NAVAL POSTGRADUATE SCHOOL

MONTEREY, CALIFORNIA

DISSERTATION

PERFORMANCE ANALYSIS OF A JTIDS/LINK-16-TYPE WAVEFORM TRANSMITTED OVER SLOW, FLAT NAKAGAMI FADING CHANNELS IN THE PRESENCE OF NARROWBAND INTERFERENCE

by

Chi-Han Kao

December 2008

Dissertation Supervisor: R. C. Robertson

Approved for public release; distribution is unlimited

THIS PAGE INTENTIONALLY LEFT BLANK

REPORT DOCUMENTATION PAGE		*Form Approved OMB No. 0704-0188*
Public reporting burden for this collection of information is estimated to average 1 hour per response, including the time for reviewing instruction, searching existing data sources, gathering and maintaining the data needed, and completing and reviewing the collection of information. Send comments regarding this burden estimate or any other aspect of this collection of information, including suggestions for reducing this burden, to Washington headquarters Services, Directorate for Information Operations and Reports, 1215 Jefferson Davis Highway, Suite 1204, Arlington, VA 22202-4302, and to the Office of Management and Budget, Paperwork Reduction Project (0704-0188) Washington DC 20503.

1. AGENCY USE ONLY *(Leave blank)*	**2. REPORT DATE** December 2008	**3. REPORT TYPE AND DATES COVERED** Dissertation

4. TITLE AND SUBTITLE: Title (Mix case letters) Performance Analysis of a JTIDS/Link-16-type Waveform Transmitted over Slow, Flat Nakagami Fading Channels in the Presence of Narrowband Interference	**5. FUNDING NUMBERS**
6. AUTHOR(S) Kao, Chi-Han	
7. PERFORMING ORGANIZATION NAME(S) AND ADDRESS(ES) Naval Postgraduate School Monterey, CA 93943-5000	**8. PERFORMING ORGANIZATION REPORT NUMBER**
9. SPONSORING / MONITORING AGENCY NAME(S) AND ADDRESS(ES) N/A	**10. SPONSORING / MONITORING AGENCY REPORT NUMBER**

11. SUPPLEMENTARY NOTES The views expressed in this dissertation are those of the author and do not reflect the official policy or position of the Department of Defense or the U.S. Government.

12a. DISTRIBUTION / AVAILABILITY STATEMENT Approved for public release; distribution is unlimited.	**12b. DISTRIBUTION CODE**

13. ABSTRACT (maximum 200 words)

   Link-16 is a tactical data link. It provides presumably secure and jam-resistant tactical information for land, sea, and air platforms. The communication terminal of Link-16 is called Joint Tactical Information Distribution System (JTIDS) and features Reed-Solomon (RS) coding, symbol interleaving, cyclic code-shift keying (CCSK) for M-ary symbol modulation, minimum-shift keying (MSK) for chip modulation, and combined frequency-hopping and direct sequence spread spectrum for transmission security. In this dissertation, the performance of a JTIDS/Link-16-type waveform in both additive white Gaussian noise (AWGN) and narrowband interference transmitted over a slow, flat Nakagami fading channel is investigated. In general, the results show that barrage noise interference (BNI) has the most effect in degrading JTIDS's performance when signal-to-interference ratio (SIR) is small, whereas pulsed-noise interference with a smaller fraction of time that interference is on causes the greatest degradation when SIR is large, whether the channel is fading or not. In addition, two modified JTIDS/Link-16-compatible systems are proposed and evaluated. The first system uses errors-and-erasures decoding (EED) in place of errors-only RS decoding, whereas the second system employs a new 32-chip CCSK sequence instead of the 32-chip CCSK sequence chosen for JTIDS. The results show that EED outperforms errors-only RS decoding in all cases and the probability of symbol error obtained for the new CCSK sequence compares favorably with the sequence chosen for JTIDS.

14. SUBJECT TERMS AWGN, CCSK, EED, JTIDS, Link-16, MSK, Nakagami fading, narrowband interference, probability of symbol error, Reed-Solomon codes.	**15. NUMBER OF PAGES** 208
	16. PRICE CODE

17. SECURITY CLASSIFICATION OF REPORT Unclassified	**18. SECURITY CLASSIFICATION OF THIS PAGE** Unclassified	**19. SECURITY CLASSIFICATION OF ABSTRACT** Unclassified	**20. LIMITATION OF ABSTRACT** UU

THIS PAGE INTENTIONALLY LEFT BLANK

PERFORMANCE ANALYSIS OF A JTIDS/LINK-16-TYPE WAVEFORM TRANSMITTED OVER SLOW, FLAT NAKAGAMI FADING CHANNELS IN THE PRESENCE OF NARROWBAND INTERFERENCE

Chi-Han Kao
Commander, Taiwan R.O.C. Navy
B.S., Chinese Naval Academy, 1989
M.S.E.E., Naval Postgraduate School, 2002

Submitted in partial fulfillment of the
requirements for the degree of

DOCTOR OF PHILOSOPHY IN ELECTRICAL ENGINEERING

from the

**NAVAL POSTGRADUATE SCHOOL
December 2008**

Author: _____
           Chi-Han Kao, Commander, Taiwan R.O.C. Navy

Approved by:

_____
R. Clark Robertson, PhD
Professor of Electrical and Computer Engineering
Dissertation Supervisor and Committee Chair

_____   _____
Roberto Cristi, PhD   Frank Kragh, PhD
Professor of Electrical and   Assistant Professor of Electrical
Computer Engineering   and Computer Engineering

_____   _____
Monique P. Fargues, PhD   Kyle Lin, PhD
Professor of Electrical and   Associate Professor of
Computer Engineering   Operation Research

Approved by: _____
              Jeffrey B. Knorr, Chair, Department of Electrical and Computer Engineering

Approved by: _____
              Douglas Moses, Associate Provost for Academic Affairs

iii

THIS PAGE INTENTIONALLY LEFT BLANK

ABSTRACT

Link-16 is a tactical data link currently employed by the United States Navy, the Joint Services, and forces of North Atlantic Treaty Organization. It provides presumably secure and jam-resistant tactical information for land, sea, and air platforms. The communication terminal of Link-16 is called Joint Tactical Information Distribution System (JTIDS) and features Reed-Solomon (RS) coding, symbol interleaving, cyclic code-shift keying (CCSK) for M-ary symbol modulation, minimum-shift keying for chip modulation, and combined frequency-hopping and direct sequence spread spectrum for transmission security. In this dissertation, we investigate the performance of a JTIDS/Link-16-type waveform in both additive white Gaussian noise (AWGN) and narrowband interference when the signal is transmitted over a slow, flat Nakagami fading channel. In general, the results show that barrage noise interference has the most effect in degrading JTIDS's performance when signal-to-interference ratio (SIR) is small, whereas pulsed-noise interference for a smaller fraction of time that the interference is on causes the greatest degradation when SIR is large, whether the channel is fading or not.

In addition, two modified JTIDS/Link-16-compatible systems are proposed and evaluated. The first system uses errors-and-erasures decoding (EED) in place of errors-only RS decoding, and the second system employs a new 32-chip CCSK sequence instead of the 32-chip CCSK sequence chosen for JTIDS. For the first modified system, the results show that EED outperforms errors-only RS decoding in all cases, whether channel is fading or not. With EED, the most significant improvement is found when both the fraction of time the interference is on is small and the signal-to-AWGN ratio is large. For the second modified system, the new 32-chip CCSK sequence, obtained from a search algorithm, allows for seven instead of six chip errors in the received sequence without making a symbol error, but the results show that the probability of symbol error obtained with the new CCSK sequence is only slightly better than that obtained with the sequence chosen for JTIDS.

THIS PAGE INTENTIONALLY LEFT BLANK

TABLE OF CONTENTS

THIS PAGE INTENTIONALLY LEFT BLANK

LIST OF FIGURES

LIST OF TABLES

THIS PAGE INTENTIONALLY LEFT BLANK

EXECUTIVE SUMMARY

Link-16 is a tactical data link currently employed by the United States Navy, the Joint Services, and forces of North Atlantic Treaty Organization. It provides presumably secure and jam-resistant tactical information for land, sea, and air platforms. The communication terminal of Link-16 is called the Joint Tactical Information Distribution System (JTIDS) and features Reed-Solomon (RS) coding, symbol interleaving, cyclic code-shift keying (CCSK) for M-ary symbol modulation, minimum-shift keying (MSK) for chip modulation, diversity, and combined frequency-hopping and direct sequence spread spectrum for transmission security. In this dissertation, the performance of a JTIDS/Link-16-type waveform is investigated for both the single- and the double-pulse structure in both additive white Gaussian noise (AWGN) and narrowband interference when the signal is transmitted over a slow, flat Nakagami fading channel. Note that the term "JTIDS/Link-16-type waveform" is used to distinguish from the actual JTIDS/Link-16 waveform, which is received noncoherently at the chip level. In this dissertation, the performance of a JTIDS/Link-16-type waveform with coherent detection is evaluated in order to ascertain the performance possible if coherent chip demodulation were practical. The analysis presented in this dissertation is easily modified to evaluate performance with noncoherent chip demodulation.

Prior to the performance analysis, the objectives of this dissertation, the fundamentals of the JTIDS/Link-16 system, and related research are introduced. The effects of narrowband interference and fading channels on the probability of symbol error of the JTIDS/Link-16-type waveform for various types of narrowband interference and fading channels are discussed. Next, a model of a JTIDS/Link-16-type transceiver is presented. The major functional blocks of the transceiver, such as a RS encoder, symbol interleaver, CCSK baseband M-ary symbol modulator, MSK chip modulator, and the JTIDS pulse structures are discussed. In addition, two modified JTIDS-compatible systems are proposed to reduce the probability of bit error. The first system uses errors-and-erasures decoding (EED) in place of errors-only RS decoding since EED can result in more coding gain for some types of fading channels and/or narrowband interference. The second system employs a new 32-chip CCSK sequence instead of the 32-chip CCSK

sequence chosen for JTIDS. Compared to the sequence chosen for JTIDS, this new sequence has a smaller maximum off-peak cross-correlation value and allows for seven instead of six chip errors in the received sequence before a symbol error occurs.

To analyze the probability of symbol error of a JTIDS/Link-16-type system, an analytic expression for the performance of CCSK is required. Since CCSK is non-orthogonal, an analytic expression for the probability of CCSK symbol error has thus far been elusive. Previously, the evaluation was done by simulation. In this dissertation, a novel analytic upper bound on the probability of symbol error for CCSK was derived for the 32-chip CCSK sequence chosen for JTIDS. The analytic upper bound is compared to two different Monte Carlo simulations. The first simulation simulates the overall probability of symbol error of CCSK for the 32-chip CCSK sequence chosen for JTIDS, while the second simulates the conditional probabilities of symbol error of CCSK for the same sequence chosen for JTIDS in order to obtain the probability of symbol error for CCSK. The results of both simulations and the results obtained with the analytic expression all are very close.

Next, the probability of symbol error for a JTIDS/Link-16-type waveform was evaluated. The evaluation was divided into three major parts. In the first part, the probability of symbol error of a JTIDS/Link-16-type waveform in AWGN-only was evaluated for both the single- and the double-pulse structure. In the second part, narrowband interference was included in the evaluation. Three types of narrowband interference, barrage noise interference (BNI), pulsed-noise interference (PNI), and combined PNI and partial-band noise interference (PBNI), were considered. In the third part, a fading channel was considered in addition to both AWGN and narrowband interference. Given the assumptions that the chip duration is smaller than the channel coherence time and that for a particular hop the signal bandwidth is smaller than the channel coherence bandwidth, the fading channel is modeled as a slow, flat Nakagami fading channel. The Nakagami fading model is assumed since it is applicable for a multipath signal with a significant line-of-sight (LOS) component such as Link-16. In general, the results show that BNI has the most effect in degrading JTIDS's performance when signal-to-interference (SIR) is small, whereas PNI causes the greatest degradation when SIR is large, whether the channel is fading or not.

To improve system performance, two modified JTIDS/Link-16-compatible systems were evaluated in the last part of this dissertation. As mentioned earlier, the first modified system uses EED, while the second modified system uses an improved 32-chip CCSK starting sequence. The probability of symbol error for a JTIDS/Link-16-type waveform obtained with EED is compared to that obtained with errors-only RS decoding, while the probability of symbol error for CCSK obtained with the new sequence is compared to that obtained with the sequence chosen for JTIDS. For the first modified system, the results show that EED outperforms errors-only RS decoding in all cases, whether the channel is fading or not and whether narrowband interference is present or not. With EED, the most significant improvement is found for PNI. For the second modified system, the results show that the probability of symbol error obtained with the new CCSK sequence is only slightly better than that obtained with the sequence chosen for JTIDS. In terms of modifying JITIDS in order to improve performance, EED is more attractive than changing the 32-chip CCSK sequence since EED is backwards compatible with existing JTIDS transceivers, while a new 32-chip CCSK sequence is not.

THIS PAGE INTENTIONALLY LEFT BLANK

ACKNOWLEDGMENTS

First and foremost I am grateful to my parents, my wonderful daughter, Jenny, and my dearest friend, Elise, for the sacrifices they made in support of my completing this dissertation. Second, I would like to thank my dissertation supervisor and chair, Prof. Clark Robertson, and my committee, Prof. Roberto Cristi, Prof. Monique Fargues, Prof. Frank Kragh, and Prof. Kyle Lin, for their endless hours of help, suggestions, ideas, and advice during the development of this dissertation. Third, I would like to thank Donna Miller, Cryptological Research Laboratory Manager, for her enthusiastic technical support. Thanks go out as well to LCDR Kendrick Macklin, USN, and Alice Lee, Program Officer and Educational Technician of Electrical and Computer Engineering Department, respectively, for their assistance. Finally, I want to express my appreciation to Col. Gary Roser and Cynthia Graham, Director and Assistant Director of International Programs, respectively, for their endless assistance throughout my second tour at Naval Postgraduate School.

THIS PAGE INTENTIONALLY LEFT BLANK

I. INTRODUCTION

A. OBJECTIVE

Link-16 is a tactical data link currently employed by the United States Navy, the Joint Services, and forces of North Atlantic Treaty Organization (NATO). It provides presumably secure and jam-resistant tactical communications for land, sea, and air platforms. Link-16 uses the Joint Tactical Information Distribution System (JTIDS) as the communication terminal to generate desired radio frequency (RF) signals. Based on a time-division multiple access (TDMA) architecture, information is exchanged to support command and control systems as well as provide situational awareness. JTIDS features Reed-Solomon (RS) coding, symbol interleaving, cyclic code-shift keying (CCSK) for M-ary baseband symbol modulation, minimum-shift keying (MSK) for chip modulation, double-pulse transmission for diversity, and combined frequency-hopping and direct sequence spread spectrum for transmission security [1].

There are several objectives for this dissertation. The first objective is to investigate the performance of a JTIDS/Link-16-type waveform for both the single- and the double-pulse structure in additive white Gaussian noise (AWGN). For any military communications systems, the anti-jam capability is an important issue in terms of design. Thus, the second objective is to investigate the vulnerability of a JTIDS/Link-16-type waveform for both the single- and the double-pulse structure to various types of narrowband interference, such as barrage noise interference (BNI), pulsed-noise interference (PNI), partial-band noise interference (PBNI), and a combination of PNI with PBNI.

In practice, the JTIDS signal is operated in the UHF band and transmitted in a fading channel. Given the assumptions that the chip duration is less than the channel coherence time and that at a particular hop the signal bandwidth is less than the channel coherence bandwidth, the fading channel is modeled as a slow, flat Nakagami fading channel. When the JTIDS signal is transmitted over a fading channel, it is reasonably to assume that narrowband interference is present most of time. Therefore, the third objective of this dissertation is to investigate the performance of a JTIDS/Link-16-type

1

waveform for both the single- and the double-pulse structure in both AWGN and narrowband interference when transmitted over a slow, flat Nakagami fading channel.

Forward error correction (FEC) coding can greatly enhance the performance of digital communication systems, especially when narrowband interference or fading channels are a factor. In addition to an (n, k) RS code with errors-only decoding, there are other decoding techniques, such as errors-and-erasures decoding (EED), can be used to improve the performance of a digital communication system; hence, the fourth objective of this dissertation is to use EED in place of errors-only RS decoding in order to see how much of an improvement would result.

For JTIDS, data modulation consists of two parts: CCSK and MSK. CCSK provides *M*-ary baseband symbol modulation, where each 5-bit symbol is represented by a 32-chip sequence, while MSK provides chip modulation for transmission. Note that CCSK is non-orthogonal; that is, the cross-correlation between the 32-chip starting sequence and its 31 cyclically shifted versions yields nonzero off-peak cross-correlation values. To improve performance, the 32-chip starting sequence must be chosen to minimize the maximum off-peak cross-correlation value; therefore, the last objective of this dissertation is to find the best 32-chip starting sequence to optimize the JTIDS performance. Note that the actual JTIDS waveform is received noncoherently at the chip level, but in this dissertation the performance of a JTIDS-type waveform with coherent detection is evaluated in order to ascertain the performance possible if coherent chip demodulation were practical. The performance analysis presented in this dissertation is easily modified to evaluate performance with noncoherent chip demodulation.

B.   JTIDS/LINK-16 FUNDAMENTALS

1.   Relationship between Link-16 and JTIDS

JTIDS/Link-16 is actually two different things: Link-16 and JTIDS. Link-16 is the name of the whole data link system, while JTIDS is the communication component of the link. Based on a TDMA architecture, Link-16 provides a secure and ostensibly jam-resistant data link so that the near real-time tactical information can be exchanged among different platforms. A representation of the Link-16 network is shown in Figure 1.
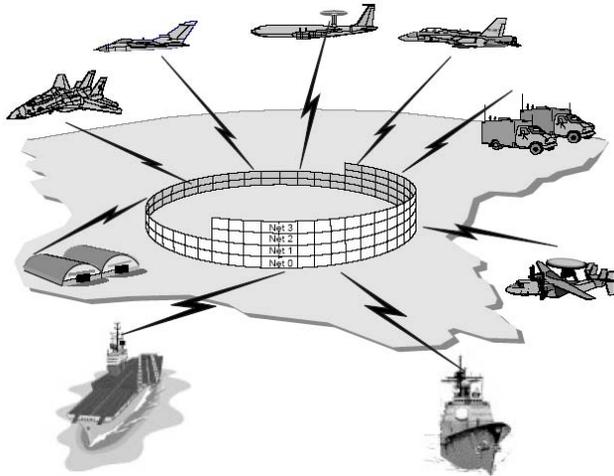
Figure 1.   Link-16 network (from [2]).

As the communication component of Link-16, JTIDS consists of software and hardware to generate, transmit, and receive the waveform in the frequency band from 960 MHz to 1215 MHz [2]. The relationship between Link-16 and JTIDS is shown in Figure 2. In general, Link-16 includes the combat system computers that generate the Link-16 messages and the JTIDS terminals. Link-16 is the NATO designation; the U.S. Navy designation for Link-16 is the Tactical Digital Information Link *J* (*TADIL J*), where *J* represents *J*-Series messages, also referred to as Link-16 tactical information.
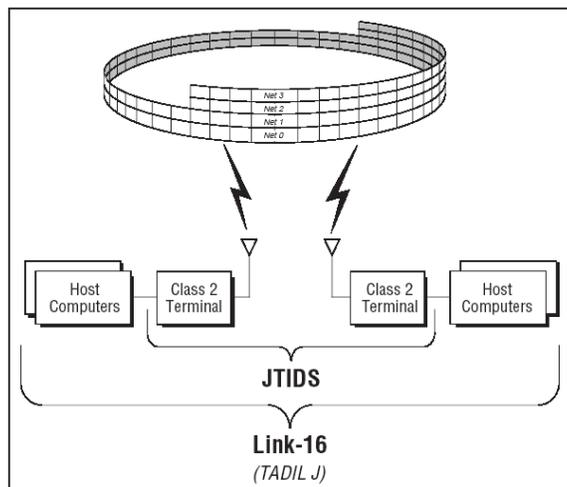
Figure 2.   Relationship between Link-16 and JTIDS (from [2]).

2.   Brief Historical Development of JTIDS

The development of JTIDS began in the late 1960s with two competing versions: TDMA for the U.S. Air Force (USAF) and distributed TDMA (DTDMA) for the U.S. Navy (USN). Early technical problems hampered both, but the problems encountered by the Navy were more severe. In 1976, the two programs were combined into a single joint program, and the USAF was given the lead to develop JTIDS/Link-16. The first operational application of JTIDS was the Class I terminal for early warning aircraft. Since the Class I terminal was too large for smaller aircraft, the development of the smaller Class II terminal was initiated in the late 1970s, and a series of operational tests were conducted in the 1980s. In the early 1990s, the Air Force conducted a series of successful operational tests of candidate Class II terminals on the F-15 aircraft. As a consequence, the Air Force started the Class IIR program in 1993 [3].

While developing the Class II JTIDS terminal, the United States and NATO collaborated in the development of Multi-functional Information Distribution System (MIDS), a JTIDS interoperable system. The MIDS program was initially led by the USAF; however, during the development of MIDS, the Class IIR program encountered both increasing cost and reliability problems, and the USAF withdrew its MIDS development on the F-16 aircraft. While USAF gave up MIDS, the USN responded by offering the F/A-18 as the new MIDS reference platform. The Navy's proposal was accepted, and the USN assumed the leadership of the MIDS development in the early 1990s. In addition to the United States, the countries funding the development are France, Germany, Italy, and Spain [4].

In 1991, the MIDS Program Memorandum of Understanding (PMOU) that governs development of the MIDS terminal was signed by the participating nations. In 1993, the MIDS program was restructured in a way that emphasized open architecture and the use of commercial parts. As of today, more than a dozen countries have installed Link-16 terminals (JTIDS or MIDS) on different land, sea, and air platforms [4]. At the user level, MIDS is essentially an evolved sibling of JTIDS; therefore, JTIDS and MIDS are assumed to be interchangeable in this dissertation.

3. Features of Link-16

Among all of the established data links, Link-16 is the most jam-resistant. In addition to jam-resistance, Link-16 has other features that outperform its predecessors: Link-4A and Link-11. Link-4A was initially developed as an automatic all-weather carrier landing system, but later it became an airborne data link to exchange status and target data between E-2C Hawkeye and F-14A Tomcat aircraft. Link-11 was developed in the 1950s to support the exchange of tactical data for maritime operations. Primarily operating in the HF band, Link-11 also supports UHF communication within the range of line-of-sight (LOS) [5]. Link-16 outperforms Link-4A and Link-11 in many ways, such as secure voice, jam resistance, security, and data throughput. We can further compare the differences between Link-4A, Link-11, and Link-16 in terms of architecture, protocol, message standard, and data rates [4]. As is seen in Table 1, Link-4A uses time-division multiplexing (TDM) and a command-and-response protocol to connect a controller (E-2C) with multiple controlled aircrafts (F-14A). The message exchange is divided into control messages (known as the V-Series messages) and aircraft replies (known as the R-Series messages). The effective two-way tactical data rate is 3,060 bits per second. Note that there is no parity check or forward error correction (FEC) coding used in Link-4A.

Table 1.   Differences between Link-4A, Link-11, and Link-16 (after [2]).

Link	Architecture	Protocol	Message Standard	Information data rate (kbps)		Channel data rate (kbps)	
						Parity	FEC
Link-4A	TDM	Command/ Response	V-Series R-Series		3.06	-	-
Link-11	Netted	Polling by Net Control	M-Series	Fast Slow	1.80 1.09	- -	2.250 1.364
Link-16	TDMA	Assigned Time Slots	J-Series	Standard Packed-2 Packed-4	26.88 53.76 107.52	28.8 57.6 115.2	59.520 119.040 238.080

Link-11 uses a netted architecture and a polling protocol in which one unit is the net control station (NCS) and calls each participating unit in turn to report its data. The Link-11 message, known as the M-Series message, consists of two 24-bit frames. For the

fast data rate, 24 bits of data are transmitted every 13.33 milliseconds (ms), which results in a data rate of 1800 bits per second. With the use of FEC coding, the channel data rate is 2250 bits per second; however, the information data rate is still the lowest among the three data links.

Link-16 uses a TDMA architecture. Each JTIDS platform is preassigned sets of time slots to transmit its data. Each time slot is 7.8125 ms in duration. One of three data packing structures can be sent in each time slot: Standard (three words), Packed-2 (six words), or Packed-4 (twelve words). The effective information data rate of Standard packing is 26,880 bps, which is much higher than that of Link-4A and Link-11. If the parity bits are included, the channel data rate is 28,800 bps. If FEC coding is considered, the channel data rate is 59,520 bps. Link-16 is a significant improvement over Link-4A and Link-11; however, it does not replace Link-4A and Link-11 entirely because Link-16 only operates in the UHF spectrum. Link-16 is limited to LOS communications unless suitable relay platforms are available.

4.   Features of JTIDS

Several features of Link-16 are a result of the unique JTIDS architecture. First, as shown in Table 2, JTIDS provides two types of security: message security (MSEC) and transmission security (TSEC). MSEC, or the encryption of message data, is applied to Link-16 messages at the link layer, while TSEC is applied to the entire transmission at the physical layer. TSEC includes random message jittering, symbol interleaving, chip scrambling, and random frequency-hopping [6]. More details on these different types of TSEC are addressed later in this chapter and in Chapter III.

Table 2.   Types of security in JTIDS (after [2]).

Cryptovariable	Type of Security
MSEC	Encryption of message data
TSEC	Encryption of JTIDS waveform -- Jitter -- Pseudorandom Noise -- Frequency-Hopping Pattern

Second, in early data links, a node is a unit required to maintain the operation of the system. In Link-11, for example, the net control station is a node. If the NCS fails, the entire link fails. In Link-16, there are no nodes required to maintain network operation so that the loss of any unit does not cause system failure. Time slots are preassigned to each participating platform, and the link operates regardless of the participation of any particular platform.

Third, in a single net, the time slots can be parceled out to one or more network participation groups (NPGs). Each NPG is grouped by its mission. For example, an NPG can be a group of platforms executing surveillance, electronic warfare, or weapons coordination. This division of the net into functional groups gives JTIDS platforms more flexibility to use the network.

Lastly, in JTIDS, the time slots can be stacked up to 127 nets by assigning a different frequency-hopping pattern to each net. Stacked nets are particularly useful for air control purposes with mutually exclusive sets of controlling units and controlled aircraft. For example, as shown in Figure 3, two mutually exclusive sets are using the stacked net structure; one is using Net-1, and the other is using Net-3. However, transmission errors increase as the number of stacked nets increases. Due to self-interference, the maximum number of stacked nets that can be operated simultaneously is about twenty [6].
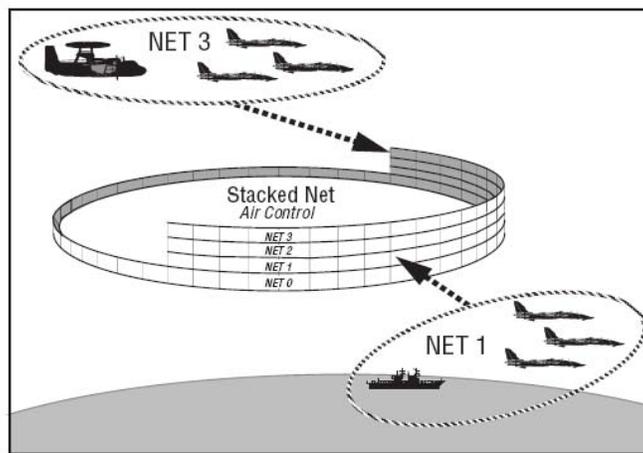
Figure 3.   JTIDS stacked nets (from [2]).

7

5.   Link-16 TDMA Architecture and Data Packing Structures

As shown in Figure 4, the Link-16 TDMA architecture divides network time into epochs, frames, and time slots. An epoch is 12.8 minutes in duration, and there are 64 frames per epoch. Each frame is twelve seconds in duration and is composed of 1536 time slots. The time slot is the basic unit of the JTIDS/Link-16 network. As mentioned earlier, each JTIDS/Link-16 platform is preassigned sets of time slots to transmit its data, and each time slot is 7.8125 ms in duration.
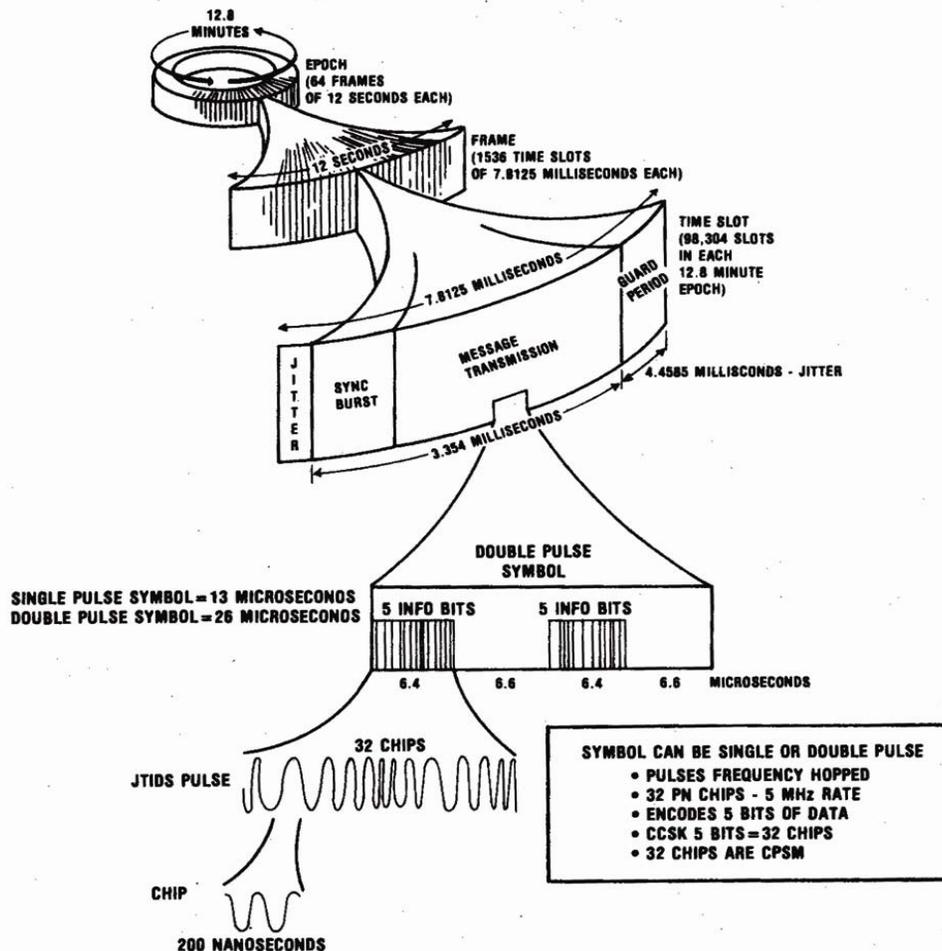
Figure 4.   JTIDS TDMA architecture (from [7]).

As previously mentioned, there are three types of data packing that can be used in each time slot: Standard (3 words), Packed-2 (6 words), or Packed-4 (12 words). The message data with Standard packing is always transmitted with a double-pulse structure (STD-DP). The message data with Packed-2 packing can be transmitted either with a

8

single-pulse (P2SP) or with a double-pulse structure (P2DP). The message data with Packed-4 packing is always transmitted with a single-pulse structure (P4SP). Thus, there are four options to transmit Link-16 messages. Note that the jam-resistance decreases as the density of the data packing increases; therefore, STD-DP is the most reliable data packing structure.

6. Time Slot Components

For the STD-DP packing structure, a single time-slot consists of several elements, including jitter, synchronization, time refinement, message (header and data), and propagation. These elements are shown in Figure 5.
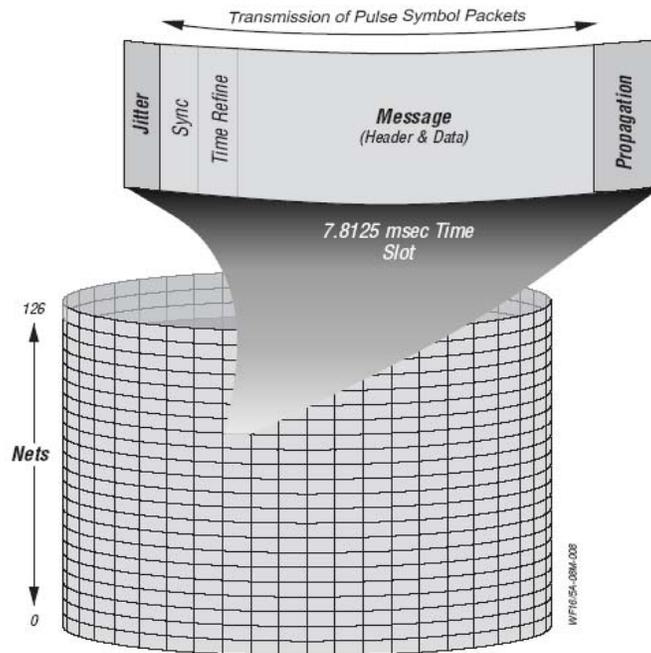
Figure 5.　Components of the time slot (from [2]).

The time-slot starts with a delay, called jitter. The amount of jitter varies from time-slot to time-slot in a pseudorandom pattern determined by the TSEC cryptovariable. Jitter contributes to the anti-jam nature of the JTIDS signal because an effective jammer needs to know when to turn the jamming signal on. After the jitter are two sets of predetermined symbols, synchronization and time refinement, which are used by the receiver to recognize and synchronize with the signal. Followed by the time refinement is

the message, which consists of header and data symbols. Since the header and data symbols are closely related to the performance analysis, more details are addressed in the next subsection. Lastly, the propagation time is a guard time which allows for the propagation of the signal. There are two possible guard times; one is for normal range$(\cong 300\,\text{nmi})$, and the other is for extended range $(\cong 500\,\text{nmi})$ [8]. Note that the jitter and propagation times are dead times in which no signal is transmitted.

7.   Link-16 Messages

Link-16 messages are exchanged during each TDMA time slot. As previously mentioned, each message consists of a header and data. The header specifies the type of data and identifies the source terminal. The format of the header is shown in Figure 6. As can be seen, it contains 35 bits. Bits 0 through 2 specify the type of data. Bit 3 provides packing or relay information. Bits 4 through 18 not only identify the source track number of the transmitting terminal, but also contribute to the calculation of parity bits. Bits 19 through 34 specify the serial number of the Secure Data Unit (SDU), which is determined by the message encryption.

Header			
SDU Serial Number	Source Track Number	P/R	Type
34	19	4 3	0
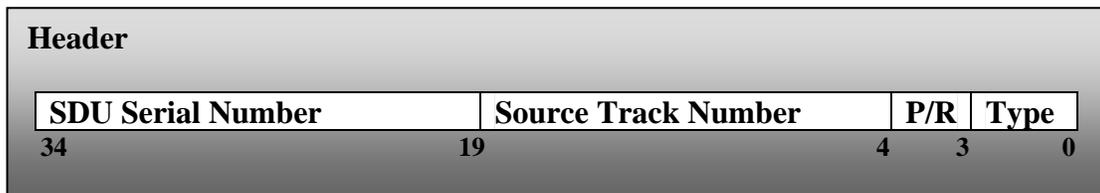
Figure 6.   Link-16 massage header (after [2]).

For message data, there are four types of format: fixed-format, variable-format, free text, and round-trip timing (RTT). A fixed-format message data is used to exchange J-Series messages, while a variable-format message data is used to provide a general way to exchange any type of user-defined message, but not used by the U.S. Navy. Free-text message data is used for digitized voice, and a RTT message data is used for terminal synchronization; a terminal must be synchronized with the net in order to receive and transmit on a JTIDS network. To facilitate the performance analysis, only the fixed-format message data is considered in this dissertation.

10

In a J-Series message, there are three types of J-Series words: initial word, extension word, and continuation word. As shown in Figure 7, each word consists of 75 bits, of which 70 are J-Series message data, four bits are used for parity checks, and one bit is reserved as a spare. J-Series messages may contain an initial word, one or more extension words, and one or more continuation words. Up to eight words may be used to form a single J-Series message. If the STD-DP packing structure is used, three J-Series words (225 bits) are formed and transmitted in each time slot.

Initial Word

Parity	Information Fields	Message length	Sub-Label	Label	Word Format 00
74 70		13 10	7	2	0

Extension Word

Parity	Information Fields	Word Format 10
74 70		2 0

Continuation Word

Parity	Information Fields	Continuation Label	Word Format 01
74 70		7	2 0
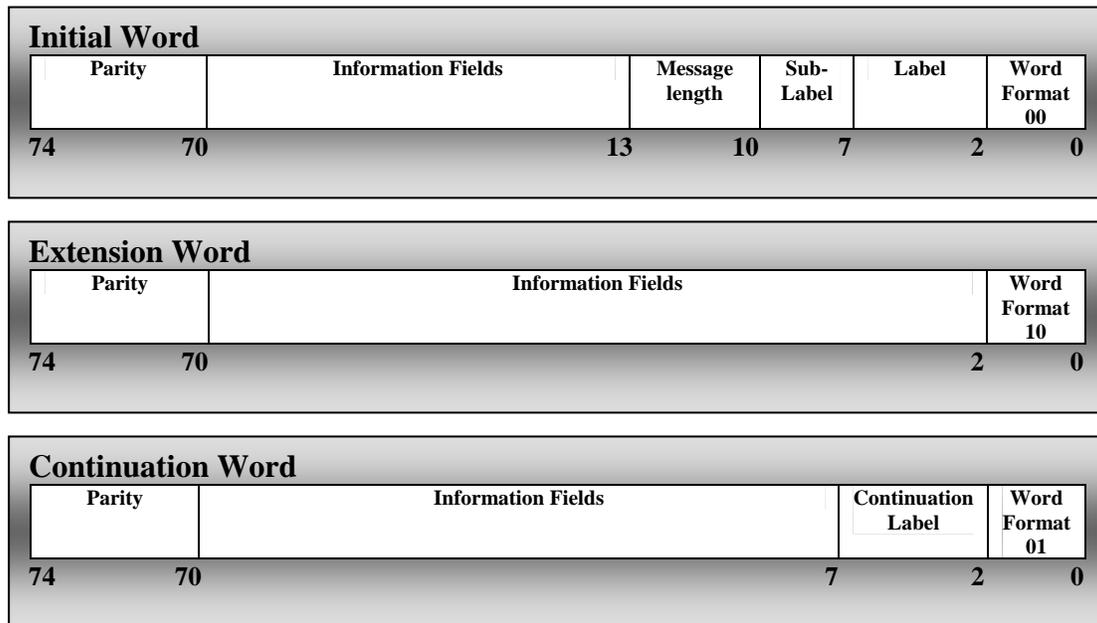
Figure 7.   Fixed-format message words (after [2]).

8.   Link Layer Operations of Link-16

The three-word J-Series triplets are assembled at the link layer of Link-16 [6]. Before the header and J-Series triplets are forwarded to the physical layer for transmission, several steps are involved. First, the data packing structure, STD-DP, P2SP, P2DP, or P4SP, is determined and recorded in the header. Second, the twelve parity bits are generated using a binary (237,225) cyclic redundancy check (CRC) error detection code, where the 225 input bits consist of three 70-bit J-Series message data and the 15-bit source track number from the header. The twelve parity bits are then distributed within the J-Series triplets shown in Figure 7. Third, the J-Series triplets are subject to encryption. The encryption process yields a SDU serial number and is stored in the

header (bits 19 through 34). Note that the header is transmitted without encryption. Lastly, the header and J-Series triplets are forwarded to the physical layer for transmission.

On reception, the link layer performs the preceding operations in reverse, and only those J-Series triplets that pass the parity check are passed to the protocol stack. Note that the header is interpreted at the link layer, but the J-Series triplets are processed at the physical layer; that is, the entire J-Series message (header and data) cannot be passed to the protocol stack in one step. The data symbols must be buffered and demodulated after the packing structure in the header is determined at the link layer [6]. More details about the Link-16 physical layer operations and JTIDS waveform are introduced in Chapter III.

C.   LITERATURE REVIEW

In most applications, an ideal conventional communication system, whether digital or analog, is one that maximizes performance with minimum transmission power, minimum transmission bandwidth, and minimum transmitter/receiver complexity. In military applications, however, there are other considerations that supersede the conventional ones. For example, the ability to reject hostile jamming, low probability of detection (LPD), and low probability of interception (LPI). To obtain these goals, usually both transmission bandwidth and transmitter/receiver complexity are sacrificed. These types of systems are called spread spectrum communication systems. There are three primary types of spread spectrum systems: direct sequence spread spectrum (DSSS), frequency-hopping spread spectrum (FHSS), and hybrid DS/FH spread spectrum. JTIDS is a hybrid DS/FH spread spectrum system that uses CCSK for symbol modulation and spreading, and its waveform hops pseudorandomly to over 51 frequency bins at a rate of around 77,000 hops per second.

There are a considerable number of published papers on the topic of hybrid DS/FH spread spectrum, but few investigated the performance of JTIDS. As mentioned earlier, JTIDS is currently used by the United States Navy, the Joint Services, NATO, and some US allies. Due to security issues, it is understandable that there are no standard or physical layer specifications of JTIDS released for public access. Since there is no

standard, different papers have interpreted the structure of the JTIDS physical layer differently, and different conclusions are reached even though the terminology used is the same. In what follows, the papers closely related to the performance analysis of JTIDS are first reviewed, and then the review is extended to those papers that are related to generic hybrid DS/FH spread spectrum systems.

In general, there are two approaches to evaluate system performance: analytical derivation and simulation. In [9] and [10], the error rate performance of the JTIDS CCSK waveform is investigated by simulation. These two papers point out that the CCSK waveform is not orthogonal, and there is no simple relationship between the symbol and bit error probabilities. Paper [9] compares the error performance between the JTIDS 32-ary CCSK waveforms and 32-ary orthogonal waveforms for a system with 32 chips per symbol. The results in this paper showed that there is no significant performance difference between the two waveforms for the multiple-access channel; however, CCSK modulation has a larger bit error probability than orthogonal modulation in additive white Gaussian noise (AWGN).

Among all of the related papers reviewed ([9] through [24]), [11] is the only one describes an analysis of the performance of a JTIDS waveform in AWGN. This paper evaluated an approximation for the probability of symbol error and probability of bit error of a JTIDS waveform with both errors-only and errors-and-erasures RS decoding. The performance analysis is based on the auto-correlation property of the CCSK sequence. With the assumption of ideal coherent demodulation and the fact that the bit error probability of MSK is same as that of binary phase-shift keying (BPSK) [12], approximate analytical expressions for the probability of symbol error and probability of bit error for both errors-only and errors-and-erasures decoding are presented. Unfortunately, the results presented in this paper are based on the overly optimistic assumption that the cross-correlation values for the CCSK symbol demodulator are independent. Actually, it can be shown that these cross-correlation values are not independent (see Appendix A).

Additional research related to the performance of JTIDS is presented in [13]. This paper compares the robustness of three airborne networking waveforms: orthogonal

frequency-division multiplexing (OFDM), single carrier DSSS, and JTIDS/Link-16, based on the assumptions that there is a LOS path between transmitter and receiver and that there is no multipath fading. Quantitative numerical results are used to compare the performance of these three waveforms against several jamming threats, such as tone jamming, partial-band jamming, and frequency-follower jamming. No analytical results are presented in the paper. This paper concluded that: (a) JTIDS/Link-16 has an advantage against tone jamming because of the DS spreading, (b) the JTIDS/Link-16 waveform is protected against partial-band jamming because it is a frequency-hop system, and (c) JTIDS/Link-16 can combat frequency-follower jamming because it transmits a single symbol per hop, and its dwell time at a particular frequency is very short, which makes implementation of a follower jammer currently impractical.

Instead of using CCSK and MSK for data modulation, [14] used BPSK to evaluate the performance for a (31,15) RS code over a bursty-noise channel. Bursty-noise is defined as background Gaussian noise plus burst noise, which is a series of finite-duration Gaussian-noise pulses with Poisson occurrence times. Using this noise model, along with ideal symbol interleaving/de-interleaving, BPSK modulation, and errors-only RS decoding, decoded bit error probability bounds were derived for the case where the noise bursts are long with respect to the channel symbol rate. Narrowband interference and multipath fading were not considered in this paper. The theoretical bounds are compared with Monte Carlo simulations in this paper. The simulation results agree well with the theoretical performance bounds; however, these results cannot represent the performance of JTIDS because CCSK is not considered.

For the past twenty years, hybrid DS/FH spread spectrum (SS) has received considerable attention because it combines the advantages of both DSSS and FHSS. Generally speaking, DSSS is effective in combating frequency-selective multipath fading, while FHSS system is effective in mitigating partial-band noise interference (PBNI). There are many papers that investigate the performance of various hybrid DS/FH spread spectrum systems. For example, the performance of coherent and non-coherent hybrid DS/slow FH (DS/SFH) spread spectrum multiple access (SSMA) communication systems in AWGN was evaluated in [15] and [16], respectively. In [15], systems employing BPSK/QPSK data modulation with arbitrary chip waveforms are investigated,

and the hopping rates are restricted to be much slower than the data rate so that coherent demodulation is feasible. In [16] the hopping rates are considered slightly smaller than or equal to the data rate, and differential phase-shift keying (DPSK), BFSK, and M-ary frequency-shift keying (M-FSK) modulation are considered. Both papers investigate the average probability of bit error and multiple access capability. The multiple access capability is defined as the maximum number of signals transmitted from different stations simultaneously that can be tolerated in the neighborhood of a receiver and the error probability for the reception of a particular signal not exceed a pre-specified maximum value. According to their results, in both coherent and noncoherent cases, the multiple-access capability of hybrid spread spectrum is superior to that of pure FHSS, but inferior to that of pure DSSS for systems with identical bandwidth expansion. Further, the hybrid systems with coherent and noncoherent demodulation are compared, and the results show that there is a considerable loss in performance for the noncoherent systems.

In addition to the performance of hybrid DS/SFH SS in AWGN, the performance of coded hybrid DS/FH SS in AWGN, PBNI, and multiple-access interference (MAI) is evaluated in [17]. The system model employs M-FSK for data modulation with several FEC codes such as convolutional codes, RS codes, and concatenated codes. Interleaving is assumed so that burst errors can be assumed to be converted to random errors. It was shown that in all cases the use of FEC coding reduced the minimum required carrier-to-interference ratio, increased the number of users that could be supported, and improved the system performance in worst case PBNI.

Instead of PBNI and MAI, the performance of coded hybrid DS/FH SS system in AWGN, multipath Ricean fading, and MAI is investigated in [18]. M-FSK was used for data modulation in combination with several FEC codes such as convolutional codes, RS codes, and concatenated codes. In this study, the effects of Ricean fading and MAI on the number of users in the network, the minimum carrier-to-interference (C/I) ratio required to guarantee a desirable probability of bit error, and the improvement in system performance obtained with FEC coding were investigated. Several conclusions are reached in their paper. First, concatenated codes offer the best performance, followed closely by RS codes; however, the use of higher modulation schemes (large M) does not

15

offer a substantial improvement in E_b/N_0 for Ricean fading channels. Second, Ricean fading degrades system performance and results in a reduction in the number of users in the network. Third, the use of FEC coding restores the performance, but the use of FEC coding adds extra complexity and delay to the system. Lastly, the use of *M*-ary signaling does not counter the degradation due to Ricean fading but does increase the number of users in the network.

Other than PBNI or multiple-tone jamming, the performance of hybrid DS/FH SS against follower jamming is investigated in [19]. This paper assumes that the jammer detects the current hop frequency and transmits an interfering signal to the satellite before the satellite finishes receiving that frequency. The probability of symbol error for hybrid DS/FH SS in the presence of a follower jammer is determined. The results show that sufficiently fast frequency hopping can combat both follower jamming and frequency-selective fading.

The performance of coherent and noncoherent asynchronous hybrid DS/FH SSMA in AWGN, PBNI, MAI, and Ricean fading are investigated in [20]. Two modulation schemes, BPSK and *M*-FSK, with several different FEC codes including dual-K convolutional codes and concatenated codes (dual-K inner code and RS outer code) are considered. Ideal interleaving is assumed so that any burst errors can be assumed to be random errors. According to this paper, coherent systems offer better performance in the presence of combined PBNI, MAI, Ricean fading, and AWGN; however, the data rates in the coherent system are restricted to be substantially lower than the hopping rate. This paper also showed that the use of FEC codes, especially concatenated codes, improves the system performance considerably.

The performance of hybrid DS/FH SS in a hostile land mobile radio channel is evaluated in [21]. The effects of a barrage jammer, Rayleigh fading, and log-normal shadowing on system performance are discussed. With DPSK signaling, an analytical expression for the probability of bit error is derived for a Rayleigh fading channel both with and without log-normal shadowing. This paper shows that log-normal shadowing degrades system performance, but the degradation is much smaller than that introduced

by multipath fading. This paper concludes that in order to achieve a better performance, diversity should be used to reduce the effect of shadowing and fast fading.

As mentioned earlier, JTIDS uses CCSK for baseband symbol modulation; however, CCSK is not orthogonal. To minimize the probability of error and increase system capacity, orthogonal sequences are often employed. For example, [22] assumes orthogonal codes to investigate the performance and capacity of a hybrid DS/FH SS mobile radio system operating over a Rayleigh fading channel. QPSK is used for data modulation. Performance is investigated for both deterministic and random signature sequences, where Hadamard codes of length eight are used for the deterministic signature sequences. The results of this paper indicate that using orthogonal signature codes minimizes the probability of bit error and increases capacity of synchronous systems; however, if the system is asynchronous, performance with Hadamard codes is degraded since the sequences are no longer orthogonal.

The performance of hybrid DS/SFH SS with MSK modulation in AWGN and partial-band multitone jamming is evaluated in [23]. With the assumptions that the DSSS signal bandwidth is equivalent to the FH slot spacing, all filters are ideal, and there is no multiple user interference, an analytic probability of bit error expression is developed. The probability of bit error is evaluated for various values of the DS processing gain, the number of jamming tones, the signal-to-noise power ratio, and the jamming-to-signal power ratio. The results show that, in some cases, the addition of DS spreading to a FH system can significantly improve the system's resistance to partial-band multitone jamming without increasing the total system bandwidth.

The performance of hybrid DS/SFH MSK in a Rayleigh fading channel with PBNI is evaluated in [24]. It is shown that in AWGN, for large signal-to-interference ratio (SIR), the worst case probability of bit error is caused by PBNI, while for a low SIR, the worst case probability of bit error is caused by the full-band interference, independent of signal-to-AWGN ratio (SNR). Furthermore, in a Rayleigh fading channel, full-band interference always causes the worst probability of bit error independent of SIR or SNR.

17

To sum up, the performance of hybrid DS/FH SS systems for various modulation schemes in the presence of different types of interference and fading has been investigated in [9]-[24], but only [11] attempts to evaluate the performance of the JTIDS waveform analytically in AWGN. Unfortunately, the results presented in [11] are based on the overly optimistic assumption that the cross-correlation values for the CCSK symbol demodulator are independent. To the best of the author's knowledge, the performance of a JTIDS/Link-16-type waveform in both AWGN and narrowband interference when the signal is transmitted over a slow, flat Nakagami fading channel has not been investigated.

The rest of this dissertation is organized as follows. Narrowband interference and multipath fading channels are introduced in Chapter II. The physical layer of a JTIDS/Link-16-type system along with proposed modifications, including a system with errors-and-erasures decoding (EED) and a system with an improved CCSK sequence, are introduced in Chapter III. The performance analysis and simulation for the 32-chip CCSK sequence chosen for JTIDS in AWGN is presented in Chapter IV. The analysis for the probability of symbol error of CCSK is considerably more difficult than an analysis of orthogonal modulation due to the non-orthogonal nature of CCSK. To the best of the author's knowledge, the analysis presented here is novel and is based on a deep understanding of the nature of the cross-correlation properties of CCSK sequences. In Chapter V, the probability of symbol error of a JTIDS/Link-16-type waveform in both AWGN and narrowband interference when the signal is transmitted over a slow, flat Nakagami fading channel is investigated. In Chapter VI, the performance analyses for the two proposed modifications are evaluated. The probabilities of symbol error obtained with the modified systems are compared with those obtained in Chapter IV and V, respectively. Finally, the important results and findings are summarized in Chapter VII.

II.   NARROWBAND INTERFERENCE AND FADING CHANNELS

For any military wireless communication systems, the effect of both hostile jammers and multipath fading channels must be considered. In this chapter, several types of narrowband interference, such as barrage noise interference (BNI), pulsed-noise interference (PNI), partial-band noise interference (PBNI), and a combination of PNI and PBNI are first considered. Next, four types of small-scale fading and three widely used multipath fading models, namely Rayleigh, Ricean, and Nakagami fading models, are introduced. Lastly, a generic expression for the performance over Nakagami fading channels is addressed.

A.   NARROWBAND INTERFERENCE

1.   Barrage Noise Interference

The most benign narrowband interference is BNI. This interference is modeled as a bandlimited, noise-like signal $n_I(t)$ with channel power spectral density (PSD) $S_{n_I}(f)$. It is usually assumed that the BNI bandwidth covers exactly the frequency band of the receiver; although, in practice an actual BNI may not be that precise. The effect of BNI on the system is simply to increase the Gaussian noise level at the receiver. Since AWGN $n(t)$ and BNI $n_I(t)$ are independent random processes, the total noise PSD can be written as

$$N_T(f) = N_0/2 + S_{n_I}(f), \tag{2.1}$$

where $N_0/2$ is the two-sided PSD of AWGN. Recall that the PSD at the output of a linear system with transfer function $H(f)$ is related to the PSD at the input by [25]

$$S_{out}(f) = S_{in}(f)|H(f)|^2, \tag{2.2}$$

and recall that the noise power at system output is given by

$$\sigma^2 = \int_{-\infty}^{\infty} S_{out}(f)\, df. \tag{2.3}$$

If a correlator (consists of a mixer and an integrator) is used to recover the signal, the total noise power at the output of the integrator is given by

$$\sigma_T^2 = \sigma_n^2 + \sigma_I^2$$
$$= N_0/T_b + \int_{-\infty}^{\infty} S_{I_{in}}(f)|H(f)|^2 \, df, \tag{2.4}$$

where $S_{I_{in}}(f)$ is the PSD of BNI at the input of the integrator, and $H(f)$ is the transfer function of the integrator, which is given by

$$H(f) = \left[\frac{\sin(\pi f T_b)}{\pi f T_b}\right]\exp(-j\pi f T_b). \tag{2.5}$$

If MSK is used for data modulation, and if the channel PSD of BNI $S_{n_I}(f)$ is $N_I/2$ within the null-to-null bandwidth of the MSK signal and zero elsewhere, Equation (2.4) simplifies to

$$\sigma_T^2 \approx \frac{N_0}{T_b} + \int_{-0.75R_b}^{+0.75R_b} N_I \left[\frac{\sin(\pi f T_b)}{\pi f T_b}\right]^2 \, df \tag{2.6}$$

since the null-to-null bandwidth of the MSK signal is $1.5R_b$ and the PSD of BNI at the integrator input is

$$S_{I_{in}}(f) = S_{n_I}(f - f_c) + S_{n_I}(f + f_c) = N_I; \tag{2.7}$$

therefore, the total noise power at the integrator output of a MSK receiver is

$$\sigma_T^2 = \frac{N_0 + 0.889N_I}{T_b}. \tag{2.8}$$

When viewed as a special case of offset QPSK (OQPSK), MSK has the same probability of bit error as BPSK, QPSK, and OQPSK [26]. Thus, the probability of bit error of MSK in AWGN is given by

$$P_b = Q\left(\sqrt{\frac{\overline{X^2}}{\sigma_n^2}}\right) = Q\left(\sqrt{\frac{2E_b}{N_0}}\right), \tag{2.9}$$

where $\overline{X}$ is the mean of the integrator output X. Since BNI is a bandlimited, noise-like signal, it has no effects on the mean of the integrator output; therefore, the mean $\overline{X}$ is the same as that without BNI, but the variance σ_T^2 is given by Equation (2.8). Modifying the result obtained for AWGN alone, we obtain the probability of bit error of MSK in the presence of both AWGN and BNI as

$$P_b = Q\left(\sqrt{\frac{\overline{X}^2}{\sigma_T^2}}\right) = Q\left(\sqrt{\frac{2E_b}{N_0 + 0.889 N_I}}\right). \tag{2.10}$$

For the case of direct sequence MSK (DS/MSK), Equation (2.10) must be modified. In essence, the bit duration T_b is replaced by the chip duration T_c, and

$$\sigma_T^2 = \frac{N_0 + 0.889 N_I}{T_c}. \tag{2.11}$$

Hence, for a DS/MSK system in both AWGN and BNI, the probability of chip error is

$$P_c = Q\left(\sqrt{\frac{2E_c}{N_0 + 0.889 N_I}}\right), \tag{2.12}$$

where E_c is the average energy per chip.

2.   Pulsed-Noise Interference

Pulsed-noise interference is similar to barrage noise interference except the interference is turned on and off systematically. Assuming a constant average interference power, the effect of PNI is to increase the noise PSD by $1/\rho_1$, where $0 < \rho_1 \leq 1$ represents the fraction of time the jammer is turned on. If $P_b(\square)$ denotes the conditional probability of bit error for the data modulation of interest, then the average probability of bit error subject to PNI is given by [27]

$$\begin{aligned} P_b = &\Pr\{\text{pulse jammer on}\} P_b(\text{pulse jammer on}) \\ &+ \Pr\{\text{pulse jammer off}\} P_b(\text{pulse jammer off}). \end{aligned} \tag{2.13}$$

For conventional MSK in both AWGN and PNI, the average probability of bit error is obtained by substituting Equations (2.9) and (2.10) into (2.13) to obtain

$$P_b = \rho_1 Q\left(\sqrt{\frac{2E_b}{N_0 + (0.889\,N_I/\rho_1)}}\right) + (1-\rho_1)Q\left(\sqrt{\frac{2E_b}{N_0}}\right). \qquad (2.14)$$

For DS/MSK in both AWGN and PNI, the analysis is analogous to that for DS/MSK in both AWGN and BNI. Replacing T_b with T_c, we obtain the probability of chip error for DS/MSK in both AWGN and PNI as

$$P_c = \rho_1 Q\left(\sqrt{\frac{2E_c}{N_0 + (0.889\,N_I/\rho_1)}}\right) + (1-\rho_1)Q\left(\sqrt{\frac{2E_c}{N_0}}\right). \qquad (2.15)$$

3.   Partial-Band Noise Interference

Partial-band noise interference is similar to the BNI except only a portion of the overall signal bandwidth has interference. Because of the smaller bandwidth, a partial-band noise interference signal may be easier to generate than a barrage noise interference signal. Furthermore, for FHSS systems, PBNI is considerably more effective than BNI since the signal can be seriously degraded when hops are in the interference band. Therefore, partial-band interference is commonly used to jam frequency-hopping communication systems [28].

Analytically, PBNI is similar to PNI. Let the fraction of the spread spectrum signal bandwidth which has interference be denoted by ρ_2. Assuming a constant average interference power for all ρ_2, the effect of PBNI is to increase the noise PSD by $1/\rho_2$ in the bins that are affected. Note that $1/\rho_2 \geq 1$ since $0 < \rho_2 \leq 1$. If $P_b(\square)$ denotes the conditional probability of bit error for the data modulation of interest, then the average probability of bit error subject to PBNI is given by

$$\begin{aligned}
P_b = &\Pr\{\text{bin jammed}\}\, P_b(\text{bin jammed})\\
&+ \Pr\{\text{bin not jammed}\}\, P_b(\text{bin not jammed}).
\end{aligned} \qquad (2.16)$$

If the frequency-hop bins are assumed to be non-overlapping in frequency and if the data modulation of interest is MSK, the average probability of bit error for a FHSS system with MSK signaling in both AWGN and PBNI is given by

$$P_b = \rho_2 Q\left(\sqrt{\frac{2E_b}{N_0 + (0.889\,N_I/\rho_2)}}\right) + (1-\rho_2)Q\left(\sqrt{\frac{2E_b}{N_0}}\right). \tag{2.17}$$

For DS/MSK in both AWGN and PBNI, the analysis is analogous to that for DS/MSK in both AWGN and BNI. The probability of chip error for DS/MSK in both AWGN and PBNI is obtained by replacing T_b with T_c in (2.17) to obtain

$$P_c = \rho_2 Q\left(\sqrt{\frac{2E_c}{N_0 + (0.889\,N_I/\rho_2)}}\right) + (1-\rho_2)Q\left(\sqrt{\frac{2E_c}{N_0}}\right). \tag{2.18}$$

Note that Equation (2.18) is identical to (2.15) if $\rho_2 = \rho_1$.

4. Combined Pulsed-Noise and Partial-Band Noise Interference

As mentioned earlier, JTIDS is a hybrid DS/FH spread spectrum system. Intuitively, an effective jamming strategy would use a combination of PNI and PBNI to engage the JTIDS waveform. Let ρ_1 represent the fraction of time the jammer is turned on and ρ_2 represent the fraction of the spread spectrum signal bandwidth that is jammed. We assume that the time the interference is on and the portion of the band that is jammed are independent. If $P_b(\square)$ denotes the conditional probability of bit error for the data modulation of interest, then the average probability of bit error is given by

$$\begin{aligned} P_b = &\ \mathrm{Pr}\{\text{jammed}\}\,P_b(\text{jammed}) \\ &+ \mathrm{Pr}\{\text{not jammed}\}\,P_b(\text{not jammed}), \end{aligned} \tag{2.19}$$

where $\mathrm{Pr}\{\text{jammed}\}$ is defined as the probability that PNI is turned on and that the hop is also jammed, which is given by

$$\mathrm{Pr}\{\text{jammed}\} = \rho_1\rho_2, \tag{2.20}$$

and $\mathrm{Pr}\{\text{not jammed}\}$ is given by

$$\mathrm{Pr}\{\text{not jammed}\} = 1 - \rho_1\rho_2 \tag{2.21}$$

since a symbol is only jammed when the interference is on and the hop is jammed. Therefore, the effect of combined PNI and PBNI is to increase the noise PSD by

23

$1/(\rho_1\rho_2)$ in the bins that are jammed. If the frequency-hop bins are assumed to be non-overlapping in frequency and if the data modulation of interest is MSK, then the average probability of chip error for a hybrid DS/FH SS system in both AWGN and combined PNI and PBNI is given by

$$P_c < \rho_1\rho_2 Q\left(\sqrt{\frac{2E_c}{(N_0+0.889N_I/\rho_1\rho_2)}}\right)+(1-\rho_1\rho_2)Q\left(\sqrt{\frac{2E_c}{N_0}}\right). \qquad (2.22)$$

Note that Equation (2.22) is identical to Equation (2.15) and Equation (2.18) if $\rho_1\rho_2$ are replaced by ρ_1 and ρ_2, respectively.

B.   FADING CHANNELS

Many wireless communication channels do not have a line-of-sight (LOS) signal path. When there is no LOS, the signal is transmitted to the receiver by a phenomenon known as multipath; that is, there are multiple signal paths from the transmitter to the receiver as a result of reflection of the original signal off of buildings, terrain features, the ionosphere or troposphere, and so on. Due to multipath, a signal will arrive at the receiver multiple times with different amplitudes, phases, and arrival times, giving rise to the term multipath fading. For JTIDS, multipath fading is not critical since JTIDS is operated in the UHF band (LOS is required); however, there are some cases where the JTIDS signal suffers from multipath fading. For example, in ship-to-ship or ship-to-low altitude air platforms communications, a two-ray path may occur. Therefore, a multipath fading channel is considered in this dissertation.

The effect of multipath fading on the received signal amplitude can be broken into large-scale and small-scale fading. Large-scale fading represents the average received signal power attenuation over large transmitter-to-receiver separation distances, whereas small-scale fading refers to the dramatic fluctuation in signal amplitude over very short distances (on the order of a half-wavelength or less). In general, large-scale fading is taken into account in the link budget analysis, whereas small-scale fading is considered in the performance analysis. Therefore, a multipath fading channel can be narrowed down to a small-scale fading channel in this dissertation. In what follows, four types of small scale

fading are first discussed followed by three common fading models, and then a slow, flat Nakagami fading channel is introduced in the last section of this chapter.

1.   Types of Small Scale Fading

There are two channel mechanisms that determine the types of small-scale fading: coherence bandwidth B_C and coherence time T_C. The former is a statistical measure of the range of frequencies over which the channel has approximately equal gain and linear phase, whereas the later is a statistical measure of the time duration over which the channel impulse response is essentially invariant. The coherence bandwidth is inversely proportional to the multipath root-mean-square (rms) delay spread σ_τ. When the coherence bandwidth is defined as the bandwidth over which the frequency correlation function is above 0.5, a more popular approximation of the coherence bandwidth is $B_C \approx 1/(5\sigma_\tau)$. Similarly, the coherence time is inversely proportional to the Doppler spread B_d. When the coherence time is defined as the time over which the time correlation function is above 0.5, a more popular approximation of the coherence time is $T_C \approx 9/(16\pi B_d)$. Typical measured values of rms delay spread and Doppler spread can be found in [29].

If the transmitted signal bandwidth B_S is less than the coherence bandwidth, then the received signal undergoes flat fading; otherwise, the received signal undergoes frequency-selective fading. If the transmitted symbol time T_S is greater than the coherence time, the received signal undergoes fast fading; otherwise, the received signal undergoes slow fading. Note that the reciprocal of the signal bandwidth is the symbol time, the reciprocal of the coherence bandwidth is the rms delay spread, and the reciprocal of the coherence time is the Doppler spread. In other words, if the transmitted symbol time T_S is greater than the rms delay spread, then the received signal also undergoes flat fading; otherwise, the received signal undergoes frequency-selective fading. If the transmitted signal bandwidth B_S is less than the Doppler spread, the received signal also undergoes fast fading; otherwise, the received signal undergoes slow fading. This is illustrated in Figure 8. To summarize, there are four types of small-scale

fading: flat fading and frequency-selective fading are related to multipath delay spread, while fast fading and slow fading are related to Doppler spread. Either frequency-selective fading or fast fading causes severe performance degradation.

Small-scale fading
related to *multipath delay spread*

Flat fading if $B_S < B_C$ or $T_S > \sigma_\tau$

Frequency-selective fading if $B_S > B_C$ or $T_S < \sigma_\tau$

Small-scale fading
related to *Doppler spread*

Fast fading if $T_S > T_C$ or $B_S < B_D$

Slow fading if $T_S < T_C$ or $B_S > B_D$
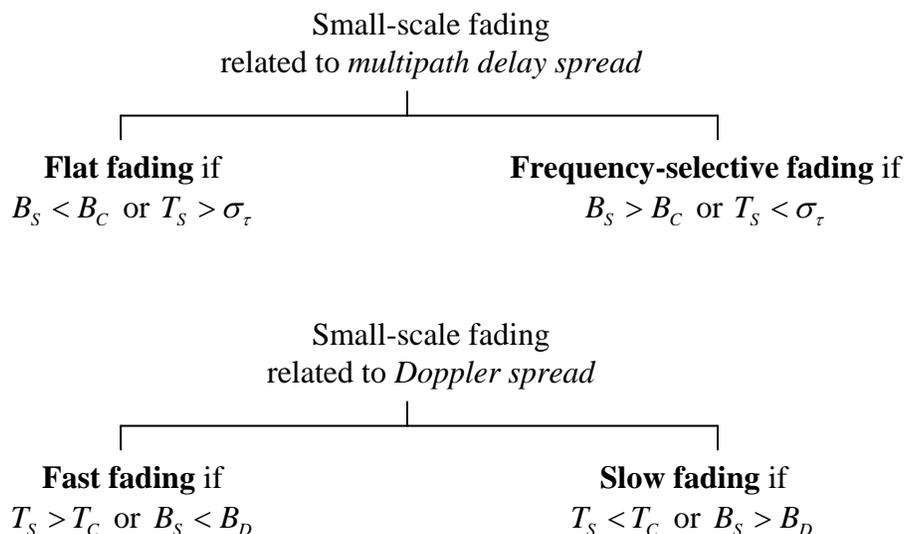
Figure 8.   Types of small scale fading (after [29]).

2.   **Fading Channel Models**

For a non-fading channel, the received signal amplitude A_c is modeled as a deterministic parameter; however, for a fading channel, the received signal amplitude fluctuates and is modeled as a random variable a_c. In wireless communications, there are three widely used models for fading channels: Rayleigh, Ricean, and Nakagami. The Rayleigh fading model is most applicable when there is no LOS propagation between transmitter and receiver and all of the received signal power is due to multipath. For Rayleigh fading model, the amplitude of the received signal varies randomly according to a Rayleigh distribution; that is, the received signal amplitude a_c has a probability density function (pdf) as [30]

$$f_{A_c}(a_c) = \frac{a_c}{\sigma^2} \exp\left(\frac{-a_c^2}{2\sigma^2}\right), \quad a_c \geq 0 \tag{2.23}$$

where $2\sigma^2$ represents the received non-LOS signal power.

26

The Ricean fading model is most applicable when there is LOS propagation between transmitter and receiver, but a substantial portion of the received signal power is still due to multipath. Note that when there is LOS between transmitter and receiver and virtually none of the received signal power is due to multipath, the channel is non-fading. For Ricean fading channels, the received signal amplitude a_c is modeled as a Ricean random variable with a pdf [30]

$$f_{A_c}(a_c) = \frac{a_c}{\sigma^2} \exp\left(\frac{-\left(a_c^2 + \alpha^2\right)}{2\sigma^2}\right) I_0\left(\frac{\alpha a_c}{\sigma^2}\right), \quad a_c \geq 0 \tag{2.24}$$

where $I_0(\square)$ is the zeroth-order modified Bessel function of the first kind, α^2 is the received LOS signal power, and $2\sigma^2$ is the non-LOS signal power. It has been shown that the average received signal power for a Ricean fading channel is [30]

$$\overline{S^2(t)} = \overline{a_c^2} = \alpha^2 + 2\sigma^2 \ . \tag{2.25}$$

Note that when there is no LOS ($\alpha^2 \to 0$), the Ricean probability density function reduces to the Rayleigh probability density function since $I_0(0) = 1$, and the average received signal power reduces to $2\sigma^2$. When the ratio $\alpha^2/2\sigma^2 \to \infty$, there is no fading.

Besides Rayleigh and Ricean, another widely used fading model is Nakagami. The Nakagami fading model was initially proposed because it matches empirical results for short wave ionospheric propagation. It became a widely used model for several reasons [31]. First, it is useful to describe the amplitude of the received signal for maximal-ratio combining with L-fold diversity. For L-branch maximal-ratio combining with Rayleigh-fading signals, the resulting signal is Nakagami with $m = L$. It can be shown that when diversity L is used and the channel is modeled as a Nakagami-m fading channel, the performance is identical to that obtained for a Rayleigh fading channel with diversity mL. Second, the Nakagami model is also applicable for a multipath signal with a significant LOS component between transmitter and receiver. Third, the Nakagami model is useful to model interference from multiple sources in a cellular system since the sum of multiple independent and identically distributed Rayleigh-fading signals have a Nakagami distributed signal amplitude. Lastly, the Nakagami distribution matches some

27

empirical data better than other models. For Nakagami fading channels, the received signal amplitude a_c is modeled as a Nakagami-*m* random variable with a pdf

$$f_{A_C}(a_c) = \frac{2}{\Gamma(m)} \left(\frac{m}{\overline{a_c^2}} \right)^m a_c^{2m-1} \exp\left(\frac{-ma_c^2}{\overline{a_c^2}} \right), \quad a_c \geq 0 \qquad (2.26)$$

where $\Gamma(\Box)$ is the Gamma function, and the parameter *m* is the fading figure, defined as

$$m = \frac{\overline{a_c^2}^2}{E\left[\left(a_c^2 - \overline{a_c^2} \right)^2 \right]}, \quad \text{where } m \geq \frac{1}{2}. \qquad (2.27)$$

It can be shown that when $m = 1$ the Nakagami-*m* pdf corresponds to the Rayleigh pdf since $\Gamma(n+1) = n!$. Generally speaking, for $m < 1$, the fading is more severe than Rayleigh fading; $m = 1$ is Rayleigh fading; when $m > 1$, there is a LOS component to the received signal, and when $m \to \infty$, there is no fading. In Figure 9 the Nakagami-*m* pdf is illustrated as a function of a_c for various values of *m* and with $\overline{a_c^2} = 1$.
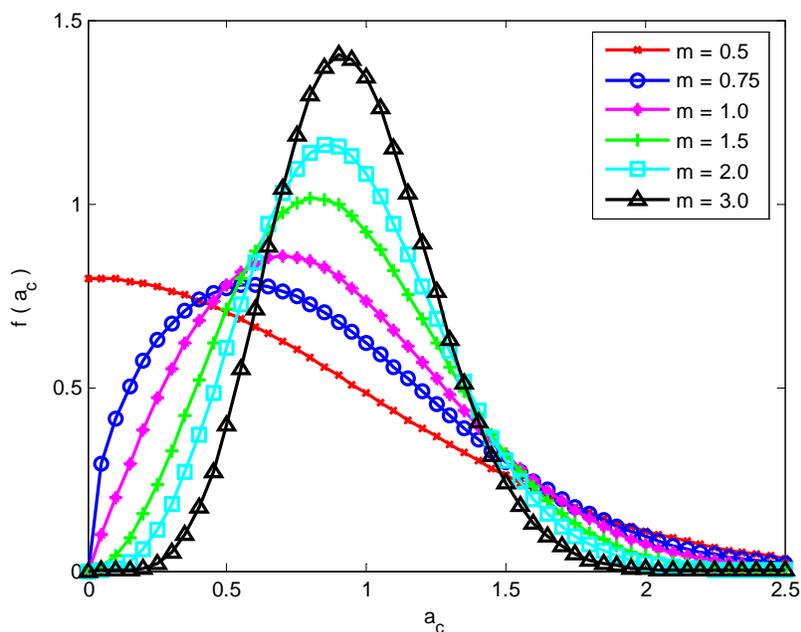
Figure 9.   Nakagami-*m* pdf for various values of *m* and with $\overline{a_c^2} = 1$.

3. Performance over Nakagami Fading Channels

Since for fading channels the received signal amplitude a_c is modeled as a random variable, $E_s = a_c^2 T_s$ is also a random variable. The probability of symbol error is now a conditional probability, denoted $P_s(a_c)$. Since $P_s(a_c)$ is a function of random variable a_c, the average probability of symbol error is the expected value of $P_s(a_c)$; that is [32],

$$P_s = \int_0^\infty P_s(a_c) f_{A_c}(a_c) da_c,$$

(2.28)

where $f_{A_c}(a_c)$ is the pdf for a_c. If we define a new random variable as

$$\gamma_s = \frac{E_s}{N_0} = \frac{a_c^2 T_s}{N_0},$$

(2.29)

then the average probability of symbol error becomes

$$P_s = \int_0^\infty P_s(\gamma_s) f_{\Gamma_s}(\gamma_s) d\gamma_s,$$

(2.30)

and the pdf in terms of γ_s is obtained from [33]

$$f_{\Gamma_s}(\gamma_s) = \left| \frac{da_c}{d\gamma_s} \right| f_{A_c}\left(a_c = \sqrt{N_0 \gamma_s / T_s} \right).$$

(2.31)

Using Equation (2.26) in (2.31), we obtain a Nakagami-m pdf in terms of γ_s as

$$f_{\Gamma_s}(\gamma_s) = \frac{m^m}{\Gamma(m)\overline{\gamma}_s^m} \gamma_s^{m-1} \exp\left(\frac{-m\gamma_s}{\overline{\gamma}_s} \right),$$

(2.32)

where $\gamma_s \geq 0$ and $\overline{\gamma}_s = \overline{a_c^2} T_s / N_0$. Substituting Equation (2.32) into (2.30), we obtain a generic expression for the average probability of symbol error over Nakagami fading channels as

$$P_s = \int_0^\infty P_s(\gamma_s) \frac{m^m}{\Gamma(m)\overline{\gamma}_s^m} \gamma_s^{m-1} \exp\left(\frac{-m\gamma_s}{\overline{\gamma}_s} \right) d\gamma_s.$$

(2.33)

29

C.   SUMMARY OF CHAPTER II

In this chapter, we began with the discussion of four types of narrowband interference, such as BNI, PNI, PBNI, and combined PNI and PBNI. We showed that the performance in PNI is the same as that in PBNI and that in combined PNI and PBNI if $\rho_1 = \rho_2 = \rho_1 \rho_2$. Next, we introduced multipath fading channels, especially small-scale fadings. Four types of small-scale fading, such as flat fading, frequency-selective fading, fast fading, and slow fading, are addressed. Either frequency-selective fading or fast fading can cause severe performance degradation. To combat severe small-scale fadings, several mitigation techniques are addressed in [26].

In this dissertation we assume that the chip duration is less than the channel coherence time and that at a particular hop the signal bandwidth is less than the channel coherence bandwidth, and thus both frequency-selective fading and fast fading are avoided. Followed by small-scale fadings, three widely used models for fading channels, such as Rayleigh, Ricean, and Nakagami, are introduced. In this dissertation, Nakagami fading model is chosen since it is a better model for maximum ratio combining with L diversity, which is the receiver assumed to recover chips when the double-pulse structure is operated in JTIDS. Finally, a generic expression for analyzing the average probability of symbol error over Nakagami fading channels is presented to facilitate the performance analysis in the later chapters. With the above assumptions, the fading channel is therefore modeled as a slow, flat Nakagami fading channel in this dissertation.

In the next chapter, the physical layer of a JTIDS/Link-16-type system is introduced followed by two proposed JTIDS/Link-16-comptible systems, including a system with errors-and-erasures decoding (EED) instead of errors-only RS decoding and a system with an improved 32-chip CCSK sequence in place of the 32-chip CCSK sequence chosen for JTIDS. These two proposed JTIDS/Link-16-comptible systems are interesting since they could improve JTIDS performance without a large-scale modification of the original system design.

III. PHYSICAL LAYER OVERVIEW AND MODIFIED JTIDS/LINK-16-TYPE SYSTEMS

Before analyzing the probability of symbol error for a JTIDS/Link-16-type waveform, the physical layer (or transceiver) of a JTIDS-type system is required. In this chapter, a JTIDS/Link-16-type system is first constructed based on some published literatures, and then each functional block of the constructed physical layer is introduced. Next, two modified JTIDS/Link-16-compatible systems are proposed to improve the performance. The first modified system uses errors-and-erasures decoding (EED) in place of errors-only RS decoding, whereas the second modified system employs a new 32-chip CCSK sequence instead of the 32-chip CCSK sequence chosen for JTIDS.

A. JTIDS/LINK-16-TYPE SYSTEM

JTIDS features RS coding, symbol interleaving, CCSK for M-ary baseband symbol modulation, MSK chip modulation for transmission, double-pulse diversity, and combined FH/DS spread spectrum for transmission security. Based on [2], [6], and [11], the physical layer (or transceiver) of a JTIDS-type system is illustrated in Figure 10.
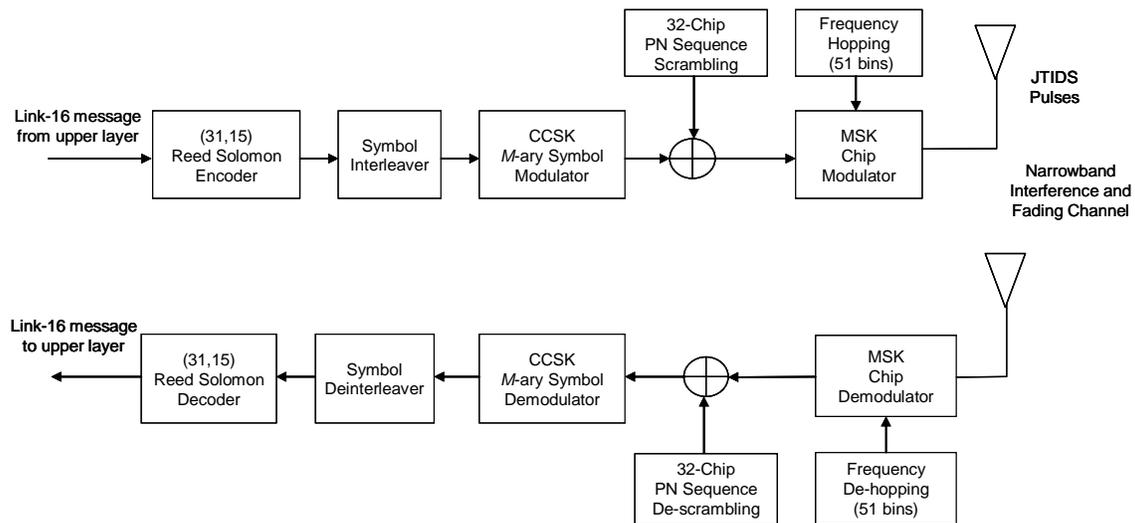
Figure 10.   A JTIDS/Link-16-type system model.

As is seen in Figure 10, the top branch is the model of a JTIDS-type transmitter, while the bottom branch is the model of the JTIDS-type receiver. In addition to AWGN, various types of narrowband interference, such as BNI, PNI, PBNI, and combined PNI and PBNI, and a slow, flat Nakagami fading channel are considered in the channel. Each functional block of Figure 10 is introduced block-by-block in this section followed by a overall model description.

1.   Reed-Solomon Codes

RS codes are nonbinary Bose-Chaudhuri-Hocquenghem (BCH) codes, the most commonly used block codes for random error correction. For nonbinary codes, m bits at a time are combined to form a symbol, and $M = 2^m$ symbols are required to represent all possible combinations of m bits. An (n, k) RS encoder takes k information symbols and generates n coded symbols. RS codes have the largest possible minimum distance for each combination of n and k. A t-error correcting RS code with symbols from the Galois field of 2^m ($GF(2^m)$) is characterized by [34]

$$
\begin{aligned}
n &= 2^m - 1 \\
n - k &= 2t \\
d_{\min} &= 2t + 1,
\end{aligned}
\tag{3.1}
$$

where t is the number of symbol errors that can be corrected and $d_{\min}$ is the minimum Hamming distance between any two code words. If $m = 5$ ($n = 31$) and $k = 15$, then $t = 8$ and $d_{\min} = 17$. In other words, an (31,15) RS code can correct up to eight symbol errors in a codeword containing 31 symbols. Since each symbol represents five bits, an (31,15) RS code can correct error bursts up to length $m \times t = 40$ bits when all errors in the error burst are confined to $t = 8$ symbols.

When Link-16 messages (bit streams) arrive at the physical layer, they are first mapped into 5-bit symbols. Thus, the 35-bit message header becomes seven symbols, and each 75-bit J-Series word (message data) becomes 15 symbols. The seven symbols of the message header are then encoded with a (16,7) block code that is related to a RS code by shortening and/or puncturing. The 15 symbols of message data are encoded with a

(31,15) RS code. After encoding, the Link-16 message header consists of 16 coded symbols, while each J-Series word consists of 31 coded symbols.

Note that there is no such thing as a (16,7) RS code since the number of RS coded symbols n must be of length $n = 2^m - 1$. A (16,7) code could possibly be obtained from puncturing a (31,7) RS code. Punctured RS codes are maximum distance separable (MDS) codes. If the code is MDS, then the minimum Hamming distance becomes [35]

$$d'_{min} = d_{min} - j,$$ (3.2)

where d_{min} is the minimum Hamming distance before puncturing and j represents the number of parity symbols that are punctured from n coded symbols of a RS code. From Equation (3.2), we see that the error correction capability of a RS code reduces as j increases. When $j = 15$, a (31,7) RS code with $d_{min} = 25$ reduces to a (16,7) code with $d'_{min} = 10$. In this case, a (16,7) code can only correct

$$t = \left\lfloor \frac{d'_{min} - 1}{2} \right\rfloor = 4$$ (3.3)

symbol errors. In other words, the message header will be less robust than the message data since a (31, 15) RS code can correct up to $t = 8$ symbol errors.

Another possibility to obtain a (16,7) code is by shortening and puncturing a RS code. Shortened RS codes are also MDS codes [36]. A (n,k) RS code is shortened by setting i information symbols equal to zero at both the encoder and the decoder to give a $(n-i, k-i)$ codeword. The shortened code corrects at least as many errors as the original, but the codewords are shorter. If a (31,15) RS code is first shortened by eight information symbols, we get a (23,7) shortened RS code. If the shortened code is then punctured by seven parity symbols, the result is a (16,7) shortened, punctured RS code. Note that whether the first or the second method is used to obtain a (16,7) code, the header is always less robust than the message data; therefore, the message header is always transmitted in double-pulse format to combat fading channels and/or narrowband interference.

2. Symbol Interleaver

A symbol interleaver is a device that mixes up the symbols from several different codewords so that the symbols from a specific codeword are not transmitted sequentially. A symbol de-interleaver in the receiver reverses the process, putting the received symbols back into the proper order before passing them on to the decoder. For JTIDS, the symbol interleaver is used to interleave both the header symbols and data symbols. Since the header specifies the type of data and identifies the source track number of the transmitting terminal, the communications link could be significantly degraded if the header symbols are jammed.

For JTIDS, the size of the symbol interleaver depends on the number of codewords in the packing structure. For example, for the STD-DP packing structure, the interleaver contains 109 symbols. The symbol interleaving process is shown in Figure 11. Note that the interleaver read-in sequence is fixed, but the starting point of the read-out is pseudo-random, which provides the first layer of transmission security [6].
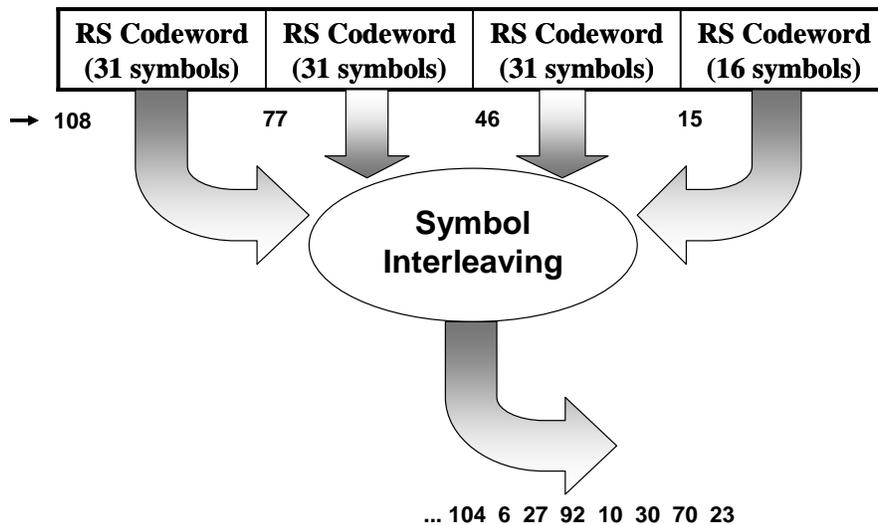
Figure 11.   Symbol interleaving process (after [2]).

3. Cyclic Code Shift Keying Baseband Symbol Modulation

After interleaving, 32 synchronization symbols and eight time refinement symbols are appended to the beginning of the interleaved, coded symbols. In order to transmit the

symbols over a radio channel, the symbols must be modulated with the RF carrier. In JTIDS, this process is done in two parts: CCSK and MSK. CCSK is a baseband symbol modulation scheme, while MSK is a chip modulation scheme. CCSK provides *M*-ary baseband modulation and spreading since each 5-bit symbol is represented by a 32-chip sequence. As shown in Figure 12, the 32-chip CCSK sequences are derived by cyclically shifting a starting sequence S_0 one place to the left between one and 31 times to obtain a unique sequence for all possible combinations of five bits. When despread, the determination of which 5-bit symbol was received is accomplished by computing the cross-correlation between the received 32-chip sequence and all possible 32 sequences. The decision is made by choosing the 5-bit symbol corresponding to the branch with the largest cross-correlation value. It can be shown that, for the 32-chip starting sequence chosen for JTIDS, the original 5-bit symbol can be recovered perfectly even though there are six chip errors occurred in the 32-chip sequence.

← Direction of shifting

5-Bit Symbol	32-Chip Sequences (CCSK Codeword)
00000	S_0 = 01111100111010010000101011101100
00001	S_1 = 11111001110100100001010111011000
00010	S_2 = 11110011101001000010101110110001
00011	S_3 = 11100111010010000101011101100011
00100	S_4 = 11001110100100001010111011000111
⋮	⋮
11111	S_{31} = 00111110011101001000010101110110

Figure 12.   The 32-chip CCSK sequences chosen for JTIDS (after [2]).

After the CCSK symbol-to-chips spreading, each 32-chip CCSK sequence is scrambled with a 32-chip pseudo-noise (PN) sequence. This process not only provides a uniform spreading of the baseband waveform but also acquires the second layer transmission security. The resulting 32-chip sequence is called a 32-chip transmission symbol. The process of converting a 5-bit symbol to a 32-chip transmission symbol is shown in Figure 13.
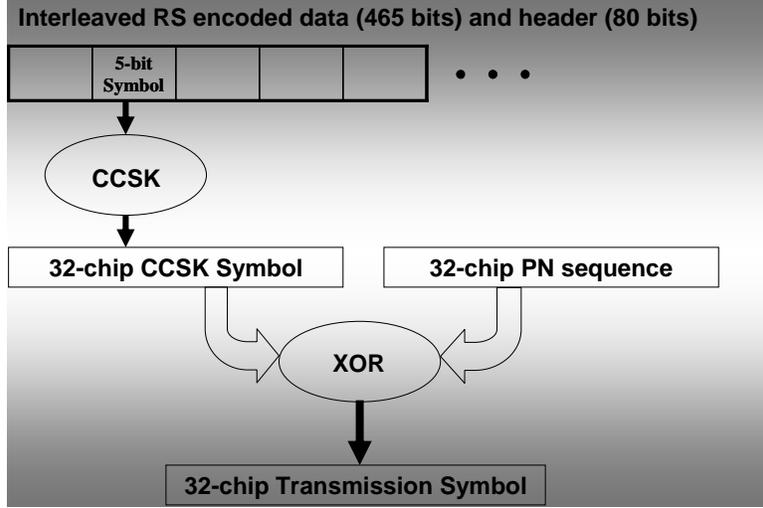
Figure 13.   From a 5-bit symbol to a 32-chip transmission symbol (after [2]).

4.   Minimum-Shift Keying Chip Modulation

After scrambling, each chip is modulated for transmission with a special case of continuous phase frequency-shift keying (CPFSK), also known as minimum-shift keying (MSK) [37]. MSK has many attractive attributes such as constant envelope, compact spectrum, the error rate performance of BPSK, and simple synchronization circuits. MSK can also be viewed as a form of OQPSK with sinusoidal pulse weighting. When viewed as an OQPSK signal with sinusoidal pulse weighting, the MSK waveform is [38]

$$s(t) = a_I(t)\cos\left(\frac{\pi t}{2T}\right)\cos(2\pi f_c t) + a_Q(t)\sin\left(\frac{\pi t}{2T}\right)\sin(2\pi f_c t), \qquad (3.4)$$

where $a_I(t)\cos(\pi t/2T)$ is the in-phase chip stream waveform with sinusoidal pulse weighting, $a_Q(t)\sin(\pi t/2T)$ is the quadrature chip stream waveform with sinusoidal pulse weighting, and f_c is the carrier frequency. Since a_I (even chips of the chip stream) and a_Q (odd chips of the chip stream) can be either $+1$ or -1, Equation (3.4) can be rewritten as

$$s(t) = \cos\left[2\pi\left(f_c + \frac{b_k}{4T}\right)t + \phi_k\right], \qquad (3.5)$$

36

where $b_k = -a_I \times a_Q = \pm 1$ and the phase ϕ_k is 0 or π corresponding to $a_I = 1$ or $a_I = -1$. From Equation (3.5), we see that the MSK waveform has a constant envelope with two signaling frequencies. The higher signaling frequency is $f_+ = f_c + 1/4T$, while the lower signaling frequency is $f_- = f_c - 1/4T$; that is, the frequency deviation is $\Delta f = 1/2T$, which is the same as that of coherent BFSK; hence, this signaling technique is named "minimum shift" keying. Based on Equation (3.4), a MSK transmission waveform is generated for a chip stream [1 0 0 0 1 1 1] with $T = 1$ sec and $f_c = 2$ Hz. Note that for JTIDS, $T = T_c = 200$ nsec. The MSK waveform corresponding to the chip stream is shown at the bottom of Figure 14, while the modulated in-phase and quadrature chip stream waveforms are shown at the top and the middle of Figure 14, respectively.
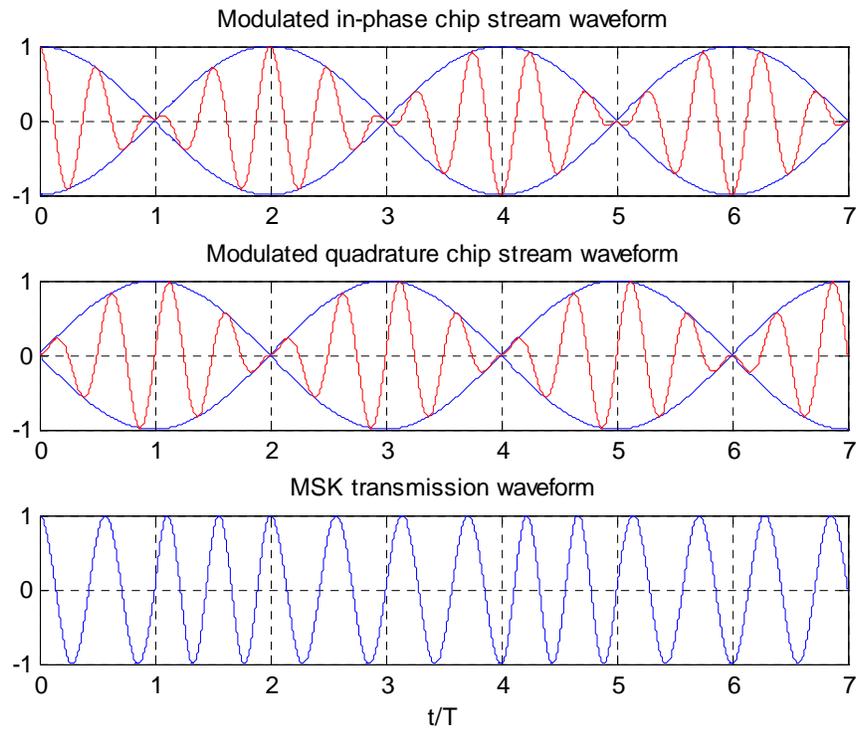
Figure 14.   The MSK waveform for the chip stream [1 0 0 0 1 1 1].

From the MSK waveform, we see that the two signaling frequencies are used to represent a change in chip value between successive chips rather than an absolute chip value. For example, from the first to the second chip, the higher signaling frequency is used since the chip value is changed, whereas from the second to the third chip, the lower

signaling frequency is used since the chip value stays the same. From the MSK waveform we also see that there is phase continuity in the RF carrier at the chip transition instants. This phase continuity can mitigate out-of-band interference arising from hardlimiting process in a satellite repeater; therefore, MSK is an excellent modulation scheme when the use of efficient amplitude-saturating transmitters is required.

5.   JTIDS Pulse Structures

As mentioned earlier, the Link-16 message data can be sent as either a single- or a double-pulse, depending on the packing structure. The single-pulse structure consists of a 6.4 μs on-time and a 6.6 μs off-time, so the total duration for a single-pulse is 13 μs. The double-pulse structure consists of two single pulses which carry the same data but use different carrier frequencies. This repetition provides robustness against fading and/or narrowband interference. The double-pulse structure is illustrated in Figure 15. From Figure 10, a MSK chip demodulator is used to recover chips for both the single- and the double-pulse structure. The process of recovering chips for both structures is addressed separately in Chapter V since different MSK chip demodulators are required to obtain the optimal performance.
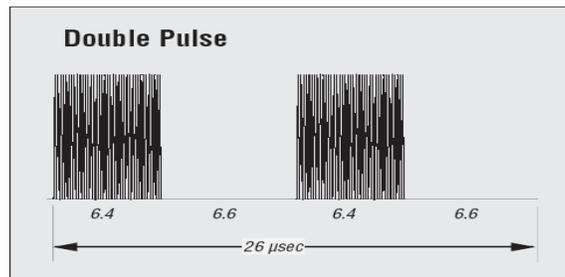
Figure 15.   The standard double-pulse structure (from [2]).

The implication of the foregoing is that the data rate for the double-pulse structure is half that of the single-pulse structure. Furthermore, the average energy per bit, both channel and data, is doubled when the double-pulse structure is used. That is, JTIDS is not a constant average energy per bit system when it changes between the single- and the double-pulse structure. In this dissertation, comparisons are made based on the average energy per bit per pulse, not the total average energy per bit.

6. Frequency Hopping

In a frequency-hopping spread spectrum system, rather than transmit all symbols with the same carrier, the carrier is changed pseudorandomly according to some predesignated PN sequence. FHSS is not immune to jamming but can reduce jammer effectiveness considerably since the jammer has to emit a jamming signal in most of the frequency-hop bins. Generally, data throughput decreases because FHSS only uses a small fraction of the available radio bandwidth at any one time.

A FHSS system can be either fast frequency-hopped (FFH) or slow frequency-hopped (SFH). If more than one symbol is transmitted prior to each frequency-hop, the system is described as SFH. If one symbol per hop is transmitted or if the same symbol is transmitted for several consecutive hops, the system is described as FFH. For JTIDS with STD-DP packing, the same symbol is transmitted for two consecutive hops. Therefore, JTIDS is considered as a hybrid DS/FFH spread spectrum system with sequential diversity $L = 2$. The JTIDS waveform hops pseudorandomly over 51 frequency bins at a rate of around 77,000 hops per second. The 51 carrier frequencies are shown in Table 3. Note that the portion of the spectrum used for JTIDS communications is in the UHF band. UHF communications are line-of-sight (LOS) [2].

Table 3.   The 51 JTIDS hopping frequencies (after [2]).

Frequency Number	Frequency (MHz)	Frequency Number	Frequency (MHz)	Frequency Number	Frequency (MHz)
0	969	17	1062	34	1158
1	972	18	1065	35	1161
2	975	19	1113	36	1164
3	978	20	1116	37	1167
4	981	21	1119	38	1170
5	984	22	1122	39	1173
6	987	23	1125	40	1176
7	990	24	1128	41	1179
8	993	25	1131	42	1182
9	996	26	1134	43	1185
10	999	27	1137	44	1188
11	1002	28	1140	45	1191
12	1005	29	1143	46	1194
13	1008	30	1146	47	1197
14	1053	31	1149	48	1200
15	1056	32	1152	49	1203
16	1059	33	1155	50	1206

7. Overall Model Description for a JTIDS-type System

When the Link-16 message bit streams arrive at the JTIDS-type transmitter (top branch of Figure 10), they are first mapped into 5-bit symbols. The seven symbols of the message header are encoded with a (16,7) block code that is related to a RS code by shortening and/or puncturing, while the 15 message data symbols are encoded with a (31,15) RS code. After encoding, the data and header symbols are interleaved for the first layer of transmission security. Next, these 5-bit interleaved symbols are modulated with a 32-ary CCSK, where each 5-bit symbol is represented by one of the cyclic-shifts of the 32-chip CCSK starting sequence. To obtain the second layer of transmission security, each 32-chip CCSK sequence is scrambled with a 32-chip pseudo-noise (PN) sequence. The resulting 32-chip sequence is modulated for transmission with MSK to generate analog pulses. Each pulse is then up-converted to one of the 51 possible carrier frequencies, which contributes a third layer of transmission security. Normally, the starting point of the pulse train is pseudo-randomly jittered, which provides a forth layer of transmission security since it can make it difficult for a jammer to decide when to turn on the jamming signal. After up-conversion, the signal is amplified, filtered, and transmitted over the channel.

At the receiver (bottom branch of Figure 10), the receiving process is the reverse of the transmission process. After frequency dehopping, MSK chip demodulation, and de-scrambling by a 32-chip PN sequence, each 5-bit symbol is recovered by a CCSK symbol demodulator. The determination of which 5-bit channel symbol was received is accomplished by computing the cross-correlation between de-scrambled 32-chip sequence and all possible 32 local sequences, and the decision is made by choosing the 5-bit channel symbol corresponding to the branch with the largest cross-correlation value. It can be shown that the original 5-bit symbol can be retrieved perfectly with as many as six chip errors in each 32-chip sequence. After symbol de-interleaving, the header symbols are first decoded by a (16,7) decoder to determine the data packing structure. Once the packing structure is read, the data symbols are decoded by a (31,15) RS decoder. If the decoding is successful, the data symbols are converted into bit streams which are sent to the link layer.

B. MODIFIED JTIDS/LINK-16-TYPE SYSTEMS

In the previous section, the physical layer of a JTIDS-type system was introduced. In this section, two JTIDS/Link-16-compatible systems are proposed in order to improve system performance. The first system uses errors-and-erasures decoding (EED) in place of errors-only RS decoding, whereas the second system employs a new 32-chip CCSK sequence instead of the 32-chip CCSK sequence chosen for JTIDS.

1. System with Errors-and-Erasures Decoding

In the previous section, we have assumed that the output of the CCSK symbol demodulator is the estimate of the received coded symbols which then must be decoded. Hence, the digital output of the CCSK symbol demodulator is the input to the decoder. This is referred to as hard decision decoding. An alternative to hard decision decoding is erasure decoding, which is the simplest form of soft decision decoding. In this case, the CCSK symbol demodulator either decides which coded symbol was received or is unable to make a decision, in which case the symbol is erased. Since a RS code can be used to correct errors and erasures simultaneously and EED can result in more coding gain for some types of fading channels [39], a JTIDS/Link-16-compatible system with EED is proposed in Figure 16.
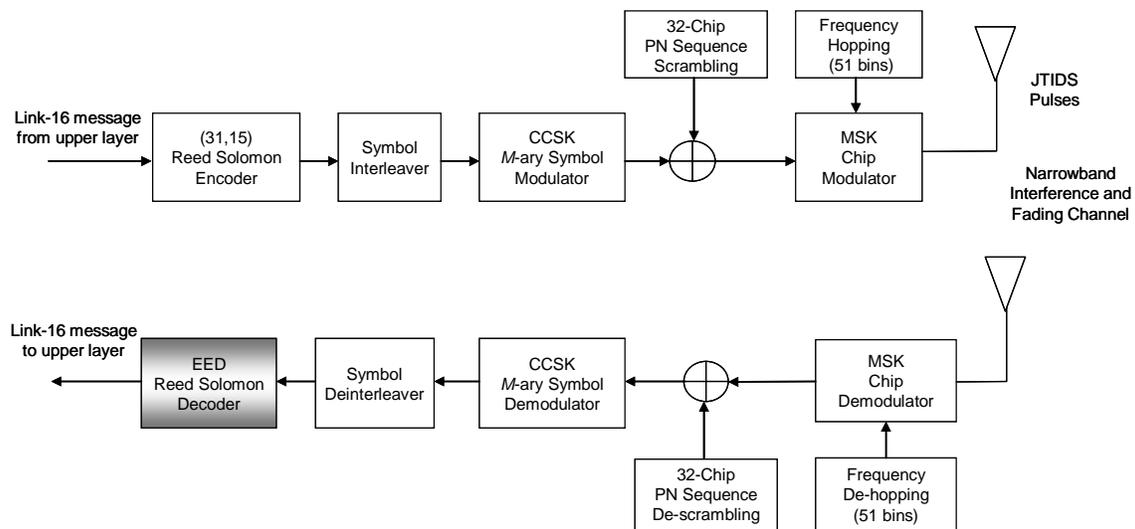
Figure 16.   A JTIDS-compatible system with errors-and-erasures decoding.

In general, when EED is implemented, the receiver replaces the symbols that are received ambiguously, or unreliably, with an erasure e. For example, in binary erasure decoding, the output of the demodulator is not binary but ternary; that is, 1, 0, and e. Recall that the error correction capability of block codes is characterized by the minimum Hamming distance $d_{\min}$. Suppose that a codeword is received with a single erased bit. Now all valid codewords are separated by a Hamming distance of at least $d_{\min} - 1$. If there are e erasures in a received codeword, all valid codewords are then separated by a Hamming distance of at least $d_{\min} - e$. Hence, the effective minimum Hamming distance between valid codewords when there are e erasures in the received codeword is $d_{\min_e} = d_{\min} - e$, and the number of errors in the non-erasured bits of the codeword that can be corrected is [40]

$$t_e = \left\lfloor \frac{d_{\min} - e - 1}{2} \right\rfloor. \tag{3.6}$$

In other words, a linear block code can correct t_e errors and e erasures as long as $2t_e + e < d_{\min}$. Hence, for a given value of $d_{\min}$, twice as many erasures as errors can be corrected. Therefore, EED can result in more coding gain for fading channels.

For JTIDS, as mentioned earlier, the decision of which 5-bit symbol was sent is based on the cross-correlation values obtained when the de-scrambled sequence is cross-correlated with the 32 valid CCSK sequences. Suppose symbol S_0 was sent and there is no chip error in the de-scrambled sequence, then the cross-correlation is given by

$$\Re_i = \begin{cases} 32 & i = 0 \\ h_i \le H & i = 1, 2, ..., 31 \end{cases}, \tag{3.7}$$

where i is the index of the cross-correlation branch, H is the maximum off-peak cross-correlation values, and the values of h_i and H depend on the 32-chip starting sequence chosen. It can be shown that for the 32-chip starting sequence chosen for JTIDS, h_i has values of -4, 0, and $+4$. In other words, $H = 4$ is the maximum off-peak cross-correlation value. Since $\Re_0 = 32 > \Re_i$ for $i = 1, 2, ..., 31$, the decision made is that S_0 was

received. To apply EED, an erasure threshold is required in the CCSK symbol demodulator. Intuitively, if the erasure threshold T is too small (e.g., $T \leq H = 4$), the result will be similar to that of errors-only RS decoding. If T is too large (e.g., $T \geq 32$), the result will be worse than that of errors-only RS decoding since most of the correct symbols will be erased even though in the absence of noise. Therefore, an optimal erasure threshold T_{opt} is required in order to obtain the best performance. How to find the optimal erasure threshold T_{opt} such that the performance of JTIDS is improved is addressed in Chapter VI.

2. A New 32-Chip CCSK Starting Sequence

From Equation (3.7), the 32-chip CCSK starting sequence chosen for JTIDS and its 31 cyclically shifted versions are not orthogonal since the off-peak cross-correlation values have values other than zero. Intuitively, performance close to that of orthogonal signaling can be expected if the maximum off-peak cross-correlation values are close to or less than zero. To find such a new 32-chip CCSK starting sequence that may improve system performance, a search algorithm is created with MATLAB codes. Fortunately, the search algorithm yields a new 32-chip sequence which has a maximum off-peak cross-correlation value $H = 0$. Furthermore, it can shown that this new sequence allows for seven instead of six chip errors in the received, de-scrambled sequence without making a symbol error. This new 32-chip sequence and its cyclically shifted versions are discussed in Chapter VI.

C. SUMMARY OF CHAPTER III

In this chapter, the physical layer of a JTIDS-type system was introduced and two JTIDS-compatible systems were proposed in order to improve system performance. With a better understanding of the JTIDS-type system, we can investigate the performance of a JTIDS-type waveform after we obtain an analytic expression for the probability of symbol error of CCSK. An analytic expression for the probability of symbol error of CCSK is derived in the next chapter.

THIS PAGE INTENTIONALLY LEFT BLANK

IV. PERFORMANCE ANALYSIS AND SIMULATION OF CCSK

CCSK is the 32-ary baseband symbol modulation scheme used by JTIDS. The system model of a JTIDS-type receiver is shown in the bottom branch of Figure 10 and is reproduced here in Figure 17 for convenience. In order to investigate the probability of symbol error of a JTIDS/Link-16-type waveform, an analytic evaluation of CCSK performance in terms of probability of symbol error is required. Since CCSK is non-orthogonal, it is complicated to evaluate its performance analytically. Previously, the evaluation has been done by simulation [9],[10],[13]. The only exception is [11]; however, the results presented in [11] are based on the overly optimistic assumption that the cross-correlation values of the CCSK symbols are independent. Actually, these cross-correlation values are not independent (see Appendix A). In this chapter, an analytic upper bound on the probability of symbol error of CCSK in AWGN is first derived for the 32-chip CCSK sequence chosen for JTIDS. The probability of symbol error obtained with the analytic upper bound is then compared with that obtained by two different Monte Carlo simulations in AWGN.
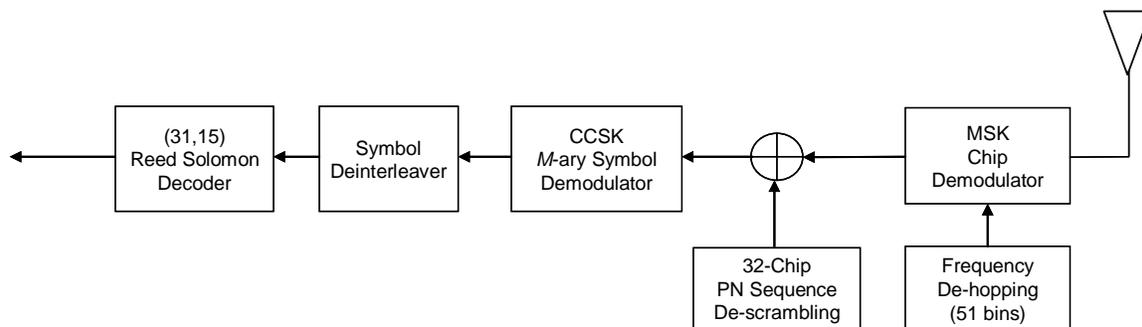
Figure 17.   Model of a JTIDS-type receiver.

A.   PERFORMANCE ANALYSIS OF CCSK

As seen in Figure 17, after de-scrambling, the received 32-chip sequence is sent to CCSK symbol demodulator to recover the original 5-bit symbol. The CCSK symbol demodulator is shown in Figure 18, where the input $\hat{S}$ is the de-scrambled 32-chip sequence, and the output of the CCSK symbol demodulator is a 5-bit symbol. The

notations S_i for $i = 0,1,...,31$ represent the 32 cyclic-shifted CCSK sequences, and $\Re_i$ for $i = 0,1,...,31$ represent the cross-correlation values for the ith branch.
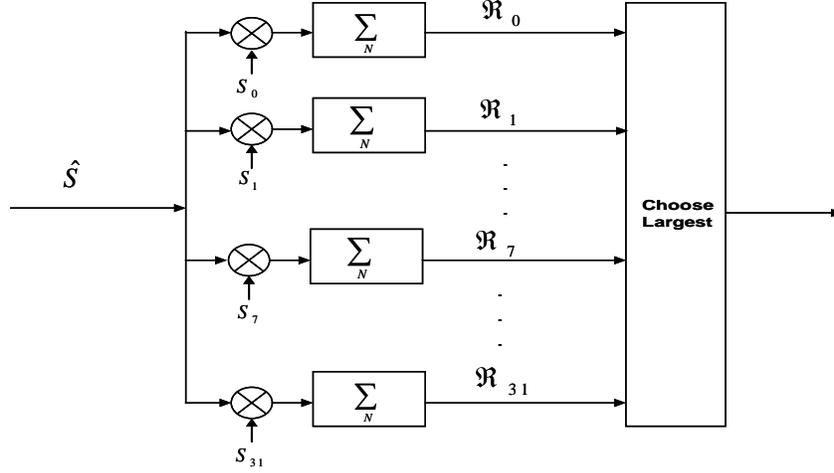
Figure 18.   CCSK symbol demodulator.

1.   CCSK Symbol Demodulation

As is seen in Figure 18, the determination of which 5-bit symbol was received is accomplished by computing the cross-correlation between the de-scrambled 32-chip sequence and all 32 cyclic-shifted CCSK sequences. The decision is made by choosing the 5-bit symbol corresponding to the branch with the largest cross-correlation value. If symbol 0 is sent and if there is no chip error in the received 32-chip sequence, the cross-correlation result is shown in Equation (3.7) and reproduced here for convenience as

$$\Re_i = \begin{cases} 32 & i = 0 \\ h_i & i = 1, 2, ..., 31, \end{cases} \tag{4.1}$$

where h_i is the off-peak cross-correlation value for branches $1 \le i \le 31$. For the 32-chip CCSK sequence chosen for JTIDS, in the absence of noise the off-peak cross-correlation has three discrete values: $h_i = -4, 0,$ or 4 for $i = 1, 2, ..., 31$; hence, the maximum off-peak cross-correlation value $H = 4$. In this case, the decision made at the CCSK symbol demodulator is that symbol 0 was sent since $\Re_0 = 32$ is the largest. Note that Equation (4.1) shows that CCSK is not orthogonal since the $h_i s$ have values other than zero.

46

Due to the nature of CCSK sequences in general, and in particular for the sequence chosen for JTIDS, the preceding off-peak cross-correlation values are the same regardless of which symbol is transmitted, but the locations of the off-peak cross-correlation values will shift according to the symbol being transmitted. For example, in the absence of noise and given that symbol 0 is sent, we get $\Re_0 = 32$, and the maximum off-peak cross-correlation value $H = 4$ occurs at the seventh, sixteenth, and twenty-fifth branches; that is, $\Re_7 = \Re_{16} = \Re_{25} = 4$. If symbol 1 is sent in the absence of noise, we get $\Re_1 = 32$, and the maximum off-peak cross-correlation value occurs at the eighth, seventeenth, and twenty-sixth branches; that is, $\Re_8 = \Re_{17} = \Re_{26} = 4$. Therefore, without loss of generality, we can assume symbol 0 is the transmitted symbol.

2.   Cross-correlation Properties of CCSK

As mentioned earlier, Equation (4.1) shows that CCSK is not orthogonal since the $h_i s$ have values other than zero for $1 \le i \le 31$. To analyze the probability of symbol error for CCSK, a better understanding of the nature of the cross-correlation properties of CCSK sequences is needed. Specifically, we need to investigate the cases where the de-scrambled sequence $\hat{S}$ consists of N chip errors for $0 \le N \le 32$. For $N = 0, N = 1$, and $N = 2$, the cross-correlation results given that symbol 0 is sent are shown in Table 4 for two specific cases each when $N = 1$ and $N = 2$.

From Table 4, several properties are observed. First, when $N = 0$ (column 2), the maximum off-peak cross-correlation value $H = 4$ occurs at $\Re_7$, $\Re_{16}$, and $\Re_{25}$. Second, when $N = 1$ (column 3 and 4), the value of $\Re_0$ decreases by two, whereas $\Re_i$ for $1 \le i \le 31$ can either increase or decrease by two, depending on where the chip error has occurred (for column 3, the first chip is assumed to be in error, whereas for column 4, the fifth chip is erroneous), and, as a result, $H = 6$. Third, when $N = 2$ (column 5 and 6), the value of $\Re_0$ decreases by four, whereas $\Re_i$ for $1 \le i \le 31$ can either increase by four, decrease by four, or stay the same. Last, the location of the maximum off-peak cross-correlation value varies based on the location and the number of chip errors in the received, descrambled 32-chip sequence. For example, when $N = 1$ and the chip error

occurs at the first chip location of the received sequence, $\mathfrak{R}_{25} = 6$ is the maximum; if the chip error occurs at the fifth chip location of the received sequence, $\mathfrak{R}_7 = 6$ is the maximum. When $N = 2$ and the chip errors occur at the fifth and the tenth chip location of the received sequence (column 5), $\mathfrak{R}_7 = 8$ (an increase of four) is the maximum; however, if the chip errors occur at the first and the second chip location of the received sequence (column 6), the maximum off-peak cross-correlation value is not eight but four for branches 5, 12, 16, 20 and 25. Five pairs of the 32-chip CCSK symbols are converted into baseband waveforms and listed in Table 5 to illustrate why this occurs.

Table 4. Partial CCSK cross-correlation results for $N = 0$, $N = 1$, and $N = 2$.

$\mathfrak{R}_i$	$N = 0$	$N = 1_{(1)}$	$N = 1_{(5)}$	$N = 2_{(5,10)}$	$N = 2_{(1,2)}$
$i = 0$	32	30	30	28	28
$i = 1$	0	2	-2	-4	0
$i = 2$	0	2	2	4	0
$i = 3$	-4	-2	-2	-4	-4
$i = 4$	0	2	-2	0	0
$i = 5$	0	2	-2	0	4
$i = 6$	-4	-6	-6	-8	-4
$i = 7$	4	2	6	8	0
$i = 8$	0	2	-2	0	0
$i = 9$	-4	-2	-2	0	-4
$i = 10$	-4	-2	-2	0	0
$i = 11$	0	-2	-2	-4	-4
$i = 12$	0	2	2	4	4
$i = 13$	0	-2	2	0	0
$i = 14$	0	-2	2	4	-4
$i = 15$	-4	-2	-2	-4	0
$i = 16$	4	2	2	0	4
$i = 17$	-4	-6	-2	-4	-4
$i = 18$	0	-2	-2	0	0
$i = 19$	0	-2	2	0	-4
$i = 20$	0	2	-2	-4	4
$i = 21$	0	-2	-2	0	-4
$i = 22$	-4	-2	-6	-4	0
$i = 23$	-4	-6	-2	0	-8
$i = 24$	0	2	-2	-4	0
$i = 25$	4	6	2	0	4
$i = 26$	-4	-2	-2	-4	0
$i = 27$	0	-2	2	0	-4
$i = 28$	0	2	2	0	0
$i = 29$	-4	-2	-6	-4	0
$i = 30$	0	-2	-2	0	0
$i = 31$	0	-2	-2	-4	0

As is seen in Table 5, the first pair consists of symbol 0 and symbol 7. When these two waveforms are cross-correlated in the absence of noise, we obtain $\Re_7 = 4$. The second pair consists of symbol 0 and symbol 16. When these two waveforms are cross-correlated in the absence of noise, we obtain $\Re_{16} = 4$. The third pair consists of symbol 0 and symbol 25. When these two waveforms are cross-correlated in the absence of noise, we again obtain $\Re_{25} = 4$. The fourth pair consists of symbol 0 and symbol 1. When these two waveforms are cross-correlated in the absence of noise, we obtain $\Re_1 = 0$. The fifth pair consists of symbol 0 and symbol 3. When these two waveforms are cross-correlated in the absence of noise, we obtain $\Re_3 = -4$. In other words, in the absence of noise, the first three symbol-pairs have the maximum off-peak cross-correlation values $h_i = H = 4$, the fourth symbol-pair (symbol 0 and symbol 1) has an off-peak cross-correlation value $h_i = 0$, and the fifth symbol-pair (symbol 0 and symbol 3) has the smallest off-peak cross-correlation value $h_i = -4$.

Table 5.　　Five pairs of the 32-chip CCSK baseband waveform.

Symbol 0	-1 1 1 1 1 1 -1 -1 1 1 1 -1 1 -1 -1 1 -1 -1 -1 -1 1 -1 1 -1 1 1 1 -1 1 1 -1 -1
Symbol 7	-1 1 1 1 -1 1 -1 -1 1 -1 -1 -1 -1 1 -1 1 -1 1 1 1 -1 1 1 -1 -1 -1 1 1 1 1 1 -1
Symbol 0	-1 1 1 1 1 1 -1 -1 1 1 1 -1 1 -1 -1 1 -1 -1 -1 -1 1 -1 1 -1 1 1 1 -1 1 1 -1 -1
Symbol 16	-1 -1 -1 -1 1 -1 1 -1 1 1 1 -1 1 1 -1 -1 -1 1 1 1 1 1 -1 -1 1 1 1 -1 1 -1 -1 1
Symbol 0	-1 1 1 1 1 1 -1 -1 1 1 1 -1 1 -1 -1 1 -1 -1 -1 -1 1 -1 1 -1 1 1 1 -1 1 1 -1 -1
Symbol 25	1 1 -1 1 1 -1 -1 -1 1 1 1 1 1 -1 -1 1 1 1 -1 1 -1 -1 1 -1 -1 -1 -1 1 -1 1 -1 1
Symbol 0	-1 1 1 1 1 1 -1 -1 1 1 1 -1 1 -1 -1 1 -1 -1 -1 -1 1 -1 1 -1 1 1 1 -1 1 1 -1 -1
Symbol 1	1 1 1 1 1 -1 -1 1 1 1 -1 1 -1 -1 1 -1 -1 -1 -1 1 -1 1 -1 1 1 1 -1 1 1 -1 -1 -1
Symbol 0	-1 1 1 1 1 1 -1 -1 1 1 1 -1 1 -1 -1 1 -1 -1 -1 -1 1 -1 1 -1 1 1 1 -1 1 1 -1 -1
Symbol 3	1 1 1 -1 -1 1 1 1 -1 1 -1 -1 1 -1 -1 -1 -1 1 -1 1 -1 1 1 1 -1 1 1 -1 -1 -1 1 1

Comparing two waveforms chip-by-chip for each symbol pair in Table 5, we see that for the first three symbol pairs, there are 18 same-sign chip pairs and 14 different-sign chip-pairs. For the fourth symbol pair, there are 16 same-sign chip pairs and 16 different-sign chip-pairs. For the fifth symbol-pair, there are 14 same-sign chip pairs and 18 different-sign chip-pairs. In general, we can divide the 32-chip waveform of each symbol pair into two groups. The first group consists of $n_1 = (32 + h_i)/2$ same-sign chip pairs, while the second group has $n_2 = (32 - h_i)/2$ different-sign chip-pairs. For example,

in Table 5, for the first three symbol pairs, $n_1 = 18$ and $n_2 = 14$; for the fourth symbol pair, $n_1 = 16$ and $n_2 = 16$; for the fifth symbol pair, $n_1 = 14$ and $n_2 = 18$.

Given these observations, we conclude the following. First, when $N = 1$, $\mathfrak{R}_i$ for $1 \leq i \leq 31$ decrease by two when the chip error occurs in the first group and increase by two when the chip error occurs in the second group. For example, when $N = 1$ and the chip error occurs at the first chip location of the received sequence (see column 3 of Table 4), $\mathfrak{R}_7 = \mathfrak{R}_{16} = 4 - 2 = 2$ (decreases by two) since the chip error occurs in the first group, while $\mathfrak{R}_{25} = 4 + 2 = 6$ (increases by two) since the chip error occurs in the second group. Similarly, $\mathfrak{R}_1 = 0 + 2 = 2$ and $\mathfrak{R}_3 = -4 + 2 = -2$ both increase by two since the chip error occurs in the second group. Second, when $N = 2$, $\mathfrak{R}_i$ for $1 \leq i \leq 31$ decrease by four when the chip errors occur in the first group, increase by four when the chip errors occur in the second group, and stay the same if one chip error occurs in the first group while the other occurs in the second group. For example, when $N = 2$ and the chip errors occur at the fifth and the tenth chip location of the received sequence (see column 5 of Table 4), $\mathfrak{R}_7 = 4 + 4 = 8$ (increases by four) since both chip errors occur in the second group, $\mathfrak{R}_{16} = \mathfrak{R}_{25} = 4 - 4 = 0$ and $\mathfrak{R}_1 = 0 - 4 = -4$ (decrease by four) since both chip errors occur in the first group, and $\mathfrak{R}_3 = -4$ stays the same since one chip error occurs in the first group and the other occurs in the second group. Furthermore, when $N = 2$ and the chip errors occur at the first and the second chip location of the received sequence (see column 6 of Table 4), $\mathfrak{R}_7 = 4 - 4 = 0$ (decreases by four) since the chip errors occur in the first group, but $\mathfrak{R}_{16} = \mathfrak{R}_{25} = 4$, $\mathfrak{R}_1 = 0$, and $\mathfrak{R}_3 = -4$ (stay the same) since one chip error occurs in the first group and the other occurs in the second group. This explains why in some cases $H = 4$ instead of eight when $N = 2$.

Observing the first three symbol pairs in Table 5, we see that the probability that one chip error occurs in the first group given that $N = 1$ is $18/32$, while the probability that one chip error occurs in the second group given that $N = 1$ is $14/32$. Let X_1 and X_2 represent the number of chip errors in the first and second group, respectively. The preceding conditional probabilities for a single chip error can also be obtained from

50

$$P\{X_1 = 1 | X_1 + X_2 = 1\} = \frac{\binom{18}{1}\binom{14}{0}}{\binom{32}{1}} = \frac{18}{32} \qquad (4.2)$$

and from

$$P\{X_1 = 0 | X_1 + X_2 = 1\} = \frac{\binom{18}{0}\binom{14}{1}}{\binom{32}{1}} = \frac{14}{32}. \qquad (4.3)$$

Note that the distributions in Equations (4.2) and (4.3) are known as the hyper-geometric distribution. The general expression for the hyper-geometric distribution is [41]

$$P\{X_1 = q | X_1 + X_2 = j\} = \frac{\binom{n_1}{q}\binom{n_2}{j-q}}{\binom{n_1+n_2}{j}}, \qquad (4.4)$$

where X_1 and X_2 are independent binomial random variables, n_1 is the number of independent trials for X_1, and n_2 is the number of independent trials for X_2. Note that $N = X_1 + X_2$. In our case, $n_1 = (32 + h_i)/2$ and $n_2 = (32 - h_i)/2$ represent the number of same-sign and different-sign chip pairs of two cross-correlated sequences, respectively.

In addition to the cases of $N = 0$, 1, and 2, the cross-correlation results for $\Re_0$ and $\Re_7$ from $N = 5$ to $N = 8$ given that symbol 0 is sent are shown in Table 6, where q is denoted as the number of chip errors in the first group (same-sign), and $N - q$ is denoted as the number of chip errors in the second group (different-sign). When $N = 5$, $\Re_0 = 22$ is independent of the locations of the chip errors, and the possible values of $\Re_7$ ranges from -6 to 14. The same results are obtained for $\Re_{16}$ and $\Re_{25}$. Since $\Re_7$, $\Re_{16}$, and $\Re_{25}$ correspond to the maximum off-peak cross-correlation values, all other $\Re_i s$ have an off-peak cross-correlation value that is less than fourteen. Since $\Re_0 > \Re_i$ for

$i = 7, 16,$ and 25, the decision is that symbol 0 was received; therefore, the CCSK symbol demodulator does not make an error in this case.

Table 6.   Cross-correlation results for $\mathfrak{R}_0$ and $\mathfrak{R}_7$ for $N = 5$ through $N = 8$.

$N = j$	q	$j - q$	$\mathfrak{R}_0$	$\mathfrak{R}_7$	Remark
5	5	0	22	-6	No error
	4	1	22	-2	No error
	3	2	22	2	No error
	2	3	22	6	No error
	1	4	22	10	No error
	0	5	22	14	No error
6	6	0	20	-8	No error
	5	1	20	-4	No error
	1	5	20	12	No error
	0	6	20	16	No error
7	7	0	18	-10	No error
	6	1	18	-6	No error
	1	6	18	14	No error
	0	7	18	18	Tie
8	8	0	16	-12	No error
	7	1	16	-8	No error
	1	7	16	16	Tie
	0	8	16	20	Error

When $N = 6$, there are seven possibilities based on the value of q, but only four possibilities are shown in Table 6. Now, $\mathfrak{R}_0 = 20$, which remains independent of the locations of chip errors, and the possible value of $\mathfrak{R}_7$ ranges from -8 to 16. The same results are obtained for $\mathfrak{R}_{16}$ and $\mathfrak{R}_{25}$. Since $\mathfrak{R}_7$, $\mathfrak{R}_{16}$, and $\mathfrak{R}_{25}$ correspond to the maximum off-peak cross-correlation values, all other $\mathfrak{R}_i s$ have an off-peak cross-correlation value that is less than sixteen. Again, since $\mathfrak{R}_0 > \mathfrak{R}_i$ for $i = 7, 16,$ and 25, the decision is that symbol 0 was received; therefore, the CCSK symbol demodulator does not make an error given that $N = 6$.

When $N = 7$, there are eight possibilities based on the value of q but only four are shown in Table 6. Now, $\mathfrak{R}_0 = 18$, and the possible value of $\mathfrak{R}_7$ ranges from -10 to 18; that is, it is possible to have a tie when $\mathfrak{R}_0 = \mathfrak{R}_7 = 18$. In this case, the CCSK symbol demodulator can make an error by choosing symbol 7. Note that when $N = 7$, it is

possible to have $\mathfrak{R}_7 = 18$, $\mathfrak{R}_{16} = 18$, or $\mathfrak{R}_{25} = 18$, but only one can have a cross-correlation value of 18 at any given time. To get $\mathfrak{R}_7 = \mathfrak{R}_{16} = \mathfrak{R}_{25} = 18$ at the same time when $N = 7$, we need to have at least seven chip locations where all three symbols (symbol 7, 16, and 25) have the same sign but have different signs from the corresponding chips of symbol 0. As can be seen from Table 5, this is not possible.

When $N = 8$, there are nine possibilities based on the value of q, but only four are shown in Table 6. Now, $\mathfrak{R}_0 = 16$, and the possible value of $\mathfrak{R}_7$ ranges from -12 to 20; that is, it is possible to have either a tie when $\mathfrak{R}_0 = \mathfrak{R}_7 = 16$ or a symbol error when $\mathfrak{R}_0 < \mathfrak{R}_7$. In either case, the CCSK symbol demodulator could make an error if symbol 7 is chosen. Note that when $N = 8$, it is possible to have both $\mathfrak{R}_7 = 16$ and $\mathfrak{R}_{25} = 16$ at the same time since there are six chip locations where symbol 7 and symbol 25 have chips with the same sign but with different signs from the corresponding chips of symbol 0 (see Table 5). If six chip errors occur at the preceding six locations, one of the remaining two chip errors occurs in the second group with respect to symbol 7 but in the first group with respect to symbol 25, and the other remaining chip error occurs in the second group with respect to symbol 25 but in the first group with respect to symbol 7, then there is a three-way tie with $\mathfrak{R}_0 = \mathfrak{R}_7 = \mathfrak{R}_{25} = 16$. Note that when $N = 8$, it is not possible to have a three-way tie with either $\mathfrak{R}_0 = \mathfrak{R}_7 = \mathfrak{R}_{16} = 16$ or $\mathfrak{R}_0 = \mathfrak{R}_{16} = \mathfrak{R}_{25} = 16$ since there are only five chip locations where symbols 7 and 16 (or symbols 16 and 25) have chips with the same sign but with different signs from the corresponding chips of symbol 0.

Based on the observations from $N = 0$ to $N = 8$, CCSK cross-correlation properties can be summarized. First, the value of $\mathfrak{R}_0$ is given by

$$\mathfrak{R}_0 = 32 - 2j, \tag{4.5}$$

where $0 \le j \le 32$ is the total number of chip errors in the received, de-scrambled 32-chip CCSK sequence. Second, the value of $\mathfrak{R}_i$ is given by

$$\mathfrak{R}_i = h_i - 2q + 2(j - q) = h_i + 2(j - 2q), \quad 0 \le q \le j, \quad 1 \le i \le 31 \tag{4.6}$$

since the value of $\Re_i$ decreases by $2q$ if q chip errors occur in the first group and increases by $2(j-q)$ if $j-q$ chip errors occur in the second group. Third, from Equation (4.6), the value of $\Re_i$ ranges from

$$h_i - 2j \leq \Re_i \leq h_i + 2j, \quad 1 \leq i \leq 31 \tag{4.7}$$

since the smallest value of $\Re_i$ is obtained when $q = N$, and the largest value of $\Re_i$ is obtained when $q = 0$. For example, as shown in Table 6, if $i = 7$, $h_7 = 4$, $N = 7$, and $q = 7$, then $\Re_7 = -10$, while if $i = 7$, $h_7 = 4$, $N = 7$, and $q = 0$, then $\Re_7 = 18$. Fourth, from Equation (4.6), $\Re_i$ is a hyper-geometric random variable with a conditional probability mass function (pmf)

$$P\{\Re_i = h_i + 2(j-2q)|N = j\} = \frac{\binom{(32+h_i)/2}{q}\binom{(32-h_i)/2}{j-q}}{\binom{32}{j}}, \tag{4.8}$$

where the left-hand-side of Equation (4.8) is obtained from the left-hand-side of Equation (4.4) by

$$\begin{aligned}
P\{X_1 = q|X_1 + X_2 = j\} &= P\{X_1 = q, X_2 = j-q|X_1 + X_2 = j\} \\
&= P\{X_1 = q, X_2 = j-q|N = j\} \\
&= P\{\Re_i = h_i - 2q + 2(j-q)|N = j\} \\
&= P\{\Re_i = h_i + 2(j-2q)|N = j\},
\end{aligned} \tag{4.9}$$

and the right-hand-side of Equation (4.8) is obtained from the right-hand-side of Equation (4.4) with $n_1 = (32+h_i)/2$ and $n_2 = (32-h_i)/2$. For example, if $i = 7$, $h_7 = 4$, $N = 1$, and $q = 1$, from Equation (4.6) $\Re_7 = 4 + 2(1-2) = 2$, and from Equation (4.8)

$$P\{\Re_7 = 2|N = 1\} = \frac{\binom{18}{1}\binom{14}{0}}{\binom{32}{1}} = \frac{18}{32}. \tag{4.10}$$

54

If $i = 7$, $h_7 = 4$, $N = 1$, and $q = 0$, from Equation (4.6) $\Re_7 = 4 + 2(1-0) = 6$, and

$$P\{\Re_7 = 6|N = 1\} = \frac{\binom{18}{0}\binom{14}{1}}{\binom{32}{1}} = \frac{14}{32}. \tag{4.11}$$

Note that Equations (4.10) and (4.11) have the same results as Equations (4.2) and (4.3), respectively. Last, the CCSK symbol demodulator does not make a symbol error when $N \leq 6$; that is

$$P\{\text{symbol error}|N = j\} = 0, \quad \text{when } 0 \leq j \leq 6. \tag{4.12}$$

Note that Equation (4.12) is the conditional probability of symbol error for CCSK when $N \leq 6$. From the principle of total probability [42], we have

$$P\{A\} = \sum_j P\{A|N = j\}P\{N = j\}. \tag{4.13}$$

If event A is defined as a CCSK symbol error, then the probability of symbol error for CCSK is obtained from Equation (4.13) as

$$P_S = \sum_{j=0}^{32} P\{\text{symbol error}|N = j\}P\{N = j\}, \tag{4.14}$$

where N is a binomial random variable with a pmf

$$P\{N = j\} = \binom{32}{j}P_c^j(1-P_c)^{32-j}, \quad j = 0,1,2,...,32 \tag{4.15}$$

and P_c is the probability of chip error at the output of the MSK chip demodulator. Note that to evaluate Equation (4.14), the conditional probabilities of symbol error for $0 \leq N \leq 32$ are required. In other words, the problem remaining is how to obtain the conditional probabilities of symbol error of CCSK for $7 \leq N \leq 32$.

3. Conditional Probabilities of Symbol Error of CCSK

Based on CCSK cross-correlation properties, the conditional probability of symbol error given that $N = 7,8,...,32$ can be obtained case by case. First, consider the

case $N = 7$. From Table 6, when symbol 0 is sent given that $N = 7$, $\Re_0 = 32 - 2N = 18$, while the possible values of $\Re_7$ are in the set $\{-10, -6, -2, 2, 6, 10, 14, 18\}$. Since a symbol error occurs when $\Re_7 \geq \Re_0$, we need to find the conditional probability that $\Re_7 = 18$ given that $N = 7$. From Equation (4.8),

$$P\{\Re_7 = 18 | N = 7\} = \frac{\binom{18}{0}\binom{14}{7}}{\binom{32}{7}} = 1.02 \times 10^{-3} \tag{4.16}$$
$$= P\{\Re_i = 18 | N = 7\},$$

where $i = 16$ and 25 since $\Re_7$, $\Re_{16}$, and $\Re_{25}$ have the same maximum off-peak cross-correlation value. As a result, the conditional probability that symbol S_7 is chosen when $N = 7$ is given by

$$
\begin{aligned}
P\{S_7 \text{ chosen} | N = 7\} &= P\{S_7 \text{ chosen} | N = 7, \Re_7 = 18\} P\{\Re_7 = 18 | N = 7\} \\
&= (1/2)(1.02 \times 10^{-3}) \\
&= P\{S_{16} \text{ chosen} | N = 7\} \\
&= P\{S_{25} \text{ chosen} | N = 7\},
\end{aligned}
\tag{4.17}
$$

where the factor $1/2$ is due to the tie when $\Re_0 = \Re_7$, and the third and the fourth line of Equation (4.17) is due to the fact that $\Re_7$, $\Re_{16}$, and $\Re_{25}$ have the same maximum off-peak cross-correlation value and it is not possible to have a tree-way tie among either $\Re_0$, $\Re_7$, and $\Re_{25}$ or $\Re_0$, $\Re_7$, and $\Re_{16}$ when $N = 7$. Therefore, the conditional probability of symbol error given that $N = 7$ is given by

$$
\begin{aligned}
P\{\text{symbol error} | N = 7\} &= \sum_{i=1}^{31} P\{S_i \text{ chosen} | N = 7\} \\
&= P\{S_7 \text{ chosen} | N = 7\} + P\{S_{16} \text{ chosen} | N = 7\} + \\
&\quad P\{S_{25} \text{ chosen} | N = 7\} \\
&= 3P\{S_7 \text{ chosen} | N = 7\} \\
&= 1.53 \times 10^{-3}.
\end{aligned}
\tag{4.18}
$$

56

Note that the second line of Equation (4.18) is due to the fact that only $\mathfrak{R}_7$, $\mathfrak{R}_{16}$, and $\mathfrak{R}_{25}$ can have a cross-correlation value of 18 when $N = 7$. For the remaining branches, the corresponding cross-correlation value is always less than eighteen.

When $N = 8$, we have $\mathfrak{R}_0 = 32 - 2N = 16$, and the possible values of $\mathfrak{R}_7$ are in the set $\{-12, -8, -4, 0, 4, 8, 12, 16, 20\}$. Since a symbol error occurs when $\mathfrak{R}_7 \geq \mathfrak{R}_0$, we need to find the conditional probabilities that $\mathfrak{R}_7 = 16$ and $\mathfrak{R}_7 = 20$ given that $N = 8$, respectively. From Equation (4.8), the conditional probability that $\mathfrak{R}_7 = 20$ given that $N = 8$ is

$$P\{\mathfrak{R}_7 = 20 | N = 8\} = \frac{\binom{18}{0}\binom{14}{8}}{\binom{32}{8}} = 2.855 \times 10^{-4}, \tag{4.19}$$

and the conditional probability that $\mathfrak{R}_7 = 16$ given that $N = 8$ is

$$P\{\mathfrak{R}_7 = 16 | N = 8\} = \frac{\binom{18}{1}\binom{14}{7}}{\binom{32}{8}} = 5.873 \times 10^{-3}. \tag{4.20}$$

Next, the conditional probability that S_7 is chosen given that $N = 8$ is

$$P\{S_7 \text{ chosen} | N = 8\} = P\{S_7 \text{ chosen} | N = 8, \mathfrak{R}_7 = 20\} P\{\mathfrak{R}_7 = 20 | N = 8\} + \\ P\{S_7 \text{ chosen} | N = 8, \mathfrak{R}_7 = 16\} P\{\mathfrak{R}_7 = 16 | N = 8\}, \tag{4.21}$$

where

$$P\{S_7 \text{ chosen} | N = 8, \mathfrak{R}_7 = 20\} = 1 \tag{4.22}$$

since $\mathfrak{R}_7 > \mathfrak{R}_0$, and $P\{S_7 \text{ chosen} | N = 8, \mathfrak{R}_7 = 16\}$ is in the range of

$$\frac{1}{3} \leq P\{S_7 \text{ chosen} | N = 8, \mathfrak{R}_7 = 16\} \leq \frac{1}{2}, \tag{4.23}$$

where the factor $1/2$ is obtained for a two-way tie when $\mathfrak{R}_0 = \mathfrak{R}_7 = 16$, and the factor $1/3$ is obtained for a three-way tie when $\mathfrak{R}_0 = \mathfrak{R}_7 = \mathfrak{R}_{25} = 16$. Note that Equation (4.23) can be verified by the following:

$$
\begin{aligned}
&P\{S_7 \text{ chosen} | N = 8, \mathfrak{R}_7 = 16\} \\
&= P\{S_7 \text{ chosen} | N = 8, \mathfrak{R}_7 = 16, \mathfrak{R}_{25} < 16\} P\{\mathfrak{R}_{25} < 16 | N = 8, \mathfrak{R}_7 = 16\} + \\
&\quad P\{S_7 \text{ chosen} | N = 8, \mathfrak{R}_7 = 16, \mathfrak{R}_{25} = 16\} P\{\mathfrak{R}_{25} = 16 | N = 8, \mathfrak{R}_7 = 16\} \quad (4.24) \\
&= \frac{1}{2} P\{\mathfrak{R}_{25} < 16 | N = 8, \mathfrak{R}_7 = 16\} + \frac{1}{3} P\{\mathfrak{R}_{25} = 16 | N = 8, \mathfrak{R}_7 = 16\} \\
&\Rightarrow \frac{1}{3} \leq P\{S_7 \text{ chosen} | N = 8, \mathfrak{R}_7 = 16\} \leq \frac{1}{2}
\end{aligned}
$$

since $P\{\mathfrak{R}_{25} < 16 | N = 8, \mathfrak{R}_7 = 16\} + P\{\mathfrak{R}_{25} = 16 | N = 8, \mathfrak{R}_7 = 16\} = 1$. Now, using Equation (4.22) and the upper bound of Equation (4.23) in Equation (4.21), we obtain

$$
\begin{aligned}
P\{S_7 \text{ chosen} | N = 8\} &\leq 1 \cdot P\{\mathfrak{R}_7 = 20 | N = 8\} + \frac{1}{2} P\{\mathfrak{R}_7 = 16 | N = 8\} \\
&\leq 3.222 \times 10^{-3}.
\end{aligned} \quad (4.25)
$$

Note that

$$
P\{S_7 \text{ chosen} | N = 8\} = P\{S_{25} \text{ chosen} | N = 8\} \leq 3.222 \times 10^{-3} \quad (4.26)
$$

since symbol 7 and symbol 25 have similar properties; however,

$$
P\{S_7 \text{ chosen} | N = 8\} \neq P\{S_{16} \text{ chosen} | N = 8\} \quad (4.27)
$$

since $P\{S_{16} \text{ chosen} | N = 8, \mathfrak{R}_{16} = 16\} = 1/2$. According to Table 5, we can see that it is not possible to have a three-way tie for symbol 16 given that $N = 8$ and $\mathfrak{R}_{16} = 16$. As a result,

$$
\begin{aligned}
P\{S_{16} \text{ chosen} | N = 8\} &= 1 \cdot P\{\mathfrak{R}_{16} = 20 | N = 8\} + \frac{1}{2} P\{\mathfrak{R}_{16} = 16 | N = 8\} \\
&= 3.222 \times 10^{-3}.
\end{aligned} \quad (4.28)
$$

In addition to $\mathfrak{R}_7$, $\mathfrak{R}_{16}$, and $\mathfrak{R}_{25}$, we need to consider other branches that have an off-peak cross-correlation value $h_i = 0$ (such as $\mathfrak{R}_1$) since these branches can also have a

cross-correlation value of 16 when $N = 8$. From Equation (4.8), the conditional probability that $\Re_1 = 16$ given that $N = 8$ is

$$P\{\Re_1 = 16 | N = 8\} = \frac{\binom{16}{0}\binom{16}{8}}{\binom{32}{8}} = 1.224 \times 10^{-3}, \qquad (4.29)$$

and the conditional probability that S_1 is chosen is

$$
\begin{aligned}
P\{S_1 \text{ chosen} | N = 8\} &= P\{S_1 \text{ chosen} | N = 8, \Re_1 = 16\} P\{\Re_1 = 16 | N = 8\} \\
&\leq \frac{1}{2} P\{\Re_1 = 16 | N = 8\} = 6.118 \times 10^{-4},
\end{aligned}
\qquad (4.30)
$$

where the factor $1/2$ is an upper bound and is obtained for the two-way tie when $\Re_0 = \Re_1 = 16$. From Equations (4.26), (4.28), and (4.30), the conditional probability of symbol error when $N = 8$ is given by

$$
\begin{aligned}
P\{\text{symbol error} | N = 8\} &= \sum_{i=1}^{31} P\{S_i \text{ chosen} | N = 8\} \\
&= P\{S_7 \text{ chosen} | N = 8\} + P\{S_{16} \text{ chosen} | N = 8\} + \\
&\quad P\{S_{25} \text{ chosen} | N = 8\} + 18 P\{S_1 \text{ chosen} | N = 8\} \\
&\leq 0.0207.
\end{aligned}
\qquad (4.31)
$$

Note that the factor 18 in the second line of Equation (4.32) is due to the fact that there are eighteen branches (including $\Re_1$) that have $h_i = 0$.

When $N = 9$, $\Re_0 = 32 - 2N = 14$, and the possible values of $\Re_7$ are in the set $\{-14, -10, -6, -2, 2, 6, 10, 14, 18, 22\}$. Since a symbol error occurs when $\Re_7 \geq \Re_0$, we need to find the probability that $\Re_7 = 14$, $\Re_7 = 18$, and $\Re_7 = 22$ given that $N = 9$, respectively. From Equation (4.8), the probability that $\Re_7 = 22$ given that $N = 9$ is

$$P\{\Re_7 = 22 | N = 9\} = \frac{\binom{18}{0}\binom{14}{9}}{\binom{32}{9}} = 7.138 \times 10^{-5}. \qquad (4.32)$$

The conditional probability that $\Re_7 = 18$ given that $N = 9$ is

$$P\{\Re_7 = 18|N = 9\} = \frac{\binom{18}{1}\binom{14}{8}}{\binom{32}{9}} = 1.927 \times 10^{-3}. \tag{4.33}$$

The conditional probability that $\Re_7 = 14$ given that $N = 9$ is

$$P\{\Re_7 = 14|N = 9\} = \frac{\binom{18}{2}\binom{14}{7}}{\binom{32}{9}} = 0.019. \tag{4.34}$$

The conditional probability that S_7 is chosen when $N = 9$ is given by

$$
\begin{aligned}
P\{S_7 \text{ chosen}|N = 9\} &= P\{S_7 \text{ chosen}|N = 9, \Re_7 = 22\} P\{\Re_7 = 22|N = 9\} + \\
&\quad P\{S_7 \text{ chosen}|N = 9, \Re_7 = 18\} P\{\Re_7 = 18|N = 9\} + \\
&\quad P\{S_7 \text{ chosen}|N = 9, \Re_7 = 14\} P\{\Re_7 = 14|N = 9\} \\
&\leq 1 \cdot P\{\Re_7 = 22|N = 9\} + 1 \cdot P\{\Re_7 = 18|N = 9\} + \\
&\quad + \frac{1}{2} P\{\Re_7 = 14|N = 9\} = 0.0115,
\end{aligned} \tag{4.35}
$$

where the factor $1/2$ is an upper bound. Similarly, if the two-way tie (the upper bound) is only considered for symbol 16 and symbol 25 given that $N = 9$, we obtain

$$P\{S_7 \text{ chosen}|N = 9\} = P\{S_i \text{ chosen}|N = 9\} \leq 0.0115, \tag{4.36}$$

where $i = 16$ and 25.

Similar to the case for $N = 8$, in addition to $\Re_7$, $\Re_{16}$, and $\Re_{25}$, we must consider other branches that have $h_i = 0$ since these branches, such as $\Re_1$, can also have a cross-correlation value greater than or equal to $\Re_0 = 14$. When $N = 9$, the possible values of $\Re_1$ are in the set $\{-18, -14, -10, -6, -2, 2, 6, 10, 14, 18\}$. Since a symbol error occurs when $\Re_1 \geq \Re_0$, we need to find the probability that $\Re_1 = 14$ and $\Re_1 = 18$. From Equation (4.8), the conditional probability that $\Re_1 = 18$ given that $N = 9$ is

$$P\{\mathfrak{R}_1 = 18 | N = 9\} = \frac{\binom{16}{0}\binom{16}{9}}{\binom{32}{9}} = 4.079 \times 10^{-4}, \tag{4.37}$$

and the conditional probability that $\mathfrak{R}_1 = 14$ given that $N = 9$ is

$$P\{\mathfrak{R}_1 = 14 | N = 9\} = \frac{\binom{16}{1}\binom{16}{8}}{\binom{32}{9}} = 7.341 \times 10^{-3}. \tag{4.38}$$

The conditional probability that S_1 is chosen given that $N = 9$ is upper bounded by

$$\begin{aligned}
P\{S_1 \text{ chosen} | N = 9\} = &P\{S_1 \text{ chosen} | N = 9, \mathfrak{R}_1 = 18\} P\{\mathfrak{R}_1 = 18 | N = 9\} + \\
&P\{S_1 \text{ chosen} | N = 9, \mathfrak{R}_1 = 14\} P\{\mathfrak{R}_1 = 14 | N = 9\} \\
\leq &1 \cdot P\{\mathfrak{R}_1 = 18 | N = 9\} + \frac{1}{2} P\{\mathfrak{R}_1 = 14 | N = 9\} = 0.0041.
\end{aligned} \tag{4.39}$$

In addition to the eighteen branches that have off-peak cross-correlation value $h_i = 0$ such as $\mathfrak{R}_1$, we must now consider branches that have off-peak cross-correlation value $h_i = -4$, such as $\mathfrak{R}_3$, since these branches can also have a cross-correlation value of 14 given that $N = 9$. In this case, the possible values of $\mathfrak{R}_3$ are in the set $\{-22, -18, -14, -10, -6, -2, 2, 6, 10, 14\}$. Since a symbol error occurs when $\mathfrak{R}_3 \geq \mathfrak{R}_0$, we need to find the probability that $\mathfrak{R}_3 = 14$. From Equation (4.8),

$$P\{\mathfrak{R}_3 = 14 | N = 9\} = \frac{\binom{14}{0}\binom{18}{9}}{\binom{32}{9}} = 1.733 \times 10^{-3}, \tag{4.40}$$

and the conditional probability that S_3 is chosen when $N = 9$ is

$$\begin{aligned}
P\{S_3 \text{ chosen} | N = 9\} = &P\{S_3 \text{ chosen} | N = 9, \mathfrak{R}_3 = 14\} P\{\mathfrak{R}_3 = 14 | N = 9\} \\
\leq &\frac{1}{2} P\{\mathfrak{R}_3 = 14 | N = 9\} = 8.665 \times 10^{-4}.
\end{aligned} \tag{4.41}$$

where the factor $1/2$ is an upper bound. Now, combining the results of Equation (4.36), Equation (4.39), and Equation (4.41), we obtain

$$
\begin{aligned}
P\{\text{symbol error}\,|\,N=9\} &= \sum_{i=1}^{31} P\{S_i \text{ chosen}\,|\,N=9\} \\
&= P\{S_7 \text{ chosen}\,|\,N=9\} + P\{S_{16} \text{ chosen}\,|\,N=9\} + \\
&\quad P\{S_{25} \text{ chosen}\,|\,N=9\} + 18P\{S_1 \text{ chosen}\,|\,N=9\} \\
&\quad + 10P\{S_3 \text{ chosen}\,|\,N=9\} \le 0.1166,
\end{aligned} \tag{4.42}
$$

where the factor 10 in Equation (4.42) is due to the fact that there are ten branches (including $\mathfrak{R}_3$) that have $h_i = -4$.

Repeating the above process, we obtain the remaining conditional probabilities of symbol error for $10 \le N \le 32$. The overall conditional probabilities of symbol error for the 32-chip CCSK sequence chosen for JTIDS are listed in Table 7. Since the non-zero values (except $N=7$) are upper bounds, the analytic conditional probabilities of symbol error are denoted as ζ_{UB_j}. Note that when $N \ge 11$, the upper bound produced by this method exceeds one, in which case the upper bound is given as one.

Table 7.   Conditional probabilities of symbol error for the 32-chip CCSK sequence chosen for JTIDS

$N = j$	ζ_{UB_j}
0	0
1	0
$\vdots$	$\vdots$
6	0
7	0.0015
8	0.0207
9	0.1166
10	0.4187
11	1.0
12	1.0
$\vdots$	$\vdots$
32	1.0

4. Probability of Symbol Error for CCSK in AWGN

Now, combining Equations (4.14) and (4.15), we get the probability of symbol error for the 32-chip CCSK sequence chosen for JTIDS as

$$P_S = \sum_{j=0}^{32} \zeta_j \binom{32}{j} P_c^j \left(1 - P_c\right)^{32-j},$$ (4.43)

where ζ_j is the conditional probabilities of symbol error for CCSK, and P_c is the probability of chip error at the output of the MSK chip demodulator. If we use ζ_{UB_j} in Equation (4.43), then an analytic upper bound on the probability of symbol error for the 32-chip CCSK sequence chosen for JTIDS is given by

$$P_S < \sum_{j=0}^{32} \zeta_{UB_j} \binom{32}{j} P_c^j \left(1 - P_c\right)^{32-j}.$$ (4.44)

MSK can be considered as a special case of offset quadrature phase-shift keying (OQPSK) with sinusoidal pulse shaping. When a coherent matched filter or correlator is used to recover the chips, MSK has the same performance as BPSK, QPSK, and OQPSK [38]; that is,

$$P_c = Q\left(\sqrt{\frac{2E_c}{N_0}}\right).$$ (4.45)

Since $E_s = 5E_b = 32E_c$, we can rewrite Equation (4.45) as

$$P_c = Q\left(\sqrt{\frac{10E_b}{32N_0}}\right).$$ (4.46)

Note that the actual JTIDS waveform is received noncoherently at the chip level, but in this dissertation the performance of a JTIDS-type waveform with coherent detection is evaluated in order to ascertain the performance possible if coherent chip demodulation were practical. The analysis presented in this paper can easily be modified to evaluate performance with noncoherent chip demodulation.

Now, substituting Equation (4.46) into (4.44), we obtain an analytic upper bound on the probability of symbol error for the 32-chip CCSK sequence chosen for JTIDS in

AWGN. The results are shown in Figure 19. To compare the difference between orthogonal signaling and non-orthogonal CCSK, the probability of symbol error of 32-ary coherent orthogonal signaling is also shown in Figure 19. As expected, the probability of symbol error of 32-chip CCSK is inferior to that of 32-ary orthogonal signaling. The relative performance degradation is about 2 dB at $P_s = 10^{-5}$; however, the advantage of using CCSK is that only one detector branch is required to recover the original symbol instead of thirty-two detector branches.
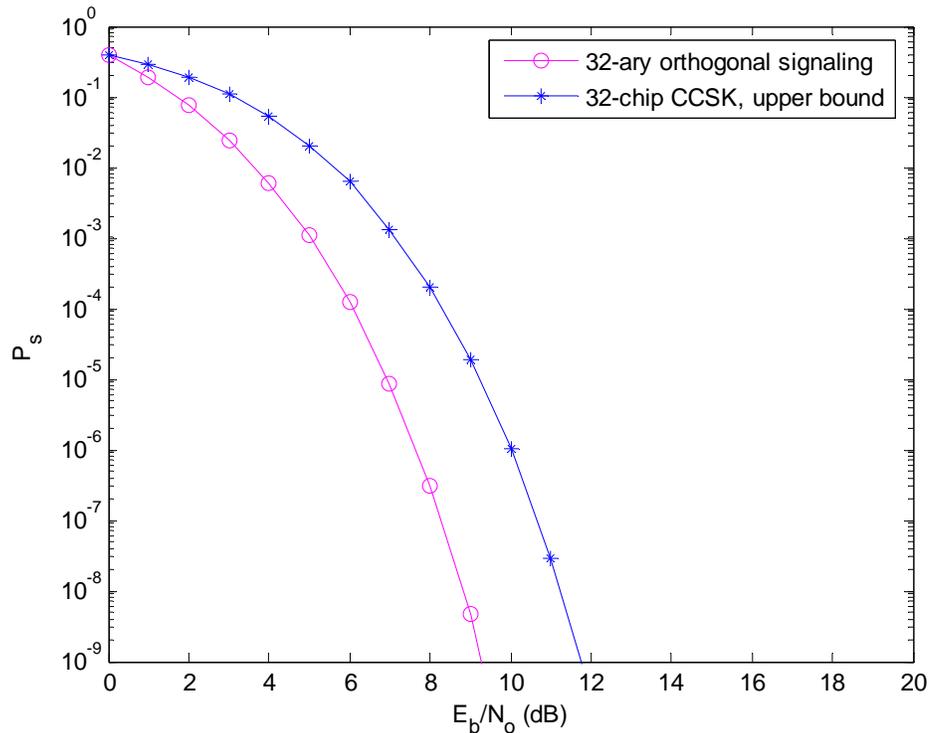
Figure 19.   Probability of symbol error for the 32-chip CCSK sequence chosen for JTIDS in AWGN.

B.   SIMULATION OF CCSK PERFORMANCE

In addition to the upper bound derived in the last section, two different Monte Carlo simulations are implemented in this section. The first simulation, a CCSK Monte Carlo Simulation, is written to simulate the detection of a JTIDS/Link-16-type waveform without considering the process of FEC coding, interleaving, scrambling, or frequency-hopping. The second simulation, a Monte Carlo simulation with stratified sampling, is

written to obtain the conditional probabilities of symbol error ζ_j for $7 \leq j \leq 32$ [43]. These two simulations are available to the interested reader by contacting either the author at chihankao@yahoo.com or Prof. Clark Robertson, Naval Postgraduate School, at CRobertson@nps.edu. In what follows, the major steps of these two simulations are introduced and their results are compared to that of the analytical upper bound.

1. CCSK Monte Carlo Simulation

A flow chart of this simulation is shown in Figure 20. As can be seen, this simulation consists of a transmitter with a CCSK symbol modulator and a coherent MSK chip modulator, an AWGN channel, and a receiver with a coherent MSK chip de-modulator and a CCSK symbol demodulator.
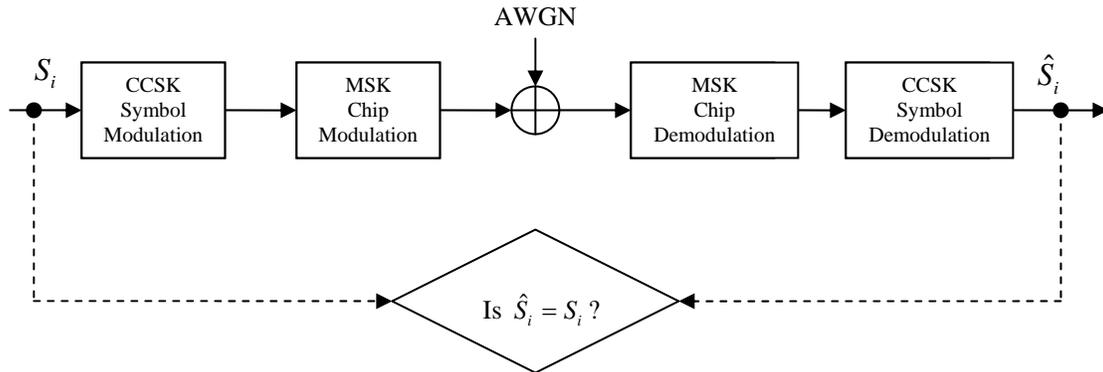
Figure 20.   CCSK Monte Carlo simulation.

In Figure 20, the input to the CCSK symbol modulator S_i is a decimal number which represents a 5-bit symbol, where $0 \leq i \leq 31$. For example, symbol 0 is denoted as $S_0 = 0 = 00000$ and symbol 1 is denoted as $S_1 = 1 = 00001$. The output of the CCSK symbol demodulator $\hat{S}_i$ is the estimate of the symbol received. The processes of the CCSK simulation are as follows: (i) in each iteration, 100 random symbols (between symbol 0 and 31) are generated and modulated with CCSK, following which the chips are modulated with MSK for transmission, (ii) the transmitted signal is added to white Gaussian noise in the channel, (iii) the noisy signal is received and demodulated with coherent MSK at the chip level and with CCSK at the symbol level to obtain an estimate of the received symbol, (iv) the transmitted and received symbols are compared to

determine if a symbol error has occurred, (v) the above process is repeated enough times to ensure sufficient accuracy of the simulation. Then the error ratio is calculated for each E_b/N_0. The result of the CCSK Monte Carlo simulation is shown in Figure 21 along with the analytical result for the CCSK upper bound. As is seen, the difference between the analytical upper bound and simulation is less than 0.2 dB from $P_S = 10^{-2}$ to $P_S = 10^{-4}$. In other words, the analytical expression given in Equation (4.44) is a tight upper bound.
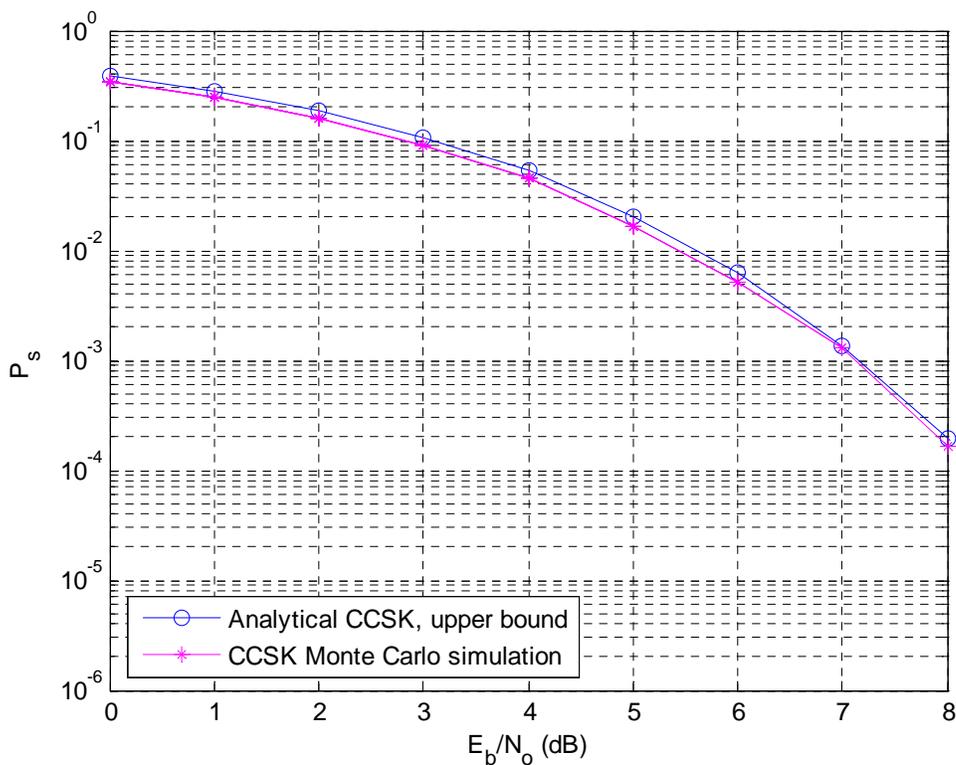
Figure 21.   Probability of symbol error of the 32-chip CCSK sequence chosen for JTIDS in AWGN: Monte Carlo simulation versus analytical upper bound.

2.   Monte Carlo Simulation with Stratified Sampling

Both the accuracy and the efficiency of the simulations are very important. In the previous section, we have shown that the result of a CCSK Monte Carlo Simulation is very close to that obtained by an analytical upper bound; however, the simulation itself is inefficient since there are few symbol errors when E_b/N_0 is large, and it can take hours

of computation time to obtain a performance plot. To improve simulation efficiency and to check the accuracy of the first simulation, a Monte Carlo simulation with stratified sampling is used to generate the conditional probabilities of symbol error ζ_j, where $7 \leq j \leq 32$. Recall that the conditional CCSK probabilities of symbol error ζ_j shown in Table 7 are analytical upper bounds for $j > 7$, hereafter denoted as ζ_{UB_j}, while in this section the conditional probabilities of symbol error obtained by simulation are denoted as ζ_{SIM_j}.

Stratified sampling is a sampling method which focuses on important sub-populations and ignores irrelevant ones. In our case, the important sub-populations are those conditional probabilities of symbol error of CCSK given that $7 \leq N \leq 32$, and the irrelevant sub-populations are those conditional probabilities of symbol error given that $N \leq 6$ since we have shown that the conditional probability of symbol error for CCSK is zero when $N \leq 6$. By not running the simulation for the irrelevant sub-populations, the simulation is more efficient compared to the previous simulation method. The question remaining is how to implement the simulation for those conditional probabilities of symbol error given that $7 \leq N \leq 32$.

A Monte Carlo simulation with stratified sampling is implemented in a manner similar to that of finding the analytic upper bound; that is, the simulation for the conditional probability of symbol error is done case-by-case for different N. For example, given $N = 7$ and that symbol 0 is sent, the major process of the simulation is as follows. In each iteration, (i) generate randomly a 32-chip sequence with $N = 7$ chip errors (with respect to the original 32-chip sequence of symbol 0) to model the noisy received 32-chip sequence at the output of the coherent MSK chip demodulator, (ii) cross-correlate the received 32-chip sequence with all of the 32 local sequences to yield 32 cross-correlation values, $\Re_0, \Re_{1,....,} \Re_{31}$, (iii) calculate the probability of symbol error based on the following: if $\Re_i > \Re_0$, where $1 \leq i \leq 31$, the conditional probability of symbol error is one; if $\Re_i = \Re_0$, where $1 \leq i \leq 31$, the conditional probability of symbol error is $\eta/(\eta+1)$, where η is the total number of ties; if $\Re_i < \Re_0$, where $1 \leq i \leq 31$, the

67

conditional probability of symbol error is zero. Next, the above iteration is repeated 10,000 times, and the average conditional probability of symbol error is calculated. Using the above approach, we obtain the conditional probabilities of symbol error given that $7 \leq N \leq 32$. The results are shown in the third column of Table 8.

Table 8.   Conditional probabilities of symbol error for the 32-chip CCSK sequence chosen for JTIDS: analytic upper bound versus Monte Carlo simulation with stratified sampling.

$N = j$	ζ_{UB_j}	ζ_{SIM_j}
0	0	0
1	0	0
2	0	0
3	0	0
4	0	0
5	0	0
6	0	0
7	0.0015	0.0015
8	0.0207	0.0194
9	0.1166	0.1126
10	0.4187	0.3669
11	1.0	0.7093
12	1.0	0.9351
13	1.0	0.9953
14	1.0	1.0
15	1.0	1.0
$\vdots$	$\vdots$	$\vdots$
32	1.0	1.0

Note that the second column of Table 8 is copied from Table 7 in order to more easily compare the difference between the analytic upper bound and the simulation. As can be seen, the analytic upper bound is close to the simulation except when $N = 10$, 11, and 12. It is interesting to note that $\zeta_{SIM_j} > (32-1)/32 = 0.9688$ when $N \geq 13$. This is due to the fact that the demodulator makes its decision chip-by-chip prior to making symbol decisions rather than making decision symbol-by-symbol as is typically done with other types of M-ary modulation techniques.

Now, substituting ζ_{SIM_j} into Equation (4.43) along with Equation (4.46), the simulation result for the probability of symbol error in AWGN is shown in Figure 22. The results of the analytical upper bound and the CCSK Monte Carlo simulation are also shown. As is seen from Figure 22, the two different simulations match well.
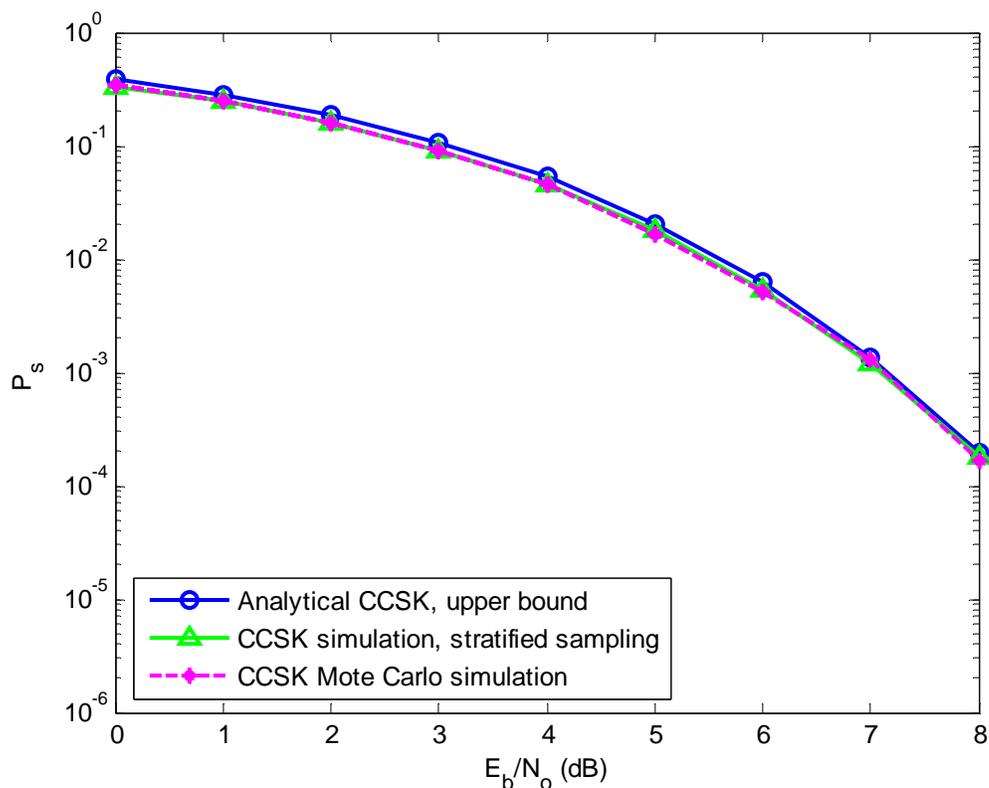
Figure 22. Probability of symbol error for the 32-chip CCSK sequence chosen for JTIDS in AWGN: two different Monte Carlo simulations versus analytic upper bound.

To examine the accuracy of the simulation with stratified sampling results, the standard error of the simulation on the probability of symbol error of CCSK at each E_b/N_0 is calculated using [43]

$$StdErr(P_s) = \sqrt{\sum_{j=0}^{32} \left(P\{N = j\} \right)^2 \left(\frac{Var_j}{n} \right)}, \qquad (4.47)$$

where Var_j is the variance of the conditional probabilities of symbol error ζ_{SIM_j}, and $n = 10,000$ is the total number of iterations for each j chip errors. The derivation of

Equation (4.47) is shown in Appendix B. The estimated probability of symbol error for the 32-chip CCSK sequence chosen for JTIDS and the associated standard error of the estimation are shown in Table 9.

Table 9.   Estimated probability of symbol error for 32-chip CCSK and the associated standard error of the estimation.

E_b/N_0	Estimated P_s	Standard Error
0	0.336	6.761×10^{-4}
1	0.244	6.087×10^{-4}
2	0.160	5.013×10^{-4}
3	0.093	3.681×10^{-4}
4	0.045	2.335×10^{-4}
5	0.018	1.233×10^{-4}
6	5.529×10^{-3}	5.195×10^{-5}
7	1.235×10^{-3}	1.658×10^{-5}
8	1.877×10^{-4}	3.763×10^{-6}

C.   SUMMARY OF CHAPTER IV

In this chapter, an analytic upper bound on the probability of symbol error of CCSK in AWGN is derived for the 32-chip CCSK sequence chosen for JTIDS. The probability of symbol error obtained with the analytic upper bound is compared with that obtained by two different Monte Carlo simulations. The results show that the analytic method yields a tight upper bound. Given the probability of symbol error of CCSK in AWGN, either analytic upper bound or simulation, we can now evaluate the probability of symbol error of a JTIDS/Link-16-type waveform in both AWGN and narrowband interference when the signal is transmitted over a slow, flat Nakagami fading channel. This is addressed in the next chapter.

V. PERFORMANCE ANALYSIS OF A JTIDS/LINK-16-TYPE WAVEFORM

For JTIDS, data demodulation consists of two parts: MSK chip demodulation and CCSK symbol demodulation. The receiver structure of a JTIDS-type system is shown in Figure 17 and is reproduced here (Figure 23) for convenience. Given the assumptions that frequency de-hopping is perfectly synchronized with the frequency hopped waveform and that the signal-to-noise ratio is large, the MSK chip demodulator recovers the original 32-chip transmitted symbol. Given that de-scrambling is perfectly synchronized, the CCSK symbol demodulator detects the original 5-bit coded symbol. As is seen in Figure 23, in order to evaluate the probability of information symbol error P_s at the output of the RS decoder for a JTIDS/Link-16-type waveform, the probability of channel chip error p_c at the output of the MSK chip demodulator and the probability of channel symbol error p_s at the output of the CCSK symbol demodulator are both required.
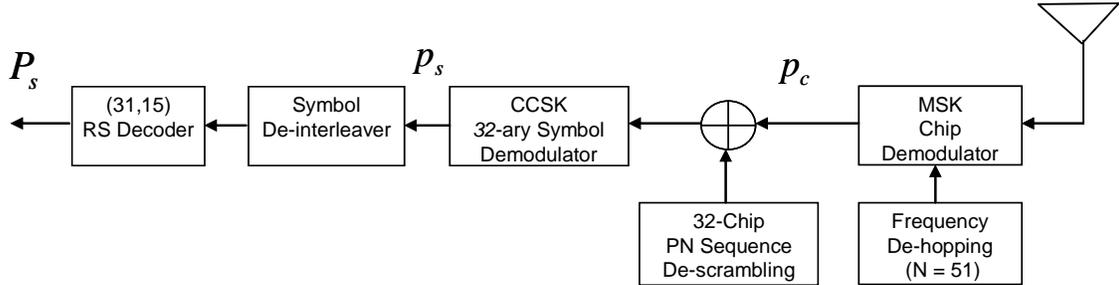
Figure 23.   Receiver structure of a JTIDS-type system.

In this chapter, an analytic expression for the probability of channel chip error of a JTIDS/Link-16-type waveform, both the single- and the double-pulse structure, in AWGN is introduced in Section A. An analytic expression for the probability of channel symbol error of a JTIDS/Link-16-type waveform is introduced in Section B. In Section C, two analytic expressions for the performance of linear, nonbinary block codes are introduced. In Section D, the probability of symbol error of a JTIDS/Link-16-type waveform in AWGN is investigated. The probability of symbol error of a JTIDS/Link-16-type waveform in both AWGN and narrowband interference is investigated in Section

71

E, and the probability of symbol error of a JTIDS/Link-16-type waveform in both AWGN and narrowband interference when the signal is transmitted over a slow, flat Nakagami fading channel is investigated in Section F.

A. PROBABILITY OF CHANNEL CHIP ERROR

1. Single-Pulse Structure

As mentioned in Chapter III, the Link-16 message data can be sent with either a single-pulse structure or a double-pulse structure. When a single-pulse structure is used, the coherent MSK chip demodulator shown in Figure 24 is assumed, where the input $r(t)$ is the received JTIDS/Link-16-type waveform, and the output $\hat{S}$ is the estimated received 32-chip CCSK sequence that is ready for de-scrambling.
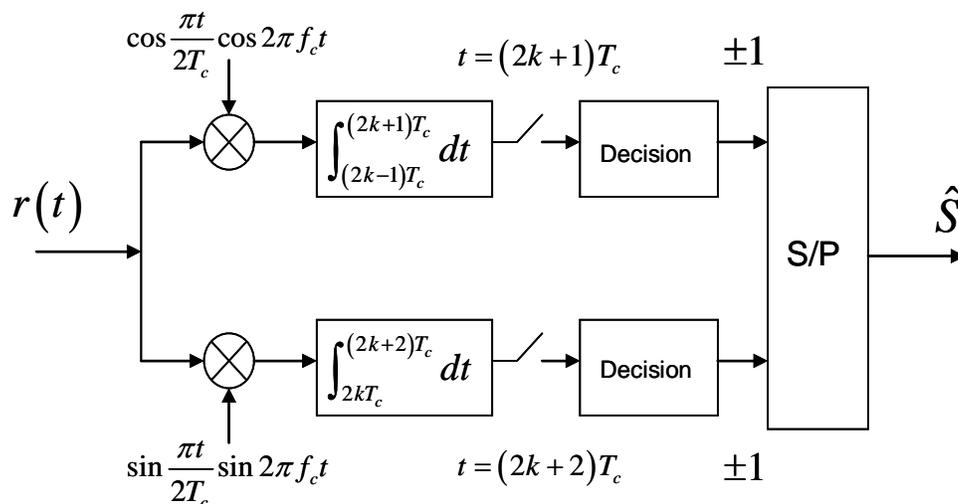
Figure 24.   MSK coherent chip demodulator (after [38]).

As mentioned in Chapter IV, MSK can be considered as a special case of OQPSK with sinusoidal pulse shaping. When a coherent matched filter or correlator (as shown in Figure 24) is used to recover the chips, MSK has the same performance as BPSK, QPSK, and OQPSK [38]; that is,

$$P_c = Q\left(\sqrt{\frac{2E_c}{N_0}}\right), \tag{5.1}$$

where E_c is the average energy per chip. Since each 5-bit symbol is converted into 32 chips,

$$E_s = 5E_b = 32E_c, \tag{5.2}$$

where E_s is the average energy per symbol and E_b is the average energy per bit. Therefore, Equation (5.1) can be expressed as

$$P_c = Q\left(\sqrt{\frac{10E_b}{32N_0}}\right). \tag{5.3}$$

Note that Equation (5.3) is not the probability of channel chip error since FEC coding has not been considered. When FEC coding is applied, for every k information data symbols, n coded symbols are transmitted where $n > k$. Since n coded symbols must be transmitted in the time it would otherwise take to transmit k data symbols, we get

$$nT_{s_c} = kT_s \Rightarrow T_{s_c} = \frac{k}{n}T_s = rT_s, \tag{5.4}$$

where T_{s_c} is the duration of a coded symbol, T_s is the duration of an information symbol, and r is the code rate. From Equation (5.4), the coded symbol rate is

$$R_{s_c} = \frac{1}{T_{s_c}} = \frac{R_s}{r}, \tag{5.5}$$

where R_s is the information (or uncoded) symbol rate. Since $r < 1$, the coded symbol rate is higher than the information symbol rate. If the average transmitted power is the same whether coded or uncoded symbols are transmitted (i.e., $P = E_{s_c}R_{s_c} = E_sR_s$), the average energy per coded symbol is given by

$$E_{s_c} = \frac{R_s}{R_{s_c}}E_s = rE_s, \tag{5.6}$$

73

and the average energy per coded bit is $E_{b_c} = rE_b$. Therefore, when FEC coding is applied, Equation (5.3) can be rewritten as

$$p_c = Q\left(\sqrt{\frac{10E_{b_c}}{32N_0}}\right) = Q\left(\sqrt{\frac{10rE_b}{32N_0}}\right), \qquad (5.7)$$

which is the probability of channel chip error of a JTIDS/Link-16-type waveform with the single-pulse structure in AWGN when chips are coherently demodulated.

2. Double-Pulse Structure

The double-pulse structure increases the anti-jam capability of the link since it provides a diversity of $L = 2$. To recover the data sent with the double-pulse structure, soft decision (SD) combining on a chip-by-chip basis is assumed in the coherent MSK chip demodulator which is shown in Figure 25.
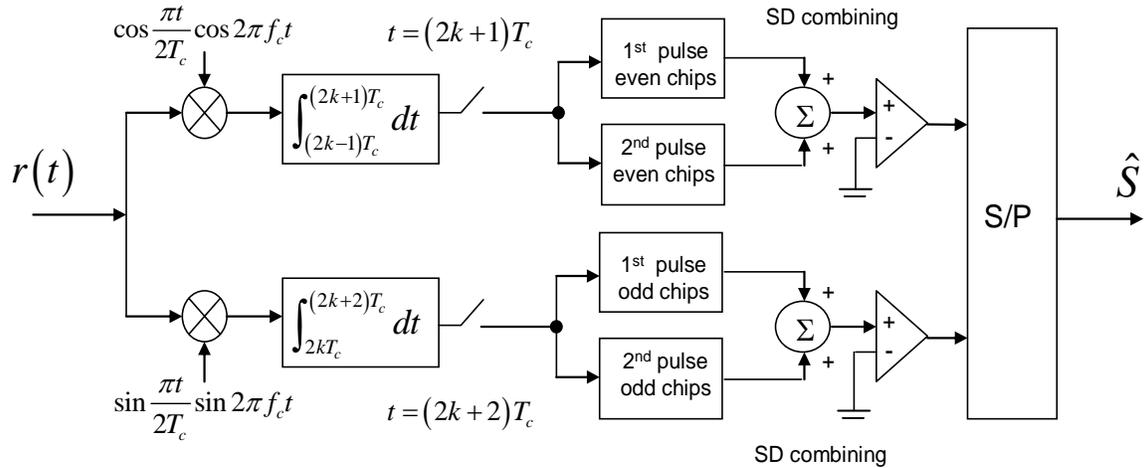
Figure 25.   MSK double-pulse coherent chip demodulator with SD combining.

As can be seen, a buffer/SD combining circuit is added to the coherent MSK chip demodulator to implement SD combining. When the double-pulse structure is used, JTIDS is a hybrid DS/FFH spread spectrum system with sequential diversity $L = 2$ since each symbol is transmitted twice on two different carrier frequencies. In this case, the average energy per symbol is

$$E_s = LE_p, \tag{5.8}$$

where E_p is the average energy per pulse. Note that for the single-pulse structure, $E_s = E_p$ since $L = 1$. Since $E_s = 5E_b$ and $E_p = 5E_{b'}$, from Equation (5.8) we get

$$E_b = LE_{b'}, \tag{5.9}$$

where $E_{b'}$ is the average energy per bit per pulse. Note that for a single-pulse, $E_b = E_{b'}$ since $L = 1$. Substituting Equation (5.9) into (5.7), we obtain a general expression for the probability of channel chip error of a JTIDS/Link-16-type waveform in AWGN as

$$p_c = Q\left(\sqrt{\frac{10rLE_{b'}}{32N_0}} \right), \tag{5.10}$$

where $L = 1$ for the single-pulse structure, and $L = 2$ for the double-pulse structure. Note that if p_c is expressed in terms of E_b instead of $LE_{b'}$, then p_c is the same for both the single- and the double-pulse structure when only AWGN is present.

B.   PROBABILITY OF CHANNEL SYMBOL ERROR

The probability of symbol error for the 32-ary CCSK used by JTIDS is given in Equation (4.43) and is reproduced here for convenience:

$$P_S = \sum_{j=0}^{32} \varsigma_j \binom{32}{j} P_c^j \left(1 - P_c\right)^{32-j}. \tag{5.11}$$

Since the demodulation of CCSK symbol is independent of the FEC coding, the analytic expression for the probability of channel symbol error of a JTIDS/Link-16-type waveform can be obtained from Equation (5.11) by replacing P_S and P_c with p_s and p_c, respectively; that is,

$$p_s = \sum_{j=0}^{32} \varsigma_j \binom{32}{j} p_c^j \left(1 - p_c\right)^{32-j}, \tag{5.12}$$

where ς_j are the conditional probabilities of channel symbol error given that $N = j$ chip errors have occurred in the received, de-scrambled 32-chip sequence, and p_c is the

75

probability of channel chip error of a JTIDS/Link-16-type waveform. In Chapter IV, the values of ζ_j were obtained both analytically and by Monte Carlo simulation. Since the analytic result yields a tight upper bound, it is used to evaluate the probability of symbol error of a JTIDS/Link-16-type waveform in this chapter. Therefore, from (5.12), the probability of channel symbol error of a JTIDS/Link-16-type waveform is given by

$$p_s < \sum_{j=0}^{32} \zeta_{UB_j} \binom{32}{j} p_c^j (1 - p_c)^{32-j}. \tag{5.13}$$

C.   PERFORMANCE OF LINEAR, NONBINARY BLOCK CODES

As mentioned earlier, JTIDS uses RS codes for FEC coding. A RS code is a linear, nonbinary block code. For a *t*-symbol error correcting, nonbinary block code, the probability of decoder, or block, error is upper bounded by [40]

$$P_E \le \sum_{i=t+1}^{n} \binom{n}{i} p_s^i (1 - p_s)^{n-i}, \tag{5.14}$$

where the equality holds for either a perfect code or a bounded distance decoder, and p_s is the probability of channel symbol error. Since each block consists of *n* coded symbols, the probability of symbol error for a linear, nonbinary block code is obtained by approximating the probability of information symbol error given i channel symbol errors per block by i/n [44]. Substituting this into Equation (5.14), we get

$$P_S \approx \frac{1}{n} \sum_{i=t+1}^{n} i \binom{n}{i} p_s^i (1 - p_s)^{n-i}. \tag{5.15}$$

Equation (5.15) can be used to evaluate the probability of symbol error of a JTIDS/Link-16-type waveform given the probability of channel symbol error p_s. Note that Equation (5.15) is independent of the types of noise and/or fading channels but requires that the performance of each of the *n* symbols per block be independent; that is, a memoryless channel is assumed.

D. PERFORMANCE ANALYSIS IN AWGN

1. Single-Pulse Structure

With Equations (5.10), (5.13), and (5.15), we are ready to investigate the probability of symbol error of a JTIDS/Link-16-type waveform for the single-pulse structure in AWGN. First, using Equation (5.10) with $r = 15/31$ and $L = 1$ in Equation (5.13) along with ζ_{UB_j} from Table 7, we obtain the probability of channel symbol error p_s. Next, using p_s in Equation (5.15), we obtain the probability of symbol error of a JTIDS/Link-16-type waveform for the single-pulse structure in AWGN. The result is shown in Figure 26. To see the difference between the coded and the uncoded system, the probability of symbol error for an uncoded JTIDS/Link-16-type waveform is also shown. As can be seen, the $E_{b'}/N_0$ required for the coded system is about 7.1 dB at $P_S = 10^{-5}$, while the $E_{b'}/N_0$ required for the uncoded system is 9.2 dB; that is, the coding gain is about 2.1 dB at $P_S = 10^{-5}$.
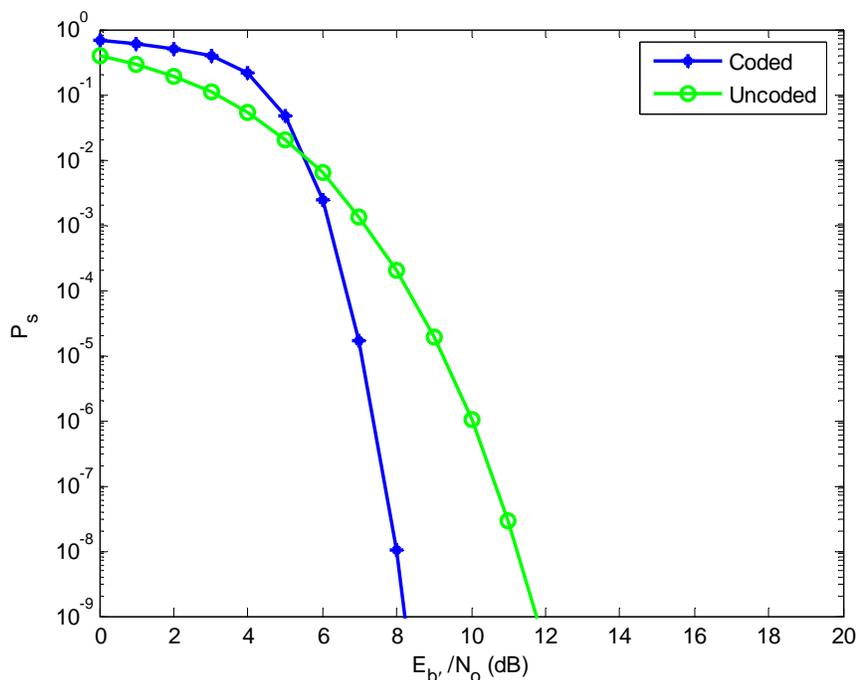
Figure 26.   Probability of symbol error of a JTIDS/Link-16-type waveform for the single-pulse structure in AWGN: coded versus uncoded system.

2. Double-Pulse Structure

The process of obtaining the probability of symbol error of a JTIDS/Link-16-type waveform for the double-pulse structure in AWGN is almost the same as the process for the single-pulse structure case except for using $L = 2$ in Equation (5.10). In order to compare the performance between the single- and the double-pulse structure, both results are shown in Figure 27. As expected, the double-pulse structure outperforms the single-pulse structure in terms of $E_{b'}$. At $P_S = 10^{-5}$, the $E_{b'}/N_0$ required for the double-pulse structure is about 4 dB, while the $E_{b'}/N_0$ required for the single-pulse structure is about 7.1 dB in AWGN. In other words, the double-pulse structure outperforms the single-pulse structure by 3.1 dB at $P_S = 10^{-5}$ in AWGN. Note that, as discussed in Chapter III, Section A.5, this comparison is made on an average energy per bit per pulse basis. If the comparisons were made on average energy per bit basis, then there would be no difference between the performances obtained for the single- and the double-pulse structure.
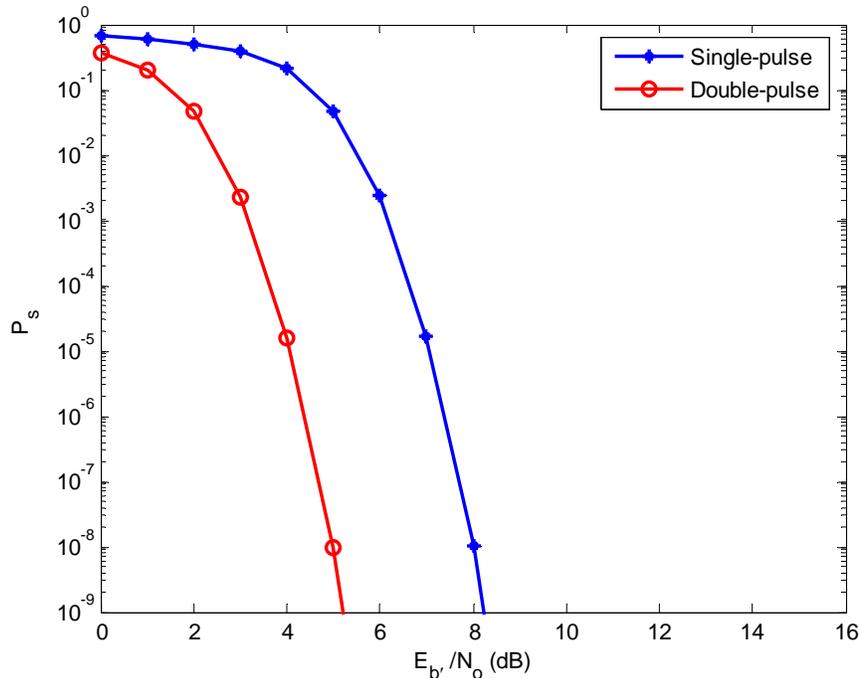
Figure 27.   Probability of symbol error of a JTIDS/Link-16-type waveform in AWGN: single-pulse versus double-pulse structure.

E. PERFORMANCE ANALYSIS IN BOTH AWGN AND NARROWBAND INTERFERENCE

In this section, the probability of symbol error of a JTIDS/Link-16-type waveform in both AWGN and narrowband interference is investigated. Three types of narrowband interference are considered: BNI, PNI, and a combined PNI and PBNI.

1. Performance in Both AWGN and BNI

As discussed in Chapter II, the effect of BNI on the system is simply to increase the Gaussian noise level at the receiver. Due to BNI, the total noise power at the integrator output of a DS/MSK receiver is given in Equation (2.11) and is reproduced here for convenience:

$$\sigma_T^2 = \frac{N_0 + 0.889 N_I}{T_c},$$

(5.16)

where the factor 0.889 comes from the assumption that the PSD of the BNI at the receiver input is $N_I/2$ within the null-to-null bandwidth (i.e., from $-0.75 R_c$ to $0.75 R_c$) of the DS/MSK signal and zero elsewhere. For JTIDS, however, the transmitted signal is hopping over the overall bandwidth of the JTIDS waveform; therefore, the total noise power is approximately equal to

$$\sigma_T^2 \approx \frac{N_0}{T_c} + \int_{-\infty}^{+\infty} N_I \left[\frac{\sin(\pi f T_c)}{\pi f T_c} \right]^2 df = \frac{N_0 + N_I}{T_c}.$$

(5.17)

Thus, the probability of channel chip error of a JTIDS/Link-16 waveform in both AWGN and BNI is given by [27]

$$p_c = Q\left(\sqrt{\frac{0.3125 r L E_{b'}}{N_0 + N_I}} \right),$$

(5.18)

where r is the code rate, $L=1$ for the single-pulse structure, and $L=2$ for the double-pulse structure. Now, using Equation (5.18) with $r=15/31$ and $L=1$ in Equation (5.13) along with ζ_{UB_j} from Table 7, we obtain the probability of channel symbol error p_s. Next, using p_s in Equation (5.15), we obtain an upper bound on the probability of

symbol error of a JTIDS/Link-16-type waveform for the single-pulse structure in both AWGN and BNI. To compare the difference between the coded and the uncoded system, both results are shown in Figure 28 where $E_{b'}/N_0 = 10$ dB. As can be seen, the required $E_{b'}/N_I$ for the coded system is about 10.2 dB at $P_S = 10^{-5}$, while the $E_{b'}/N_I$ required for the uncoded system is about 17.2 dB; that is, the coding gain for the single-pulse structure in both AWGN and BNI is 7 dB at $P_S = 10^{-5}$ when $E_{b'}/N_0 = 10$ dB.
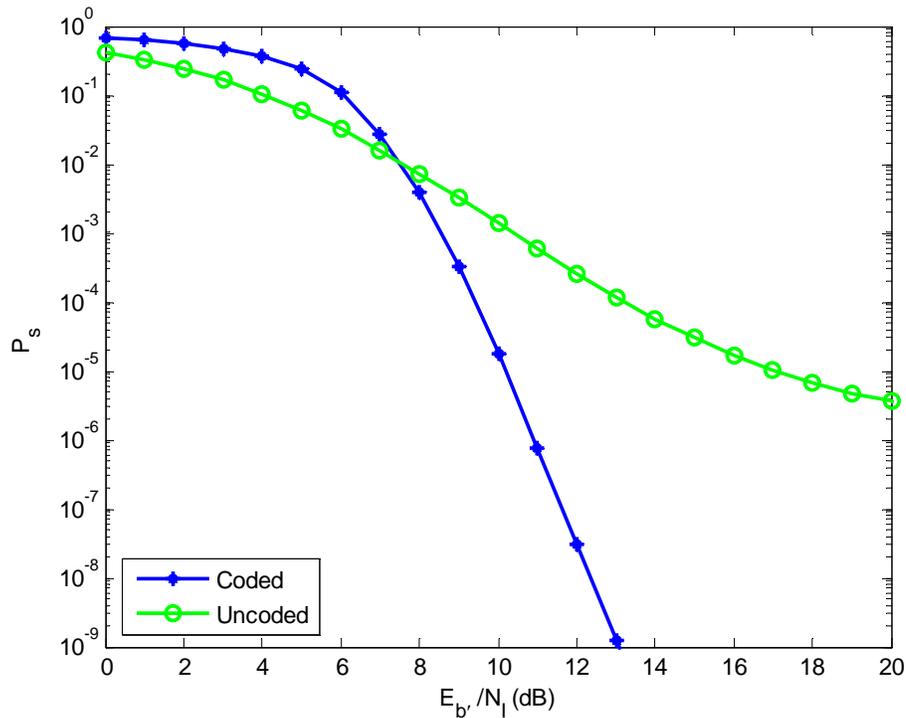
Figure 28.   Probability of symbol error of a JTIDS/Link-16-type waveform for the single-pulse structure in both AWGN and BNI where $E_{b'}/N_0 = 10\,\text{dB}$: coded versus uncoded system.

When $E_{b'}/N_0$ is increased to $15\,\text{dB}$, the probability of symbol error of a JTIDS/Link-16-type waveform for the single-pulse structure in both AWGN and BNI is shown in Figure 29. As can be seen, the $E_{b'}/N_I$ required for the coded system is reduced to 7.8 dB at $P_S = 10^{-5}$, while the $E_{b'}/N_I$ required for the uncoded system is reduced to 10.5 dB at $P_S = 10^{-5}$ for a coding gain of 2.7 dB. Comparing Figure 29 with Figure 28, we see that the effect of BNI on the system decreases as $E_{b'}/N_0$ increases, whether the

system is coded or uncoded. In addition, the coding gain is small when $E_{b'}/N_0$ is large, whereas the coding gain is large when $E_{b'}/N_0$ is small. In other words, FEC coding improves the system performance with a greater margin when $E_{b'}/N_0$ is poorer.
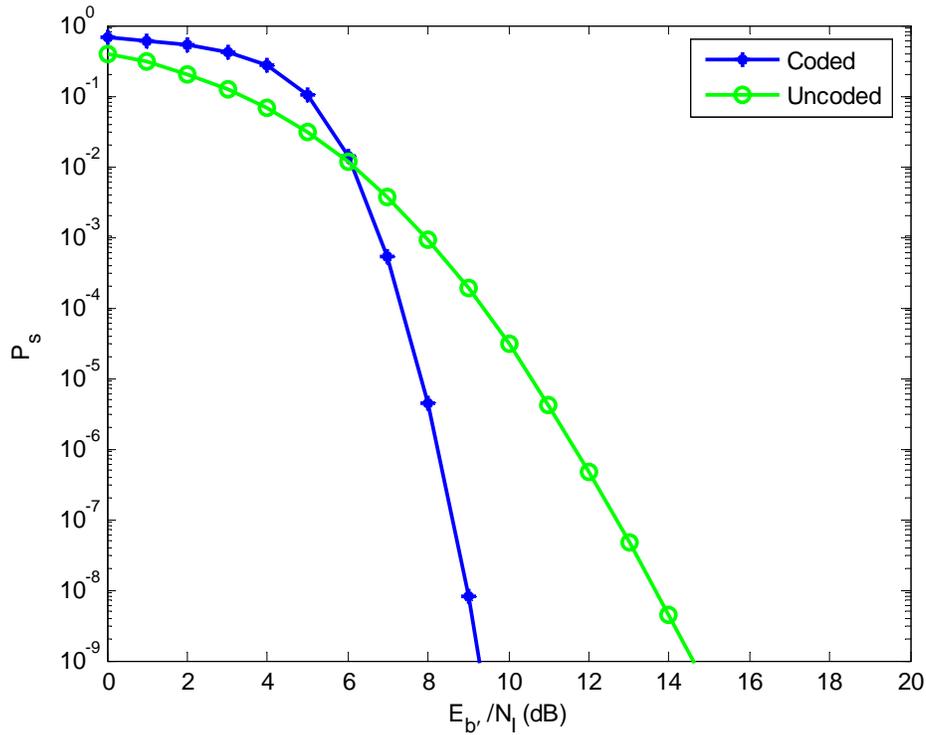
Figure 29.   Probability of symbol error of a JTIDS/Link-16-type waveform for the single-pulse structure in both AWGN and BNI where $E_{b'}/N_0 = 15\,\text{dB}$: coded versus uncoded system.

For our analysis, a proper value of $E_{b'}/N_0$ is required. In Figure 30, $E_{b'}/N_I$ versus $E_{b'}/N_0$ is plotted for the single-pulse structure of a JTIDS/Link-16-type waveform in both AWGN and BNI when $P_S = 10^{-5}$. As is seen in Figure 30, $E_{b'}/N_I$ approaches 7 dB when $E_{b'}/N_0 \geq 15\,\text{dB}$, while $E_{b'}/N_I$ approaches infinity when $E_{b'}/N_0 \leq 10\,\text{dB}$. Based on this observation, it is reasonable to investigate the performance of a JTIDS/Link-16-type waveform in both AWGN and narrowband interference for $10\,\text{dB} \leq E_{b'}/N_0 \leq 15\,\text{dB}$.

81
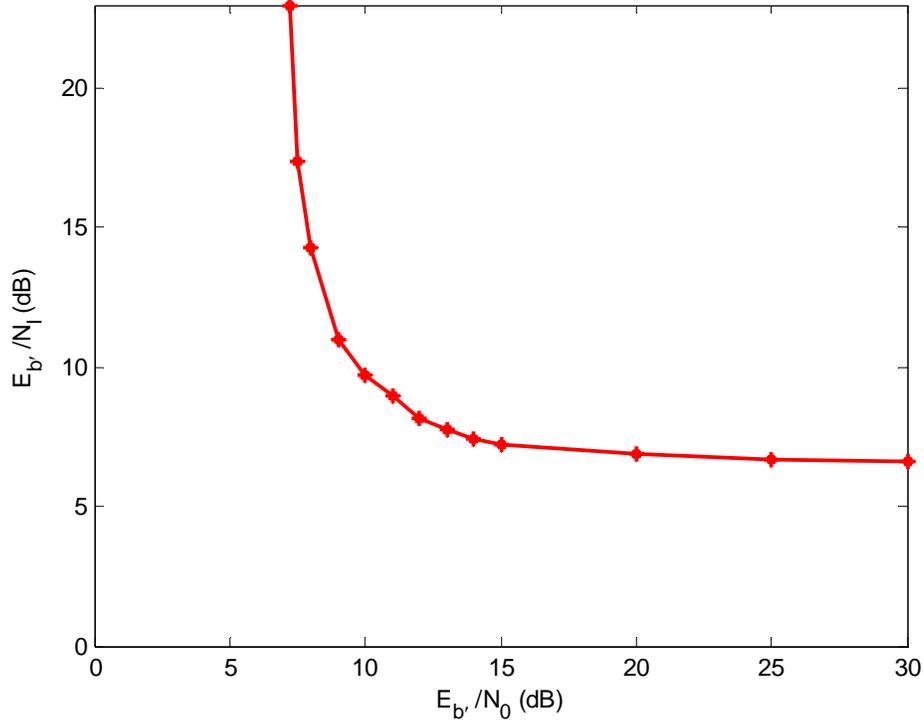
Figure 30. $E_{b'}/N_0$ versus $E_{b'}/N_I$ when $P_S = 10^{-5}$ for a JTIDS/Link-16-type waveform with the single-pulse structure in both AWGN and BNI.

For the double-pulse structure, the process of obtaining the probability of symbol error of a JTIDS/Link-16-type waveform in both AWGN and BNI is the same as that for the single-pulse structure except $L = 2$ in Equation (5.18). To compare the performance between the single- and the double-pulse structure, both results are shown in Figure 31 and 32 where $E_{b'}/N_0 = 10$ dB and 15 dB, respectively. As is seen in Figure 31, when $E_{b'}/N_0 = 10$ dB, the $E_{b'}/N_I$ required for the double-pulse structure is 5.2 dB at $P_S = 10^{-5}$, which outperforms the single-pulse structure by 5 dB. When $E_{b'}/N_0$ is increased to 15 dB (see Figure 32), the required $E_{b'}/N_I$ for the double-pulse structure is 4.4 dB at $P_S = 10^{-5}$, which outperforms the single-pulse structure by 3.4 dB (a decrease of 1.6 dB if compared to when $E_{b'}/N_0 = 10$ dB). This is consistent with our intuition that a stronger signal benefits less from the added robustness of the double-pulse structure.
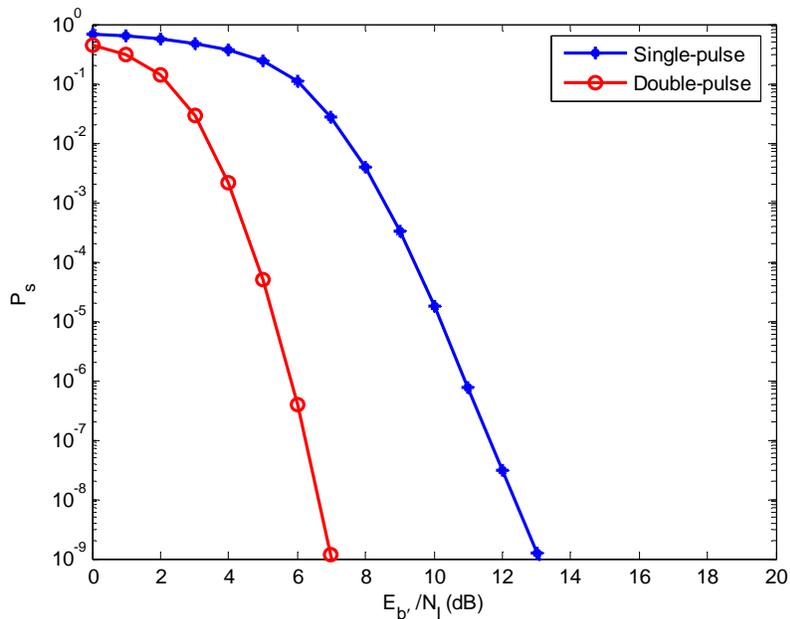
Figure 31.   Probability of symbol error of a JTIDS/Link-16-type waveform in both AWGN and BNI where $E_{b'}/N_0 = 10\,\text{dB}$: double- versus single-pulse structure.
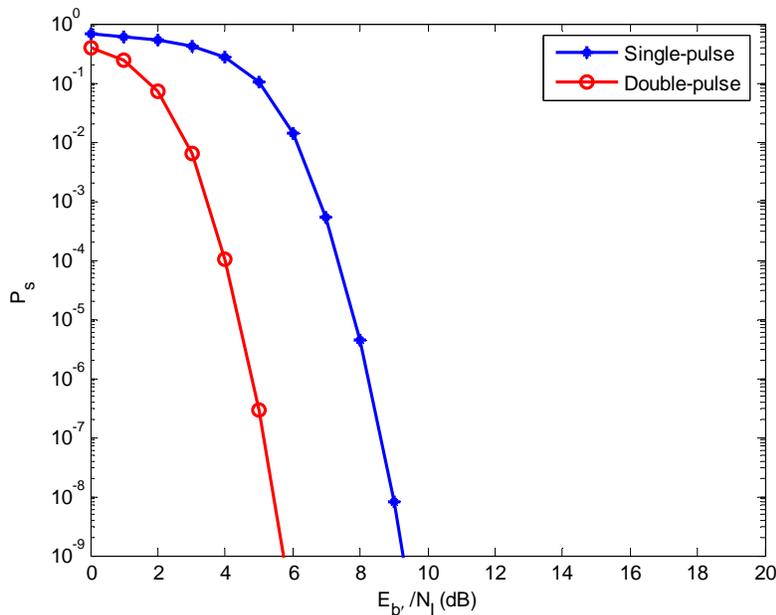
Figure 32.   Probability of symbol error of a JTIDS/Link-16-type waveform in both AWGN and BNI where $E_{b'}/N_0 = 15\,\text{dB}$: double- versus single-pulse structure.

2.   Performance in Both AWGN and PNI

When a JTIDS/Link-16-type waveform is subjected to both AWGN and PNI, Equation (5.15) can still be used to evaluate the probability of symbol error since Equation (5.15) is independent on the types of noise and/or fading channels; however, the probability of channel symbol error p_s shown in Equation (5.12) must be modified as

$$p_s = \Pr\{\text{jammer off}\}\, p_s\,(\text{jammer off}) + \Pr\{\text{jammer on}\}\, p_s\,(\text{jammer on}) \quad (5.19)$$

since the probability of channel symbol error is determined at the symbol level instead of at the chip level and since the PNI is assumed. If $0 < \rho_1 \leq 1$ represents the fraction of time the PNI is on, Equation (5.19) can be rewritten as

$$p_s = (1 - \rho_1)\, p_{s_0} + \rho_1\, p_{s_1}, \quad (5.20)$$

where p_{s_0} is the probability of channel symbol error when the single-pulse is not jammed (PNI is off), and p_{s_1} is the probability of channel symbol error when the single-pulse is jammed (PNI is on). Note that we assume that either all the chips of a symbol experience PNI or none of them do. The probability of channel symbol error when the single-pulse is not jammed is given by

$$p_{s_0} = \sum_{j=0}^{32} \zeta_j \binom{32}{j} p_{c_0}^j \left(1 - p_{c_0}\right)^{32-j}, \quad (5.21)$$

where ζ_j is the conditional probabilities of channel symbol error given that $N = j$ chip errors have occurred in the received, de-scrambled 32-chip sequence, and p_{c_0} is the probability of channel chip error when the single-pulse is not jammed, given by

$$p_{c_0} = Q\left(\sqrt{\frac{0.3125 r E_{b'}}{N_0}}\right), \quad (5.22)$$

where r is the code rate. Similarly, the probability of channel symbol error when the single-pulse is jammed is given by

$$p_{s_1} = \sum_{j=0}^{32} \zeta_j \binom{32}{j} p_{c_1}^j \left(1 - p_{c_1}\right)^{32-j}, \quad (5.23)$$

where p_{c_1} is the probability of channel chip error when the single-pulse is jammed, given by

$$p_{c_1} = Q\left(\sqrt{\frac{0.3125rE_{b'}}{N_0 + N_I/\rho_1}}\right) \qquad (5.24)$$

since the effect of PNI is to increase the noise power spectral density by $1/\rho_1$ if a constant average interference power is assumed.

From Equation (5.13), the probability of channel symbol error when the single-pulse is not jammed is upper-bounded by

$$p_{s_0} < \sum_{j=0}^{32} \zeta_{UB_j} \binom{32}{j} p_{c_0}^j \left(1-p_{c_0}\right)^{32-j} \qquad (5.25)$$

and the probability of channel symbol error when the single-pulse is jammed is upper-bounded by

$$p_{s_1} < \sum_{j=0}^{32} \zeta_{UB_j} \binom{32}{j} p_{c_1}^j \left(1-p_{c_1}\right)^{32-j}. \qquad (5.26)$$

Now, using Equation (5.22) with code rate $r = 15/31$ in Equation (5.25) along with ζ_{UB_j} from Table 7, we obtain the probability of channel symbol error when the single-pulse is not jammed p_{s_0}. Similarly, using Equation (5.24) with code rate $r = 15/31$ in Equation (5.26) along with ζ_{UB_j} from Table 7, we obtain the probability of channel symbol error when the single-pulse is jammed p_{s_1}. Next, substituting the obtained p_{s_0} and p_{s_1} into Equation (5.20), we obtain the average probability of channel symbol error p_s. Finally, substituting the average probability of channel symbol error p_s into Equation (5.15), we obtain the probability of symbol error of a JTIDS/Link-16-type waveform for the single-pulse structure in both AWGN and PNI. The results are shown in Figure 33 where $E_{b'}/N_0 = 10\,\text{dB}$ and in Figure 34 where $E_{b'}/N_0 = 15\,\text{dB}$ for different values of ρ_1.
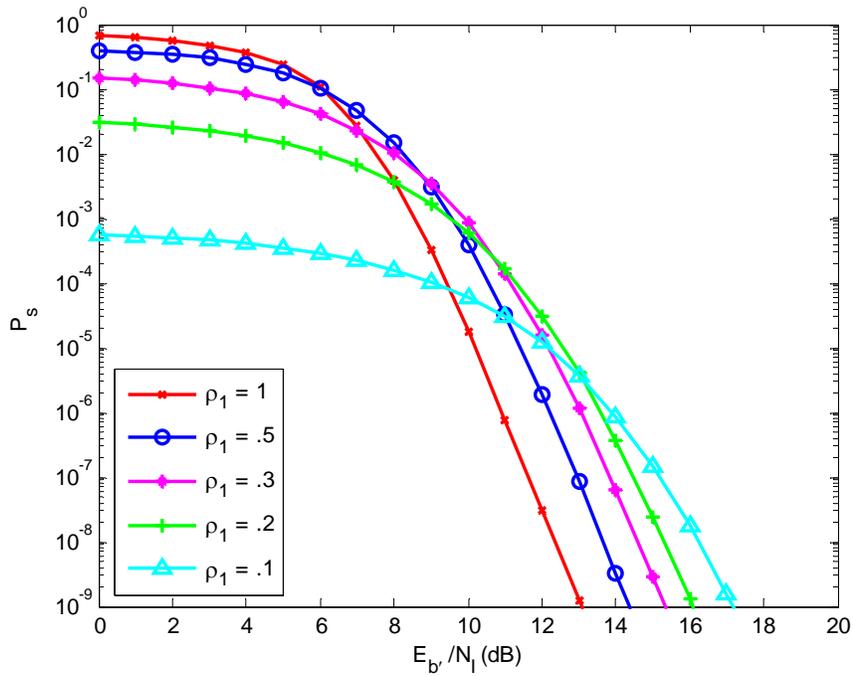
Figure 33.   Probability of symbol error of a JTIDS/Link-16-type waveform for the single-pulse structure in both AWGN and PNI where $E_{b'}/N_0 = 10\,\text{dB}$.
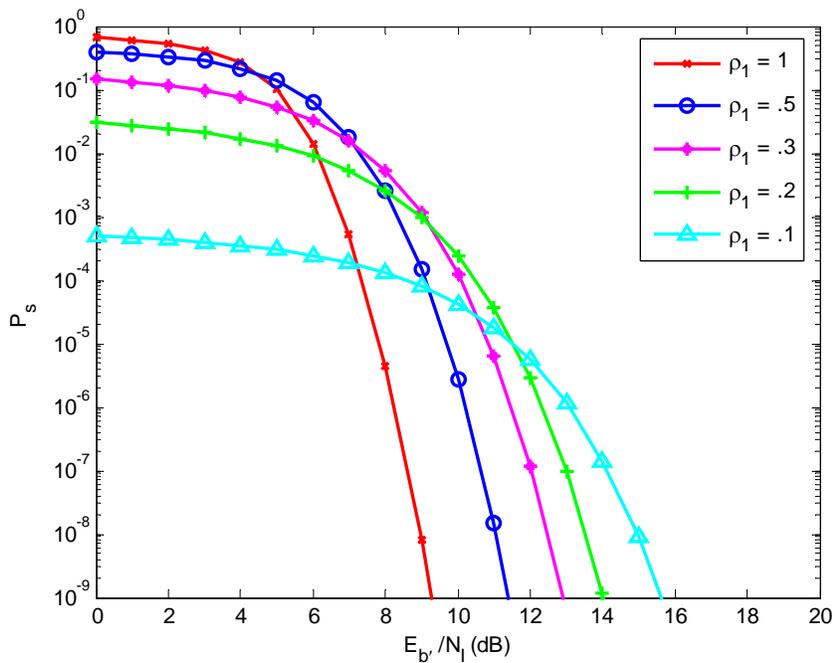
Figure 34.   Probability of symbol error of a JTIDS/Link-16-type waveform for the single-pulse structure in both AWGN and PNI where $E_{b'}/N_0 = 15\,\text{dB}$.

As expected, when $\rho_1 = 1$ (BNI), the performance is the same as that of a JTIDS/Link-16-type waveform for the single-pulse structure in both AWGN and BNI. Furthermore, for both Figures 33 and 34, as $E_{b'}/N_I$ increases, the value of ρ_1 that maximizes the probability of symbol error decreases. In other words, $\rho_1 = 1$ has the most effect in degrading performance when $E_{b'}/N_I$ is relatively small, whereas $\rho_1 = 0.1$ causes the greatest degradation when $E_{b'}/N_I$ is relatively large. This is consistent with our intuition that for strong signals, the jammer power must be large during a symbol in order to make a symbol error likely.

Note that the average probability of channel symbol error in Equation (5.20) is only valid for the single-pulse structure. In general, we can rewrite Equation (5.20) as

$$p_s = \sum_{\ell=0}^{L} \binom{L}{\ell} \rho_1^{\ell} \left(1 - \rho_1\right)^{L-\ell} p_{s_\ell},$$

(5.27)

where $L = 1$ for the single-pulse structure, $L = 2$ for the double-pulse structure, and p_{s_ℓ} is the probability of channel symbol error given that ℓ pulses are jammed and is upper-bounded by

$$p_{s_\ell} < \sum_{j=0}^{32} \zeta_{UB_j} \binom{32}{j} p_{c_\ell}^{j} \left(1 - p_{c_\ell}\right)^{32-j},$$

(5.28)

where $\ell = 0, \ldots, L$, and p_{c_ℓ} is the probability of channel chip error given that ℓ pulses are jammed. For coherent detection, p_{c_ℓ} is given by

$$p_{c_\ell} = Q\left(\sqrt{\frac{0.3125 r L E_{b'}}{N_0 + \left(\ell N_I / L \rho_1\right)}}\right).$$

(5.29)

Now, using $L = 2$ in Equation (5.27), we get

$$p_s = \left(1 - \rho_1\right)^2 p_{s_0} + 2\rho_1 \left(1 - \rho_1\right) p_{s_1} + \rho_1^2 p_{s_2},$$

(5.30)

where p_{s_0} is the probability of channel symbol error given that neither pulse is jammed, p_{s_1} is the probability of channel symbol error given that one pulse is jammed, and p_{s_2} is

the probability of channel symbol error given that both pulses are jammed. From Equation (5.28), p_{s_0} is upper-bounded by

$$p_{s_0} < \sum_{j=0}^{32} \zeta_{UB_j} \binom{32}{j} p_{c_0}^j \left(1 - p_{c_0}\right)^{32-j},$$ (5.31)

and from Equation (5.29) with $\ell = 0$ and $L = 2$, p_{c_0} is given by

$$p_{c_0} = Q\left(\sqrt{\frac{0.625 r E_{b'}}{N_0}}\right).$$ (5.32)

Similarly, from Equation (5.28), p_{s_1} is upper-bounded by

$$p_{s_1} < \sum_{j=0}^{32} \zeta_{UB_j} \binom{32}{j} p_{c_1}^j \left(1 - p_{c_1}\right)^{32-j},$$ (5.33)

and from Equation (5.29) with $\ell = 1$ and $L = 2$, p_{c_1} is given by

$$p_{c_1} = Q\left(\sqrt{\frac{0.625 r E_{b'}}{N_0 + \left(N_I / 2\rho_1\right)}}\right).$$ (5.34)

From Equation (5.28), p_{s_2} is upper-bounded by

$$p_{s_2} < \sum_{j=0}^{32} \zeta_{UB_j} \binom{32}{j} p_{c_2}^j \left(1 - p_{c_2}\right)^{32-j},$$ (5.35)

and from Equation (5.29) with $\ell = 2$ and $L = 2$, p_{c_2} is given by

$$p_{c_2} = Q\left(\sqrt{\frac{0.625 r E_{b'}}{N_0 + N_I / \rho_1}}\right).$$ (5.36)

Now, using Equation (5.32) with $r = 15/31$ in (5.31) along with ζ_{UB_j} from Table 7, we obtain the probability of channel symbol error given that neither pulse is jammed p_{s_0}. Using Equation (5.34) with $r = 15/31$ in (5.33) along with ζ_{UB_j} from Table 7, we obtain the probability of channel symbol error given that one pulse is jammed p_{s_1}. Finally, using (5.36) with $r = 15/31$ in (5.35) along with ζ_{UB_j} from Table 7, we obtain

probability of channel symbol error given that both pulses are jammed p_{s_2}. Next, substituting p_{s_0}, p_{s_1}, and p_{s_2} into Equation (5.30), we obtain the average probability of channel symbol error p_s. Lastly, using p_s in Equation (5.15), we obtain the probability of symbol error of a JTIDS/Link-16-type waveform for the double-pulse structure in both AWGN and PNI.

To compare the difference between the single- and the double-pulse structure, both results are shown in Figure 35 and 36 where $E_{b'}/N_0 = 10$ dB and 15 dB, respectively. From both Figures 35 and 36, several observations can be made. First, for both the single- and the double-pulse structure, the value of ρ_1 that maximizes the probability of symbol error decreases as $E_{b'}/N_I$ increases. Second, when $E_{b'}/N_I$ is relatively large (such as 10 dB), the double-pulse structure always outperforms the single-pulse structure for the same value of ρ_1. However, when $E_{b'}/N_I$ is relatively small (such as 6 dB), the single-pulse structure can outperform the double-pulse structure for smaller values of ρ_1. This is consistent with our intuition that for a particular value of ρ_1, the double-pulse structure is more likely to have at least one pulse jammed. Consequently, when $E_{b'}/N_I$ is small, the performance of the double-pulse structure tends to be poorer than that of the single-pulse structure. Lastly, the double-pulse structure outperforms the single-pulse structure by a smaller margin as $E_{b'}/N_0$ increases. For example, in Figure 36 where $E_{b'}/N_0$ is increased to 15 dB, for $\rho_1 = 0.5$, the double-pulse structure outperforms the single-pulse structure by 4.2 dB (a decrease of 1 dB compared to when $E_{b'}/N_0 = 10$ dB) at $P_S = 10^{-5}$. This is consistent with our intuition that a stronger signal benefits less from the added robustness of the double-pulse structure. Note that since PNI is identical to PBNI mathematically, the above results can be applied to the case when a JTIDS/Link-16-type waveform is subject to both AWGN and PBNI when $\rho_2 = \rho_1$, where ρ_2 represents the fraction of the spread spectrum signal bandwidth that is jammed.
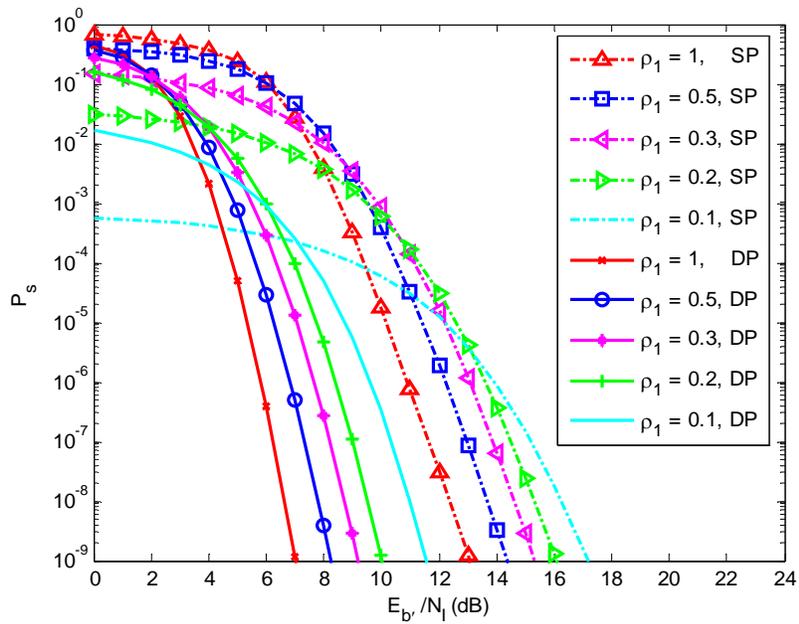
Figure 35. Probability of symbol error of a JTIDS/Link-16-type waveform in both AWGN and PNI where $E_{b'}/N_0 = 10$ dB: single- versus double-pulse structure.
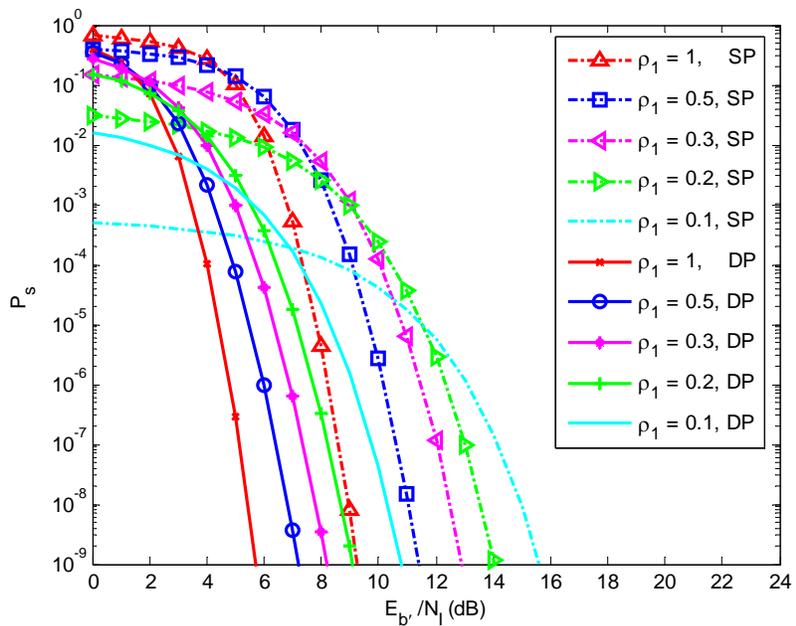
Figure 36. Probability of symbol error of a JTIDS/Link-16-type waveform in both AWGN and PNI where $E_{b'}/N_0 = 15$ dB: single- versus double-pulse structure.

3. Performance in Both AWGN and PNI with Perfect Side Information

In some cases, the system performance can be improved further if we have some information regarding which pulse is jammed and which is not. When available, this information is called side information. Perfect side information (PSI) is not realistic but gives us a benchmark against which to measure receivers which have imperfect or no side information. For PSI, we assume that the jammed pulse is disregarded except when all pulses are jammed. Given this assumption, PSI has no effect on the single-pulse structure but will affect the double-pulse structure since there is a possibility that one of the two pulses will experience jamming. With PSI, Equation (5.34) becomes

$$p_{c_1} = Q\left(\sqrt{\frac{0.3125rE_{b'}}{N_0}}\right), \tag{5.37}$$

while p_{c_0} and p_{c_2}, shown in Equations (5.32) and (5.36), respectively, stay the same. Now, using Equation (5.32) with $r = 15/31$ in (5.31) along with ζ_{UB_j} from Table 7, we obtain the probability of channel symbol error given that neither pulse is jammed p_{s_0}. Using Equation (5.37) with $r = 15/31$ in (5.33) along with ζ_{UB_j} from Table 7, we obtain the probability of channel symbol error given that one pulse is jammed p_{s_1}. Finally, using (5.36) with $r = 15/31$ in (5.35) along with ζ_{UB_j} from Table 7, we obtain probability of channel symbol error given that both pulses are jammed p_{s_2}. Next, using p_{s_0}, p_{s_1}, and p_{s_2} in (5.30), we obtain the average probability of channel symbol error p_s. Finally, using p_s in (5.15), we obtain the probability of symbol error of a JTIDS/Link-16-type waveform for the double-pulse structure with PSI in both AWGN and PNI.

To compare the difference between the double-pulse structure with and without PSI, both results are shown in Figure 37 and 38 where $E_{b'}/N_0 = 10\,\mathrm{dB}$ and 15 dB, respectively. From both Figures 37 and 38, several observations can be made. First, for $\rho_1 = 1$, the probability of symbol error is same, whether the double-pulse structure has PSI or not. This is expected since $\rho_1 = 1$ implies both pulses are subjected to BNI. In this case, no jammed pulse is disregarded and PSI has no effect. Second, the double-pulse

structure with PSI outperforms that without PSI for the same ρ_1 (except $\rho_1 = 1$), and the superiority increases as the value of ρ_1 decreases. For example, in Figure 37, for $\rho_1 = 0.5$, the double-pulse structure with PSI outperforms that without PSI by 0.8 dB at $P_S = 10^{-5}$, while for $\rho_1 = 0.3$, the double-pulse structure with PSI outperforms that without PSI by 4 dB at $P_S = 10^{-5}$. Next, the double-pulse structure with PSI outperforms that without PSI by a smaller margin as $E_{b'}/N_0$ increases. For example, in Figure 38 where $E_{b'}/N_0$ is increased to 15 dB, for $\rho_1 = 0.5$, the double-pulse structure with PSI outperforms that without PSI by 0.4 dB (a decrease of 0.4 dB compared to when $E_{b'}/N_0 = 10\,\text{dB}$) at $P_S = 10^{-5}$, while for $\rho_1 = 0.3$, the double-pulse structure with PSI outperforms that without PSI by 3.4 dB (a decrease of 0.6 dB compared to when $E_{b'}/N_0 = 10\,\text{dB}$) at $P_S = 10^{-5}$. Finally, we see that PSI effectively mitigates the degradation of the system due to PNI.
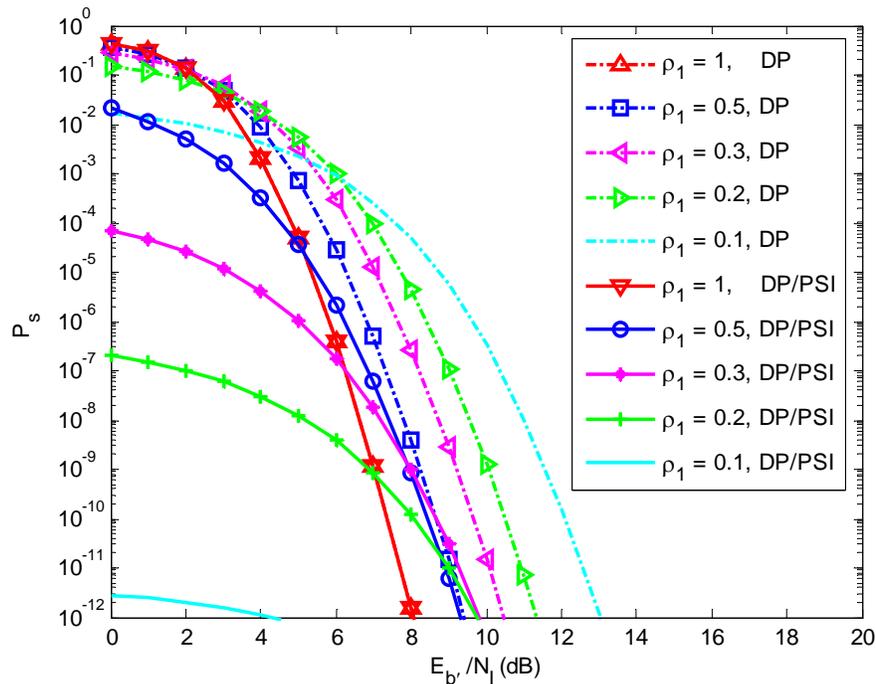
Figure 37.   Probability of symbol error of a JTIDS/Link-16-type waveform for the double-pulse (DP) structure in both AWGN and PNI where $E_{b'}/N_0 = 10\,\text{dB}$: DP without PSI versus DP with PSI.
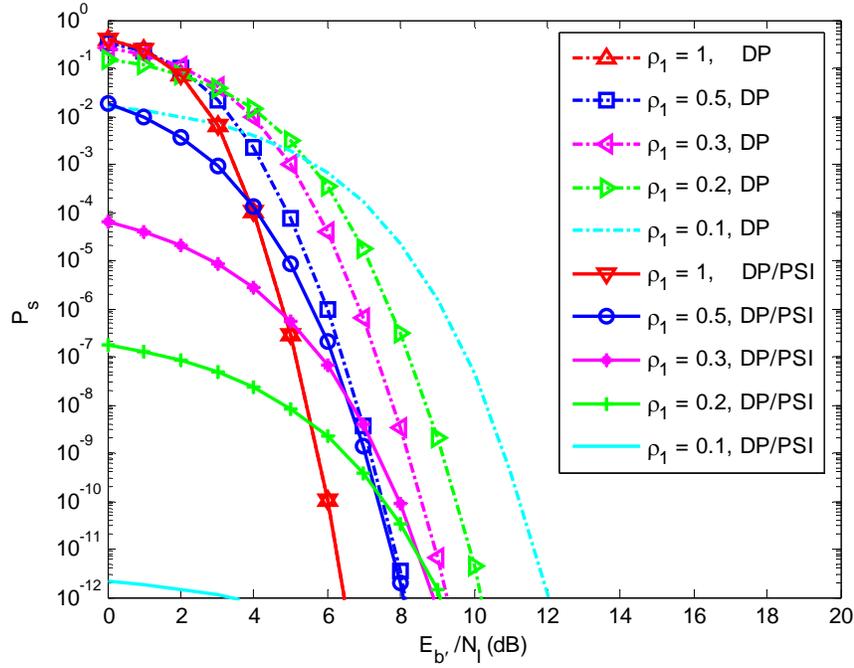
Figure 38.   Probability of symbol error of a JTIDS/Link-16-type waveform for the double-pulse (DP) structure in both AWGN and PNI where $E_{b'}/N_0 = 15\,\text{dB}$: DP without PSI versus DP with PSI.

4.   Performance in Both AWGN and Combined PNI and PBNI

As mentioned earlier, JTIDS is a hybrid DS/FH spread spectrum system where adjacent frequency-hop bins overlap in frequency. Intuitively, an effective jamming strategy would use a combination of PNI and PBNI to interfere with the JTIDS waveform. Since the design of the JTIDS waveform results in each symbol being received independently, Equation (5.15) can be used to evaluate the probability of symbol error of a JTIDS/Link-16-type waveform for the single-pulse structure in both AWGN and a combination of PNI and PBNI; however, the average probability of channel symbol error p_s shown in Equation (5.12) must be modified as

$$
\begin{aligned}
p_s = \Pr\{\text{not jammed}\}\, p_s\,(\text{not jammed}) \\
+ \Pr\{\text{jammed}\}\, p_s\,(\text{jammed}),
\end{aligned}
\tag{5.38}
$$

where $\Pr\{\text{not jammed}\}$ is the probability that PNI is off and that the hop is not in the bin that is jammed, which is given by Equation (2.21) and reproduced here for convenience:

$$\Pr\{\text{not jammed}\} = 1 - \rho_1 \rho_2 , \tag{5.39}$$

where ρ_1 represents the fraction of time the PNI is on and ρ_2 represents the fraction of the spread spectrum signal bandwidth that is jammed. The term $\Pr\{\text{jammed}\}$ in Equation (5.38) is the probability that PNI is on and that the hop is in the bin that is jammed, which is given by Equation (2.20) and reproduced here for convenience:

$$\Pr\{\text{jammed}\} = \rho_1 \rho_2 . \tag{5.40}$$

Note that Equations (5.38) through (5.40) are based on the assumption that when the jammer is on is independent of which portion of the band is jammed. Substituting Equations (5.39) and (5.40) into Equation (5.38), the average probability of channel symbol error is given by

$$p_s = (1 - \rho_1 \rho_2) p_{s_0} + (\rho_1 \rho_2) p_{s_1} . \tag{5.41}$$

The probability of channel symbol error given that the single-pulse is not jammed is p_{s_0} and is upper-bounded by

$$p_{s_0} < \sum_{j=0}^{32} \zeta_{UB_j} \binom{32}{j} p_{c_0}^j \left(1 - p_{c_0}\right)^{32-j} , \tag{5.42}$$

where p_{c_0} is the probability of channel chip error given that the single-pulse is not jammed, which is given by Equation (5.22) and reproduced here for convenience:

$$p_{c_0} = Q\left(\sqrt{\frac{0.3125 r E_{b'}}{N_0}}\right). \tag{5.43}$$

Similarly, p_{s_1} is the probability of channel symbol error given that the single-pulse is jammed and is upper-bounded by

$$p_{s_1} < \sum_{j=0}^{32} \zeta_{UB_j} \binom{32}{j} p_{c_1}^j \left(1 - p_{c_1}\right)^{32-j} , \tag{5.44}$$

94

where p_{c_1} is the probability of channel chip error given that the single-pulse is jammed. From Equation (5.24), p_{c_1} is upper-bounded by

$$p_{c_1} < Q\left(\sqrt{\frac{0.3125 r E_{b'}}{N_0 + N_I/(\rho_1 \rho_2)}}\right) \tag{5.45}$$

since for PBNI the noise interference bandwidth may at times be only slightly larger than the hop bandwidth. Now, substituting Equations (5.42) through (5.45) along with ζ_{UB_j} from Table 7 into (5.41), we obtain the average probability of channel symbol error p_s. Next, substituting p_s into (5.15), we obtain the probability of symbol error for a JTIDS/Link-16-type waveform with the single-pulse structure in both AWGN and a combination of PNI and PBNI. Note that from (5.45), the effect of combined PNI and PBNI is to increase the noise PSD by $1/(\rho_1 \rho_2)$ in the bins that are jammed. For the single-pulse structure, the probability of symbol error for a JTIDS/Link-16-type waveform in both AWGN and combined PNI and PBNI is identical to that for a JTIDS/Link-16-type waveform in both AWGN and PNI if $\rho_1 \rho_2$ is replaced by ρ_1. Therefore, there is no need to regenerate performance plots for combined PNI and PBNI. Similarly, for the double-pulse structure, the probability of symbol error for a JTIDS/Link-16-type waveform without PSI in both AWGN and combined PNI and PBNI can be obtained from Figures 35 and 36 when ρ_1 is replaced by $\rho_1 \rho_2$.

F.   PERFORMANCE ANALYSIS IN BOTH AWGN AND NARROWBAND INTERFERENCE WHEN THE SIGNAL IS TRANSMITTED OVER A SLOW, FLAT NAKAGAMI FADING CHANNEL

In addition to both AWGN and narrowband interference, the probability of symbol error for a JTIDS/Link-16-type waveform transmitted over a fading channel is considered in this section. Since Nakagami fading channels encompass line-of-sight (LOS) fading channels as well as Rayleigh fading channels, and given the assumptions that the chip duration is less than the channel coherence time and that at a particular frequency hop the signal bandwidth is less than the channel coherence bandwidth, the channel is modeled as a slow, flat Nakagami fading channel.

1. Performance in AWGN and BNI When the Signal is Transmitted over a Slow, Flat Nakagami Fading Channel

The process of evaluating the performance of a JTIDS/Link-16-type waveform for the single-pulse structure in both AWGN and BNI when the signal is transmitted over a slow, flat Nakagami fading channel is similar to that for channels with no fading. The only difference is that Equation (5.18) with $L=1$ is now a conditional probability of channel chip error since the received signal amplitude a_c fluctuates and is modeled as a Nakagami-m random variable with a probability density function (pdf)

$$f_{A_C}(a_c) = \frac{2}{\Gamma(m)}\left(\frac{m}{\overline{a_c^2}}\right)^m a_c^{2m-1} \exp\left(\frac{-ma_c^2}{\overline{a_c^2}}\right), \quad a_c \geq 0, \tag{5.46}$$

where $\Gamma(\square)$ is the Gamma function, the parameter m is the fading figure, and $\overline{a_c^2}$ is the average power of the received signal. When $m<1$, the fading is more severe than Rayleigh fading; $m=1$ is Rayleigh fading. When $m>1$, there is a LOS component to the received signal, and when $m \to \infty$, there is no fading. Replacing $E_{b'}$ with $a_c^2 T_{b'}$ in Equation (5.18) with $L=1$, we get

$$p_c(a_c) = Q\left(\sqrt{\frac{0.3125 r a_c^2 T_{b'}}{N_0 + N_I}}\right), \tag{5.47}$$

where $T_{b'}$ is the bit duration per pulse. If

$$\gamma_T = \frac{a_c^2 T_{b'}}{N_0 + N_I}, \tag{5.48}$$

then Equation (5.47) can be rewritten as

$$p_c(\gamma_T) = Q\left(\sqrt{0.3125 r \gamma_T}\right). \tag{5.49}$$

The Nakagami-m pdf in terms of γ_T is obtained from

$$f_{\Gamma_T}(\gamma_T) = \left|\frac{da_c}{d\gamma_T}\right| f_{A_c}\left(a_c = \sqrt{\left(\frac{N_0 + N_I}{T_{b'}}\right)\gamma_T}\right). \tag{5.50}$$

Substituting Equation (5.46) into (5.50), we get

$$f_{\Gamma_T}(\gamma_T) = \frac{1}{\Gamma(m)}\left(\frac{m}{\overline{\gamma_T}}\right)^m \gamma_T^{m-1} \exp\left(\frac{-m\gamma_T}{\overline{\gamma_T}}\right), \quad \gamma_T \geq 0. \tag{5.51}$$

where

$$\overline{\gamma_T} = \frac{\overline{a_c^2}T_{b'}}{N_0 + N_I}. \tag{5.52}$$

The average probability of channel chip error of a JTIDS/Link-16-type waveform for the single-pulse structure in both AWGN and BNI when the signal is transmitted over a slow, flat Nakagami fading channel is obtained from

$$p_c = \int_0^\infty p_c(\gamma_T) f_{\Gamma_T}(\gamma_T) d\gamma_T. \tag{5.53}$$

Substituting Equations (5.49) and (5.51) into (5.53), the average probability of channel chip error is given by

$$p_c = \int_0^\infty Q\left(\sqrt{0.3125r\gamma_T}\right)\frac{1}{\Gamma(m)}\left(\frac{m}{\overline{\gamma_T}}\right)^m \gamma_T^{m-1} \exp\left(\frac{-m\gamma_T}{\overline{\gamma_T}}\right) d\gamma_T. \tag{5.54}$$

It has been shown that [45]

$$\begin{aligned}
&\int_0^\infty Q\left(\sqrt{2\gamma}\right)\frac{1}{\Gamma(L)}\left(\frac{L}{\overline{\gamma}}\right)^L \gamma^{L-1} \exp\left(\frac{-L\gamma}{\overline{\gamma}}\right) d\gamma \\
&= \left(\frac{1-\varsigma}{2}\right)^L \sum_{k=0}^{L-1}\binom{L-1+k}{k}\left(\frac{1+\varsigma}{2}\right)^k,
\end{aligned} \tag{5.55}$$

where $\varsigma = \sqrt{\overline{\gamma}/(L+\overline{\gamma})}$ and L is an integer. From Equation (5.55), when m is an integer, Equation (5.54) can be evaluated to obtain

$$p_c = \left(\frac{1-\alpha}{2}\right)^m \sum_{k=0}^{m-1}\binom{m-1+k}{k}\left(\frac{1+\alpha}{2}\right)^k, \tag{5.56}$$

where $\alpha = \sqrt{\overline{\gamma_1}/(m+\overline{\gamma_1})}$ and $\overline{\gamma_1} = 0.3125r\overline{\gamma_T}/2$.

Now, using Equation (5.56) with $r = 15/31$ in (5.13) along with ζ_{UB_j} from Table 7, we obtain the probability of channel symbol error p_s. Next, using p_s in (5.15), we obtain the probability of symbol error of a JTIDS/Link-16-type waveform for the single-pulse structure in both AWGN and BNI when the signal is transmitted over a slow, flat Nakagami fading channel. Recall that, for JTIDS, communications are LOS [2]; hence, the range of the fading figure is $1 < m < \infty$. The results are shown in Figure 39 and 40 where $E_{b'}/N_0 = 10\,\text{dB}$ and 15 dB, respectively. Note that in both figures, performance is evaluated for $1 \le m \le 30$, where $m = 1$ (Rayleigh fading) is only for purposes of comparison and $m = 30$ approaches no fading. As expected, when $m = 30$, the results of Figures 39 and 40 are virtually identical to those for no fading as shown in Figures 28 and 29, respectively. In Figure 39, where $E_{b'}/N_0 = 10\,\text{dB}$, at $P_S = 10^{-5}$, the $E_{b'}/N_I$ required when $m = 1$ is about 16.8 dB, the $E_{b'}/N_I$ required when $m = 2$ is about 12.5 dB, and the $E_{b'}/N_I$ required when $m = 30$ is about 10.3 dB.
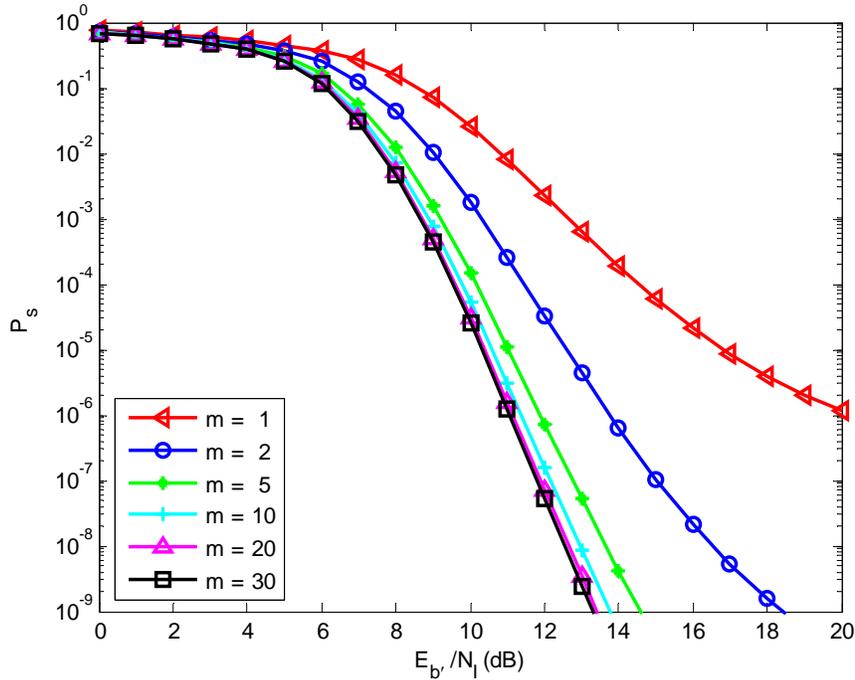
Figure 39.   Probability of symbol error of a JTIDS/Link-16-type waveform for the single-pulse structure in both AWGN and BNI when transmitted over a slow, flat Nakagami fading channel where $E_{b'}/N_0 = 10\,\text{dB}$.

In Figure 40, where $E_{b'}/N_0 = 15\,\text{dB}$, at $P_S = 10^{-5}$, the $E_{b'}/N_I$ required when $m = 1$ is about 10.5 dB, the $E_{b'}/N_I$ required when $m = 2$ is about 9.1 dB, and the $E_{b'}/N_I$ required when $m = 30$ is about 7.9 dB. In either case, performance for $m \geq 10$ is relatively insensitive to the value of m.
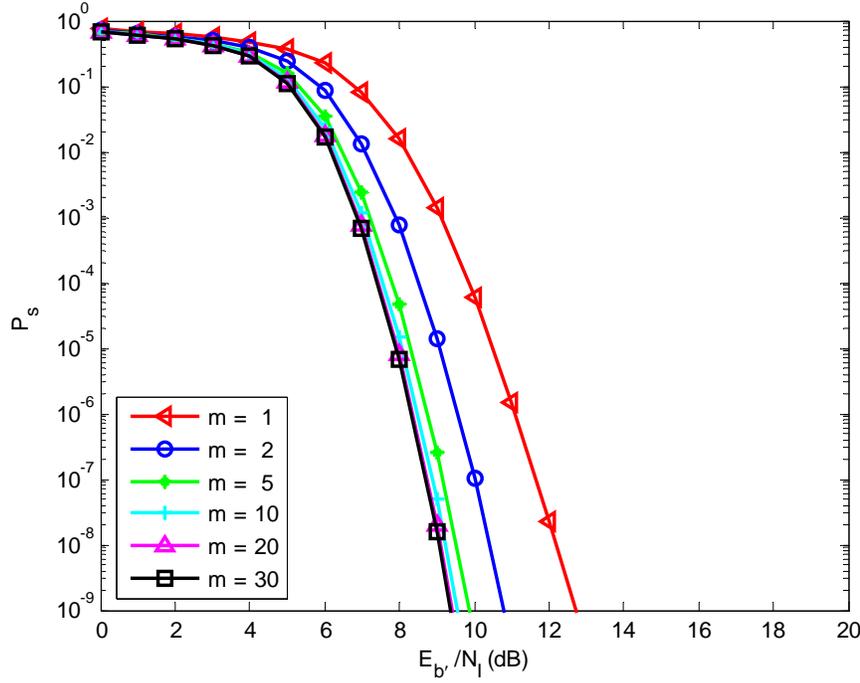

Figure 40.   Probability of symbol error of a JTIDS/Link-16-type waveform for the single-pulse structure in both AWGN and BNI when transmitted over a slow, flat Nakagami fading channel where $E_{b'}/N_0 = 15\,\text{dB}$.

When the double-pulse structure is chosen, the conditional probability of channel chip error of a JTIDS/Link-16-type waveform in both AWGN and BNI when the signal is transmitted over a slow, flat Nakagami fading channel is obtained from

$$p_c\left(a_{c_k}\right) = Q\left(\sqrt{\frac{0.3125r\sum_{k=1}^{2}a_{c_k}^2 T_{b'}}{N_0 + N_I}}\right),\tag{5.57}$$

where a_{c_k} are independent, identical distributed (iid) Nakagami random variables. If $\gamma_{T_k} \sqsubset a_{c_k}^2 T_{b'}/\left(N_0 + N_I\right)$, we can rewrite Equation (5.57) as

$$p_c\left(\gamma_{T_k}\right)=Q\left(\sqrt{0.3125r\sum_k\gamma_{T_k}}\right). \tag{5.58}$$

If $\gamma_T^* \square \sum_{k=1}^{2}\gamma_{T_k}$, then Equation (5.58) becomes

$$p_c\left(\gamma_T^*\right)=Q\left(\sqrt{0.3125r\gamma_T^*}\right), \tag{5.59}$$

and the pdf in terms of γ_T^* is given by

$$f_{\Gamma_T^*}\left(\gamma_T^*\right)=f_{\Gamma_{T_1}}\left(\gamma_{T_1}\right)\otimes f_{\Gamma_{T_2}}\left(\gamma_{T_2}\right), \tag{5.60}$$

where the symbol $\otimes$ denotes convolution, and $f_{\Gamma_{T_k}}\left(\gamma_{T_k}\right), k=1,2,$ is identical to $f_{\Gamma_T}\left(\gamma_T\right)$ that is shown in Equation (5.51). Instead of using convolution, Equation (5.60) can be solved by using the Laplace transform and then the inverse Laplace transform; that is,

$$F_{\Gamma_T^*}\left(s\right)=F_{\Gamma_T}\left(s\right)\times F_{\Gamma_T}\left(s\right)=\left[F_{\Gamma_T}\left(s\right)\right]^2, \tag{5.61}$$

where $F_{\Gamma_T}\left(s\right)$ is the Laplace transform of $f_{\Gamma_T}\left(\gamma_T\right)$. Since [46]

$$\mathcal{L}\left\{\frac{t^n e^{at}}{n!}\right\}=\frac{1}{\left(s-a\right)^{n+1}}, \tag{5.62}$$

where $n=1,2,3,...$, the Laplace transform of $f_{\Gamma_T}\left(\gamma_T\right)$, Equation (5.51), is given by

$$F_{\Gamma_T}\left(s\right)=\frac{1}{\left(\dfrac{\overline{\gamma_T}}{m}\right)^m\left(s+\dfrac{m}{\overline{\gamma_T}}\right)^m} \tag{5.63}$$

when m is an integer. Substituting Equation (5.63) into Equation (5.61), we get

$$F_{\Gamma_T^*}\left(s\right)=\frac{1}{\left(\dfrac{\overline{\gamma_T}}{m}\right)^{2m}\left(s+\dfrac{m}{\overline{\gamma_T}}\right)^{2m}}. \tag{5.64}$$

Next, using Equation (5.62), we obtain the inverse Laplace transform of Equation (5.64) as

$$f_{\Gamma_T^*}\left(\gamma_T^*\right)=\frac{1}{\Gamma(2m)}\left(\frac{m}{\overline{\gamma_T}}\right)^{2m}\left(\gamma_T^*\right)^{2m-1}\exp\left(\frac{-m\gamma_T^*}{\overline{\gamma_T}}\right),\quad \gamma_T^*\geq 0. \tag{5.65}$$

The average probability of channel chip error given that both pulses are affected by BNI is given by

$$p_c=\int_{-\infty}^{\infty}p_c\left(\gamma_T^*\right)f_{\Gamma_T^*}\left(\gamma_T^*\right)d\gamma_T^*. \tag{5.66}$$

Substituting Equations (5.59) and (5.65) into Equation (5.66), we obtain

$$p_c=\int_0^{\infty}Q\left(\sqrt{0.3125r\gamma_T^*}\right)\frac{\left(\gamma_T^*\right)^{2m-1}}{\Gamma(2m)}\left(\frac{m}{\overline{\gamma_T}}\right)^{2m}\exp\left(\frac{-m\gamma_T^*}{\overline{\gamma_T}}\right)d\gamma_T^*. \tag{5.67}$$

From Equation (5.55), when m is an integer, Equation (5.67) can be evaluated to obtain

$$p_c=\left(\frac{1-\beta}{2}\right)^{2m}\sum_{k=0}^{2m-1}\binom{2m-1+k}{k}\left(\frac{1+\beta}{2}\right)^k, \tag{5.68}$$

where $\beta=\sqrt{\overline{\gamma_2}/\left(2m+\overline{\gamma_2}\right)}$ and $\overline{\gamma_2}=0.3125r\overline{\gamma_T}$.

Now, substituting Equation (5.68) with $r=15/31$ into Equation (5.13) along with the values of ζ_{UB_j} from Table 7, we obtain the probability of channel symbol error p_s. Next, substituting p_s into Equation (5.15), we obtain the probability of symbol error of a JTIDS/Link-16-type waveform for the double-pulse structure in both AWGN and BNI when the signal is transmitted over a slow, flat Nakagami fading channel. To compare the difference between the single- and the double-pulse structure, both results are shown in Figures 41 and 42 where $E_{b'}/N_0=10$ dB and 15 dB, respectively. As expected, when $m=30$, the results for the double-pulse structure shown in both Figures 41 and 42 are virtually identical to those obtained for no fading that were shown in Figures 31 and 32, respectively. The $E_{b'}/N_I$ required for $P_s=10^{-5}$ for a JTIDS/Link-16-type waveform with the single- and the double-pulse structure in both AWGN and BNI when the signal is transmitted over a slow, flat Nakagami fading channel are summarized in Table 10.
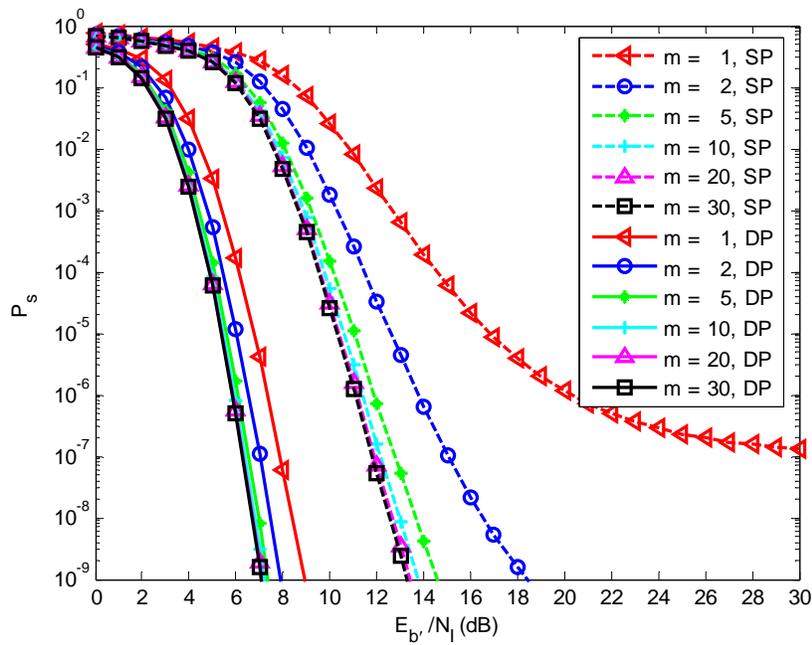
Figure 41.   Probability of symbol error of a JTIDS/Link-16-type waveform in both AWGN and BNI when the signal is transmitted over a slow, flat Nakagami fading channel where $E_{b'}/N_0 = 10$ dB: single-versus double-pulse structure.
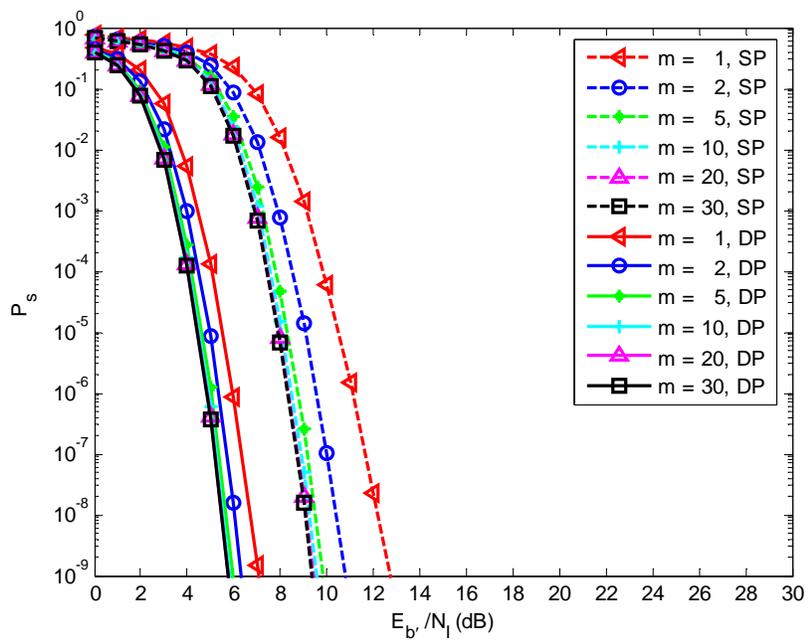
Figure 42.   Probability of symbol error of a JTIDS/Link-16-type waveform in both AWGN and BNI when the signal is transmitted over a slow, flat Nakagami fading channel where $E_{b'}/N_0 = 15$ dB: single-versus double-pulse structure.

Several observations are summarized from Table 10. First, when $P_s = 10^{-5}$, the double-pulse structure outperforms the single-pulse structure for a fixed $E_{b'}/N_0$, whether the channel is fading or not. Second, the double-pulse structure outperforms the single-pulse structure, but the superiority increases as the value of m decreases for a fixed $E_{b'}/N_0$. This is consistent with our intuition that the robustness of the double-pulse structure enhances performance more when the channel is strongly faded. Third, the double-pulse structure outperforms the single-pulse structure, but the superiority decreases as $E_{b'}/N_0$ increases for a fixed value of m. This is consistent with our intuition that a stronger signal benefits less from the robustness of the double-pulse structure. Lastly, the single-pulse structure is very sensitive to m, while the double-pulse structure is relatively insensitive to m. This is consistent with our intuition that the single-pulse structure is less robust and therefore suffers more as fading worsens.

Table 10. Required $E_{b'}/N_I$ when $P_s = 10^{-5}$ for a JTIDS/Link-16-type waveform with the single- and the double-pulse structure in both AWGN and BNI when the signal is transmitted over a slow, flat Nakagami fading channel.

m	SP/DP	$E_{b'}/N_0 = 10$ dB	$E_{b'}/N_0 = 15$ dB
1	SP	16.8 dB	10.4 dB
1	DP	6.8 dB	5.5 dB
2	SP	12.6 dB	9.1 dB
2	DP	6.0 dB	5.0 dB
30	SP	10.3 dB	7.9 dB
30	DP	5.3 dB	4.4 dB

2. Performance in AWGN and PNI When the Signal is Transmitted over a Slow, Flat Nakagami Fading Channel

The process of investigating the performance of a JTIDS/Link-16-type waveform for the single-pulse structure in both AWGN and PNI transmitted over a slow, flat

Nakagami fading channel is similar to that for channels with no fading. The only difference is that Equations (5.22) and (5.24) are now conditional probabilities of channel chip error. Replacing $E_{b'}$ with $a_c^2 T_{b'}$ in Equations (5.22) and (5.24), we obtain

$$p_{c_0}(a_c) = Q\left(\sqrt{\frac{0.3125 r a_c^2 T_{b'}}{N_0}}\right), \tag{5.69}$$

and

$$p_{c_1}(a_c) = Q\left(\sqrt{\frac{0.3125 r a_c^2 T_{b'}}{N_0 + N_I/\rho_1}}\right), \tag{5.70}$$

where $0 < \rho_1 \leq 1$ represents the fraction of time the PNI is on. If $\gamma_b = a_c^2 T_{b'}/N_0$, then Equation (5.69) can be rewritten as

$$p_{c_0}(\gamma_b) = Q\left(\sqrt{0.3125 r \gamma_b}\right). \tag{5.71}$$

The pdf in terms of γ_b is obtained from

$$f_{\Gamma_b}(\gamma_b) = \left|\frac{da_c}{d\gamma_b}\right| f_{A_c}\left(a_c = \sqrt{\frac{N_0}{T_{b'}}\gamma_b}\right). \tag{5.72}$$

Substituting Equation (5.46) into (5.72), we get,

$$f_{\Gamma_b}(\gamma_b) = \frac{1}{\Gamma(m)}\left(\frac{m}{\overline{\gamma_b}}\right)^m \gamma_b^{m-1} \exp\left(\frac{-m\gamma_b}{\overline{\gamma_b}}\right), \quad \gamma_b \geq 0, \tag{5.73}$$

where $\overline{\gamma_b} = \overline{a_c^2} T_{b'}/N_0$ is the ratio of the average energy per bit per pulse-to-noise power spectral density. If $\gamma_P = a_c^2 T_{b'}/\left[N_0 + (N_I/\rho_1)\right]$, then (5.70) can be rewritten as

$$p_{c_1}(\gamma_P) = Q\left(\sqrt{0.3125 r \gamma_P}\right). \tag{5.74}$$

The pdf in terms of γ_P is obtained from

$$f_{\Gamma_P}(\gamma_P) = \left|\frac{da_c}{d\gamma_P}\right| f_{A_c}\left(a_c = \sqrt{\left(\frac{N_0 + N_I/\rho_1}{T_{b'}}\right)\gamma_P}\right). \tag{5.75}$$

104

Substituting Equation (5.46) into (5.75), we get,

$$f_{\Gamma_P}(\gamma_P) = \frac{1}{\Gamma(m)}\left(\frac{m}{\overline{\gamma_P}}\right)^m \gamma_P^{m-1}\exp\left(\frac{-m\gamma_P}{\overline{\gamma_P}}\right), \quad \gamma_P \geq 0. \tag{5.76}$$

where $\overline{\gamma_P} = \overline{a_c^2 T_{b'}}\big/\big[N_0 + (N_I/\rho_1)\big]$.

The average probability of channel chip error when the PNI is off is

$$p_{c_0} = \int_{-\infty}^{\infty} p_{c_0}(\gamma_b) f_{\Gamma_b}(\gamma_b) d\gamma_b. \tag{5.77}$$

Substituting Equations (5.71) and (5.73) into (5.77), we obtain the average probability of channel chip error when the PNI is off as

$$p_{c_0} = \int_0^{\infty} Q\left(\sqrt{0.3125r\gamma_b}\right)\frac{1}{\Gamma(m)}\left(\frac{m}{\overline{\gamma_b}}\right)^m \gamma_b^{m-1}\exp\left(\frac{-m\gamma_b}{\overline{\gamma_b}}\right)d\gamma_b. \tag{5.78}$$

From Equation (5.55), when m is an integer, Equation (5.78) can be evaluated to obtain

$$p_{c_0} = \left(\frac{1-\mu}{2}\right)^m \sum_{k=0}^{m-1}\binom{m-1+k}{k}\left(\frac{1+\mu}{2}\right)^k, \tag{5.79}$$

where $\mu = \sqrt{\overline{\gamma_3}\big/(m+\overline{\gamma_3})}$ and $\overline{\gamma_3} = 0.3125r\overline{\gamma_b}/2$. The average probability of channel chip error when the PNI is on is obtained from

$$p_{c_1} = \int_{-\infty}^{\infty} p_{c_1}(\gamma_P) f_{\Gamma_P}(\gamma_P) d\gamma_P. \tag{5.80}$$

Substituting Equations (5.74) and (5.76) into (5.80), we obtain the average probability of channel chip error when the PNI is on as

$$p_{c_1} = \int_0^{\infty} Q\left(\sqrt{0.3125r\gamma_P}\right)\frac{1}{\Gamma(m)}\left(\frac{m}{\overline{\gamma_P}}\right)^m \gamma_P^{m-1}\exp\left(\frac{-m\gamma_P}{\overline{\gamma_P}}\right)d\gamma_P. \tag{5.81}$$

From Equation (5.55), when m is an integer, Equation (5.81) can be evaluated to obtain

$$p_{c_1} = \left(\frac{1-v}{2}\right)^m \sum_{k=0}^{m-1}\binom{m-1+k}{k}\left(\frac{1+v}{2}\right)^k, \tag{5.82}$$

where $v = \sqrt{\overline{\gamma_4}\big/(m+\overline{\gamma_4})}$ and $\overline{\gamma_4} = 0.3125r\overline{\gamma_P}/2$.

105

Now, substituting Equation (5.79) with $r = 15/31$ into Equation (5.25) along with the values of ζ_{UB_j} from Table 7, we obtain the probability of channel symbol error given that the PNI is off p_{s_0}. Similarly, substituting Equation (5.82) with $r = 15/31$ into (5.26) along with the values of ζ_{UB_j} from Table 7, we obtain the probability of channel symbol error given that the PNI is on p_{s_1}. Next, substituting p_{s_0} and p_{s_1} into Equation (5.20), we obtain the average probability of channel symbol error p_s. Finally, using the average probability of channel symbol error p_s in Equation (5.15), we obtain the probability of symbol error of a JTIDS/Link-16-type waveform for the single-pulse structure in both AWGN and PNI when the signal is transmitted over a slow, flat Nakagami fading channel. The results are shown in Figures 43 to 48 and summarized in Table 11 for different values of m, ρ_1, and $E_{b'}/N_0$.

From Figures 43 to 48, several observations can be made. First, as expected, when $m = 30$, the results of Figures 43 and 44 are virtually identical to those for no fading shown in Figures 33 and 34, respectively. Second, as expected, when both ρ_1 and $E_{b'}/N_0$ are fixed, performance improves as m increases. For example, for $\rho_1 = 0.5$ and $E_{b'}/N_0 = 10 \, \text{dB}$, the required $E_{b'}/N_I$ at $P_S = 10^{-5}$ is 13.4 dB when $m = 2$, while the required $E_{b'}/N_I$ at $P_S = 10^{-5}$ is 11.5 dB when $m = 30$. Lastly, the value of ρ_1 that maximizes the probability of symbol error decreases as $E_{b'}/N_I$ increases, whether m is large or small. In other words, barrage noise interference ($\rho_1 = 1$) has the most effect in degrading performance when $E_{b'}/N_I$ is small. When $E_{b'}/N_I$ is large, PNI with a smaller value of ρ_1 causes the greatest degradation. For example, when $m = 2$ and $E_{b'}/N_0$ is 10 dB, $\rho_1 = 1$ has the most effect in degrading performance when $E_{b'}/N_I$ is less than 7 dB, while $\rho_1 = 0.1$ causes the greatest degradation when $E_{b'}/N_I$ is greater than 15 dB. Similar results are seen when m is large. This is consistent with our intuition that, for strong signals, the jammer power must be large during a symbol in order to make a symbol error likely.

106
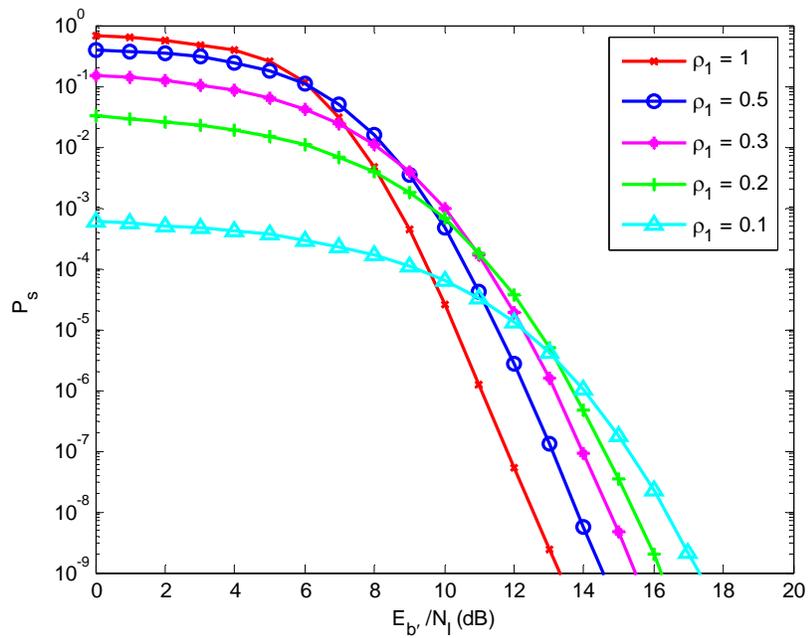
Figure 43.   Probability of symbol error of a JTIDS/Link-16-type waveform for the single-pulse structure in both AWGN and PNI transmitted over a slow, flat Nakagami fading channel where $m = 30$ and $E_{b'}/N_0 = 10$ dB.
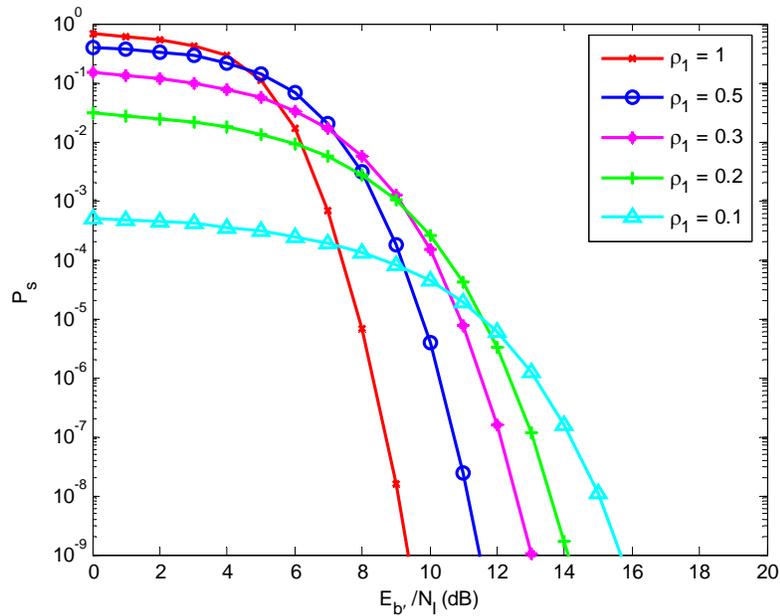
Figure 44.   Probability of symbol error of a JTIDS/Link-16-type waveform for the single-pulse structure in both AWGN and PNI transmitted over a slow, flat Nakagami fading channel where $m = 30$ and $E_{b'}/N_0 = 15$ dB.
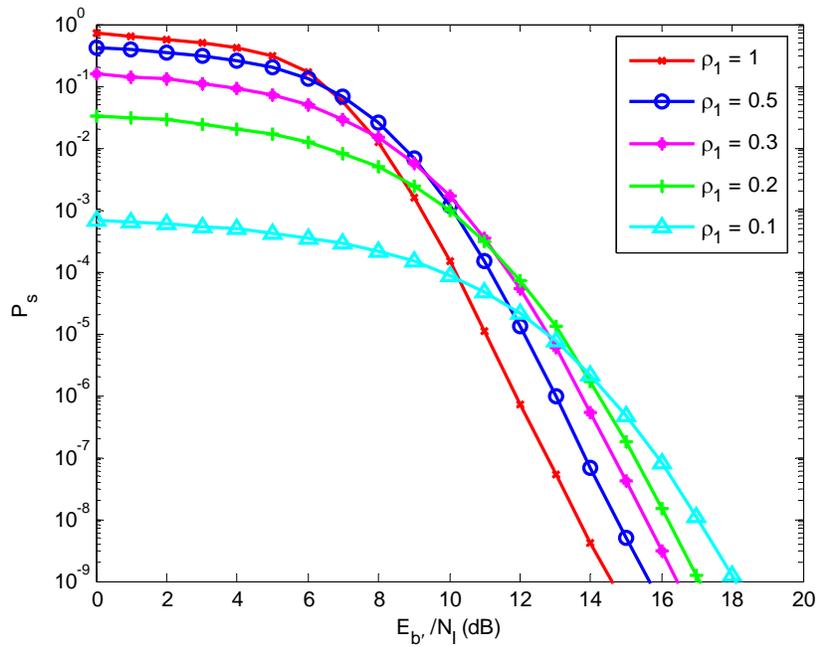
Figure 45.   Probability of symbol error of a JTIDS/Link-16-type waveform for the single-pulse structure in both AWGN and PNI transmitted over a slow, flat Nakagami fading channel where $m = 5$ and $E_{b'}/N_0 = 10\,\text{dB}$.
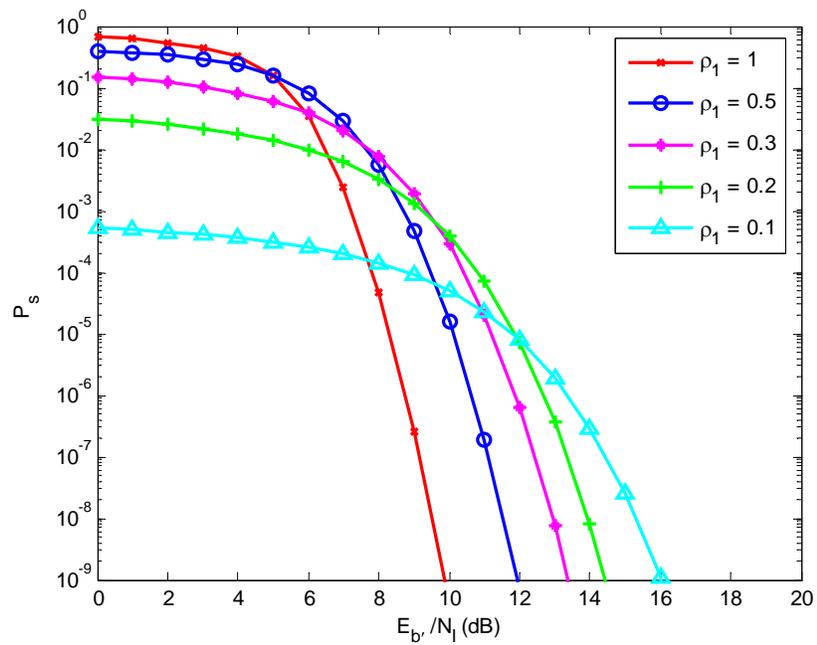
Figure 46.   Probability of symbol error of a JTIDS/Link-16-type waveform for the single-pulse structure in both AWGN and PNI transmitted over a slow, flat Nakagami fading channel where $m = 5$ and $E_{b'}/N_0 = 15\,\text{dB}$.
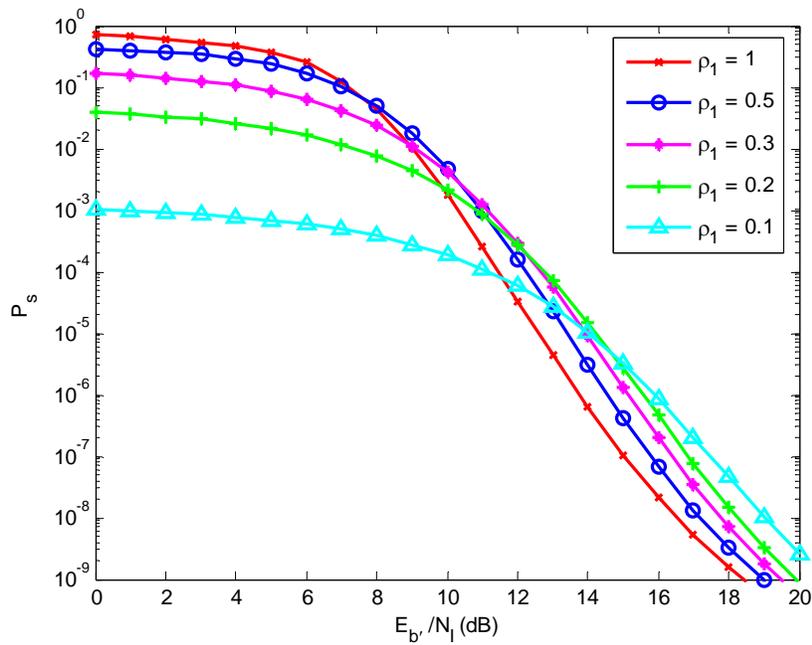
Figure 47.   Probability of symbol error of a JTIDS/Link-16-type waveform for the single-pulse structure in both AWGN and PNI transmitted over a slow, flat Nakagami fading channel where $m = 2$ and $E_{b'}/N_0 = 10\,\text{dB}$.
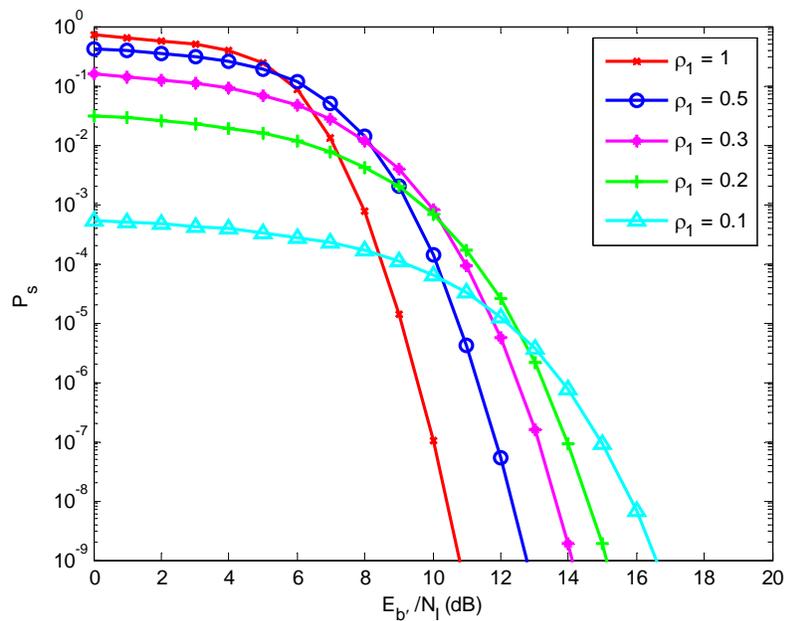
Figure 48.   Probability of symbol error of a JTIDS/Link-16-type waveform for the single-pulse structure in both AWGN and PNI transmitted over a slow, flat Nakagami fading channel where $m = 2$ and $E_{b'}/N_0 = 15\,\text{dB}$.

Table 11.   Required $E_{b'}/N_I$ in dB when $P_s = 10^{-5}$ for a JTIDS/Link-16-type waveform with the single-pulse structure in both AWGN and PNI when the signal is transmitted over a slow, flat Nakagami fading channel.

| m	$E_{b'}/N_0$ (dB)	$\rho_1 = 1$	$\rho_1 = 0.5$	$\rho_1 = 0.3$	$\rho_1 = 0.2$	$\rho_1 = 0.1$
30	10	10.3	11.5	12.3	12.7	12.3
	15	7.9	9.8	10.9	11.5	11.5
5	10	11.0	12.1	12.8	13.2	12.7
	15	8.3	10.1	11.2	11.9	11.9
2	10	12.6	13.4	13.9	14.2	13.9
	15	9.0	10.7	11.7	12.3	12.2

The process of investigating the performance of a JTIDS/Link-16-type waveform for the double-pulse structure in AWGN and PNI when the signal is transmitted over a slow, flat Nakagami fading channel is different from that for channels with no fading. In this case, we assume maximal-ratio detection with linear combining [47]. It is well known that this type of receiver is equivalent to maximum-likelihood detection when only AWGN is present. For maximal-ratio detection with linear combining when both AWGN and PNI are present, Equation (5.29) must be modified as

$$p_{c_\ell}\left(a_{c_k}\right) = Q\left(\sqrt{\frac{0.3125r\left(\sum_{k=1}^{L} a_{c_k}^2\right)^2 T_{b'}}{N_0\left(\sum_{k=1}^{L} a_{c_k}^2\right)+\left(N_I/\rho_1\right)\sum_{k=1}^{\ell} a_{c_k}^2}}\right), \tag{5.83}$$

where a_{c_k} are iid Nakagami random variables. When $L = 2$ and $\ell = 0$, (5.83) becomes

$$p_{c_0}\left(a_{c_k}\right) = Q\left(\sqrt{\frac{0.3125r\sum_{k=1}^{2} a_{c_k}^2 T_{b'}}{N_0}}\right). \tag{5.84}$$

110

When $L = 2$ and $\ell = 1$, Equation (5.83) reduces to

$$p_{c_1}\left(a_{c_k}\right) = Q\left(\sqrt{\frac{0.3125r\left(\sum_{k=1}^{2}a_{c_k}^2\right)^2 T_{b'}}{N_0\left(a_{c_1}^2 + a_{c_2}^2\right) + \left(N_I/\rho_1\right)a_{c_m}^2}}\right),$$ (5.85)

where $m = 1$ or 2. Finally, when $L = 2$ and $\ell = 2$, Equation (5.83) simplifies to

$$p_{c_2}\left(a_{c_k}\right) = Q\left(\sqrt{\frac{0.3125r\sum_{k=1}^{2}a_{c_k}^2 T_{b'}}{N_0 + \left(N_I/\rho_1\right)}}\right).$$ (5.86)

If $\gamma_{b_k} \Box a_{c_k}^2 T_{b'}/N_0$ and $\gamma_b^* \Box \sum_k \gamma_{b_k}$, $k = 1, 2$, Equation (5.84) can be rewritten as

$$p_{c_0}\left(\gamma_b^*\right) = Q\left(\sqrt{0.3125r\gamma_b^*}\right).$$ (5.87)

From Equations (5.60) to (5.64), the pdf in terms of γ_b^* is given by

$$f_{\Gamma_b^*}\left(\gamma_b^*\right) = \frac{1}{\Gamma(2m)}\left(\frac{m}{\overline{\gamma_b}}\right)^{2m}\left(\gamma_b^*\right)^{2m-1}\exp\left(\frac{-m\gamma_b^*}{\overline{\gamma_b}}\right), \quad \gamma_b^* \geq 0,$$ (5.88)

where $\overline{\gamma_b} \Box \overline{a_c^2}T_{b'}/N_0$. The average probability of channel chip error given that neither pulse is jammed is obtained from

$$p_{c_0} = \int_{-\infty}^{\infty} p_{c_0}\left(\gamma_b^*\right)f_{\Gamma_b^*}\left(\gamma_b^*\right)d\gamma_b^*.$$ (5.89)

Substituting Equations (5.87) and (5.88) into (5.89), we obtain the average probability of channel chip error given that neither pulse is jammed as

$$p_{c_0} = \int_0^{\infty} Q\left(\sqrt{0.3125r\gamma_b^*}\right)\frac{1}{\Gamma(2m)}\left(\frac{m}{\overline{\gamma_b}}\right)^{2m}\left(\gamma_b^*\right)^{2m-1}\exp\left(\frac{-m\gamma_b^*}{\overline{\gamma_b}}\right)d\gamma_b^*.$$ (5.90)

From Equation (5.55), when m is an integer, Equation (5.90) can be evaluated to obtain

$$p_{c_0} = \left(\frac{1-\omega}{2}\right)^{2m}\sum_{k=0}^{2m-1}\binom{2m-1+k}{k}\left(\frac{1+\omega}{2}\right)^k,$$ (5.91)

111

where $\omega = \sqrt{\overline{\gamma_5}/(2m+\overline{\gamma_5})}$ and $\overline{\gamma_5} = 0.3125r\overline{\gamma_b}$. Similarly, (5.86) can be rewritten as

$$p_{c_2}\left(\gamma_{T2}^*\right) = Q\left(\sqrt{0.3125r\gamma_{T2}^*}\right), \tag{5.92}$$

where $\gamma_{T2}^* \ \square \ \sum_k \gamma_{p_k}$, $k = 1, 2$, and $\gamma_{p_k} \ \square \ a_{c_k}^2 \ T_{b'}\big/\left[N_0 + \left(N_I/\rho_1\right)\right]$. From Equations (5.60) to (5.64), the pdf in terms of γ_{T2}^* is given by

$$f_{\Gamma_{T2}^*}\left(\gamma_{T2}^*\right) = \frac{1}{\Gamma(2m)}\left(\frac{m}{\overline{\gamma_p}}\right)^{2m} \left(\gamma_{T2}^*\right)^{2m-1} \exp\left(\frac{-m\gamma_{T2}^*}{\overline{\gamma_p}}\right), \quad \gamma_{T2}^* \geq 0, \tag{5.93}$$

where $\overline{\gamma_p} \ \square \ \overline{a_c^2}T_{b'}\big/\left[N_0 + \left(N_I/\rho_1\right)\right]$. The average probability of channel chip error given that both pulses are jammed is obtained from

$$p_{c_2} = \int_{-\infty}^{\infty} p_{c_2}\left(\gamma_{T2}^*\right) f_{\Gamma_{T2}^*}\left(\gamma_{T2}^*\right) d\gamma_{T2}^*. \tag{5.94}$$

Substituting Equations (5.92) and (5.93) into (5.94), we obtain the average probability of channel chip error given that both pulses are jammed as

$$p_{c_2} = \int_0^{\infty} Q\left(\sqrt{0.3125r\gamma_{T2}^*}\right)\frac{1}{\Gamma(2m)}\left(\frac{m}{\overline{\gamma_p}}\right)^{2m} \left(\gamma_{T2}^*\right)^{2m-1} \exp\left(\frac{-m\gamma_{T2}^*}{\overline{\gamma_p}}\right) d\gamma_{T2}^*. \tag{5.95}$$

From Equation (5.55), when m is an integer, Equation (5.95) can be evaluated to obtain

$$p_{c_2} = \left(\frac{1-\psi}{2}\right)^{2m} \sum_{k=0}^{2m-1}\binom{2m-1+k}{k}\left(\frac{1+\psi}{2}\right)^k, \tag{5.96}$$

where $\psi = \sqrt{\overline{\gamma_6}/(2m+\overline{\gamma_6})}$ and $\overline{\gamma_6} = 0.3125r\overline{\gamma_p}$.

Unfortunately, an analytic expression for p_{c_1}, the average probability of channel chip error given that one pulse is jammed, is extremely complex since its associated pdf is difficult to obtain. Therefore, the probability of symbol error of a JTIDS/Link-16-type waveform for the double-pulse structure in both AWGN and PNI when the signal is transmitted over a slow, flat Nakagami fading channel is not evaluated. Similarly, the probability of symbol error for a JTIDS/Link-16-type waveform for the double-pulse

112

structure in both AWGN and combined PNI and PBNI when transmitted over a slow, flat Nakagami fading channel is not investigated. However, if PSI is assumed, an analytic expression for p_{c_1} can be found. This is discussed in the next sub-section.

3.   Performance in AWGN and PNI When the Signal is Transmitted over a Slow, Flat Nakagami Fading Channel with Perfect Side Information

As discussed earlier, for the double-pulse structure in both AWGN and PNI with no fading, the probability of channel chip error given that neither pulse is jammed and the probability of channel chip error given that both pulses are jammed are given in Equations (5.32) and (5.36), respectively, whether PSI is assumed or not. When PSI is assumed, the probability of channel chip error given that one pulse is jammed is given in Equation (5.37) instead of (5.34) since we ignore the pulse that is jammed. When the signal is transmitted over a slow, flat Nakagami fading channel, Equations (5.32) and (5.36) are replaced by Equations (5.91) and (5.96), respectively, whether PSI is assumed or not. When the signal is transmitted over a slow, flat Nakagami fading channel and PSI is assumed, Equation (5.37), the conditional probability of channel chip error given that one pulse is jammed becomes

$$p_{c_1}(a_c) = Q\left(\sqrt{\frac{0.3125 r a_c^2 T_{b'}}{N_0}}\right). \tag{5.97}$$

Note that the right hand side of Equation (5.97) is the same as Equation (5.69); therefore, the average probability of channel chip error given that one pulse is jammed can be obtained from Equation (5.79) if m is an integer; that is,

$$p_{c_1} = \left(\frac{1-\xi}{2}\right)^m \sum_{k=0}^{m-1} \binom{m-1+k}{k}\left(\frac{1+\xi}{2}\right)^k, \tag{5.98}$$

where $\xi = \sqrt{\overline{\gamma_7}/\left(m+\overline{\gamma_7}\right)}$ and $\overline{\gamma_7} = 0.3125 r \overline{\gamma_b}/2$.

Now, using Equation (5.91) with $r = 15/31$ in Equation (5.31) along with ζ_{UB_j} from Table 7, we obtain the probability of channel symbol error given that neither pulse is jammed p_{s_0}. Using Equation (5.98) with $r = 15/31$ in Equation (5.33) along with ζ_{UB_j}

113

from Table 7, we obtain the probability of channel symbol error given that either pulse is jammed p_{s_1}. Finally, using Equation (5.96) with $r = 15/31$ in Equation (5.35) along with ζ_{UB_j} from Table 7, we obtain probability of channel symbol error given that both pulses are jammed p_{s_2}. Next, using p_{s_0}, p_{s_1}, and p_{s_2} in Equation (5.30), we obtain the average probability of channel symbol error p_s. Finally, using p_s in Equation (5.15), we obtain the probability of symbol error of a JTIDS/Link-16-type waveform for the double-pulse structure with PSI in both AWGN and PNI when the signal is transmitted over a slow, flat Nakagami fading channel. The results are shown in Figures 49 to 54 for different values of m, ρ_1, and $E_{b'}/N_0$.

From Figures 49 to 54, several observations can be made. First, for a fixed $E_{b'}/N_0$, the double-pulse structure with PSI outperforms the single-pulse structure by a greater margin for smaller m. For example, for $\rho_1 = 0.5$ in Figure 49, where $m = 30$, the double-pulse structure with PSI outperforms the single-pulse structure by 6.0 dB at $P_S = 10^{-5}$, while for $\rho_1 = 0.5$ in Figure 53, where $m = 2$, the double-pulse structure with PSI outperforms the single-pulse structure by 7.2 dB at $P_S = 10^{-5}$. Second, for a fixed m, the double-pulse structure with PSI outperforms the single-pulse structure by a smaller margin as $E_{b'}/N_0$ increases. For example, in Figure 53, where $m = 2$ and $E_{b'}/N_0$ is 10 dB, the double-pulse structure with PSI outperforms the single-pulse structure by 7.2 dB for $\rho_1 = 0.5$ at $P_S = 10^{-5}$, while in Figure 54, where $m = 2$ and $E_{b'}/N_0 = 15$ dB, the double-pulse structure with PSI outperforms the single-pulse structure by 5.4 dB for $\rho_1 = 0.5$ at $P_S = 10^{-5}$. Lastly, for the single-pulse structure, the value of ρ_1 that maximizes the probability of symbol error decreases as $E_{b'}/N_I$ increases, but for the double-pulse structure with PSI this is not the case. However, it can be inferred from either Figure 35 or Figure 36 that the value of ρ_1 that maximizes the probability of symbol error decreases as $E_{b'}/N_I$ increases for the double-pulse structure without PSI when the signal is transmitted over a slow, flat Nakagami fading channel.
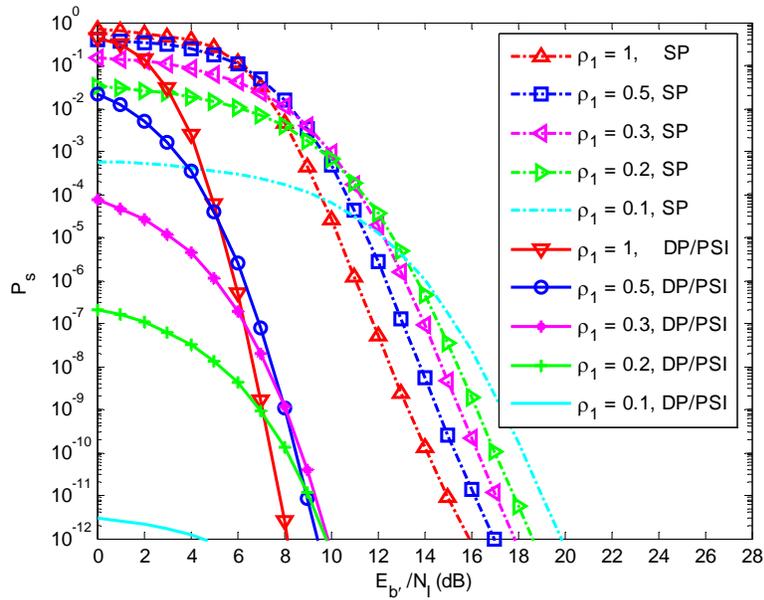
Figure 49. Probability of symbol error of a JTIDS/Link-16-type waveform in both AWGN and PNI transmitted over a slow, flat Nakagami fading channel where $m = 30$ and $E_{b'}/N_0 = 10$ dB: double-pulse structure with perfect side information versus single-pulse structure.
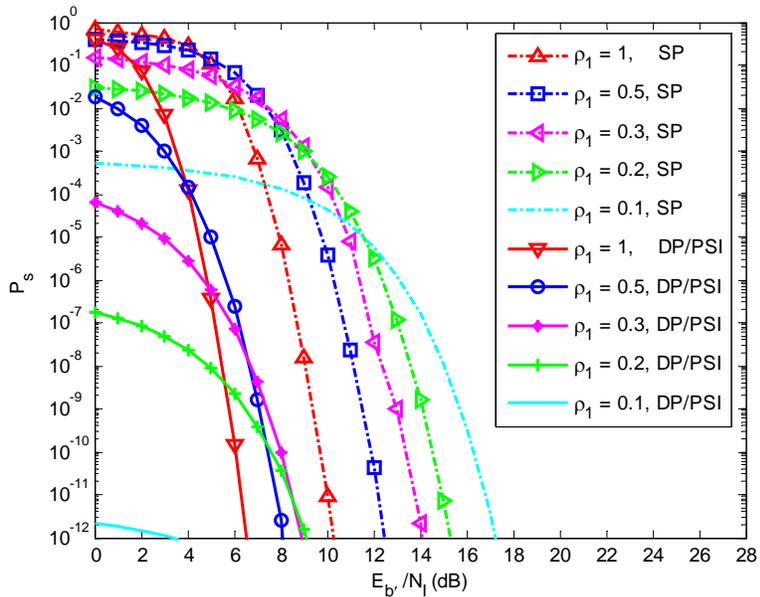
Figure 50. Probability of symbol error of a JTIDS/Link-16-type waveform in both AWGN and PNI transmitted over a slow, flat Nakagami fading channel where $m = 30$ and $E_{b'}/N_0 = 15$ dB: double-pulse structure with perfect side information versus single-pulse structure.

115
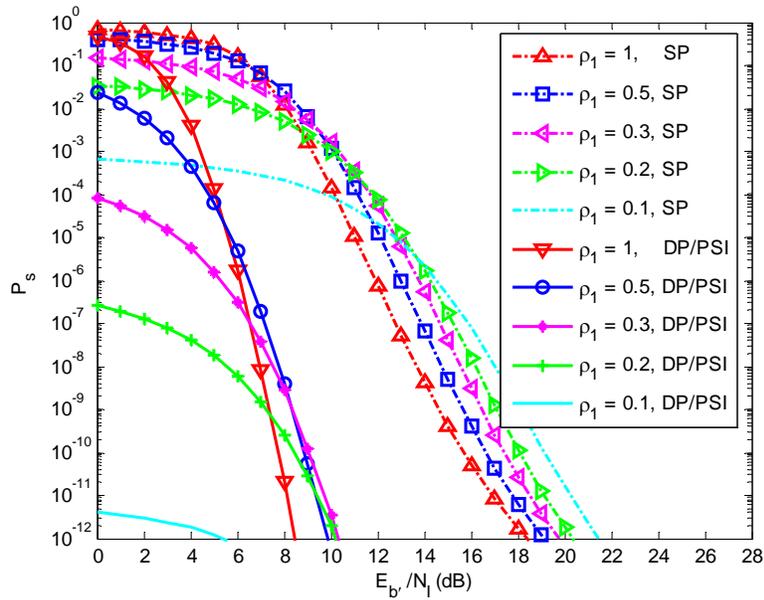
Figure 51. Probability of symbol error of a JTIDS/Link-16-type waveform in both AWGN and PNI transmitted over a slow, flat Nakagami fading channel where $m = 5$ and $E_{b'}/N_0 = 10\,\text{dB}$: double-pulse structure with perfect side information versus single-pulse structure.
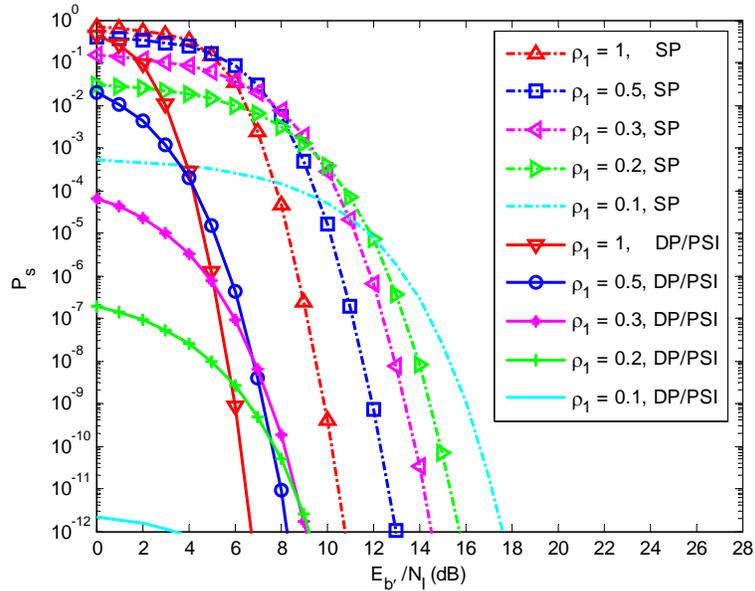
Figure 52. Probability of symbol error of a JTIDS/Link-16-type waveform in both AWGN and PNI transmitted over a slow, flat Nakagami fading channel where $m = 5$ and $E_{b'}/N_0 = 15\,\text{dB}$: double-pulse structure with perfect side information versus single-pulse structure.

116
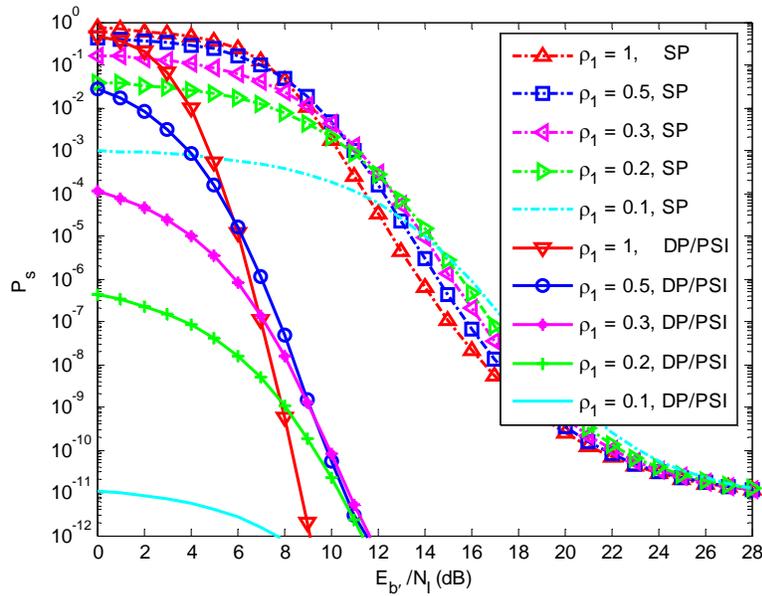
Figure 53.   Probability of symbol error of a JTIDS/Link-16-type waveform in both AWGN and PNI transmitted over a slow, flat Nakagami fading channel where $m = 2$ and $E_{b'}/N_0 = 10$ dB: double-pulse structure with perfect side information versus single-pulse structure.
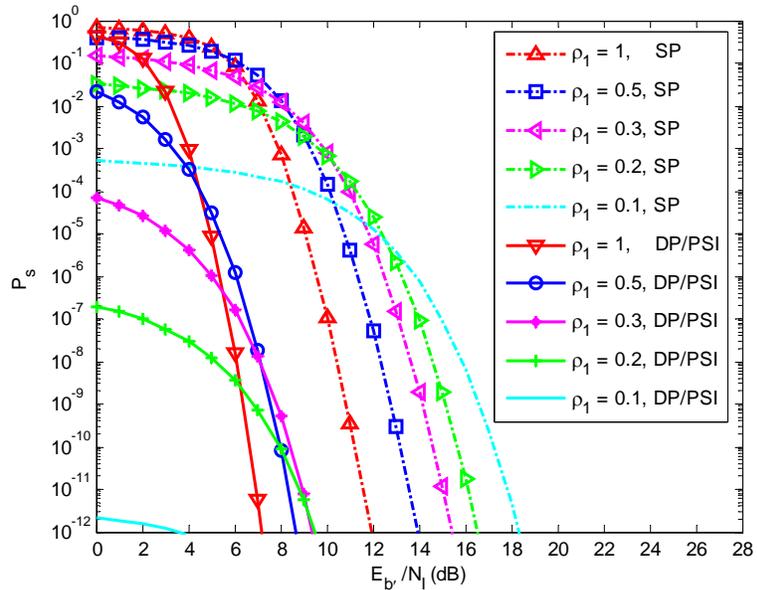
Figure 54.   Probability of symbol error of a JTIDS/Link-16-type waveform in both AWGN and PNI transmitted over a slow, flat Nakagami fading channel where $m = 2$ and $E_{b'}/N_0 = 15$ dB: double-pulse structure with perfect side information versus single-pulse structure.

117

G.   SUMMARY OF CHAPTER V

In this chapter, the probability of symbol error for a JTIDS/Link-16-type waveform was investigated. The evaluation was divided into three major sections: Section D, E, and F. In Section D, the probability of symbol error of a JTIDS/Link-16-type waveform in AWGN for both the single- and the double-pulse structure was evaluated. The results show that, in AWGN, the $E_{b'}/N_0$ required for the single-pulse structure is about 7.1 dB at $P_S = 10^{-5}$, while the $E_{b'}/N_0$ required for the double-pulse structure is about 4 dB at $P_S = 10^{-5}$; that is, in AWGN the double-pulse structure outperforms the single-pulse structure by 3.1 dB at $P_S = 10^{-5}$. In Section E, the probability of symbol error of a JTIDS/Link-16-type waveform in both AWGN and narrowband interference for both the single- and the double-pulse structure was evaluated. Three types of narrowband interference, BNI, PNI, and combined PNI and PBNI, were considered.

When the signal is subjected to both AWGN and BNI, the results show that the $E_{b'}/N_I$ required for the single-pulse structure is 10.2 dB at $P_S = 10^{-5}$ given that $E_{b'}/N_0 = 10\,\text{dB}$, while the $E_{b'}/N_I$ required for the double-pulse structure is 5.2 dB at $P_S = 10^{-5}$; that is, in both AWGN and BNI, the double-pulse structure outperforms the single-pulse structure in terms of $E_{b'}/N_0$ by 5 dB at $P_S = 10^{-5}$ when $E_{b'}/N_0 = 10\,\text{dB}$. When $E_{b'}/N_0$ is increased to 15 dB, the double-pulse structure still outperforms the single-pulse structure but with a smaller margin (a decrease of 1.6 dB) at $P_S = 10^{-5}$. This is consistent with our intuition that a stronger signal benefits less from the added robustness of the double-pulse structure.

Several conclusions can be drawn when the signal is subjected to both AWGN and PNI. First, for both the single- and the double-pulse structure, the value of ρ_1 that maximizes the probability of symbol error decreases as $E_{b'}/N_I$ increases. In other words, $\rho_1 = 1$ has the most effect in degrading performance when $E_{b'}/N_I$ is relatively small, while $\rho_1 = 0.1$ causes the greatest degradation when $E_{b'}/N_I$ is relatively large. This is

consistent with our intuition that, for strong signals, the jammer power must be large during a symbol in order to make a symbol error likely. Second, when $E_{b'}/N_I$ is relatively large (such as 10 dB), the double-pulse structure always outperforms the single-pulse structure for the same value of ρ_1. However, when $E_{b'}/N_I$ is relatively small (such as 6 dB), the single-pulse structure can outperform the double-pulse structure for smaller values of ρ_1. This is consistent with our intuition that for a particular value of ρ_1, the double-pulse structure is more likely to have at least one pulse jammed. Consequently, when $E_{b'}/N_I$ is small, the performance of the double-pulse structure tends to be poorer than that of the single-pulse structure. Lastly, the double-pulse structure outperforms the single-pulse structure by a smaller margin as $E_{b'}/N_0$ increases. This is consistent with our intuition that a stronger signal benefits less from the added robustness of the double-pulse structure.

When the signal is subjected to both AWGN and PNI and PSI is assumed, the preceding conclusions regarding the double-pulse structure change. First, for $\rho_1 = 1$, the performance is same for the double-pulse structure regardless of PSI. Second, the double-pulse structure with PSI outperforms that without PSI for the same ρ_1 (except $\rho_1 = 1$), and the superiority increases as the value of ρ_1 decreases. Third, the double-pulse structure with PSI outperforms that without PSI by a smaller margin as $E_{b'}/N_0$ increases. Lastly, we see that PSI effectively mitigates the degradation of the system due to PNI

When the signal is transmitted in both AWGN and combined PNI and PBNI, the performance curves for neither the single- nor the double-pulse structure were generated since the analytic expressions are identical to that in both AWGN and PNI when ρ_1 is replaced by $\rho_1 \rho_2$. Therefore, for the single-pulse structure, the probability of symbol error for a JTIDS/Link-16-type waveform in both AWGN and combined PNI and PBNI can be obtained from Figure 33 or 34 when ρ_1 is replaced by $\rho_1 \rho_2$. For the double-pulse structure without PSI, the probability of symbol error for a JTIDS/Link-16-type waveform in both AWGN and combined PNI and PBNI can be obtained from Figure 35

or Figure 36 when ρ_1 is replaced by $\rho_1\rho_2$. For the double-pulse structure with PSI, the probability of symbol error for a JTIDS/Link-16-type waveform in both AWGN and combined PNI and PBNI can be obtained from Figure 37 or 38.

In Section F, the probability of symbol error of a JTIDS/Link-16-type waveform in both AWGN and narrowband interference for both the single- and the double-pulse structure when the signal is transmitted over a slow, flat Nakagami fading channel was evaluated. Only two types of narrowband interference, BNI and PNI, were considered in this section. Several conclusions can be drawn when the signal is transmitted over a slow, flat Nakagami fading channel and subjected to both AWGN and BNI. First, the double-pulse structure outperforms the single-pulse structure for fixed $E_{b'}/N_0$, whether m is large or small. Second, when m is large, such as $m = 30$, the results are virtually identical to those obtained for a channel with no fading. Third, the double-pulse structure outperforms the single-pulse structure, and the superiority increases as the value of m decreases. This is consistent with our intuition that the robustness of the double-pulse structure enhances performance more when the channel is strongly faded. Fourth, for a fixed value of m, the double-pulse structure outperforms the single-pulse structure, and the superiority decreases as $E_{b'}/N_0$ increases. This is consistent with our intuition that a stronger signal benefits less from the added robustness of the double-pulse structure. Lastly, the single-pulse structure is very sensitive to m, while the double-pulse structure is relatively insensitive to m. This is consistent with our intuition that the single-pulse structure is less robust and therefore suffers more as fading worsens.

Several conclusions can be drawn when the signal is transmitted over a slow, flat Nakagami fading channel and subjected to both AWGN and PNI when PSI is not assumed. First, for the single-pulse structure, when $m = 30$, the results are virtually identical to those for no fading. Second, for a fixed value of ρ_1 and $E_{b'}/N_0$, the probability of symbol error for a JTIDS/Link-16-type waveform improves as m increases. This is consistent with our intuition that, when m is large, the channel approaches to no fading. Lastly, for the single-pulse structure, the value of ρ_1 that maximizes the probability of symbol error decreases as $E_{b'}/N_I$ increases, whether m is

120

large or small. For the double-pulse structure, the probability of symbol error of a JTIDS/Link-16-type waveform in both AWGN and PNI transmitted over a slow, flat Nakagami fading channel was not evaluated since an analytic expression for p_{c_1} has not been found.

When the signal is transmitted over a slow, flat Nakagami fading channel and subjected to both AWGN and PNI when PSI is assumed, the preceding conclusions regarding the double-pulse structure change. First, as expected, when $m = 30$, the results for the double-pulse structure with PSI are virtually identical to those for channels with no fading. Second, for a fixed $E_{b'}/N_0$, the double-pulse structure with PSI outperforms the single-pulse structure by a greater margin for smaller m. Lastly, for a fixed m, the double-pulse structure with PSI outperforms the single-pulse structure by a smaller margin as $E_{b'}/N_0$ increases. PSI is not realistic but gives us a benchmark against which to measure receivers which have imperfect or no side information.

In the next chapter, two modified JTIDS/Link-16-type systems are introduced and their performances are evaluated. The first modified system uses errors-and-erasures decoding (EED) in place of errors-only RS decoding, and the second modified system uses an improved 32-chip CCSK starting sequence in place of the 32-chip CCSK sequence chosen for JTIDS. The probabilities of symbol error obtained with the modified systems are compared with those obtained in this chapter.

THIS PAGE INTENTIONALLY LEFT BLANK

# VI. PERFORMANCE ANALYSES OF MODIFIED JTIDS/LINK-16-COMPATIBLE WAVEFORM

In the previous chapter, the probability of symbol error of a JTIDS/Link-16-type waveform transmitted over a slow, flat Nakagami fading channel with both AWGN and various types of narrowband interference was investigated. In this chapter, two modified JTIDS/Link-16-compatible systems are evaluated. The first system uses errors-and-erasures decoding (EED) in place of errors-only RS decoding since erasure decoding can result in more coding gain for some types of fading channels and/or narrowband interference [39]. The second system employs a new 32-chip CCSK sequence instead of the 32-chip CCSK sequence chosen for JTIDS. The new 32-chip CCSK sequence has a smaller maximum off-peak cross-correlation value and allows for seven instead of six chip errors in the received sequence before a symbol error occurs. The probability of symbol error obtained for this new 32-chip CCSK sequence is compared with that obtained for the 32-chip sequence chosen for JTIDS in AWGN.

A.   PERFORMANCE ANALYSIS WITH EED

Up to this point, we have assumed that the output of the CCSK symbol demodulator is the estimate of the received coded symbols which then must be decoded. Hence, the digital output of the CCSK symbol demodulator is the input to the decoder. This is referred to as hard decision decoding. An alternative to hard decision decoding is erasure decoding, which is the simplest form of soft decision decoding. A RS code can be used to correct errors and erasures simultaneously [40]. The receiver structure of the modified system with EED is shown in Figure 55.
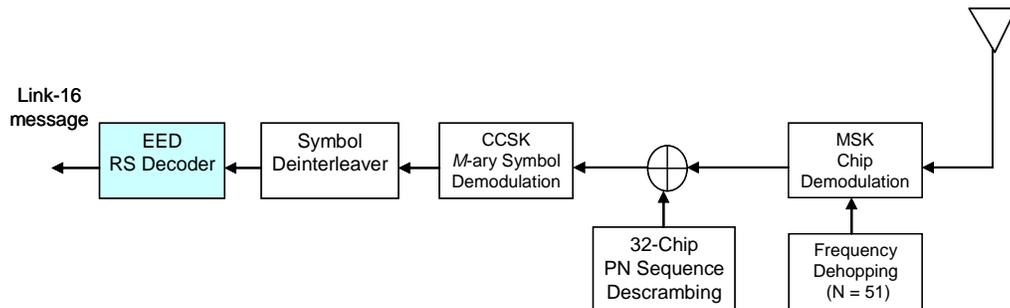
Figure 55.   Receiver structure of JTIDS/Link-16-type system with EED.

To implement EED at the RS decoder, the CCSK symbol demodulator yields thirty-three possible outputs corresponding to symbol '0' through '31' as well as symbol erasure. A channel symbol is erased when the CCSK symbol demodulator cannot make a decision as to which symbol was received with sufficient confidence, which occurs when the largest CCSK cross-correlation value is less than a specific preset threshold; that is, $\Re_i < T$ for $0 \leq i \leq 31$ where $\Re_i$ is the cross-correlation value at branch i of CCSK symbol demodulator and T is the erasure threshold. Denote T_{opt} as an optimal erasure threshold such that the overall probability of symbol error can be minimized. To implement EED, T_{opt} is required. Up to this point, T_{opt} is undetermined, but we know that T_{opt} is in the range of $[-32, 32]$ since the possible CCSK cross-correlation values are in the range of $-32 \leq \Re_i \leq 32$.

Intuitively, T_{opt} can be obtained by trial-and-error; that is, we evaluate the probability of symbol error of a JTIDS/Link-16-type waveform with EED case-by-case for all possible values of T in the range of $[-32, 32]$, and then we determine T_{opt} from the case which has the best performance. Before implementing such a trial-and-error experiment, an analytic expression for the probability of symbol error of a JTIDS/Link-16-type waveform with EED is required.

1.   Performance of Linear, Non-binary Block Codes with EED

For a linear, non-binary block code that can correct up to t symbol errors in every block of n symbols, with EED, a block error occurs either when the number of symbol errors i is greater than t regardless of the number of the symbol erasures or when the number of erasures j is greater than $d_{\min} - 2i - 1$ (since a block error will not occur as long as $d_{\min} \geq 2i + j + 1$) even when the number of symbol errors i is less than or equal to t. As a result, the probability of block error with EED is given by [40]

$$P_E = \sum_{i=t+1}^{n} \binom{n}{i} p_s^i \sum_{j=0}^{n-i} \binom{n-i}{j} p_e^j p_o^{n-i-j} + \sum_{i=0}^{t} \binom{n}{i} p_s^i \sum_{j=d_{\min}-2i}^{n-i} \binom{n-i}{j} p_e^j p_o^{n-i-j}, \qquad (6.1)$$

where p_s is the probability of channel symbol error, p_e is the probability of channel symbol erasure, and p_o is the probability of channel symbol correct. When a total of i symbol errors and j symbol erasures result in a block error, the probability of symbol error given that a block error has occurred is approximately equal to $(i+j)/n$. Using this approximation for the conditional probability of symbol error, we obtain the probability of symbol error with EED from Equation (6.1) as [40]

$$
\begin{aligned}
P_S &= P\{\text{symbol error}|\text{block error}\}\,P\{\text{block error}\} \\
&\approx \frac{1}{n}\left[\sum_{i=t+1}^{n}\binom{n}{i}p_s^i \sum_{j=0}^{n-i}(i+j)\binom{n-i}{j}p_e^j p_o^{n-i-j} + \sum_{i=0}^{t}\binom{n}{i}p_s^i \sum_{j=d_{\min}-2i}^{n-i}(i+j)\binom{n-i}{j}p_e^j p_o^{n-i-j} \right].
\end{aligned} \tag{6.2}
$$

Note that to evaluate Equation (6.2), the probability of channel symbol error p_s, the probability of channel symbol erasure p_e, and the probability of channel symbol correct p_o are required. For EED, the probability of channel symbol error is obtained by using the same approach as for errors-only RS decoding; that is, from Equation (5.12), we get

$$
\begin{aligned}
p_s &= \sum_{j=0}^{32} P\{\text{channel symbol error}|N=j\}P\{N=j\} \\
&= \sum_{j=0}^{32} \zeta_{s_j}\binom{32}{j}p_c^j(1-p_c)^{32-j},
\end{aligned} \tag{6.3}
$$

where ζ_{s_j} are the conditional probabilities of channel symbol error with EED. Similarly, the probability of channel symbol erasure with EED is obtained as

$$
\begin{aligned}
p_e &= \sum_{j=0}^{32} P\{\text{channel symbol erasure}|N=j\}P\{N=j\} \\
&= \sum_{j=0}^{32} \zeta_{e_j}\binom{32}{j}p_c^j(1-p_c)^{32-j},
\end{aligned} \tag{6.4}
$$

where ζ_{e_j} are the conditional probabilities of channel symbol erasure. Finally, the probability of channel symbol correct with EED is obtained as

$$
p_o = \sum_{j=0}^{32} \zeta_{c_j}\binom{32}{j}p_c^j(1-p_c)^{32-j}, \tag{6.5}
$$

125

where ζ_{o_j} are the conditional probabilities of channel symbol correct with EED. Note that the probability of channel chip error p_c shown in Equations (6.3) through (6.5) is obtained from (5.10), but ζ_{s_j}, ζ_{e_j} and ζ_{o_j} are unknown and must be obtained.

2. Conditional Probabilities of Channel Symbol Error, Channel Symbol Erasure, and Channel Symbol Correct

Recall that in Chapter IV, the conditional probabilities of symbol error are obtained both analytically and by Monte Carlo simulation. In this chapter, only Monte Carlo simulation is used to estimate ζ_{s_j}, ζ_{e_j} and ζ_{o_j} for all possible values of T since analytic expressions for ζ_{s_j}, ζ_{e_j} and ζ_{o_j} are difficult to obtain. As mentioned earlier, we do not know T_{opt} up to this point; thus, the worst case is to run the simulation for $-32 \leq T \leq 32$. To make the process more efficient, we can narrow down the range of T. Intuitively, if the erasure threshold T is too small, the result will be similar to that of errors-only RS decoding. If T is too large, the result will be worse than that of errors-only RS decoding since most of the correct symbols will be erased. Therefore, it is reasonable to choose $0 \leq T \leq 20$ for the initial trial-and-error. Note that when $T = 0$, we expect to obtain similar results as that of errors-only RS decoding since $T = 0$ is less than the maximum off-peak cross-correlation value $H = 4$ in the absence of noise.

For each T chosen in the range of $[0, 20]$, a Monte Carlo simulation with stratified sampling is run 10,000 times for $7 \leq N \leq 32$ to obtain ζ_{s_j}, ζ_{e_j} and ζ_{o_j}, where N is the total number of chip errors in the received sequence at the input of the CCSK symbol demodulator. As before, the simulation does not consider the cases where $N \leq 6$ since the CCSK symbol demodulator does not make a symbol error for $N \leq 6$. For symbol 0 sent, the Monte Carlo simulation with stratified sampling is implemented case-by-case for different N and T. For example, for $N = 7$ and $T = 0$, the major steps of the simulation are as follows. First, in each iteration, generate randomly a 32-chip sequence with seven chip errors corresponding to the original 32-chip sequence of symbol 0 to model the noisy received 32-chip sequence at the CCSK symbol demodulator input. Second, cross-correlate the received 32-chip sequence with all of the 32 local sequences

to yield 32 cross-correlation values: $\Re_0, \Re_1, \ldots, \Re_{31}$. Third, calculate the conditional probability of symbol erasure, the conditional probability of symbol error, and the conditional probability of symbol correct based on the following rules: (i) if the maximum $\Re_i$ is less than T for $0 \leq i \leq 31$, the conditional probability of symbol erasure is one; (ii) if the maximum $\Re_i$ is greater than or equal to T for $1 \leq i \leq 31$ and the maximum $\Re_i$ is not equal to $\Re_0$, the conditional probability of symbol error is one; (iii) if the maximum $\Re_i$ is greater than or equal to T for $1 \leq i \leq 31$ and the maximum $\Re_i$ is equal to $\Re_0$, the conditional probability of symbol error is $\tau/(\tau+1)$, and the conditional probability of symbol correct is $1 - [\tau/(\tau+1)]$, where τ is the total number of ties. Lastly, the above iteration is repeated 10,000 times, and then average values for ζ_{s_7}, ζ_{e_7}, and ζ_{o_7} are calculated. Similarly, the same approach is applied for $N = 8, 9, .., 32$. For $T = 0$, the simulation results for $7 \leq N \leq 32$ are shown in Table 12. For $T = 4$, 6, 8, 10, 12, 14, 16, 18, and 20, simulation results are shown in Appendix C.

Table 12.   Simulation results for ζ_{s_j}, ζ_{e_j}, and ζ_{o_j} when $T = 0$.

N = j	ζ_{s_j}		ζ_{e_j}		ζ_{o_j}	
	estimate	std. error	estimate	std. error	estimate	std. error
0	0	0	0	0	1	0
⋮	⋮	⋮	⋮	⋮	⋮	⋮
6	0	0	0	0	1	0
7	0.0015	0.0003	0	0	0.9885	0.0003
8	0.0208	0.0010	0	0	0.9792	0.0010
9	0.1144	0.0023	0	0	0.8856	0.0023
10	0.3656	0.0032	0	0	0.6344	0.0032
11	0.7108	0.0026	0	0	0.2892	0.0026
12	0.9363	0.0011	0	0	0.0637	0.0011
13	0.9954	0.0003	0	0	0.0046	0.0003
14	0.9999	0.0002	0	0	0.0001	0.0002
15	1	0	0	0	0	0
⋮	⋮	⋮	⋮	⋮	⋮	⋮
32	1	0	0	0	0	0

3. Optimal Erasure Threshold

Now, using ζ_{s_j}, ζ_{e_j}, and ζ_{o_j} from Table 12 in Equations (6.3), (6.4), and (6.5), respectively, along with the probability of channel chip error in Equation (5.10), we obtain the probability of channel symbol error p_s, the probability of channel symbol erasure p_e, and the probability of channel symbol correct p_o. Next, using p_s, p_e, and p_o in Equation (6.2), we obtain the probability of symbol error of a JTIDS/Link-16-type waveform with EED ($T = 0$) for the single- and the double-pulse structure in AWGN.

To compare the difference between EED ($T = 0$) and errors-only RS decoding in terms of probability of symbol error of a JTIDS/Link-16-type waveform for the single-pulse structure in AWGN, both results are shown in Figure 56. As expected, both results are virtually identical since $T = 0$ is less than the maximum off-peak cross-correlation value $H = 4$ of CCSK in the absence of noise. Note that in Figure 56, the performance with errors-only RS decoding is slightly better than was shown in Figure 27 since Equations (6.3), (6.4), and (6.5) are exact expressions, not upper bounds.
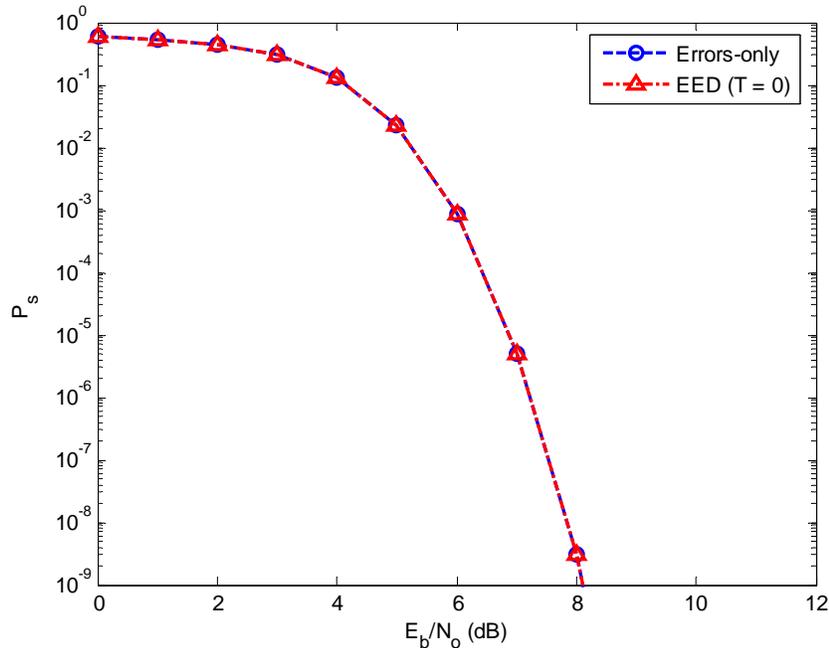
Figure 56. Probability of symbol error of a JTIDS/Link-16-type waveform for the single-pulse structure in AWGN: EED ($T = 0$) versus errors-only RS decoding.

If the erasure threshold is increased to $T = 10$ (with ζ_{s_j}, ζ_{e_j}, and ζ_{o_j} from Appendix C.5), the results are shown in Figure 57. As can be seen, the performance for EED with $T = 10$ is still virtually identical to that for errors-only RS decoding. Clearly, $T = 10$ is not the optimal threshold for EED.
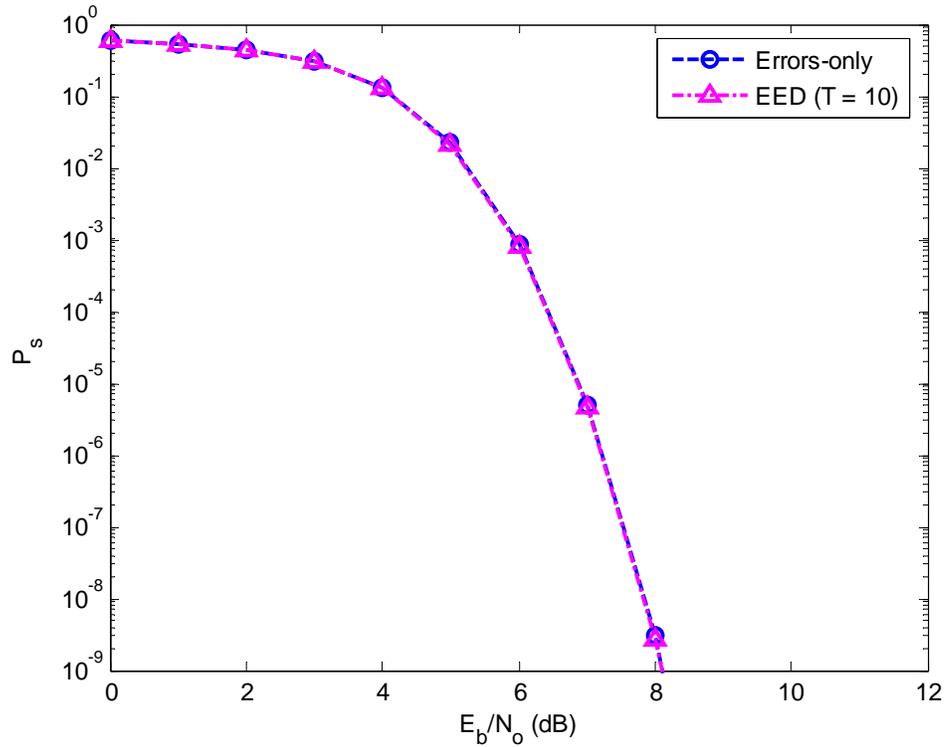
Figure 57.   Probability of symbol error of a JTIDS/Link-16-type waveform for the single-pulse structure in AWGN: EED ($T = 0$) versus EED ($T = 10$).

Now, the erasure threshold is increased to $T = 12$, 14, 16, 18, and 20, respectively. The overall results for both the single- and the double-pulse structure are shown in Figure 58. As can be seen, for both the single- and the double-pulse structure at $P_s = 10^{-5}$, the performance slightly improves when $T = 12$. The best performance is obtained when $T = 14$, and the performance begins to degrade for $T \geq 16$. Next, we need to find the optimal erasure threshold for a JTIDS/Link-16-type waveform in both AWGN and PNI since it is possible that $T = 14$ is not the optimal erasure threshold when PNI is present; although, it is intuitively obvious that BNI will not affect the optimal erasure threshold.

129
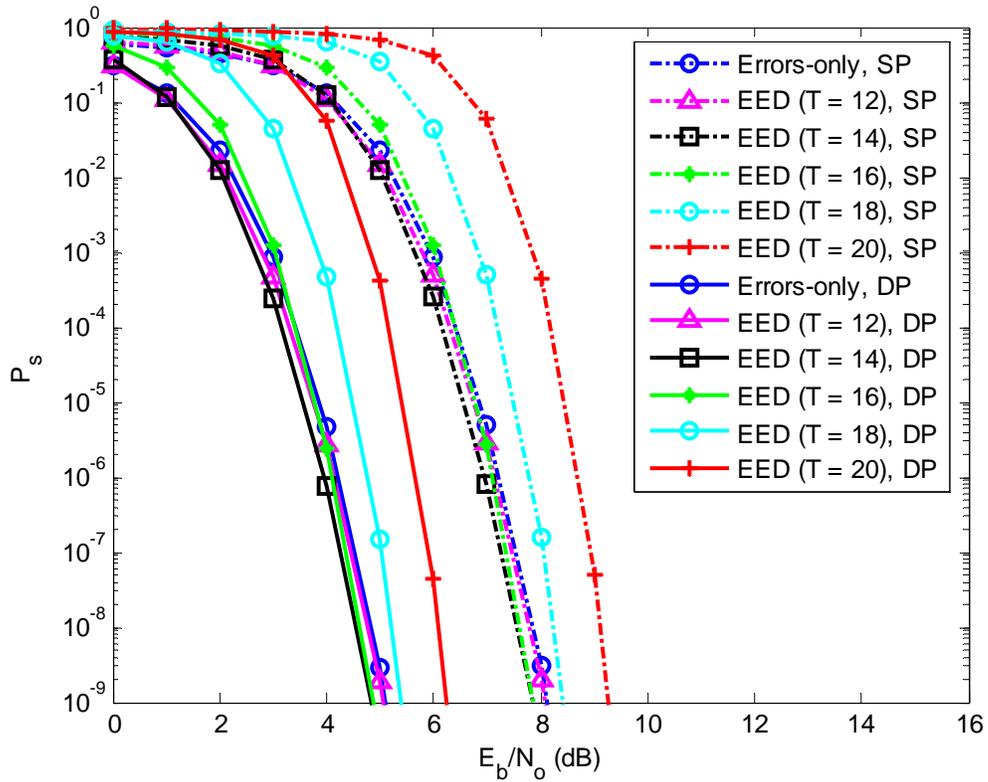
Figure 58.   Probability of symbol error of a JTIDS/Link-16-type waveform for both the single- and the double-pulse structure in AWGN: errors-only RS decoding versus EED with erasure threshold $T = 12$, 14, 16, 18 and 20.

The process of finding T_{opt} for a JTIDS/Link-16-type waveform in both AWGN and PNI is more complex than that for AWGN. For the single-pulse structure, we proceed as follows. First, the probability of channel chip error when the jammer is off p_{c_0} is obtained from Equation (5.22), and the probability of channel chip error when the jammer is on p_{c_1} is obtained from Equation (5.24). Second, substituting p_{c_0} and p_{c_1} into (5.21) and (5.23), respectively, along with ζ_{s_j} from Appendix C corresponding to the value of threshold chosen, we obtain the probability of channel symbol error when the single-pulse is not jammed p_{s_0} and the probability of channel symbol error when the single-pulse is jammed p_{s_1}. Next, substituting p_{s_0} and p_{s_1} into Equation (5.20), we obtain the average probability of channel symbol error p_s. Third, substituting p_{c_0} and

p_{c_1} into Equations (5.21) and (5.23), respectively, along with ζ_{e_j} from Appendix C corresponding to the value of threshold chosen, we obtain the probability of channel symbol erasure when the single-pulse is not jammed p_{e_0} and the probability of channel symbol erasure when the single-pulse is jammed p_{e_1}. Next, substituting p_{e_0} and p_{e_1} into Equation (5.20), we obtain the average probability of channel symbol erasure p_e. Fourth, substituting p_{c_0} and p_{c_1} into Equations (5.21) and (5.23), respectively, along with ζ_{o_j} from Appendix C corresponding to the value of threshold chosen, we obtain the probability of channel symbol correct when the single-pulse is not jammed p_{o_0} and the probability of channel symbol correct when the single-pulse is jammed p_{o_1}. Next, substituting p_{o_0} and p_{o_1} into Equation (5.20), we obtain the average probability of channel symbol correct p_o. Finally, substituting p_s, p_e, and p_o into Equation (6.2), we obtain the probability of symbol error of a JTIDS/Link-16-type waveform for the single-pulse structure with EED for a given erasure threshold in both AWGN and PNI. For each T chosen, the required $E_{b'}/N_I$ (in dB) when $P_s = 10^{-5}$ is summarized in Table 13 for various ρ_1.

Table 13.   Required $E_{b'}/N_I$ in dB when $P_s = 10^{-5}$ for the single-pulse structure of a JTIDS/Link-16-type waveform in both AWGN and PNI.

$E_{b'}/N_0$ (dB)	T	$\rho_1 = 1$	$\rho_1 = 0.5$	$\rho_1 = 0.3$	$\rho_1 = 0.2$
	0	9.80	11.01	11.68	12.04
	12	9.60	10.69	11.29	11.36
10	14	9.26	10.20	10.46	10.05
	16	9.64	10.33	10.21	8.78
	18	11.21	11.63	11.31	9.10
	20	13.77	14.06	13.83	12.59
	0	7.57	9.40	10.47	11.14
	12	7.47	9.20	10.14	10.52
15	14	7.26	8.81	9.48	9.37
	16	7.50	8.91	9.25	7.97
	18	8.37	9.70	9.86	6.73
	20	9.53	10.91	11.07	5.99

As can be seen in Table 13, for the single-pulse structure, $T_{opt} = 14$ when $0.5 \leq \rho_1 \leq 1$, while $T_{opt} = 16$ when $\rho_1 = 0.3$, whether $E_{b'}/N_0$ is large or small. When $\rho_1 = 0.2$, $T_{opt} = 16$ for small $E_{b'}/N_0$, while $T_{opt} = 20$ for large $E_{b'}/N_0$. Note that when $E_{b'}/N_0$ is large, the difference between the best T for a particular ρ_1 and $T = 14$ can exceed 3 dB.

For the double-pulse structure, we proceed as follows. First, the probability of channel chip error when neither pulse is jammed p_{c_0} is obtained from Equation (5.32), the probability of channel chip error when one pulse is jammed p_{c_1} is obtained from Equation (5.34), and the probability of channel chip error when both pulses are jammed p_{c_2} is obtained from Equation (5.36). Second, substituting p_{c_0}, p_{c_1}, and p_{c_2} into Equations (5.31), (5.33), and (5.35), respectively, along with ζ_{s_j} from Appendix C corresponding to the value of threshold chosen, we obtain the probability of channel symbol error given that neither pulse is jammed p_{s_0}, the probability of channel symbol error given that one pulse is jammed p_{s_1}, and the probability of channel symbol error given that both pulses are jammed p_{s_2}. Next, substituting p_{s_0}, p_{s_1}, and p_{s_2} into (5.30), we obtain the average probability of channel symbol error p_s. Similarly, the average probability of channel symbol erasure p_e and the average probability of channel symbol correct p_o are obtained with ζ_{e_j} and ζ_{o_j} from Appendix C corresponding to the value of threshold chosen. Lastly, substituting p_s, p_e, and p_o into Equation (6.2), we obtain the probability of symbol error of a JTIDS/Link-16-type waveform with EED for the double-pulse structure in both AWGN and PNI.

For each T examined, the required $E_{b'}/N_I$ (in dB) when $P_s = 10^{-5}$ is summarized in Table 14 for various ρ_1. It is interesting to note that, for the double-pulse structure, $T_{opt} = 14$ when $0.3 \leq \rho_1 \leq 1$, while $T_{opt} = 16$ when $\rho_1 = 0.2$, whether $E_{b'}/N_0$ is large or small. It is also interesting to note that for the double-pulse structure the performance is relatively insensitive as to whether the best T is used or not. For example, when

$E_{b'}/N_0 = 15\,\text{dB}$ and $\rho_1 = 0.2$, the difference in performance between the erasure threshold $T = 16$ and $T = 14$ is only 0.17 dB when $P_s = 10^{-5}$.

With the knowledge of the optimal erasure threshold for each case mentioned above, we are ready to investigate the probability of symbol error for a JTIDS/Link-16-type waveform with EED in both AWGN and narrowband interference.

Table 14.   Required $E_{b'}/N_I$ in dB when $P_s = 10^{-5}$ for the double-pulse structure of a JTIDS/Link-16-type waveform in both AWGN and PNI.

$E_{b'}/N_0$ (dB)	T	$\rho_1 = 1$	$\rho_1 = 0.5$	$\rho_1 = 0.3$	$\rho_1 = 0.2$
10	0	5.07	5.96	6.71	7.38
	12	4.95	5.73	6.43	7.05
	14	4.70	5.35	6.00	6.43
	16	5.01	5.51	6.05	6.29
	18	5.98	6.43	6.92	7.07
	20	7.33	7.82	8.24	8.37
15	0	4.19	5.22	6.06	6.82
	12	4.10	5.03	5.79	6.50
	14	3.90	4.65	5.37	6.01
	16	4.13	4.76	5.40	5.84
	18	4.93	5.50	6.15	6.49
	20	5.99	6.56	7.22	7.62

4.   Performance with EED in AWGN

The process of investigating the probability of symbol error of a JTIDS/Link-16-type waveform for both the single- and the double-pulse structure with EED in AWGN was mentioned at the beginning of the previous subsection. Now, with the optimal erasure threshold $T_{opt} = 14$, we obtain the best performance of a JTIDS/Link-16-type waveform for both the single- and the double-pulse structure with EED in AWGN. To compare the difference between EED and errors-only RS decoding, both results are shown in Figure 59 for both the single- and the double-pulse structure. As can be seen, EED outperforms errors-only RS decoding by 0.3 dB at $P_s = 10^{-5}$ for both the single- and the double-pulse structure. Clearly, the advantages of EED with only AWGN and no fading are minimal.
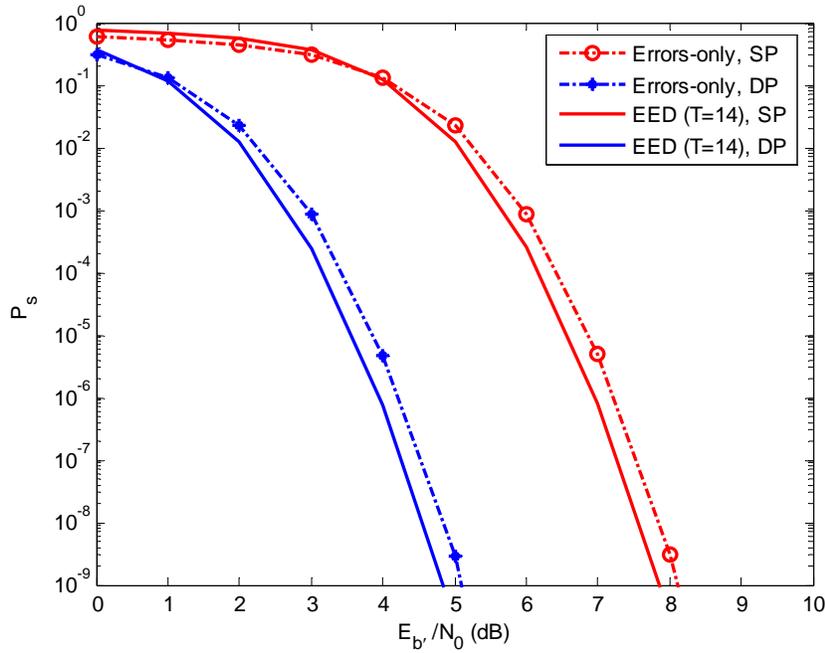
Figure 59.   Probability of symbol error of a JTIDS/Link-16-type waveform for both the single- and the double pulse structure in AWGN: EED ($T = 14$) versus errors-only RS decoding.

5.   Performance with EED in Both AWGN and PNI

To evaluate the performance of a JTIDS/Link-16-type waveform for the single-pulse structure with EED in both AWGN and PNI, we proceed as follows. First, the probability of channel chip error when the jammer is off p_{c_0} is obtained from (5.22), and the probability of channel chip error when the jammer is on p_{c_1} is obtained from (5.24). Second, using p_{c_0} and p_{c_1} in Equations (5.21) and (5.23), respectively, along with ζ_{s_j} from either Appendix C.7, C.8, or C.10 depending on the value of ρ_1, we obtain the probability of channel symbol error when the single-pulse is not jammed p_{s_0} and the probability of channel symbol error when the single-pulse is jammed p_{s_1}. Next, using p_{s_0} and p_{s_1} in (5.20) we obtain the average probability of channel symbol error p_s. Third, using p_{c_0} and p_{c_1} in (5.21) and (5.23), respectively, along with ζ_{e_j} from either Appendix C.7, C.8, or C.10 depending on the value of ρ_1, we obtain the probability of

134

channel symbol erasure when the single-pulse is not jammed p_{e_0} and the probability of channel symbol erasure when the single-pulse is jammed p_{e_1}. Next, using p_{e_0} and p_{e_1} in Equation (5.20), we obtain the average probability of channel symbol erasure p_e. Fourth, substituting p_{c_0} and p_{c_1} into Equations (5.21) and (5.23), respectively, along with ζ_{o_j} from either Appendix C.7, C.8 or C.10 depending on the value of ρ_1, we obtain the probability of channel symbol correct when the single-pulse is not jammed p_{o_0} and the probability of channel symbol correct when the single-pulse is jammed p_{o_1}. Next, substituting p_{o_0} and p_{o_1} into Equation (5.20), we obtain the average probability of channel symbol correct p_o. Finally, using p_s, p_e, and p_o in Equation (6.2), we obtain the probability of symbol error of a JTIDS/Link-16-type waveform for the single-pulse structure with EED in both AWGN and PNI. To compare the difference between EED and errors-only RS decoding, both results with various ρ_1 are shown in Figures 60 and 61 where $E_{b'}/N_0 = 10\,\text{dB}$ and 15 dB, respectively.
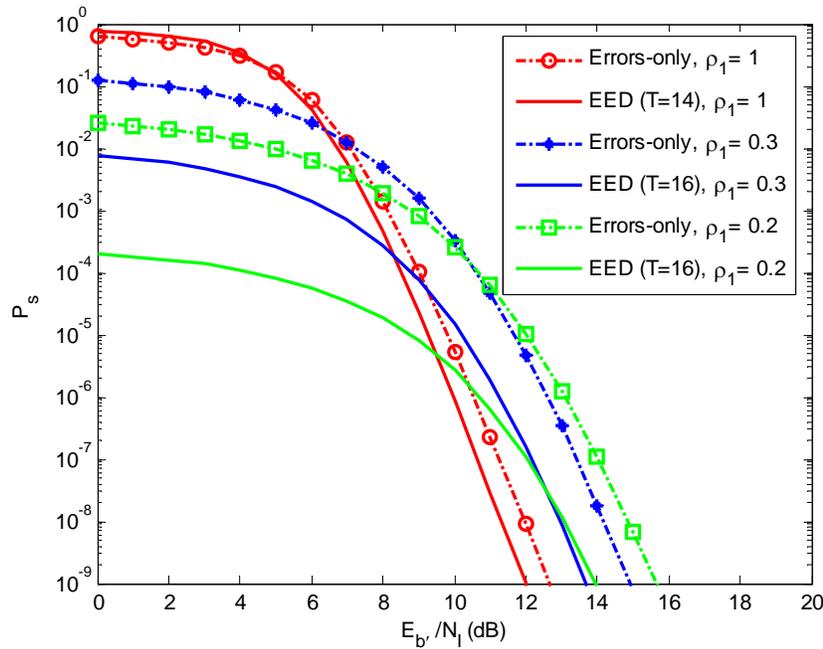
Figure 60.   Probability of symbol error of a JTIDS/Link-16-type waveform for the single-pulse structure in both AWGN and PNI where $E_{b'}/N_0 = 10\,\text{dB}$: EED versus errors-only RS decoding.
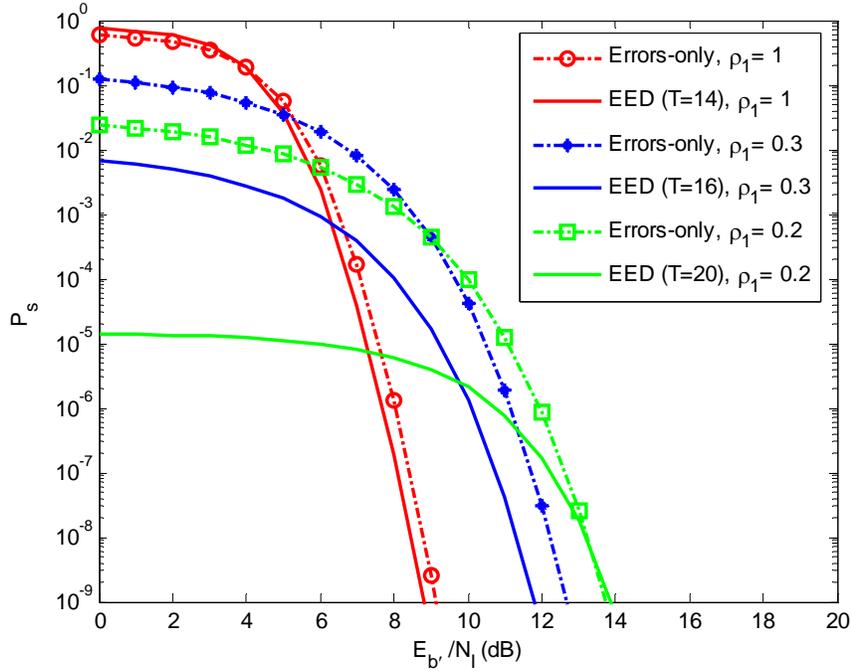
Figure 61. Probability of symbol error of a JTIDS/Link-16-type waveform for the single-pulse structure in both AWGN and PNI where $E_{b'}/N_0 = 15$ dB: EED versus errors-only RS decoding.

From Figures 60 and 61, several observations can be made. First, for all cases in both figures, EED outperforms errors-only RS decoding at $P_s = 10^{-5}$. Second, when $E_{b'}/N_0$ is fixed, EED outperforms errors-only RS decoding by a greater margin as ρ_1 decreases. For example, in Figure 60 at $P_s = 10^{-5}$, for $\rho_1 = 1$, EED outperforms errors-only RS decoding by 0.5 dB, while for $\rho_1 = 0.2$, EED outperforms errors-only RS decoding by 3.3 dB. Lastly, EED outperforms errors-only RS decoding, and the superiority increases as $E_{b'}/N_0$ increases. For example, in Figure 61 where $E_{b'}/N_0$ is 15 dB, for $\rho_1 = 0.2$, EED with $T_{opt} = 20$ outperforms errors-only RS decoding by 5.1 dB (an increase of 1.7 dB compared to when $E_{b'}/N_0 = 10$ dB) at $P_s = 10^{-5}$. Noting the trends as ρ_1 decreases and $E_{b'}/N_0$ increases, we see that for sufficiently large $E_{b'}/N_0$, EED completely eliminates the effect of PNI for probabilities of symbol error greater than some specified value such as 10^{-5}.

For the double-pulse structure, the process of investigating the probability of symbol error of a JTIDS/Link-16-type waveform with EED in both AWGN and PNI proceeds as follows. First, the probability of channel chip error when neither pulse is jammed p_{c_0} is obtained from Equation (5.32), the probability of channel chip error when one pulse is jammed p_{c_1} is obtained from Equation (5.34), and the probability of channel chip error when both pulses are jammed p_{c_2} is obtained from Equation (5.36). Second, substituting p_{c_0}, p_{c_1}, and p_{c_2} into Equations (5.31), (5.33), and (5.35), respectively, along with ζ_{s_j} from either Appendix C.7 or C.8 depending on the value of ρ_1, we obtain the probability of channel symbol error when neither pulse is jammed p_{s_0}, when one pulse is jammed p_{s_1}, and when both pulses are jammed p_{s_2}. Next, using p_{s_0}, p_{s_1}, and p_{s_2} in Equation (5.30) we obtain the average probability of channel symbol error p_s. Similarly, the average probability of channel symbol erasure p_e and the average probability of channel symbol correct p_o are obtained by replacing ζ_{s_j} with ζ_{e_j} and ζ_{o_j} from either Appendix C.7 or C.8 depending on the value of ρ_1. Lastly, substituting p_s, p_e, and p_o into Equation (6.2), we obtain the probability of symbol error of a JTIDS/Link-16-type waveform with EED for the double-pulse structure in both AWGN and PNI.

To compare the difference between EED and errors-only RS decoding for the double-pulse structure, both results with various ρ_1 are shown in Figures 62 and 63 where $E_{b'}/N_0 = 10\,\mathrm{dB}$ and 15 dB, respectively. Several observations can be made. First, as before, for all cases in both figures, EED outperforms errors-only RS decoding. Second, EED outperforms errors-only RS decoding by a greater margin as ρ_1 decreases. For example, in Figure 62, when $\rho_1 = 1$, EED outperforms errors-only RS decoding by 0.4 dB at $P_s = 10^{-5}$, while when $\rho_1 = 0.2$, EED outperforms errors-only RS decoding by 1.1 dB at $P_s = 10^{-5}$. Lastly, EED outperforms errors-only RS decoding but, unlike for the single-pulse structure, the superiority is relatively insensitive to an increase in $E_{b'}/N_0$.

137
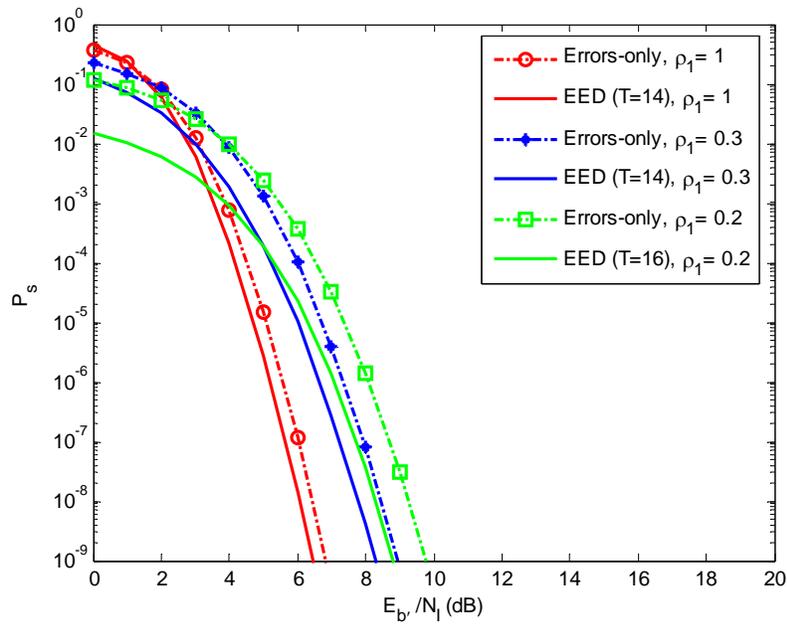
Figure 62.   Probability of symbol error of a JTIDS/Link-16-type waveform for the double-pulse structure in both AWGN and PNI where $E_{b'}/N_0 = 10\,\text{dB}$: EED versus errors-only RS decoding.
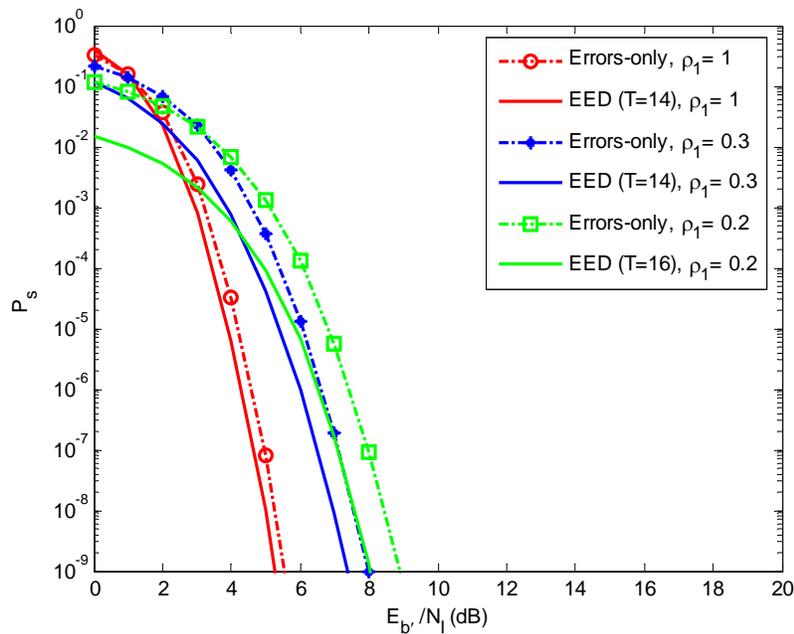
Figure 63.   Probability of symbol error of a JTIDS/Link-16-type waveform for the double-pulse structure in both AWGN and PNI where $E_{b'}/N_0 = 15\,\text{dB}$: EED versus errors-only RS decoding.

6.   Performance with EED and PSI in Both AWGN and PNI

As mentioned earlier, PSI has no effect on the single-pulse structure. In this subsection, only the performance for the double-pulse structure of a JTIDS/Link-16-type waveform with EED and PSI in both AWGN and PNI is investigated. The process is similar to that without PSI, which was discussed in the previous subsection. The only difference is that Equation (5.34) is used in place of (5.37) and $T_{opt} = 16$ is used in place of $T_{opt} = 14$ for $\rho_1 = 0.5$. For this case, $T_{opt} = 14$ for $\rho_1 = 1$, while $T_{opt} = 16$ for $\rho_1 = 0.5$ (see Table 15). To compare the difference between EED and errors-only RS decoding when PSI is assumed, both results are shown in Figures 64 and 65 where $E_{b'}/N_0 = 10\,\text{dB}$ and 15 dB, respectively. As before, for all cases in both figures, EED outperforms errors-only RS decoding when PSI is assumed. Second, EED outperforms errors-only RS decoding with a greater margin as ρ_1 decreases. For example, in Figure 64, when $\rho_1 = 1$, EED outperforms errors-only RS decoding by 0.4 dB at $P_s = 10^{-5}$, while when $\rho_1 = 0.5$, EED outperforms errors-only RS decoding by 1.8 dB at $P_s = 10^{-5}$. Lastly, EED outperforms errors-only RS decoding but, as for the double-pulse structure without PSI, the superiority is insensitive to an increase in $E_{b'}/N_0$.

Table 15.   Required $E_{b'}/N_I$ in dB when $P_s = 10^{-5}$ for the double-pulse structure of a JTIDS/Link-16-type waveform in both AWGN and PNI when PSI is assumed.

$E_{b'}/N_0$ (dB)	T	$\rho_1 = 1$	$\rho_1 = 0.5$
10	0	5.07	5.04
	12	4.95	4.62
	14	4.70	3.74
	16	5.01	3.20
	18	5.98	3.91
	20	7.33	5.91
15	0	4.19	4.57
	12	4.10	4.14
	14	3.90	3.34
	16	4.13	2.80
	18	4.93	3.11
	20	5.99	4.21
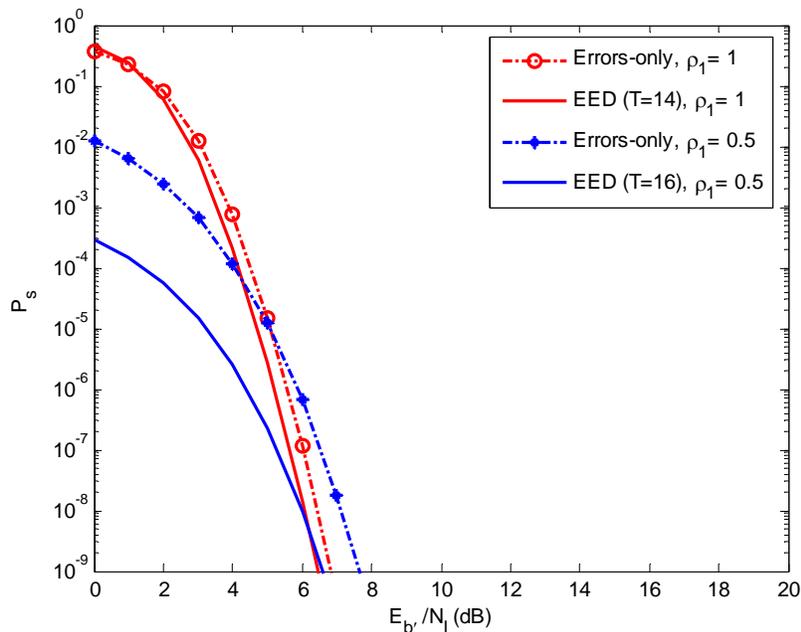
Figure 64.   Probability of symbol error of a JTIDS/Link-16-type waveform for the double-pulse structure when PSI is assumed in both AWGN and PNI where $E_{b'}/N_0 = 10\,\text{dB}$: EED versus errors-only RS decoding.
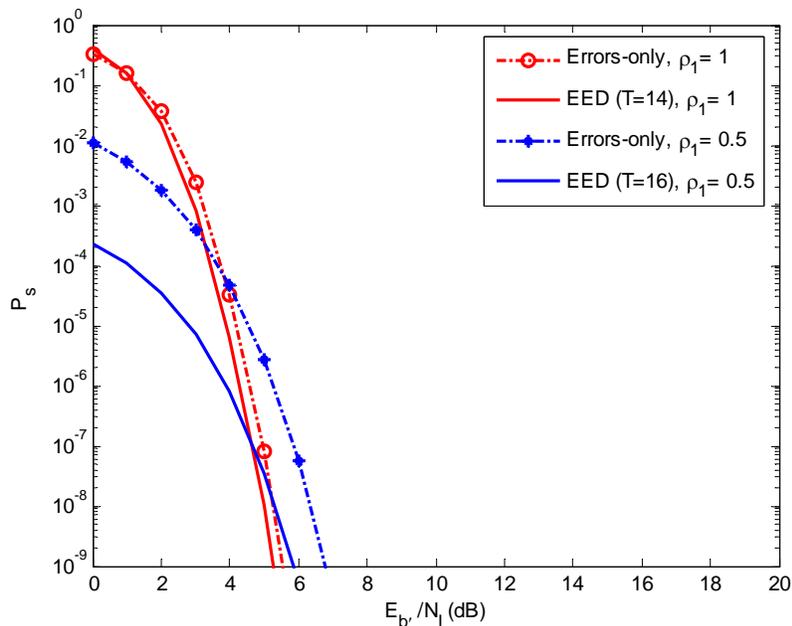
Figure 65.   Probability of symbol error of a JTIDS/Link-16-type waveform for the double-pulse structure when PSI is assumed in both AWGN and PNI where $E_{b'}/N_0 = 15\,\text{dB}$: EED versus errors-only RS decoding.

7. Performance with EED in AWGN, BNI, and Nakagami Fading Channels

To evaluate the probability of symbol error of a JTIDS/Link-16-type waveform with EED for the single-pulse structure in both AWGN and BNI when the signal is transmitted over a slow, flat Nakagami fading channel, we proceed as follows. First, the probability of channel chip error p_c is obtained from Equation (5.56) with code rate $r = 15/31$. Second, substituting p_c into (6.3), (6.4), and (6.5) along with ζ_{s_j}, ζ_{e_j}, and ζ_{o_j} from Appendix C.7, respectively, we obtain the probability of channel symbol error p_s, the probability of channel symbol erasure p_e, and the probability of channel symbol correct p_o. Lastly, using p_s, p_e, and p_o in (6.2), we obtain the probability of symbol error of a JTIDS/Link-16-type waveform with EED for the single-pulse structure in both AWGN and BNI when the signal is transmitted over a slow, flat Nakagami fading channel. To compare the difference between EED and errors-only RS decoding, both results are shown in Figure 66 and 67 where $E_{b'}/N_0 = 10$ and 15 dB, respectively.
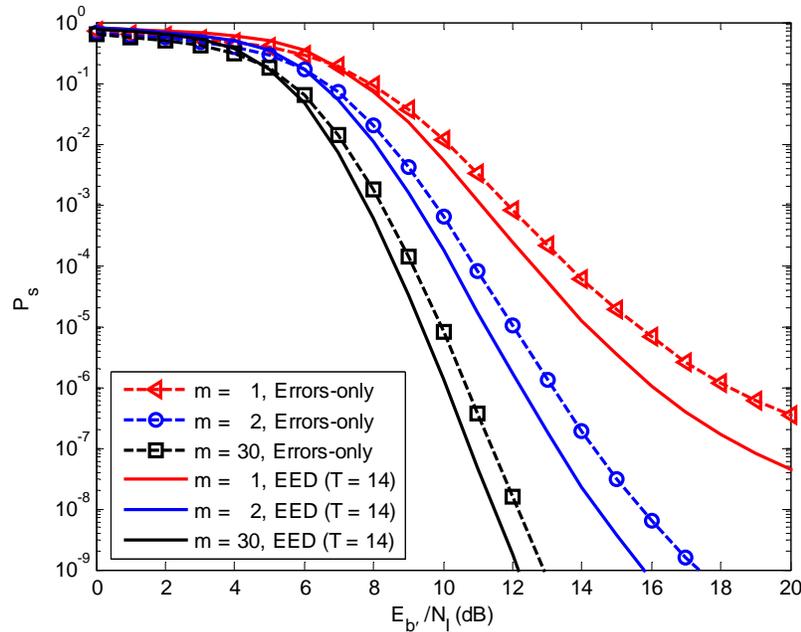
Figure 66.   Probability of symbol error of a JTIDS/Link-16-type waveform for the single-pulse structure in AWGN and BNI when transmitted over a slow, flat Nakagami fading channel where $E_{b'}/N_0 = 10\,\mathrm{dB}$: EED versus errors-only RS decoding.
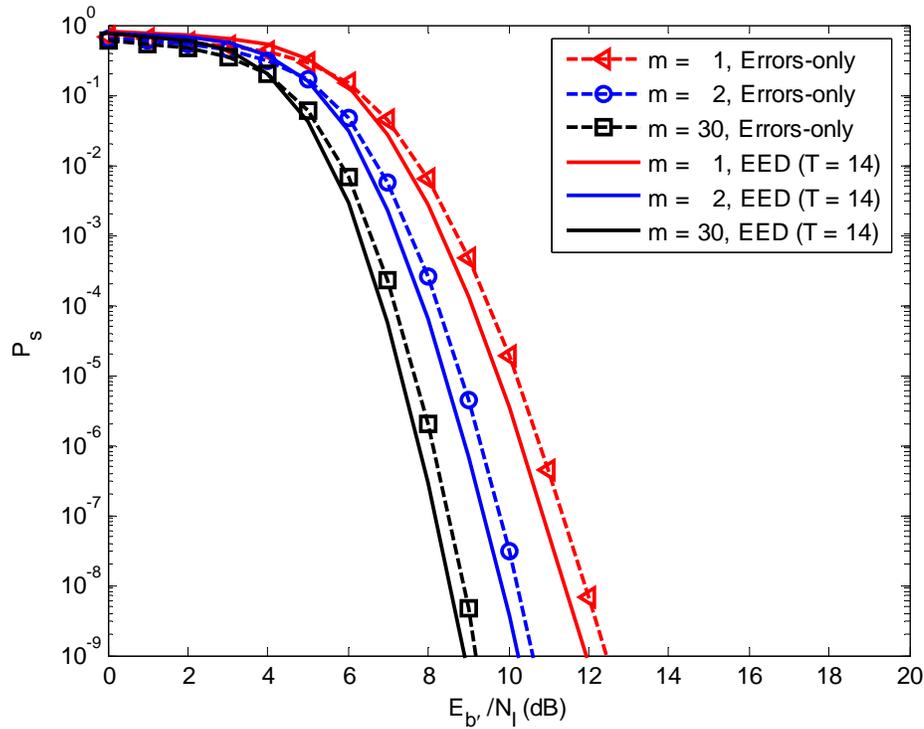
Figure 67.   Probability of symbol error of a JTIDS/Link-16-type waveform for the single-pulse structure in AWGN and BNI when transmitted over a slow, flat Nakagami fading channel where $E_{b'}/N_0 = 15\,\text{dB}$: EED versus errors-only RS decoding.

From Figures 66 and 67, several observations can be made. First, for all m and $E_{b'}/N_0$, EED outperforms errors-only RS decoding. Second, EED outperforms errors-only RS decoding by a greater margin for smaller m. For example, in Figure 66, when $m = 30$, EED outperforms errors-only RS decoding by 0.6 dB at $P_s = 10^{-5}$, while when $m = 1$, EED outperforms errors-only RS decoding by 1.4 dB at $P_s = 10^{-5}$. Lastly, EED outperforms errors-only RS decoding by a smaller margin as $E_{b'}/N_0$ increases. For example, in Figure 67 where $E_{b'}/N_0$ is increased to 15 dB, when $m = 30$, EED outperforms errors-only RS decoding by 0.3 dB (a decrease of 0.3 dB compared to when $E_{b'}/N_0 = 10\,\text{dB}$) at $P_s = 10^{-5}$, while when $m = 1$, EED outperforms errors-only RS decoding by 0.5 dB (a decrease of 0.9 dB compared to when $E_{b'}/N_0 = 10\,\text{dB}$) at $P_s = 10^{-5}$.

For the double-pulse structure, the process of evaluating the performance of a JTIDS/Link-16-type waveform with EED in both AWGN and PNI when the signal is transmitted over a slow, flat Nakagami fading channel is similar to that for the single-pulse structure except Equation (5.68) is used instead of Equation (5.56). To compare the difference between EED and errors-only RS decoding, both results are shown in Figure 68 and 69 where $E_{b'}/N_0 = 10$ and 15 dB, respectively. From both figures, we see that for all m and $E_{b'}/N_0$, EED outperforms errors-only RS decoding but with a smaller margin as compared to that for the single-pulse structure. For example, in Figure 68, for $m = 30$, EED outperforms errors-only RS decoding by 0.4 dB (a decrease of 0.2 dB compared to Figure 66) at $P_s = 10^{-5}$, while when $m = 1$, EED outperforms errors-only RS decoding by 0.5 dB (a decrease of 0.9 dB compared to Figure 66) at $P_s = 10^{-5}$. Furthermore, while the single-pulse structure is very sensitive to the value of m, the double-pulse structure is relatively insensitive to the value of m.
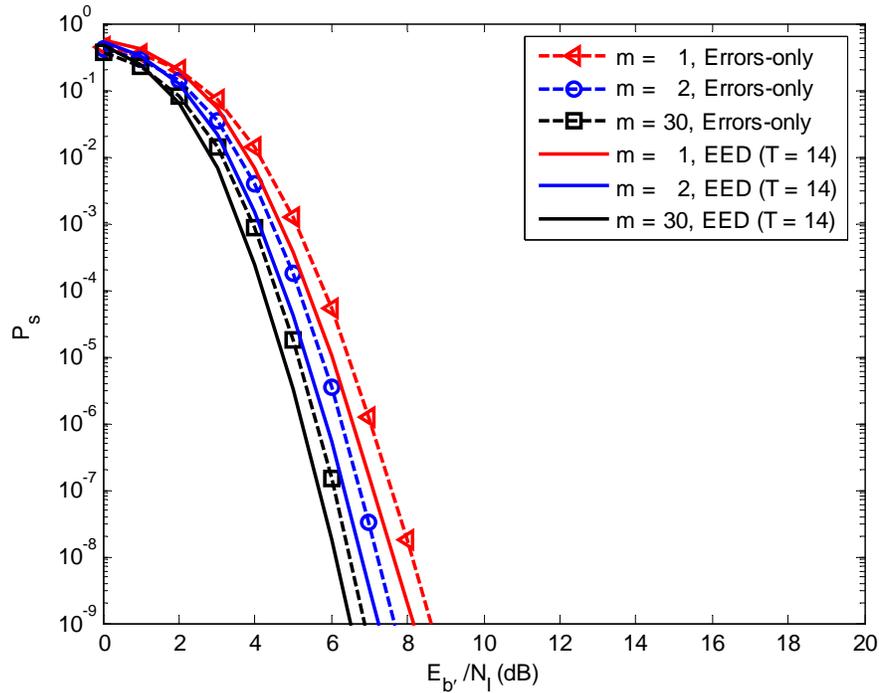
Figure 68.   Probability of symbol error of a JTIDS/Link-16-type waveform for the double-pulse structure in both AWGN and BNI when the signal is transmitted over a slow, flat Nakagami fading channel where $E_{b'}/N_0 = 10$ dB: EED versus errors-only RS decoding.

143
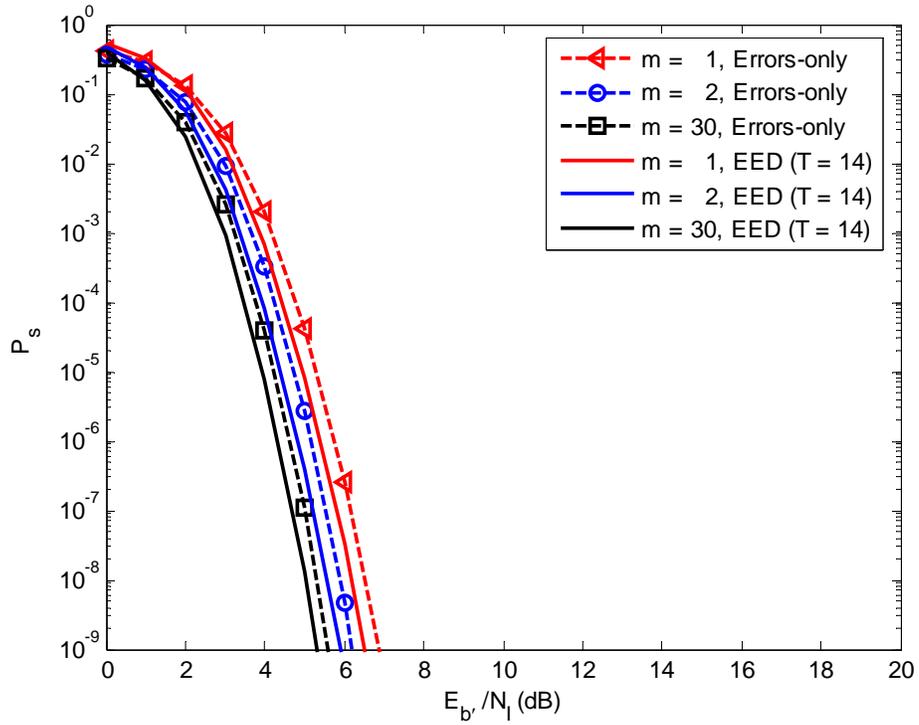
Figure 69. Probability of symbol error of a JTIDS/Link-16-type waveform for the double-pulse structure in both AWGN and BNI when the signal is transmitted over a slow, flat Nakagami fading channel where $E_{b'}/N_0 = 15$ dB: EED versus errors-only RS decoding.

8. Performance with EED in AWGN, PNI, and Nakagami Fading Channels

The process of investigating the performance of a JTIDS/Link-16-type waveform with EED for the single-pulse structure in both AWGN and PNI when the signal is transmitted over a slow, flat Nakagami fading channel is similar to that for channels with no fading. The only difference is that Equations (5.22) and (5.24) are replaced by Equations (5.79) and (5.82), respectively. For the double-pulse structure, the performance is not investigated since an analytic expression for the average probability of channel chip error given that one pulse is jammed is not available; however, when PSI is assumed, the performance with EED for the double-pulse structure is investigated in the next subsection. To compare the difference between EED and errors-only RS decoding for the single-pulse structure, both results are shown in Figures 70 to 75 for different m, ρ_1, and $E_{b'}/N_0$.

144
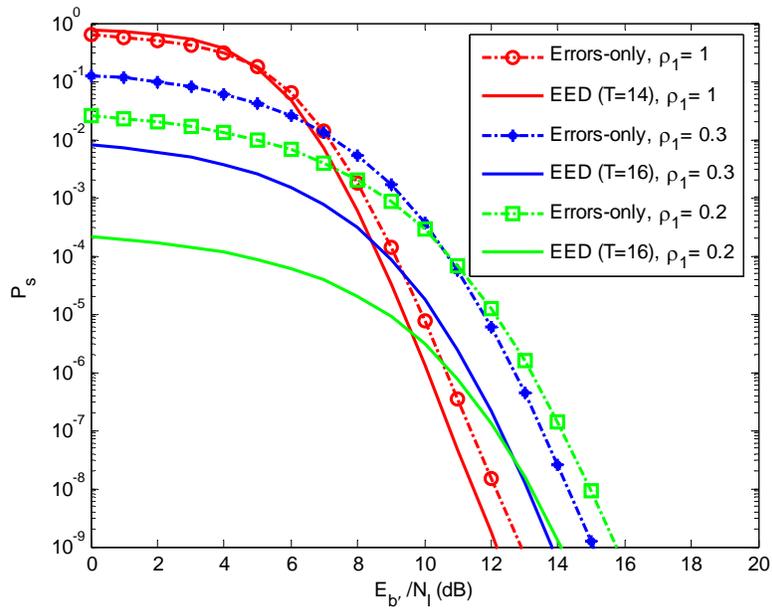
Figure 70. Probability of symbol error of a JTIDS/Link-16-type waveform for the single-pulse structure in both AWGN and PNI when the signal is transmitted over a slow, flat Nakagami fading channel where $m = 30$ and $E_{b'}/N_0 = 10\,\text{dB}$: EED versus errors-only RS decoding.
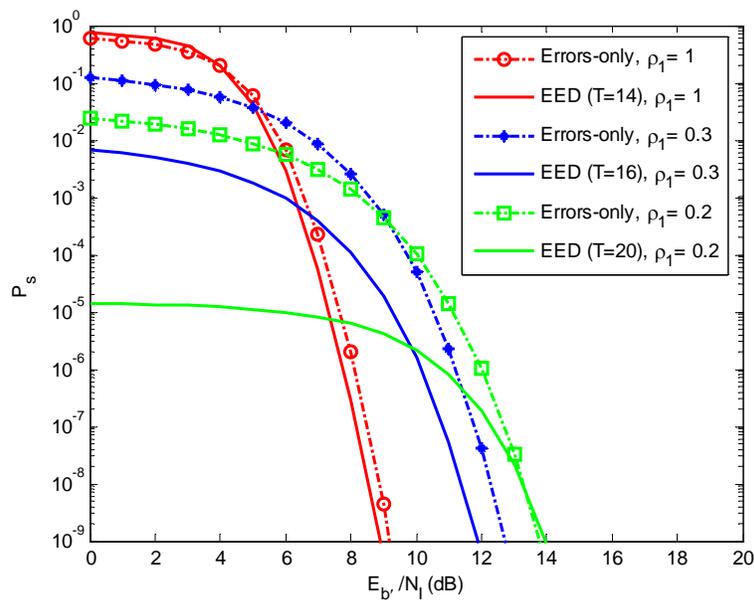
Figure 71. Probability of symbol error of a JTIDS/Link-16-type waveform for the single-pulse structure in both AWGN and PNI when the signal is transmitted over a slow, flat Nakagami fading channel where $m = 30$ and $E_{b'}/N_0 = 15\,\text{dB}$: EED versus errors-only RS decoding.

145
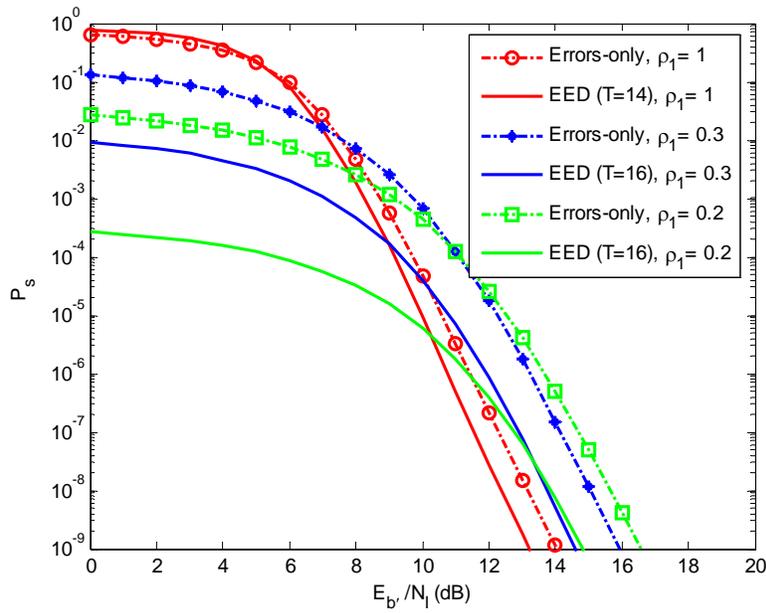
Figure 72. Probability of symbol error of a JTIDS/Link-16-type waveform for the single-pulse structure in both AWGN and PNI when the signal is transmitted over a slow, flat Nakagami fading channel where $m = 5$ and $E_{b'}/N_0 = 10\,\text{dB}$: EED versus errors-only RS decoding.
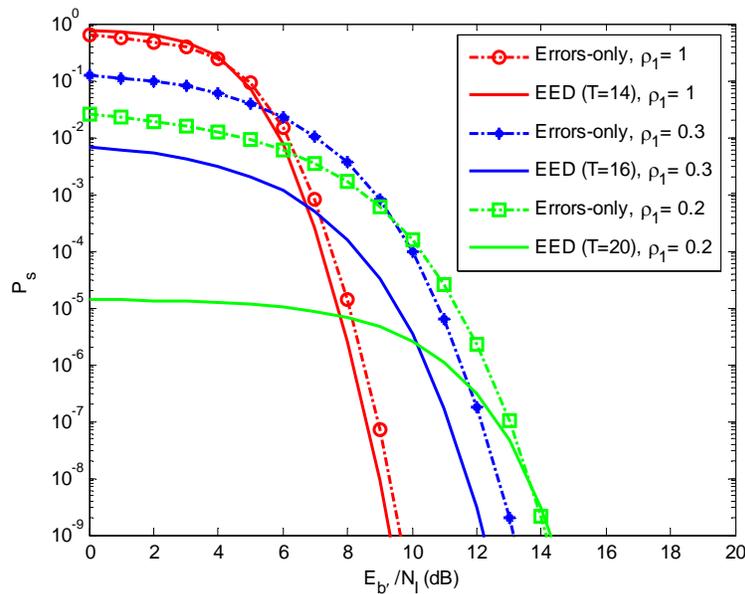
Figure 73. Probability of symbol error of a JTIDS/Link-16-type waveform for the single-pulse structure in both AWGN and PNI when the signal is transmitted over a slow, flat Nakagami fading channel where $m = 5$ and $E_{b'}/N_0 = 15\,\text{dB}$: EED versus errors-only RS decoding.
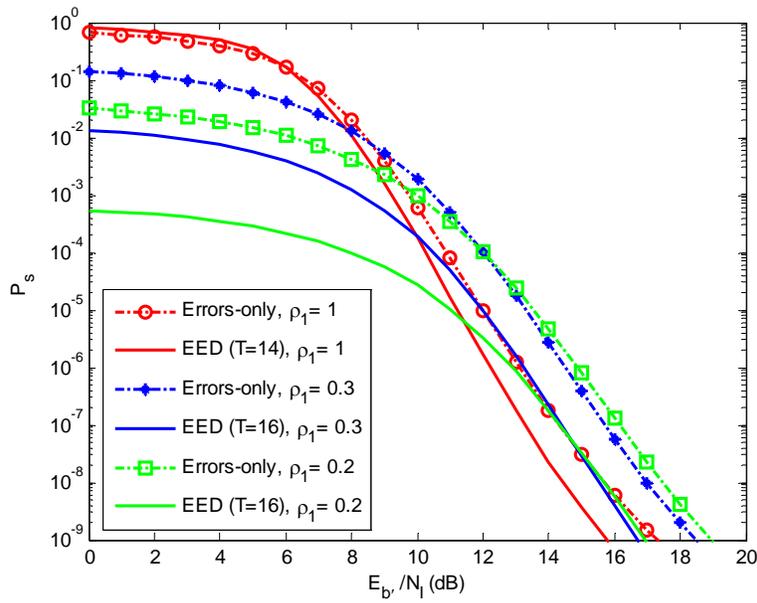
Figure 74. Probability of symbol error of a JTIDS/Link-16-type waveform for the single-pulse structure in both AWGN and PNI when the signal is transmitted over a slow, flat Nakagami fading channel where $m = 2$ and $E_{b'}/N_0 = 10\,\text{dB}$: EED versus errors-only RS decoding.
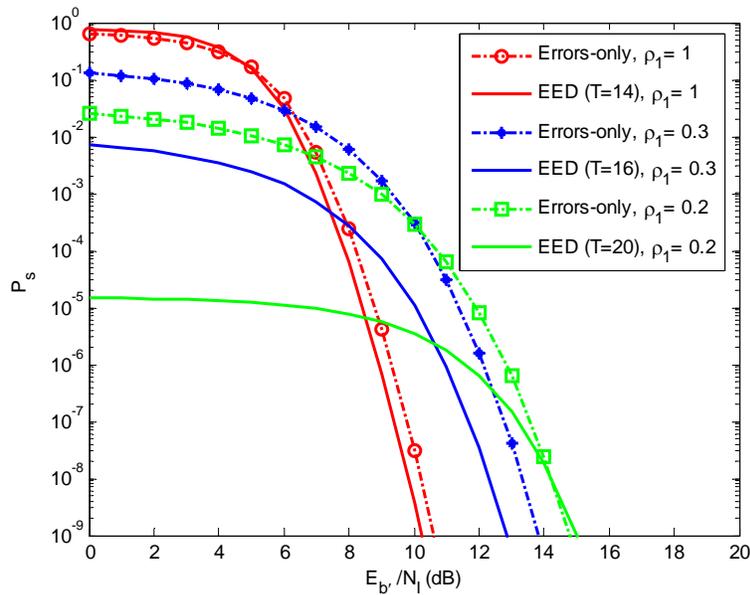

Figure 75. Probability of symbol error of a JTIDS/Link-16-type waveform for the single-pulse structure in both AWGN and PNI when the signal is transmitted over a slow, flat Nakagami fading channel where $m = 2$ and $E_{b'}/N_0 = 15\,\text{dB}$: EED versus errors-only RS decoding.

147

From Figures 70 to 75, several observations can be made. First, when $m = 30$, the results of Figures 70 and 71 are virtually identical to those for no fading shown in Figures 60 and 61, respectively. Second, when both ρ_1 and $E_{b'}/N_0$ are fixed, performance degrades as m decreases. For example, for $\rho_1 = 0.3$ and $E_{b'}/N_0 = 10\,\text{dB}$, the required $E_{b'}/N_I$ for EED at $P_S = 10^{-5}$ is 10.3 dB when $m = 30$ (see Figure 70), while the required $E_{b'}/N_I$ for EED at $P_S = 10^{-5}$ is 12 dB when $m = 2$ (see Figure 74). Third, for all cases shown in Figures 70 to 75, when both m and $E_{b'}/N_0$ are fixed, EED outperforms errors-only RS decoding and the superiority increases as ρ_1 decreases. For example, in Figure 72 where $m = 5$ and $E_{b'}/N_0 = 10\,\text{dB}$, for $\rho_1 = 1$, EED outperforms errors-only RS decoding by 0.6 dB at $P_S = 10^{-5}$, while for $\rho_1 = 0.2$, EED outperforms errors-only RS decoding by 3 dB. Lastly, from Figures 70 to 75, EED outperforms errors-only RS decoding and the largest margin (about 5 dB) is obtained when $\rho_1 = 0.2$ and $E_{b'}/N_0 = 15\,\text{dB}$, whether m is large or small. It can be shown that a larger margin (more than 5 dB) can be obtained for $\rho_1 = 0.1$ and $E_{b'}/N_0 = 15\,\text{dB}$. As was found for non-fading channels, for sufficiently large $E_{b'}/N_I$ and small ρ_1, PNI is completely ineffective for probabilities of symbol error greater than some specified value such as 10^{-5}.

9. Performance with EED in AWGN, PNI, and Nakagami Fading Channels When PSI is Assumed

When PSI is assumed, the process of investigating the performance of a JTIDS/Link-16-type waveform with EED for the double-pulse structure in both AWGN and PNI when the signal is transmitted over a slow, flat Nakagami fading channel is similar to that for channels with no fading. The only difference is that Equations (5.32), (5.37), and (5.36) are replaced by Equations (5.91), (5.98), and (5.96), respectively. To compare the difference between EED and errors-only RS decoding when PSI is assumed, both results are shown in Figures 76 to 81 for different values of m, ρ_1, and $E_{b'}/N_0$. Note that the results for $\rho_1 < 0.5$ are not shown in Figures 76 to 81 since their associated probability of symbol error is less than 10^{-5} for the entire range of $E_{b'}/N_I$.
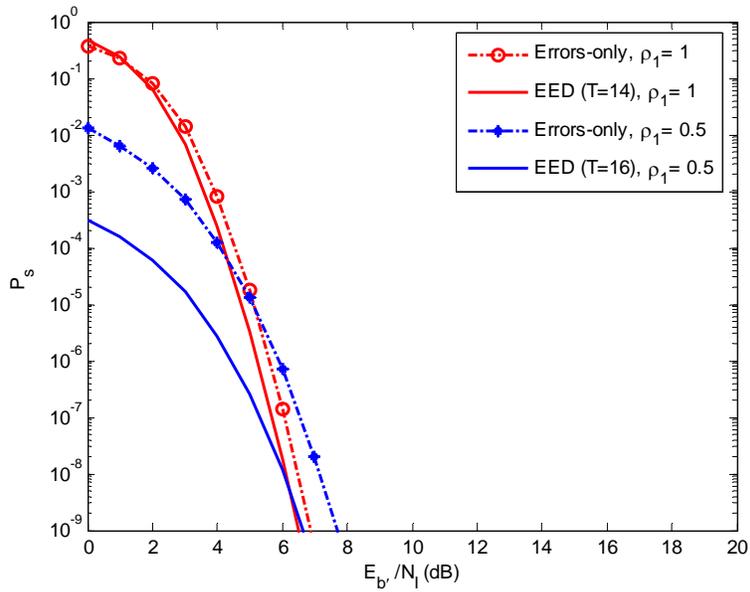
Figure 76.   Probability of symbol error of a JTIDS/Link-16-type waveform for the double-pulse structure with PSI in both AWGN and PNI when the signal is transmitted over a slow, flat Nakagami fading channel where $m = 30$ and $E_{b'}/N_0 = 10\,\text{dB}$: EED versus errors-only RS decoding.
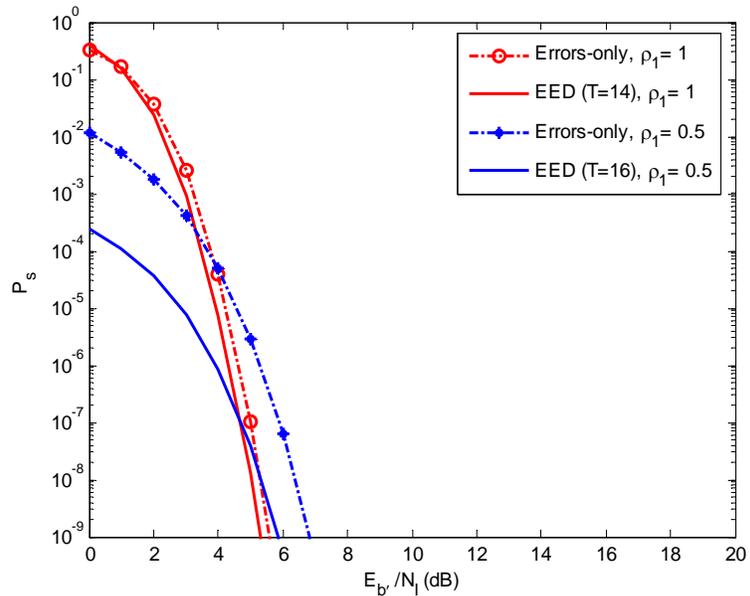
Figure 77.   Probability of symbol error of a JTIDS/Link-16-type waveform for the double-pulse structure with PSI in both AWGN and PNI when the signal is transmitted over a slow, flat Nakagami fading channel where $m = 30$ and $E_{b'}/N_0 = 15\,\text{dB}$: EED versus errors-only RS decoding.

149
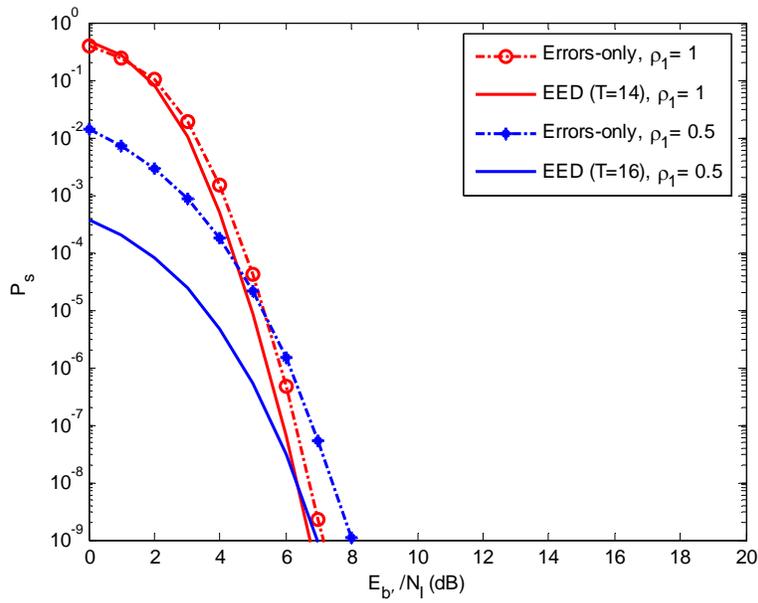
Figure 78.   Probability of symbol error of a JTIDS/Link-16-type waveform for the double-pulse structure with PSI in both AWGN and PNI when the signal is transmitted over a slow, flat Nakagami fading channel where $m = 5$ and $E_{b'}/N_0 = 10\,\text{dB}$: EED versus errors-only RS decoding.
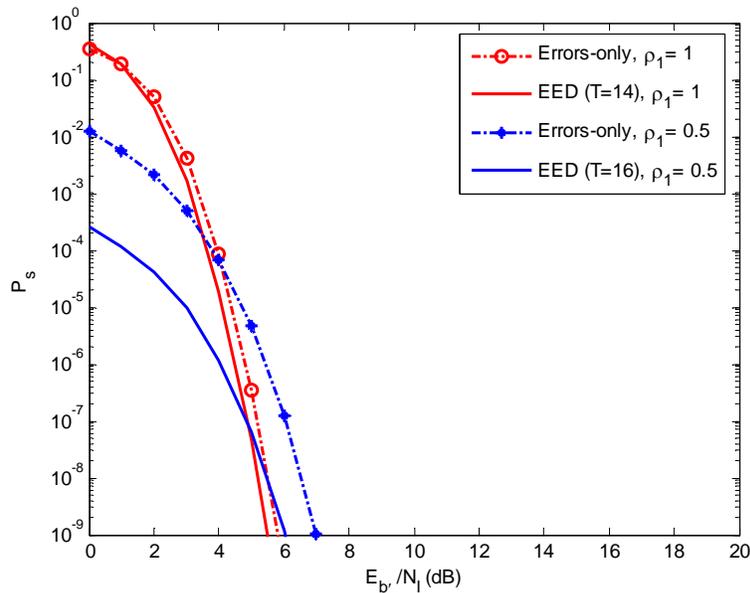
Figure 79.   Probability of symbol error of a JTIDS/Link-16-type waveform for the double-pulse structure with PSI in both AWGN and PNI when the signal is transmitted over a slow, flat Nakagami fading channel where $m = 5$ and $E_{b'}/N_0 = 15\,\text{dB}$: EED versus errors-only RS decoding.
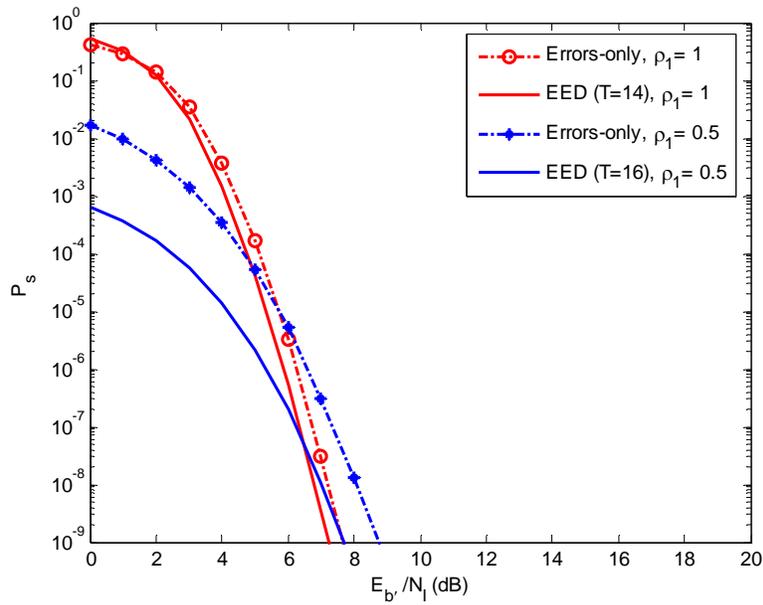
Figure 80.   Probability of symbol error of a JTIDS/Link-16-type waveform for the double-pulse structure with PSI in both AWGN and PNI when the signal is transmitted over a slow, flat Nakagami fading channel where $m = 2$ and $E_{b'}/N_0 = 10$ dB: EED versus errors-only RS decoding.
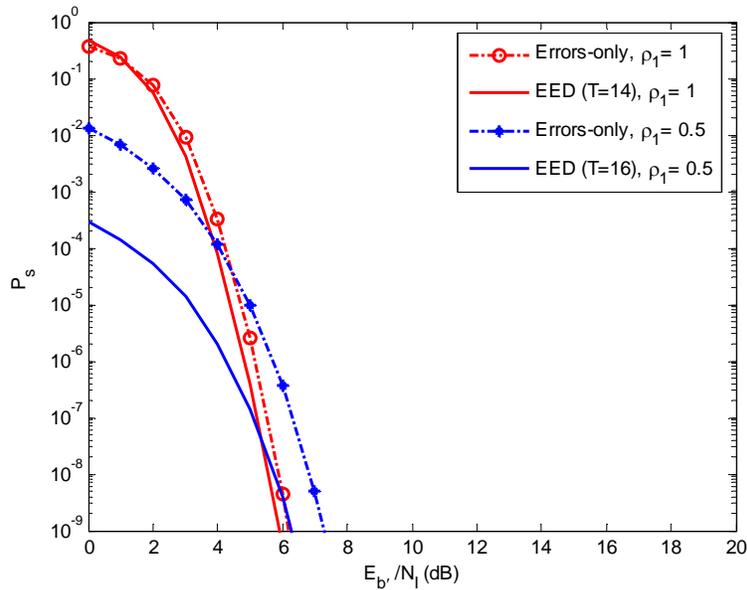

Figure 81.   Probability of symbol error of a JTIDS/Link-16-type waveform for the double-pulse structure with PSI in both AWGN and PNI when the signal is transmitted over a slow, flat Nakagami fading channel where $m = 2$ and $E_{b'}/N_0 = 15$ dB: EED versus errors-only RS decoding.

151

From Figures 76 to 81, several observations can be made. First, as expected, when $m = 30$, the results of Figures 76 and 77 are virtually identical to those obtained for no fading shown in Figures 64 and 65, respectively. Second, when both ρ_1 and $E_{b'}/N_0$ are fixed, performance degrades as m decreases, but the degradation is relatively small as compared to that for the single-pulse structure. For example, for $\rho_1 = 0.5$ and $E_{b'}/N_0 = 10 \, \text{dB}$, the required $E_{b'}/N_I$ for EED at $P_S = 10^{-5}$ is 3.3 dB when $m = 30$ (see Figure 76), while the required $E_{b'}/N_I$ for EED at $P_S = 10^{-5}$ is 4.2 dB when $m = 2$ (see Figure 80). Third, for all cases shown in Figures 76 to 81, when both m and $E_{b'}/N_0$ are fixed, EED outperforms errors-only RS decoding, and the superiority increases as ρ_1 decreases. For example, in Figure 78 where $m = 5$ and $E_{b'}/N_0 = 10 \, \text{dB}$, for $\rho_1 = 1$, EED outperforms errors-only RS decoding by 0.4 dB at $P_S = 10^{-5}$, while for $\rho_1 = 0.5$, EED outperforms errors-only RS decoding by 1.8 dB at $P_S = 10^{-5}$. Lastly, EED outperforms errors-only RS decoding, and the superiority virtually remains the same, whether the channel is fading or not. For example, for $\rho_1 = 0.5$ in Figure 76 where $m = 30$, EED outperforms errors-only RS decoding by 1.8 dB at $P_S = 10^{-5}$, while for $\rho_1 = 0.5$ in Figure 80 where $m = 2$, EED outperforms errors-only RS decoding by 1.6 dB at $P_S = 10^{-5}$.

B. PERFORMANCE ANALYSIS WITH AN IMPROVED CCSK SEQUENCE

Recall that the 32-chip CCSK starting sequence chosen for JTIDS and its 31 cyclically shifted versions are not orthogonal since the off-peak cross-correlation have values other than zero, and the maximum off-peak cross-correlation value is four. Intuitively, we can improve the performance of CCSK if the maximum off-peak cross-correlation value is less than four. Based on this idea, a search algorithm was created, and a new 32-chip CCSK starting sequence was found. This new starting sequence and its 31 cyclically shifted versions are shown in Table 16. Given that symbol 0 is sent and no chip error in the received 32-chip sequence, the off-peak cross-correlation of the new starting sequence has two discrete values: 0 and -4; that is, the maximum off-peak cross-correlation for the new starting sequence is zero instead of four.

Table 16.   New 32-chip CCSK starting sequence and its 31 cyclically shifted versions.

5-Bit Symbol	New 32-Chip CCSK Sequences
00000	S_0 = 10111010001111010010000001100110
00001	S_1 = 01110100011110100100000011001101
00010	S_2 = 11101000111101001000000110011010
00011	S_3 = 11010001111010010000001100110101
00100	S_4 = 10100011110100100000011001101011
⋮	⋮
11111	S_{31} = 01011101000111101001000000110011

Based on the same approach as we used to evaluate the 32-chip CCSK sequence chosen for JTIDS, this new 32-chip CCSK sequence is also evaluated both analytically and by Monte Carlo simulation with stratified sampling to obtain the conditional probabilities of symbol errors (denoted as ζ'_{UB_j} and ζ'_{SIM_j}, respectively). The results are shown in Table 17.

Table 17.   Conditional probabilities of symbol error for the new CCSK sequence.

$N = j$	ζ'_{UB_j}	ζ'_{SIM_j}
0	0	0
1	0	0
⋮	⋮	⋮
7	0	0
8	0.0147	0.0143
9	0.1040	0.1025
10	0.4023	0.3550
11	1.0	0.7140
12	1.0	0.9367
13	1.0	0.9956
14	1.0	0.9999
15	1.0	1.0
⋮	⋮	⋮
32	1.0	1.0

From Table 17, it is interesting to note that ζ_7' is zero for both the upper bound and the simulation results; that is, while the starting sequence chosen for JTIDS allows for six chip errors without making any symbol error, this new starting sequence allows for seven chip errors in the received 32-chip sequence without making any symbol error.

Now, substituting ζ_{SIM_j}' into Equation (4.43) along with the probability of chip error given in Equation (4.46), we obtain the probability of symbol error for the new CCSK sequence in AWGN. To compare the difference between the original CCSK sequence chosen for JTIDS and the new CCSK sequence, both results are shown in Figure 82. As can be seen, the results obtained with the new CCSK sequence are only slightly better than those obtained with the original sequence chosen for JTIDS since ultimate performance is determined at the symbol level rather than at the chip level. In essence, for practical values of the probability of chip error P_c, the first non-zero term in Equation (4.43) in not dominant.
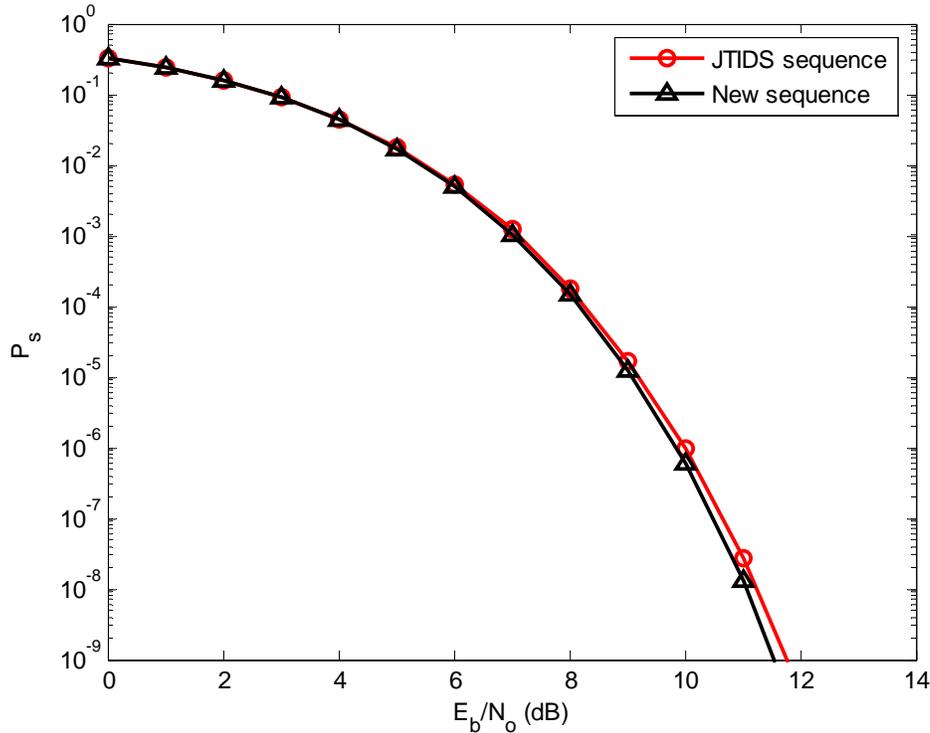
Figure 82.   Probability of symbol error for CCSK (uncoded JTIDS) in AWGN: the new CCSK sequence versus the CCSK sequence chosen for JTIDS.

Furthermore, substituting ζ'_{UB_j} into Equation (4.44) along with the probability of chip error given in Equation (4.46), we obtain an upper bound on the probability of symbol error for the new CCSK sequence in AWGN. To compare the difference between the simulation and the analytic upper bound for the new CCSK sequence, both results are shown in Figure 83. As before, the analytic method yields a tight upper bound.
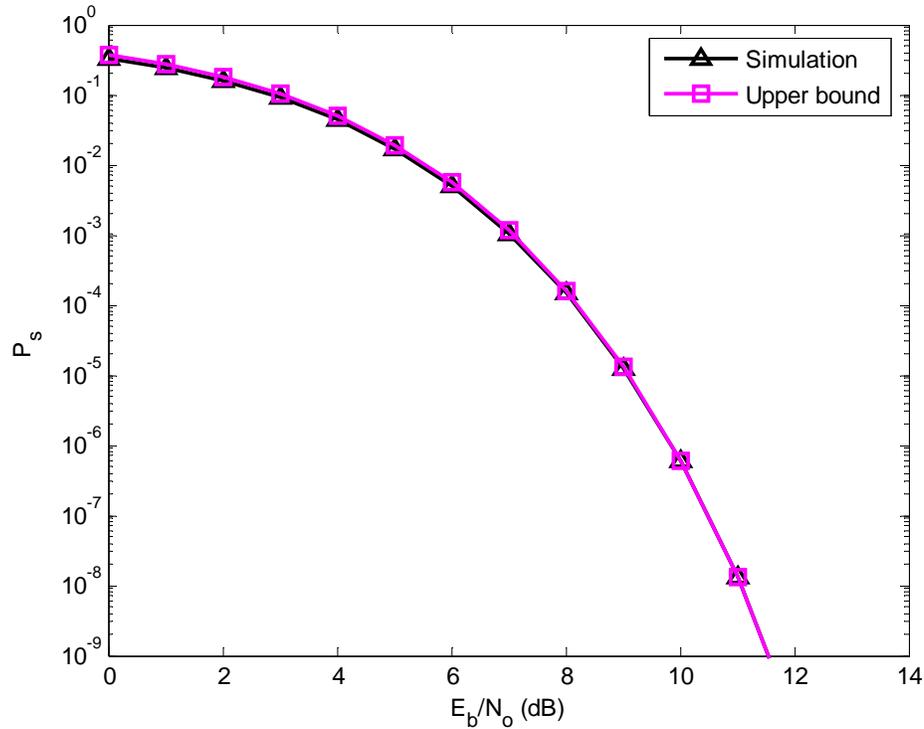
Figure 83.   Probability of symbol error for CCSK (uncoded JTIDS) with the new CCSK sequence in AWGN: analytic upper bound versus simulation results.

C.   SUMMARY OF CHAPTER VI

In this chapter, the probability of symbol error for a JTIDS/Link-16-type waveform with EED was investigated in Section A, and the probability of symbol error of CCSK (uncoded JTIDS) in AWGN was evaluated in Section B for a new 32-chip CCSK sequence. In Section A, before the performance was investigated, the conditional probabilities of channel symbol error ζ_{s_j}, channel symbol erasure ζ_{e_j}, and channel symbol correct ζ_{c_j} for EED were obtained from Monte Carlo simulation. Next, the optimal erasure threshold in terms of minimum probability of symbol error for a

JTIDS/Link-16-type waveform was obtained by trial-and-error for various types of narrowband interference, such as BNI and PNI. We found that for both the single-pulse structure and the double-pulse structure, the optimal erasure threshold is $T_{opt} = 14$, whether a JTIDS/Link-16-type waveform is transmitted over AWGN only or is transmitted in both AWGN and BNI.

When a JTIDS/Link-16-type waveform is transmitted in both AWGN and PNI, the optimal erasure threshold varies depending on (i) either the single- or the double-pulse structure, (ii) the value of $E_{b'}/N_0$ and ρ_1, and (iii) whether PSI is assumed or not. For example, for the single-pulse structure and $E_{b'}/N_0 = 10$ dB when PSI is not assumed, $T_{opt} = 14$ when $0.5 \le \rho_1 \le 1$, while $T_{opt} = 16$ when $0.2 \le \rho_1 < 0.5$. For the single-pulse structure and $E_{b'}/N_0 = 15$ dB when PSI is not assumed, $T_{opt} = 14$ when $0.5 \le \rho_1 \le 1$, $T_{opt} = 16$ when $\rho_1 = 0.3$, and $T_{opt} = 20$ when $\rho_1 = 0.2$. For the double-pulse structure when PSI is not assumed, $T_{opt} = 14$ when $0.3 \le \rho_1 \le 1$, while $T_{opt} = 16$ when $\rho_1 = 0.2$, whether $E_{b'}/N_0 = 10$ dB or 15 dB. When PSI is assumed, $T_{opt} = 14$ for $\rho_1 = 1$, while $T_{opt} = 16$ for $\rho_1 = 0.5$, whether $E_{b'}/N_0$ is 10 dB or 15 dB.

With the knowledge of ζ_{s_j}, ζ_{e_j}, ζ_{o_j}, and T_{opt}, the probability of symbol error for a JTIDS/Link-16-type waveform with EED for both the single- and the double-pulse structure were investigated for both fading channels and channels with no fading, and the results were compared to those obtained with errors-only RS decoding in Chapter V. The results show that EED outperforms errors-only RS decoding in all cases, whether the channel is fading or not and whether the narrowband interference is present or not. In general, with EED, the probability of symbol error is significantly improved (more than 5 dB for the single-pulse structure) when ρ_1 is small and $E_{b'}/N_0$ is large as compared to errors-only RS decoding, whether the channel is fading or not.

In Section B, the probability of symbol error for CCSK (uncoded JTIDS) in AWGN was investigated based on a new 32-chip CCSK sequence. The new 32-chip CCSK sequence has a smaller maximum off-peak cross-correlation value and allows for seven instead of six chip errors in the received sequence without making a symbol error.

The results obtained with the new CCSK sequence are only slightly better than those obtained with the original sequence chosen for JTIDS since performance is determined at the symbol level rather than at the chip level. Note that, in terms of modifying JITIDS in order to improve performance, EED is more attractive than changing the 32-chip CCSK sequence since EED is backwards compatible with existing JTIDS transceivers, while a new 32-chip CCSK sequence is not.

In the next chapter, the contributions of this dissertation are summarized, and some recommendations for future research are made.

THIS PAGE INTENTIONALLY LEFT BLANK

VII. CONCLUSIONS

A.   NOVEL CONTRIBUTIONS AND FINDINGS

In this dissertation, the probability of symbol error for a JTIDS/Link-16-type waveform with errors-only RS decoding in both AWGN and narrowband interference when the signal is transmitted over a slow, flat Nakagami fading channel was investigated. To improve the performance in terms of probability of symbol error, two modified systems were also proposed and evaluated. The first system uses EED in place of errors-only RS decoding, while the second system employs a new 32-chip CCSK sequence instead of the 32-chip CCSK sequence chosen for JTIDS. Several novel contributions and major findings that result from the analysis of this dissertation are summarized below.

To the best of the author's knowledge, the performance analysis and simulation of CCSK shown in Chapter IV is a novel contribution of this dissertation. Even though [11] was the first to publish an analysis of CCSK performance, the analysis is unsound due to the overly optimistic assumption that the cross-correlation values of CCSK symbols are statistically independent. In Chapter IV, the cross-correlation properties of CCSK are first formulated, and then an analytic upper bound on the probability of symbol error of CCSK in AWGN is derived for the 32-chip CCSK sequence chosen for JTIDS. The analytic upper bound is shown to be a tight upper bound by comparing the analytic results with two different Monte Carlo simulations. Based on two totally different approaches, the two Monte Carlo simulations yield a virtually identical result, which in turn is very close to the analytic result.

In Chapter V, the performance analysis of a JTIDS/Link-16 type waveform for both the single- and the double-pulse structure with errors-only RS decoding in both AWGN and narrow-band interference when the signal is transmitted over a slow, flat Nakagami fading channel is another novel contribution of this dissertation. Several major findings can be summarized. First, the double-pulse structure outperforms the single-pulse structure in most cases except when both PNI is present with small ρ_1 (such as $\rho_1 = 0.1$) and $E_{b'}/N_I$ is relatively small (such as $E_{b'}/N_I \leq 6\,\mathrm{dB}$). When this occurs, the

performance for the double-pulse structure tends to be poorer than that of the single-pulse structure since the double-pulse structure is more likely to have at least one pulse jammed. Second, for both the single- and the double-pulse structure in both AWGN and narrowband interference (without fading), the value of ρ_1 that maximizes the probability of symbol error decreases as $E_{b'}/N_I$ increases; that is, barrage noise interference ($\rho_1 = 1$) has the most effect in degrading performance when $E_{b'}/N_I$ is relatively small, while PNI with smaller ρ_1 (such as $\rho_1 = 0.1$) causes the greatest degradation when $E_{b'}/N_I$ is relatively large. This is consistent with our intuition that, for strong signals, the jammer power must be large during a symbol in order to make symbol error likely. Third, when a JTIDS/Link-16-type waveform transmitted over a slow, flat Nakagami fading channel in the presence of both AWGN and PNI, the probability of symbol error for the single-pulse structure increases as m decreases for a fixed value of ρ_1 and $E_{b'}/N_0$. This is consistent with our intuition that the single-pulse structure is less robust and therefore suffers more as fading worsens. Lastly, when the signal is transmitted over a slow, flat Nakagami fading channel and subjected to both AWGN and PNI when PSI is assumed, the double-pulse structure with PSI outperforms the single-pulse structure by a greater margin for smaller m when $E_{b'}/N_0$ is fixed. Perfect side information (PSI) is not realistic but gives us a benchmark against which to measure receivers that have imperfect or no side information.

In Section A of Chapter VI, the performance analysis of a JTIDS/Link-16 type waveform for both the single- and the double-pulse structure with EED in both AWGN and narrow-band interference when the signal is transmitted over a slow, flat Nakagami fading channel is another novel contribution of this dissertation. Two major findings are summarized. First, EED outperforms errors-only RS decoding in all cases, whether the channel is fading or not and whether the narrowband interference is present or not. Second, when ρ_1 is small and $E_{b'}/N_0$ is large, with EED, the performance of a JTIDS/Link-16 type waveform is significantly improved (more than 5 dB is observed for the single-pulse structure) as compared to errors-only RS decoding, whether the channel is fading or not.

In Section B of Chapter VI, the probability of symbol error for CCSK in AWGN was investigated based on a new 32-chip CCSK sequence obtained from a search algorithm. This new 32-chip CCSK sequence has a smaller maximum off-peak cross-correlation value ($H = 0$ instead of $H = 4$) and allows for seven chip errors instead of six chip errors in the received sequence without making a symbol error. This new CCSK sequence is the fourth novel contribution of this dissertation. The results show that the probability of symbol error obtained for the new 32-chip CCSK sequence is only slightly smaller than that obtained with the 32-chip CCSK sequence chosen for JTIDS. There is an appreciable improvement in performance for an extremely small probability of symbol error P_S, but for $P_S \approx 0.01$ as required for JTIDS, the difference is negligible.

B.   RECOMMENDATIONS FOR FURTHER RESEARCH

There are four primary areas in which follow-on research is recommended. First, recall that in Chapter V, the probability of symbol error of a JTIDS/Link-16-type waveform in both AWGN and PNI when transmitted over a slow, flat Nakagami fading channel was not investigated for the double-pulse structure. This is an area for a future effort that will allow the performance analysis for a JTIDS/Link-16-type waveform transmitted over fading channels to be extended to account for PNI when PSI is not available.

Second, in Chapter VI, the performance of a JTIDS/Link-16 type waveform for both the single- and the double-pulse structure with EED in both AWGN and narrow-band interference when the signal is transmitted over a slow, flat Nakagami fading channel was investigated based on Monte Carlo simulation to obtain the conditional probabilities of channel symbol error ζ_{s_j}, the conditional probabilities of channel symbol erasure ζ_{e_j}, and the conditional probabilities of channel symbol correct ζ_{c_j}. As a consequence, a derivation of analytic expressions for ζ_{s_j}, ζ_{e_j}, and ζ_{c_j} is a natural outgrowth of this dissertation.

Third, in Chapter VI, a new 32-chip CCSK sequence was obtained from a simple search algorithm written in MatLab. The new 32-chip CCSK sequence has a smaller maximum off-peak cross-correlation value ($H = 0$) and compares favorably to the 32-

chip sequence chosen for JTIDS. If a 32-chip CCSK sequence with a maximum off-peak cross-correlation value less than zero can be found, then system performance can be further improved. Therefore, a superior search algorithm that can find best 32-chip CCSK sequence would be an interesting topic for follow-on research.

Lastly, as mentioned at the beginning of this dissertation, the actual JTIDS waveform is received noncoherently at the chip level, but here the performance with coherent detection was evaluated in order to see how much of an improvement would result if coherent chip demodulation were practical. The performance analysis developed in this dissertation can be easily modified to evaluate noncoherent chip demodulation.

C.   CLOSING COMMENTS

The tactical data link (TDL) has played an important role on the battlefield since the late 1950s. Starting from an unsecured and low data rate system, such as Link-4A, the TDL has evolved into a more secure, more jam-resistant, and higher data rate system. To meet the requirements of tomorrow's battlefield, the demand for a more robust, higher data rate TDL is rapidly growing. Therefore, the modifications proposed in this dissertation may prove beneficial to those seeking to design a more robust TDL. Note that, in terms of modifying JITIDS in order to improve performance, EED is more attractive than changing the 32-chip CCSK sequence since EED is backwards compatible with existing JTIDS transceivers, while a new 32-chip CCSK sequence is not.

APPENDIX A. DEPENDENCE OF CCSK CROSS-CORRELATION VALUES

Let two events A and B have nonzero probabilities of occurrence; that is, assume $P\{A\} \neq 0$ and $P\{B\} \neq 0$. If A and B are conditionally independent given event C, then

$$P\{A \cap B|C\} = P\{A|C\} P\{B|C\}. \tag{A.1}$$

Now, let event $A = \{\mathfrak{R}_7 = 18\}$, event $B = \{\mathfrak{R}_{16} = 18\}$, and event $C = \{N = 7\}$, where $\mathfrak{R}_i$ is the cross-correlation value corresponding to the ith branch of the CCSK symbol demodulator (see Figure 21) and N is the total number of chip errors in the received 32-chip sequence at the input of the CCSK symbol demodulator. From Equation (4.16),

$$\begin{aligned} P\{A|C\} &= P\{\mathfrak{R}_7 = 18|N = 7\} = 1.02 \times 10^{-3} \\ &= P\{\mathfrak{R}_{16} = 18|N = 7\} \\ &= P\{B|C\}; \end{aligned} \tag{A.2}$$

that is,

$$P\{A|C\} P\{B|C\} > 0. \tag{A.3}$$

Furthermore, from Table 5, by enumerating all possibilities, it is not possible to have $R_7 = R_{16} = 18$ given that $N = 7$; that is,

$$P\{\mathfrak{R}_7 = 18 \cap \mathfrak{R}_{16} = 18|N = 7\} = 0, \tag{A.4}$$

or

$$P\{A \cap B|C\} = 0. \tag{A.5}$$

Since Equation (A.3) is not equal to (A.5), Equation (A.1) is not satisfied. Therefore, the cross-correlation values of CCSK are not conditionally independent.

THIS PAGE INTENTIONALLY LEFT BLANK

APPENDIX B. STANDARD ERRORS OF CCSK SIMULATION

Recall from Chapter IV that the probability of symbol error for CCSK is given by

$$P_S = \sum_{j=0}^{32} P\{\text{symbol error}|N = j\}P\{N = j\}$$
$$= \sum_{j=0}^{32} \zeta_{SIM_j} P\{N = j\},$$

(B.1)

where the conditional probabilities of symbol error are evaluated both analytically and by Monte Carlo simulation. The second line of Equation (B.1) indicates that the probability of symbol error for CCSK is evaluated by simulation. To check the accuracy of the simulation results, it is usual to find the standard error of the simulation.

The standard error of Equation (B.1) was shown in Equation (4.47), which is obtained as follows. The variance of Equation (B.1) is given by

$$Var(P_S) = Var\left(\sum_{j=0}^{32} \zeta_{SIM_j} P\{N = j\}\right)$$
$$= \sum_{j=0}^{32} (P\{N = j\})^2 Var(\zeta_{SIM_j})$$

(B.2)

since the pmf $P\{N = j\}$ is known. Now, from Equation (B.2), the standard error of Equation (B.1) is given by [43]

$$StdErr(P_S) = \sqrt{Var(P_S)}$$
$$= \sqrt{\sum_{j=0}^{32} (P\{N = j\})^2 Var(\zeta_{SIM_j})}$$
$$= \sqrt{\sum_{j=0}^{32} (P\{N = j\})^2 \left(\frac{Var_j}{n}\right)},$$

(B.3)

where Var_j is the variance of the conditional probabilities of symbol error ζ_j and n is the number of simulation iterations.

THIS PAGE INTENTIONALLY LEFT BLANK

APPENDIX C. CONDITIONAL PROBABILITIES OF CCSK

C.1   Simulation results for EED with $T = 0$ (10,000 iterations).

$N = j$	ζ_{s_j}		ζ_{e_j}		ζ_{o_j}	
	estimate	std. error	estimate	std. error	estimate	std. error
0	0	0	0	0	1	0
1	0	0	0	0	1	0
2	0	0	0	0	1	0
3	0	0	0	0	1	0
4	0	0	0	0	1	0
5	0	0	0	0	1	0
6	0	0	0	0	1	0
7	0.0015	0.0003	0	0	0.9885	0.0003
8	0.0208	0.0010	0	0	0.9792	0.0010
9	0.1144	0.0023	0	0	0.8856	0.0023
10	0.3656	0.0032	0	0	0.6344	0.0032
11	0.7108	0.0026	0	0	0.2892	0.0026
12	0.9363	0.0011	0	0	0.0637	0.0011
13	0.9954	0.0003	0	0	0.0046	0.0003
14	0.9999	0.0002	0	0	0.0001	0.0002
15	1	0	0	0	0	0
16	1	0	0	0	0	0
17	1	0	0	0	0	0
18	1	0	0	0	0	0
19	1	0	0	0	0	0
20	1	0	0	0	0	0
21	1	0	0	0	0	0
22	1	0	0	0	0	0
23	1	0	0	0	0	0
24	1	0	0	0	0	0
25	1	0	0	0	0	0
26	1	0	0	0	0	0
27	1	0	0	0	0	0
28	1	0	0	0	0	0
29	1	0	0	0	0	0
30	1	0	0	0	0	0
31	1	0	0	0	0	0
32	1	0	0	0	0	0

C.2   Simulation results for EED with $T = 4$ (10,000 iterations).

$N = j$	ζ_{s_j}		ζ_{e_j}		ζ_{o_j}	
	estimate	std. error	estimate	std. error	estimate	std. error
0	0	0	0	0	1	0
1	0	0	0	0	1	0
2	0	0	0	0	1	0
3	0	0	0	0	1	0
4	0	0	0	0	1	0
5	0	0	0	0	1	0
6	0	0	0	0	1	0
7	0.0013	0.0002	0	0	0.9987	0.0002
8	0.0180	0.0009	0	0	0.9820	0.0009
9	0.1114	0.0023	0	0	0.8886	0.0023
10	0.3646	0.0032	0	0	0.6354	0.0032
11	0.7128	0.0025	0	0	0.2872	0.0025
12	0.9344	0.0011	0	0	0.0656	0.0011
13	0.9956	0.0002	0	0	0.0044	0.0002
14	1	0	0	0	0	0
15	1	0	0	0	0	0
16	1	0	0	0	0	0
17	1	0	0	0	0	0
18	1	0	0	0	0	0
19	1	0	0	0	0	0
20	1	0	0	0	0	0
21	1	0	0	0	0	0
22	1	0	0	0	0	0
23	1	0	0	0	0	0
24	1	0	0	0	0	0
25	1	0	0	0	0	0
26	1	0	0	0	0	0
27	1	0	0	0	0	0
28	1	0	0	0	0	0
29	1	0	0	0	0	0
30	1	0	0	0	0	0
31	1	0	0	0	0	0
32	1	0	0	0	0	0

C.3   Simulation results for EED with $T = 6$ (10,000 iterations).

$N = j$	ζ_{s_j}		ζ_{e_j}		ζ_{o_j}	
	estimate	std. error	estimate	std. error	estimate	std. error
0	0	0	0	0	1	0
1	0	0	0	0	1	0
2	0	0	0	0	1	0
3	0	0	0	0	1	0
4	0	0	0	0	1	0
5	0	0	0	0	1	0
6	0	0	0	0	1	0
7	0.0012	0.0002	0	0	0.9988	0.0002
8	0.0211	0.0010	0	0	0.9789	0.0010
9	0.1088	0.0022	0	0	0.8912	0.0022
10	0.3654	0.0032	0	0	0.6346	0.0032
11	0.7181	0.0025	0	0	0.2819	0.0025
12	0.9341	0.0011	0	0	0.0659	0.0011
13	0.9959	0.0002	0	0	0.0041	0.0002
14	0.9994	0.0002	0.0006	0.0002	0	0
15	1	0	0	0	0	0
16	0.9999	0.0001	0.0001	0.0001	0	0
17	1	0	0	0	0	0
18	0.9997	0.0002	0.0003	0.0002	0	0
19	1	0	0	0	0	0
20	0.9998	0.0001	0.0002	0.0001	0	0
21	1	0	0	0	0	0
22	0.9998	0.0001	0.0002	0.0001	0	0
23	1	0	0	0	0	0
24	0.9996	0.0002	0.0004	0.0002	0	0
25	1	0	0	0	0	0
26	0.9981	0.0004	0.0019	0.0004	0	0
27	1	0	0	0	0	0
28	0.9933	0.0008	0.0067	0.0008	0	0
29	1	0	0	0	0	0
30	0.9181	0.0027	0.0819	0.0027	0	0
31	1	0	0	0	0	0
32	0	0	1	0	0	0

C.4   Simulation results for EED with $T = 8$ (10,000 iterations).

$N = j$	ζ_{s_j}		ζ_{e_j}		ζ_{o_j}	
	estimate	std. error	estimate	std. error	estimate	std. error
0	0	0	0	0	1	0
1	0	0	0	0	1	0
2	0	0	0	0	1	0
3	0	0	0	0	1	0
4	0	0	0	0	1	0
5	0	0	0	0	1	0
6	0	0	0	0	1	0
7	0.0013	0.0003	0	0	0.9987	0.0003
8	0.0205	0.0010	0	0	0.9795	0.0010
9	0.1109	0.0022	0	0	0.8891	0.0022
10	0.3611	0.0032	0	0	0.6389	0.0032
11	0.7122	0.0025	0	0	0.2878	0.0025
12	0.9339	0.0011	0	0	0.0061	0.0011
13	0.9649	0.0018	0.0351	0.0018	0	0
14	0.9996	0.0002	0.0004	0.0002	0	0
15	0.9745	0.0016	0.0255	0.0016	0	0
16	0.9998	0.0001	0.0002	0.0001	0	0
17	0.9813	0.0014	0.0187	0.0014	0	0
18	0.9997	0.0002	0.0003	0.0002	0	0
19	0.9811	0.0014	0.0189	0.0014	0	0
20	0.9998	0.0001	0.0002	0.0001	0	0
21	0.9755	0.0015	0.0245	0.0015	0	0
22	0.9998	0.0001	0.0002	0.0001	0	0
23	0.9646	0.0018	0.0354	0.0018	0	0
24	0.9996	0.0002	0.0004	0.0002	0	0
25	0.9331	0.0025	0.0669	0.0025	0	0
26	0.9982	0.0004	0.0018	0.0004	0	0
27	0.8430	0.0036	0.1570	0.0036	0	0
28	0.9922	0.0009	0.0078	0.0009	0	0
29	0.5858	0.0049	0.4142	0.0049	0	0
30	0.9214	0.0027	0.0786	0.0027	0	0
31	0	0	1	0	0	0
32	0	0	1	0	0	0

C.5   Simulation results for EED with $T = 10$ (10,000 iterations).

$N = j$	ζ_{s_j}		ζ_{e_j}		ζ_{o_j}	
	estimate	std. error	estimate	std. error	estimate	std. error
0	0	0	0	0	1	0
1	0	0	0	0	1	0
2	0	0	0	0	1	0
3	0	0	0	0	1	0
4	0	0	0	0	1	0
5	0	0	0	0	1	0
6	0	0	0	0	1	0
7	0.0012	0.0002	0	0	0.9988	0.0002
8	0.0202	0.0010	0	0	0.9798	0.0010
9	0.1111	0.0022	0	0	0.8889	0.0022
10	0.3577	0.0032	0	0	0.6423	0.0032
11	0.7143	0.0025	0	0	0.2857	0.0025
12	0.6934	0.0046	0.3066	0.0046	0	0
13	0.9624	0.0019	0.0376	0.0019	0	0
14	0.7569	0.0043	0.2431	0.0043	0	0
15	0.9749	0.0016	0.0251	0.0016	0	0
16	0.7920	0.0041	0.2080	0.0041	0	0
17	0.9807	0.0014	0.0193	0.0014	0	0
18	0.7928	0.0041	0.2072	0.0041	0	0
19	0.9798	0.0014	0.0202	0.0014	0	0
20	0.7867	0.0041	0.2133	0.0041	0	0
21	0.9774	0.0015	0.0226	0.0015	0	0
22	0.7418	0.0044	0.2582	0.0044	0	0
23	0.9619	0.0019	0.0381	0.0019	0	0
24	0.6578	0.0047	0.3422	0.0047	0	0
25	0.9396	0.0024	0.0604	0.0024	0	0
26	0.5017	0.0050	0.4983	0.0050	0	0
27	0.8466	0.0036	0.1534	0.0036	0	0
28	0.2636	0.0044	0.7364	0.0044	0	0
29	0.5822	0.0049	0.4178	0.0049	0	0
30	0	0	1	0	0	0
31	0	0	1	0	0	0
32	0	0	1	0	0	0

C.6   Simulation results for EED with $T = 12$ (10,000 iterations).

$N = j$	ζ_{s_j}		ζ_{e_j}		ζ_{o_j}	
	estimate	std. error	estimate	std. error	estimate	std. error
0	0	0	0	0	1	0
1	0	0	0	0	1	0
2	0	0	0	0	1	0
3	0	0	0	0	1	0
4	0	0	0	0	1	0
5	0	0	0	0	1	0
6	0	0	0	0	1	0
7	0.0011	0.0002	0	0	0.9989	0.0002
8	0.0204	0.0010	0	0	0.9796	0.0010
9	0.1164	0.0023	0	0	0.8836	0.0023
10	0.3617	0.0032	0	0	0.6383	0.0032
11	0.2966	0.0046	0.7034	0.0046	0	0
12	0.7029	0.0046	0.2971	0.0046	0	0
13	0.3778	0.0048	0.6222	0.0048	0	0
14	0.7597	0.0043	0.2403	0.0043	0	0
15	0.4205	0.0049	0.5795	0.0049	0	0
16	0.7946	0.0040	0.2054	0.0040	0	0
17	0.4483	0.0050	0.5517	0.0050	0	0
18	0.7932	0.0041	0.2068	0.0041	0	0
19	0.4337	0.0050	0.5663	0.0050	0	0
20	0.7863	0.0041	0.2137	0.0041	0	0
21	0.4053	0.0049	0.5947	0.0049	0	0
22	0.7366	0.0044	0.2634	0.0044	0	0
23	0.3253	0.0047	0.6747	0.0047	0	0
24	0.6561	0.0048	0.3439	0.0048	0	0
25	0.2262	0.0042	0.7738	0.0042	0	0
26	0.5096	0.0050	0.4904	0.0050	0	0
27	0.0986	0.0030	0.9014	0.0030	0	0
28	0.2642	0.0044	0.7358	0.0044	0	0
29	0	0	1	0	0	0
30	0	0	1	0	0	0
31	0	0	1	0	0	0
32	0	0	1	0	0	0

C.7   Simulation results for EED with $T = 14$ (10,000 iterations).

$N = j$	ζ_{s_j}		ζ_{e_j}		ζ_{o_j}	
	estimate	std. error	estimate	std. error	estimate	std. error
0	0	0	0	0	1	0
1	0	0	0	0	1	0
2	0	0	0	0	1	0
3	0	0	0	0	1	0
4	0	0	0	0	1	0
5	0	0	0	0	1	0
6	0	0	0	0	1	0
7	0.0018	0.0003	0	0	0.9982	0.0003
8	0.0194	0.0010	0	0	0.9806	0.0010
9	0.1116	0.0022	0	0	0.8884	0.0022
10	0.0772	0.0027	0.9228	0.0027	0	0
11	0.3033	0.0046	0.6967	0.0046	0	0
12	0.1217	0.0033	0.8783	0.0033	0	0
13	0.3715	0.0048	0.6285	0.0048	0	0
14	0.1624	0.0037	0.8376	0.0037	0	0
15	0.4313	0.0050	0.5687	0.0050	0	0
16	0.1711	0.0038	0.8289	0.0038	0	0
17	0.4429	0.0050	0.5571	0.0050	0	0
18	0.1876	0.0039	0.8124	0.0039	0	0
19	0.4339	0.0050	0.5661	0.0050	0	0
20	0.1675	0.0037	0.8325	0.0037	0	0
21	0.4032	0.0049	0.5968	0.0049	0	0
22	0.1331	0.0034	0.8669	0.0034	0	0
23	0.3263	0.0047	0.6737	0.0047	0	0
24	0.0837	0.0028	0.9163	0.0028	0	0
25	0.2129	0.0041	0.7871	0.0041	0	0
26	0.0311	0.0017	0.9689	0.0017	0	0
27	0.0981	0.0030	0.9019	0.0030	0	0
28	0	0	1	0	0	0
29	0	0	1	0	0	0
30	0	0	1	0	0	0
31	0	0	1	0	0	0
32	0	0	1	0	0	0

C.8   Simulation results for EED with $T = 16$ (10,000 iterations).

$N = j$	ζ_{s_j}		ζ_{e_j}		ζ_{o_j}	
	estimate	std. error	estimate	std. error	estimate	std. error
0	0	0	0	0	1	0
1	0	0	0	0	1	0
2	0	0	0	0	1	0
3	0	0	0	0	1	0
4	0	0	0	0	1	0
5	0	0	0	0	1	0
6	0	0	0	0	1	0
7	0.0015	0.0003	0	0	0.9985	0.0003
8	0.0191	0.0010	0	0	0.9809	0.0010
9	0.0115	0.0011	0.9885	0.0011	0	0
10	0.0813	0.0027	0.9187	0.0027	0	0
11	0.0268	0.0016	0.9732	0.0016	0	0
12	0.1178	0.0032	0.8822	0.0032	0	0
13	0.0408	0.0020	0.9592	0.0020	0	0
14	0.1512	0.0036	0.8488	0.0036	0	0
15	0.0583	0.0023	0.9417	0.0023	0	0
16	0.1820	0.0039	0.8180	0.0039	0	0
17	0.0606	0.0024	0.9394	0.0024	0	0
18	0.1800	0.0038	0.8200	0.0038	0	0
19	0.0532	0.0022	0.9468	0.0022	0	0
20	0.1712	0.0038	0.8288	0.0038	0	0
21	0.0461	0.0021	0.9539	0.0021	0	0
22	0.1286	0.0033	0.8714	0.0033	0	0
23	0.0296	0.0017	0.9704	0.0017	0	0
24	0.0815	0.0027	0.9185	0.0027	0	0
25	0.0088	0.0009	0.9912	0.0009	0	0
26	0.0354	0.0018	0.9646	0.0018	0	0
27	0	0	1	0	0	0
28	0	0	1	0	0	0
29	0	0	1	0	0	0
30	0	0	1	0	0	0
31	0	0	1	0	0	0
32	0	0	1	0	0	0

C.9   Simulation results for EED with $T = 18$ (10,000 iterations).

$N = j$	ζ_{s_j}		ζ_{e_j}		ζ_{o_j}	
	estimate	std. error	estimate	std. error	estimate	std. error
0	0	0	0	0	1	0
1	0	0	0	0	1	0
2	0	0	0	0	1	0
3	0	0	0	0	1	0
4	0	0	0	0	1	0
5	0	0	0	0	1	0
6	0	0	0	0	1	0
7	0.0018	0.0003	0	0	0.9982	0.0003
8	0.0004	0.0002	0.9996	0.0002	0	0
9	0.0133	0.0011	0.9867	0.0011	0	0
10	0.0041	0.0006	0.9959	0.0006	0	0
11	0.0270	0.0016	0.9730	0.0016	0	0
12	0.0098	0.0010	0.9902	0.0010	0	0
13	0.0457	0.0021	0.9543	0.0021	0	0
14	0.0114	0.0011	0.9886	0.0011	0	0
15	0.0558	0.0023	0.9442	0.0023	0	0
16	0.0168	0.0013	0.9832	0.0013	0	0
17	0.0562	0.0023	0.9438	0.0023	0	0
18	0.0161	0.0013	0.9839	0.0013	0	0
19	0.0555	0.0023	0.9445	0.0023	0	0
20	0.0128	0.0011	0.9872	0.0011	0	0
21	0.0449	0.0021	0.9551	0.0021	0	0
22	0.0085	0.0009	0.9915	0.0009	0	0
23	0.0283	0.0017	0.9717	0.0017	0	0
24	0.0027	0.0005	0.9973	0.0005	0	0
25	0.0086	0.0009	0.9914	0.0009	0	0
26	0	0	1	0	0	0
27	0	0	1	0	0	0
28	0	0	1	0	0	0
29	0	0	1	0	0	0
30	0	0	1	0	0	0
31	0	0	1	0	0	0
32	0	0	1	0	0	0

C.10   Simulation results for EED with $T = 20$ (10,000 iterations).

$N = j$	ζ_{s_j}		ζ_{e_j}		ζ_{o_j}	
	estimate	std. error	estimate	std. error	estimate	std. error
0	0	0	0	0	1	0
1	0	0	0	0	1	0
2	0	0	0	0	1	0
3	0	0	0	0	1	0
4	0	0	0	0	1	0
5	0	0	0	0	1	0
6	0	0	0	0	1	0
7	0	0	1	0	0	0
8	0.0011	0.0003	0.9989	0.0003	0	0
9	0.0005	0.0002	0.9995	0.0002	0	0
10	0.0038	0.0006	0.9962	0.0006	0	0
11	0.0008	0.0003	0.9992	0.0003	0	0
12	0.0086	0.0009	0.9914	0.0009	0	0
13	0.0021	0.0005	0.9979	0.0005	0	0
14	0.0131	0.0011	0.9869	0.0011	0	0
15	0.0032	0.0006	0.9968	0.0006	0	0
16	0.0170	0.0013	0.9830	0.0013	0	0
17	0.0031	0.0006	0.9969	0.0006	0	0
18	0.0138	0.0012	0.9862	0.0012	0	0
19	0.0028	0.0005	0.9972	0.0005	0	0
20	0.0122	0.0011	0.9878	0.0011	0	0
21	0.0017	0.0004	0.9983	0.0004	0	0
22	0.0086	0.0009	0.9914	0.0009	0	0
23	0.0005	0.0002	0.9995	0.0002	0	0
24	0.0034	0.0006	0.9966	0.0006	0	0
25	0	0	1	0	0	0
26	0	0	1	0	0	0
27	0	0	1	0	0	0
28	0	0	1	0	0	0
29	0	0	1	0	0	0
30	0	0	1	0	0	0
31	0	0	1	0	0	0
32	0	0	1	0	0	0

LIST OF REFERENCES

[1]   C. Kopp, "Network Centric Warfare Fundamentals—Part 3: JTIDS/MIDS," *DefenceTODAY Magazine*, pp. 12-19, September 2005.

[2]   Northrop Grumman Corporation, *Understanding Link-16: A Guidebook for New User*, San Diego, CA, September 2001.

[3]   D. Gonzales, D. M. Norton, and M. Hura, *Multifunctional Information Distribution System (MIDS) Program Case Study*, Project AIR FORCE, RAND, DB-292-AF, April 2000.

[4]   J. Asenstorfer, T. Cox, and D. Wilksch, *Tactical Data Link Systems and the Australian Defence Force (ADF)- Technology Developments and Interoperability Issues*, Information Networks Division, Information Science Laboratory, DSTO-TR-1470, revised February 2004.

[5]   C. R. Bell and R. E. Conley, "Navy Communications Overview," *IEEE Transactions on Communications*, vol. COM-28, no. 9, September 1980.

[6]   W. J. Wilson, "Applying Layering Principles to Legacy Systems: Link 16 as a Case Study," *Proc. IEEE Military Commun. Conf.*, vol. 1, pp. 526-531, October 2001.

[7]   C. Leslie Golliday, JR., "Data Link Communications in Tactical Air Command and Control Systems", *IEEE Journal On Selected Area in Communications*, vol. SAC-3, no. 5, pp. 779-791, September 1985.

[8]   D. B. Brick and F. W. Ellersick, "Future Air Force Tactical Communications," *IEEE Transactions on Communications*, vol. COM-28, no. 9, pp. 1551-1572, September 1980.

[9]   M. B. Pursely, T. C. Royster, IV, and M. Y. Tan, "High-Rate Direct-Sequence Spread Spectrum," *Proc. IEEE Military Commun. Conf.*, vol. 2, pp. 1101-1106, October 2003.

[10]   M. B. Pursley and T. C. Royster, "High-Rate Direct-Sequence Spread Spectrum with Error-Control Coding," *IEEE Transactions on Communications*, vol. 54, no. 9, pp. 1693-1702, September 2006.

[11]   H. Wang, J. Kuang, Z. Wang, and H. Xu, "Transmission performance Evaluation of JTIDS," *Proc. IEEE Military Commun. Conf.*, vol. 4, pp. 2264-2268, 2005.

[12]   J. Proakis, *Digital Communications*: 4th ed., Boston, MA, McGraw-Hill, 2001.

[13]   F. J. Block, "Comparison of Jamming Robustness of Airborne Networking Waveforms," *Proc. IEEE Military Commun. Conf.*, vol. 4, pp. 2119-2125, 2005.

[14]   W. J. Ebel and W. H. Tranter, "The Performance of Reed-Solomon Codes on a Bursty-Noise Channel," *IEEE Transactions on Communications*, vol. 43, no. 2/3/4, pp. 298-306, February/March/April 1995.

[15]   E. Geraniotis, "Coherent Hybrid DS-SFH Spread-Spectrum Multiple-Access Communications," *IEEE Journals on Selected Areas in Communications*, vol. SAC-3, no. 5, pp. 695-705, September 1985.

[16]   E. Geraniotis, "Noncoherent Hybrid DS-SFH Spread-Spectrum Multiple-Access Communications," *IEEE Transactions on Communications*, vol. COM-34, no. 9, pp. 862-872, September 1986.

[17]   L. Sadiq and A. H. Aghvami, "Performance of A Coded Hybrid Spread Spectrum Communication System in the Presence of Partial Band Noise and Multiple Access Interference," *Proc. IEEE Military Commun. Conf.*, vol. 3, pp. 817-821, October 1988.

[18]   L. Sadiq and A. H. Aghvami, "Performance of Coded Hybrid Spread-Spectrum Communication System in Presence of Ricean Fading and Multiple Access Interference," *Electronics Letters*, vol. 25, no. 5, pp. 328-329, 2 March 1989.

[19]   L. P. Riddle, "Performance of a Hybrid Spread Spectrum System Against Follower Jamming," *Proc. IEEE Military Commun. Conf.*, vol. 1, pp. 420-424, October 1990.

[20]   L. Sadiq, and A. H. Aghvami, "Performance of an Asynchronous Hybrid Spread Spectrum System in the presence of Interference, Ricean Fading and AWGN," in *IEE Proc. I. Commun. Speech vis.*, vol. 138, no. 2, pp. 117-122, April 1991.

[21]   R. Muammar, "Performance Evaluation of a Hybrid Spread Spectrum System in a Hostile Land Mobile Radio Channel," *Vehicular Technology Conference 1991, IEEE*, pp. 108-113, May 1991.

[22]   H. Asmer, A. U. Sheikh, and T. Aaron Gulliver, "A Hybrid DS/FH Spread Spectrum System for Mobil Radio Channel: Performance and Capacity Analysis," *Vehicular Technology Conference 1993, IEEE*, pp. 305-308, May 1993.

[23]   Z. Haiou and Z. Naitong, "Performance Analysis of Hybrid DS-SFH/MSK Spread-Spectrum System under Multitone Jamming," *Proc. IEEE Military Commun. Conf.*, vol. 1, pp. 567-570, October 1999.

[24]   H. G. Ryu and Y. Y. Kim, "Effects of Partial-band Noise Interference on Hybrid DS/SFH MSK System in Rayleigh Fading Channel," *IEE Electronics Letters*, vol. 37, no. 16, pp. 1039-1041, 2 August 2001.

[25]   R. E. Ziemer and R. L. Peterson, *Introduction to Digital Communication*, 2nd ed., Upper Saddle River, NJ, Prentice Hall, 2001.

[26]   B. Sklar, *Digital Communications: Fundamentals and Applications*, 2nd ed., Upper Saddle River, NJ, Prentice Hall PTR, 2001.

[27]   C. Robertson, Notes for EC4560 (Spread Spectrum Communications), Naval Postgraduate School, Monterey, CA, 2005 (unpublished).

[28]   R. L. Peterson, R. E. Ziemer, and D. E. Borth, *Introduction to Spread Spectrum Communications*, Upper Saddle River, NJ, Prentice Hall, 1995.

[29]   T. S. Rappaport, *Wireless Communications Principles and Practice*, 2nd ed., Prentice Hall, Upper Saddle River, NJ, 2002.

[30]   C. Robertson, Notes for EC4550 (Digital Communications), Naval Postgraduate School, Monterey, CA, 2005 (unpublished).

[31]   J. P. Linnartz (2008, September 14). *Wireless Communication*. Available: http://wireless.per.nl/reference/chaptr03/ricenaka/nakagami.htm.

[32]   P. Z. Peebles, Jr., *Probability, Random Variables and Random Signal Principles*, 4th ed., McGraw-Hill, New York, NY, 2001.

[33]   C. W. Therrien and M. Tummala, *Probability for electrical and computer engineers*, CRC Press, Boca Raton, Florida, 2004.

[34]   S. Lin and D. J. Costello, Jr., *Error Control Coding*, 2nd ed., Upper Saddle River, NJ, Pearson Prentice Hall, 2004.

[35]   S. B. Wicker, "Type-II Hybrid-ARQ Protocols Using Punctured Reed-Solomon Codes," *Proc. IEEE Military Commun. Conf.*, vol. 3, pp. 1229-1234, November 1991.

[36]   C. V. Verikoukis and J. J. Olmos, "An efficient Type-II Hybrid-ARQ Protocols Using Punctured R-S Codes for Wireless ATM Networks," *Vehicular Technology Conference, 1999*, vol. 3, pp. 1725-1729, September 1999.

[37]   W. R. Smith, "SAW Filters For CPSM Spread Spectrum Communication," *Ultrasonics Symposium Proceedings, IEEE*, pp. 524-528, 1977.

[38]   S. Pasupathy, "Minimum Shift Keying: A Spectrally Efficient Modulation," *Communications Magazine, IEEE*, vol. 17, no. 4, pp. 14-22, July, 1979.

[39]   S. B. Wicker, *Error Control Systems: for Digital Communication and Storage*, Upper Saddle River, NJ, Prentice Hall, 1995.

[40]   C. Robertson, Notes for EC4580 (Error Control Coding), Naval Postgraduate School, Monterey, CA, 2005 (unpublished).

[41]   S. M. Ross, *Introduction to Probability Models*, 8th ed., San Diego, CA, Academic Press, p.99, 2003.

[42]   A. Leon-Garcia, *Probability and Random Processes for Electrical Engineering*, 2nd ed., NY, Addison-Wesley, 2000.

[43]   S. M. Ross, *Simulation*, 3rd ed., Academic Press, San Diego, CA, pp. 158-167, 2002.

[44]   G. C. Clark, Jr. and J. Bibb Cain, *Error-Correction Coding for Digital Communications*, Plenum Press, New York, NT, p. 22, 1981.

[45]   J. Proakis, *Digital Communications*: 4th ed., Boston, MA, McGraw-Hill, p. 825, 2001.

[46]   Mathematics Department, *Mathematics Tables*, Naval postgraduate School, Monterey, CA, p. 9, 2008.

[47]   J. Proakis, *Digital Communications*: 4th ed., Boston, MA, McGraw-Hill, p. 823, 2001.

INITIAL DISTRIBUTION LIST

1.   Defense Technical Information Center
   Ft. Belvoir, Virginia

2.   Dudley Knox Library
   Naval Postgraduate School
   Monterey, California

3.   Chairman
   Department of Electrical and Computer Engineering
   Naval Postgraduate School
   Monterey, California

4.   Prof. Clark Robertson
   Department of Electrical and Computer Engineering
   Naval Postgraduate School
   Monterey, California

5.   Prof. Roberto Cristi
   Department of Electrical and Computer Engineering
   Naval Postgraduate School
   Monterey, California

6.   Prof. Monique P. Fargues
   Department of Electrical and Computer Engineering
   Naval Postgraduate School
   Monterey, California

7.   Prof. Frank Kragh
   Department of Electrical and Computer Engineering
   Naval Postgraduate School
   Monterey, California

8.   Prof. Kyle Lin
   Department of Operational Research
   Naval Postgraduate School
   Monterey, California

9.   Rich North
   Technical Director for JTRS, JPEO JTRS
   San Diego, California

10.   Howard Pace
       Duty Program Executive Officer for JTRS, JPEO JTRS
       San Diego, California

11.   Captain Steven McPhillips
       Program Manager for Command and Control Systems (PMW 150), PEO C4I
       San Diego, California

12.   Captain John Pope
       Program Manager for Communications Systems (PMW 170), PEO C4I
       San Diego, California

13.   Commander Chi-Han Kao
       Taiwan Navy
       Taipei, Taiwan, R.O.C